



NUREG/CR-6994
ANL-08/37

Argonne Model Boiler Test Results

Argonne Model Boiler Test Results

Manuscript Completed: November 2008
Date Published: December 2009

Prepared by
C.B. Bahn, K.E. Kasza, J. Park, C. Vulyak, and W.J. Shack

Argonne National Laboratory
9700 South Cass Avenue
Argonne, IL 60439

C. Harris, NRC Project Manager

NRC Job Code Y6588

This page is intentionally left blank.

Abstract

Various corrosion phenomena have been observed in the steam generator (SG) tubes of pressurized water reactors. One such type of corrosion involves impurity concentration in the narrow gap between SG tubes and supporting structures or sludge piles (“crevices”). The purpose of this study is to characterize accumulation of impurities in the crevices for varying Na-to-Cl molar ratios in water, temperature, and packing type (diamond or magnetite). This characterization is based on tests carried out at Argonne National Laboratory in a model boiler system which can simulate prototypic SG conditions. Diamond powder, which has a higher thermal conductivity than magnetite powder, can enhance the boiling rate and lead to a rapid rate of impurity accumulation. Magnetite-packed crevices, which have lower permeability, are more appropriate for the simulation of actual SG crevices than a diamond-packed crevice. A radial chemistry gradient was observed in a crevice packed tightly with magnetite powder, a finding supported by earlier experimental work. Near the tube wall, the crevice chemistry tends to vary actively because of the increased volatility effect of Cl at the heated tube wall where boiling occurs. Initially, the crevice pH near the tube wall appears to be alkaline. As the concentration progresses, however, the crevice pH becomes neutralized and even acidic because of preferential Cl concentration, enabled by a reduced boiling rate near the tube wall due to the presence of a Na-rich liquid film. Based on the test results, the chemistry variation in actual SG crevice deposits near the tube wall was estimated. Unless some impurities remain and accumulate in the crevice after each fuel cycle, during most of a typical fuel cycle, the crevice chemistry would be in a transient rather than a steady-state condition because of low impurity concentrations in the secondary system. The kinetic data obtained for the crevice chemistry evolution with low bulk impurity concentration is valuable for the estimation of actual SG crevice chemistries. Based on the crevice and bulk solution sample analyses, the volatility effect of Cl in the diamond-packed crevices becomes significant as the molar ratio decreases. Data are limited but it is likely that the volatility effect of Cl in the magnetite-packed crevices is not strongly influenced by the molar ratio variation in the bulk solution. Tests showed that once a tube crack is formed, the crack itself can act as a crevice, and in the presence of NaOH bulk chemistry, it can grow even if the sludge or debris is cleaned out of the SG.

This page is intentionally left blank.

FOREWORD

This report discusses a study conducted by Argonne National Laboratory (ANL) under contract with the U.S. Nuclear Regulatory Commission (NRC), to study the effects of steam generator secondary side water chemistry on crack initiation and propagation near crevices.

The purpose of this study is to characterize accumulation of impurities in the crevices adjacent to steam generator (SG) tubes. A model boiler system to simulate prototypical thermal hydraulic and chemistry conditions of the secondary side of SGs in pressurized water reactors was developed at ANL. The facility has prototypic crevice heat fluxes and temperatures, thus permitting the development of more prototypic crevice chemistry conditions. A crevice simulator equipped with various instruments, including thermocouples, electro-chemical potential electrodes, pH electrodes, conductivity probes, and solution sampling lines, was developed and successfully operated.

This work produced many findings regarding SG tube corrosion and deposits. The crevice pH predicted by an analytical code was compared with the measured crevice pH as a function of boiling point elevation. Initially, the crevice pH near the tube wall appears to be alkaline, however, as the impurity concentration progresses, the crevice pH becomes neutralized and even acidic. In a less permeable crevice, the volatility of Cl becomes less significant because Cl does not easily escape. This condition leads to a lowering of the crevice pH near the tube wall. The kinetic data obtained for the crevice chemistry evolution with low bulk impurity concentration is valuable for the estimation of actual SG crevice chemistries.

The chemistry variations in the deposits in an actual SG crevice near the tube wall were estimated. The Model Boiler tests showed some initial evidence that once a crack is formed, the crack itself can act as a crevice. In NaOH bulk chemistry the crack can grow even if the sludge or debris is cleaned out of the SG.

The NRC may use this research in the evaluation of industry assessments of steam generator (SG) tube integrity. These assessments are provided in support of license amendments and other licensing tasks. Additionally, these products may also provide guidance to regionally based NRC inspectors who verify proper implementation of the licensee steam generator programs.

Michael J. Case, Director
Division of Engineering
Office of Nuclear Regulatory Research
U.S. Nuclear Regulatory Commission

This page is intentionally left blank.

Contents

Abstract	iii
Foreword	v
Contents	vii
Figures	xiii
Tables	xxvii
Executive Summary	xxix
Acknowledgments.....	xxx
Acronyms and Abbreviations	xxxiii
Symbols	xxxv
1 Introduction	1
1.1 Model Development.....	1
1.2 Literature Review	4
1.2.1 Laboratory Heated Crevice Testing	4
1.2.2 Crevice Numerical Modeling.....	6
1.3 Objectives & Approach.....	8
2 Experimental	9
2.1 Model Boiler.....	9
2.2 Secondary Water Control & Instrumentations.....	10
2.2.1 Water Chemistry Control	10
2.2.2 Instrumentation	14
2.3 Crevice Simulator	19
2.3.1 Design	19
2.3.2 Instrumentation	21

2.3.3 Packing Materials.....	23
2.4 Test Procedures	25
2.5 Test Matrix	26
3. Preliminary Crevice Tests	29
3.1 Unpacked Crevice Tests.....	29
3.2 Packed Crevice Test with NaOH	30
3.2.1 Packed Crevice Test: NaOH-01	31
3.2.2 Packed Crevice Test: NaOH-02	32
4. Sodium Chloride Tests with Two Crevices	35
4.1 NaCl-01: NaCl (MR=1.0) Test	35
4.1.1 Test Conditions	35
4.1.2 High Purity Water Test	35
4.1.3 Temperature and Conductivity.....	36
4.1.4 ECP Measurement	40
4.2 NaCl-02: NaCl (MR=1.0) Test	41
4.2.1 Temperature Data.....	41
4.2.2 Bulk and Crevice Chemistry	44
4.2.3 ECP Measurement	48
4.2.4 Summary	52
4.3 NaCl-03: NaCl (MR=0.3) Test	53
4.3.1 Temperature Data.....	53
4.3.2 Bulk & Crevice Chemistry.....	56
4.3.3 ECP Measurement	59
4.3.4 Discussion	62
4.3.5 Summary	67

4.4 NaCl-04: NaCl (MR=0.7) Test	67
4.4.1 Temperature Data.....	68
4.4.2 Bulk & Crevice Chemistry.....	70
4.4.3 ECP Measurement	72
4.4.4 Discussion of ECP and Solution Analysis	74
4.4.5 Post-test Examination	77
4.4.6 Comparing the Results for NaCl-02 through -04 Tests.....	83
4.4.7 Summary	84
5. Single Crevice Test	87
5.1 Background	87
5.2 NaOH-03: NaOH Test	87
5.2.1 Temperature Data.....	87
5.2.2 Bulk & Crevice Chemistry.....	89
5.2.3 ECP Measurement	92
5.2.4 Post-Test Examination	95
5.2.5 Discussion	99
5.2.6 Summary	106
5.3 NaCl-05: NaCl (MR=0.7) Test with Diamond Packing.....	107
5.3.1 Background.....	107
5.3.2 Temperature Data.....	107
5.3.3 Bulk and Crevice Chemistry	108
5.3.4 ECP Measurements	111
5.3.5 Post-Test Examination	113
5.3.6 Discussion	116
5.3.7 Summary	122

5.4 NaCl-06: NaCl (MR=0.7) Test with Magnetite Packing	123
5.4.1 Background	123
5.4.2 Temperature Data.....	123
5.4.3 Bulk and Crevice Chemistry	125
5.4.4 ECP Measurement	129
5.4.5 Post-Test Examination	135
5.4.6 Discussion	139
5.4.7 Summary	150
6. Overall Discussion	153
6.1 Comparison with Literature Data.....	153
6.1.1 NaOH Test	153
6.1.2 NaCl Test	155
6.1.3 ECP Data Comparison	157
6.2 Comparison with MULTEQ Prediction.....	159
6.3 Implication of MB Test Results for Operating Steam Generator.....	165
6.3.1 Crack Propagation in an Unpacked Crevice	165
6.3.2 Diamond vs. Magnetite	166
6.3.3 Hideout Kinetics Estimation in Actual SG Crevices	166
6.3.4 Dependency of Cl Volatility Effect on Molar Ratio	169
6.3.5 Cl Adsorption to Magnetite.....	171
6.3.6 Electromigration Effect in the Crevice	171
6.3.7 Hard Scales Formed on the Tube Surfaces	172
7. Summary	173
7.1 Conclusions	173
7.2 Future Work	174

8. References	175
Appendix A: Preliminary Crevice Test with NaOH Bulk Chemistries	A1
A.1 Packed Crevice Test: NaOH-01	A1
A.2 Packed Crevice Test: NaOH-02	A8
References	A19
Appendix B: Mass Balance Analysis with Simple Analytical Model	B1
Reference.....	B7

This page is intentionally left blank.

Figures

Figure 1.	Mann’s model of impurity hideout in a heated, loosely packed crevice (reprinted from Figure 4-1 of EPRI Report NP-5015). ²	2
Figure 2.	Mann’s model of impurity hideout in a heated, highly packed crevice (reprinted from Figure 4-4 of EPRI Report NP-5015). ²	3
Figure 3.	Schematic showing crevice solution transport processes. ⁵	3
Figure 4.	Schematic of Argonne model boiler system. ²⁵	9
Figure 5.	Photograph showing the MB equipped with insulation and instrumentation and a discharge collection tank.	10
Figure 6.	Schematic of injection pump system for secondary bulk solution.	11
Figure 7.	Photograph of the injection pump system for controlling/changing secondary bulk water chemistry (cart on right side).....	12
Figure 8.	Photograph (bottom) and schematic (top) of the MB high-pressure manifold (upper left) access for secondary-chamber bulk-solution feed/sampling lines, overpressure safety rupture disc, pressure transducer, and filling/drain line.....	13
Figure 9.	Photograph of internal model boiler.....	16
Figure 10.	Photograph showing bulk ECP electrode assembly and the tip of the external pressure-balanced Ag/AgCl (0.01M KCl) reference electrode.....	17
Figure 11.	Close-up photograph of an ECP electrode assembly for bulk water chemistry measurement.	17
Figure 12.	Secondary chamber parallel-plate fluid conductivity probe for measuring changes in bulk water chemistry of MB.....	18
Figure 13.	Photograph of bulk secondary micro-bore sampling (shorter 1/16-in. OD tubing at center) and injection tube (longer 1/16-in. OD tubing at center).	18
Figure 14.	Schematic of crevice simulator design.	20
Figure 15.	Close-up of 10-mil gap crevice showing new Teflon seal ring on bottom of crevice to reduce SG tube stressing and facilitate crevice removal.....	20
Figure 16.	Photograph of 10-mil gap crevice simulator showing various instrumentation ports.	22
Figure 17.	Assembled diamond-packed crevice with 0.010-in. radial gap. Photograph shows two ECP electrode probes (right), four installed mid-crevice gap thermocouples, and Ni-Cr-Mo alloy porous foam mesh for retaining packing.	23

Figure 18.	Micro-bore crevice sampling tube assembly and SS frit used to prevent plugging of the tube.	23
Figure 19.	Photograph of crevice A (0.010-in. radial gap) showing diamond grit packing, three equally spaced wire shims, two micro-bore sampling lines, ECP electrodes connections, thermocouple leads, and an unused crevice port (right).	24
Figure 20.	Photograph of crevice B (0.020-in. radial gap) showing magnetite packing and equally spaced wire shims.	25
Figure 21.	Primary chamber bleed line and valve which exits the pressure vessel and purges primary non-condensable gases.	26
Figure 22.	Concentration factors vs. time for 0.25-mm (0.010-in.) radial gap unpacked crevice and primary-to-secondary temperature differences of 56°C and 69°C (100°F and 125°F).	30
Figure 23.	Concentration factors vs. time for 0.25- and 0.51-mm (0.010- and 0.020-in.) radial gap unpacked crevice and a 56°C (100°F) primary-to-secondary temperature difference.	30
Figure 24.	Photograph of gouging in tube wall in the vicinity of the 0.25-mm (0.010-in.) radial gap crevice.	32
Figure 25.	Crevice SCC flaw photographed using dye penetrant to enhance visualization. The flaw is longer than 18 mm (0.71 in.).	33
Figure 26.	Normalized temperature variation at 10-mil-gap crevice with high purity water in the bulk (NaCl-01).	36
Figure 27.	Bulk conductivity variation with time in high purity water (NaCl-01).	36
Figure 28.	Crevice temperature variation with time in the 10-mil radial gap crevice packed with diamond powder and with NaCl in the bulk solution (NaCl-01).	37
Figure 29.	Normalized temperature variation at the 10-mil gap crevice with NaCl in the bulk solution (NaCl-01).	38
Figure 30.	Crevice temperature variation with time in the 20-mil radial gap crevice packed with diamond powder (NaCl-01).	39
Figure 31.	Normalized temperature variation at 20-mil gap crevice (NaCl-01).	39
Figure 32.	Bulk conductivity variation and Cl ion concentration versus time in bulk water samples measured by an ISE (NaCl-01).	40
Figure 33.	Ni electrode potential variation in crevice with respect to Ag/AgCl (0.01 N KCl) reference electrode in bulk (NaCl-01).	41
Figure 34.	Crevice temperature variation with time and ΔT in a 10-mil radial gap crevice packed with diamond powder (NaCl-02).	42

Figure 35.	Normalized temperature variation at 10-mil gap crevice (NaCl-02).....	43
Figure 36.	Crevice temperature variation with time and ΔT in a 20-mil radial gap crevice packed with diamond powder (NaCl-02).....	43
Figure 37.	Normalized temperature variation at 20-mil gap crevice (NaCl-02).....	44
Figure 38.	Comparison of bulk conductivity and measured bulk impurity concentration determined by solution sampling (NaCl-02).	45
Figure 39.	Comparison of measured bulk conductivity in the NaCl-01 test and NaCl-02 test.....	46
Figure 40.	Normalized bulk conductivity variation as a function of ΔT in the NaCl-02 test comparing the bulk conductivity decreasing rates.	46
Figure 41.	Concentrations from crevice-solution sample analysis as functions of time and ΔT in the NaCl-02 test.....	47
Figure 42.	[Na]/[Cl] ratios in crevice versus bulk as a function of ΔT for (a) 10-mil gap and (b) 20-mil gap crevices in the NaCl-02 test.	48
Figure 43.	Electrode potential variation with respect to Ag/AgCl (0.01N KCl) (NaCl-02).....	49
Figure 44.	Predictions of solution pH variation at 260°C (500°F) with Na-to-Cl molar ratio and ion concentration.	50
Figure 45.	Electrode potential difference between crevice and bulk (NaCl-02).....	50
Figure 46.	Measured Ni electrode potential in crevice in the NaCl-01 and NaCl-02 tests.....	51
Figure 47.	Pt potential difference between crevice and bulk as a function of pH difference calculated by MULTEQ (NaCl-02).	52
Figure 48.	Schematics of the precipitation and concentration phenomena in the crevice for (a) higher ΔT (80°F and 100°F) and (b) lower ΔT (40°F and 60°F).	53
Figure 49.	Crevice temperature variation with time in a 10-mil gap crevice packed with diamond powder (NaCl-03).....	54
Figure 50.	Normalized crevice temperature variation with time in a 10-mil gap crevice packed with diamond powder (NaCl-03).....	55
Figure 51.	Crevice temperature variation with time in a 20-mil gap crevice packed with magnetite powder (NaCl-03).....	55
Figure 52.	Normalized crevice temperature variation with time in a 20-mil gap crevice packed with magnetite powder (NaCl-03).....	56
Figure 53.	Variation in bulk conductivity and ion concentration with time (NaCl-03).....	57

Figure 54.	Variation in bulk and crevice conductivity with time in a 10-mil gap crevice packed with diamond powder (NaCl-03).....	58
Figure 55.	Concentration results for crevice solution samples by using ICP/OES for Na, IC for Cl, and ISE for Na and Cl (NaCl-03).....	58
Figure 56.	Crevice conductivity variation with time in the 10-mil gap crevice packed with diamond along with analysis results of crevice samples (NaCl-03).....	59
Figure 57.	Variations in Pt electrode potential with time in bulk and 10-mil gap crevice packed with diamond (NaCl-03).....	60
Figure 58.	Variations in Ni electrode potential with time in bulk and 10-mil gap crevice packed with diamond (NaCl-03).....	60
Figure 59.	Tungsten electrode potential variations with time in bulk and 10-mil gap crevice packed with diamond (NaCl-03).....	61
Figure 60.	Tungsten potential difference between crevice and bulk compared with crevice conductivity variation in 10-mil gap crevice packed with diamond (NaCl-03).	62
Figure 61.	Plot of MULTEQ-predicted pH difference and tungsten potential difference between bulk and 10-mil gap crevice packed with diamond (NaCl-03).....	64
Figure 62.	Tungsten potential measured in crevice and bulk as a function of predicted pH by MULTEQ (initial [Na]/[Cl]=0.3; NaCl-03).	64
Figure 63.	Tungsten potentials as a function of the calculated pH based on solution samples from crevice and bulk (NaCl-03).	65
Figure 64.	Molar ratio variations as a function of time in bulk and crevices (NaCl-03).	65
Figure 65.	Total accumulated moles of Na and Cl in crevices as a function of time (NaCl-03).	66
Figure 66.	Total accumulated moles of Na and Cl in crevices as a function of exposure (NaCl-03).....	67
Figure 67.	Temperature variation in 10-mil gap crevice with time and locations of TCs (initial [Na]/[Cl]=0.7; NaCl-04).....	68
Figure 68.	Normalized temperature variation in 10-mil gap crevice (initial [Na]/[Cl]=0.7; NaCl-04). ..	69
Figure 69.	Temperature variation in 20-mil gap crevice with time and locations of TCs (initial [Na]/[Cl]=0.7; NaCl-04).....	69
Figure 70.	Normalized temperature variation in 20-mil gap crevice (initial [Na]/[Cl]=0.7; NaCl-04). ..	70
Figure 71.	Bulk conductivity variation and measured Na and Cl concentrations in bulk water samples (NaCl-04).....	71

Figure 72.	Crevice conductivity variation with time in the 10-mil gap crevice packed with diamond powder (NaCl-04).....	71
Figure 73.	Chemical analysis results for crevice samples from 10-mil gap crevice packed with diamond and 20-mil gap crevice packed with magnetite (NaCl-04).....	72
Figure 74.	Variations of Pt electrode potential in bulk and 10-mil gap crevice packed with diamond (NaCl-04).....	73
Figure 75.	Variations in Ni electrode potential in bulk and 10-mil gap crevice packed with diamond (NaCl-04).....	73
Figure 76.	Variations in tungsten electrode potential in bulk and 10-mil gap crevice packed with diamond (NaCl-04).....	74
Figure 77.	Calculated pH and tungsten potential difference between the 10-mil gap crevice and bulk (NaCl-04).....	75
Figure 78.	Tungsten potential measured in bulk and 10-mil gap crevice as a function of calculated pH for the samples taken at the same time when tungsten potentials were measured (NaCl-04).76	
Figure 79.	Na-to-Cl molar ratio variations with time in bulk and crevices (NaCl-04).....	76
Figure 80.	Total accumulated moles of Na and Cl in crevices and their molar ratio as a function of time after the solution injection (NaCl-04).....	77
Figure 81.	Total accumulated moles of Na and Cl in crevices as a function of exposure after the solution injection (NaCl-04).....	77
Figure 82.	Photograph of 10-mil gap crevice assembly after the NaCl-03 and -04 tests showing disintegrated Ni foam.	79
Figure 83.	Tube surfaces in the 10-mil gap crevice packed with diamond powder after removal of the crevice ring.	79
Figure 84.	Bare tube surfaces in the 10-mil gap crevice after removal of deposits and diamond powders, showing gouges (the same area as shown in Fig. 83).....	80
Figure 85.	Top view of 20-mil gap crevice after removal of Ni foam and retaining ring, showing the magnetite powder in the crevice after the NaCl-03 and -04 tests.....	80
Figure 86.	Tube surfaces of 20-mil gap crevice after removal of the crevice assembly showing the deposit formed on the upper crevice region and magnetite powder.....	81
Figure 87.	Bare tube surfaces in the 20-mil gap crevice after removal of the deposit and magnetite powder, showing neither pitting nor gouges.	81
Figure 88.	Ni solubility as a function of pH and Cl concentration.....	82

Figure 89.	Pt potential data measured in crevice and bulk water as a function of MULTEQ calculated pH based on solution sample analysis.	83
Figure 90.	Tungsten potential measured in bulk and crevice as a function of sample pH, including all data from NaCl-03 and -04 tests plotted in a potential-pH diagram of W-H ₂ O system predicted by the thermodynamic code HSC Chemistry.	84
Figure 91.	Crevice temperature variation in the 10-mil gap crevice packed with diamond (NaOH-03).	88
Figure 92.	Crevice temperature variation in the 20-mil gap crevice without packing (NaOH-03).	88
Figure 93.	Normalized crevice temperature in the 10-mil gap crevice packed with diamond (NaOH-03).	89
Figure 94.	Bulk conductivity variation with time and impurity concentrations in bulk solution (NaOH-03).	90
Figure 95.	Crevice conductivity variation in the 10-mil gap crevice packed with diamond (NaOH-03).	90
Figure 96.	Chemical analyses of the samples taken from the 10-mil gap crevice packed with diamond dust (NaOH-03).	91
Figure 97.	Chemical analyses of crevice samples corrected for sampling time (10-mil gap crevice: diamond packed, 20-mil gap crevice: open crevice).	92
Figure 98.	Tungsten potential variation in bulk and 10-mil gap crevice packed with diamond powder (NaOH-03).	93
Figure 99.	Pt potential variations in bulk and 10-mil gap crevice packed with diamond powder (NaOH-03).	94
Figure 100.	Alloy 600 potential variations in bulk and 10-mil gap crevice packed with diamond powder (NaOH-03).	94
Figure 101.	Tungsten and alloy 600 potentials in 10-mil gap crevice packed with diamond as compared with crevice conductivity variation (NaOH-03).	95
Figure 102.	Bare surface of alloy 600 tubing showing severe gouging due to caustic crevice chemistry.	96
Figure 103.	Gas bubbles coming out of a through-wall crack detected underneath the Teflon swaging ferrule and developed inside the 10-mil gap crevice packed with diamond dust.	96
Figure 104.	Axial cracks developed inside the 10-mil gap crevice packed with diamond dust and visually enhanced by dye penetration (left side: crevice top, right side: crevice bottom).	97
Figure 105.	Gas bubbles coming out of through-wall cracks developed inside the unpacked crevice region having a 20-mil radial gap.	98

Figure 106. Axial cracks developed inside the unpacked crevice region and visually enhanced by dye penetration.....	98
Figure 107. Primary and secondary water temperature variation with time (NaOH-03).....	99
Figure 108. Primary and secondary pressure variation with time (NaOH-03).	100
Figure 109. Cooling fan speed and crevice temperature (T3) variations with time (NaOH-03).	100
Figure 110. Crevice and bulk tungsten potential variation as a function of crevice pH based on samples (NaOH-03).....	102
Figure 111. Tungsten potentials in bulk and crevice as a function of pH by sampling results in a potential-pH diagram of W-H ₂ O system predicted by the thermodynamic code HSC Chemistry.	103
Figure 112. Volume-averaged crevice Na concentration estimated from bulk chemistry data, tungsten potential in crevice, and temperature data in crevice as compared with the analyses for crevice samples (NaOH-03).	105
Figure 113. Calculated pH and boiling point elevation variation as a function of total Na concentration in crevice predicted by MULTEQ.....	105
Figure 114. Measured tungsten potentials as a function of pH based on bulk solution samples plotted in a potential-pH diagram of W-H ₂ O system predicted by the thermodynamic code HSC Chemistry.	106
Figure 115. Crevice temperature variation with time in the 10-mil gap crevice packed with diamond powder (initial MR=0.7; NaCl-05).....	108
Figure 116. Normalized crevice temperature variation with time (initial MR=0.7; NaCl-05).....	108
Figure 117. Bulk conductivity variation with time and the chemical analysis results for bulk samples (initial MR=0.7; NaCl-05).....	109
Figure 118. Bulk and crevice conductivity variation with time (initial MR=0.7; NaCl-05).	110
Figure 119. Chemical analyses of the crevice samples (initial MR=0.7; NaCl-05).	111
Figure 120. Tungsten potential variation with time in the bulk and 10-mil gap crevice packed with diamond powder (initial MR=0.7; NaCl-05).....	112
Figure 121. Ta potential variation with time in the bulk and the 10-mil gap crevice packed with diamond powder (initial MR=0.7; NaCl-05).....	112
Figure 122. Top of the crevice ring after removal of the Inconel foam and retaining ring, which shows the diamond dust was secure inside the crevice.	114

Figure 123. Alloy 690 TT tubing surface after removal of the crevice ring and diamond dust showing gouging in the crevice region.	114
Figure 124. Bare alloy 690 TT tubing surface (left: crevice top, right: crevice bottom).	115
Figure 125. Dye penetrant test results after removal of the hard scale underneath the SS back ferrule showing no visible cracks in the crevice region.	115
Figure 126. Tungsten and Ta potentials in bulk and crevice as a function of pH estimated from the solution samples by MULTEQ (initial MR=0.7; NaCl-05).	116
Figure 127. Tungsten potentials measured during NaCl-05 compared to the data from previous tests plotted in a phase diagram of W-H ₂ O system predicted by the thermodynamic code HSC Chemistry.	117
Figure 128. Molar ratio variations in bulk and crevice samples with time (NaCl-05).	118
Figure 129. Total mass of Na and Cl in crevice as a function of time for the previous MR=0.7 test with single diamond-packed crevice (estimates from the analysis of bulk samples; NaCl-05). ..	120
Figure 130. Total moles of Na and Cl in crevice as a function of time for the previous MR=0.7 test with single diamond-packed crevice (estimates from the analysis of bulk samples; NaCl-05). ..	120
Figure 131. Total mass of Na or Cl in crevice as a function of bulk Na or Cl exposure for the previous MR=0.7 test with single diamond-packed crevice (estimates from the analysis of bulk samples; NaCl-05).	121
Figure 132. Total moles of Na or Cl in crevice as a function of bulk Na or Cl exposure for the previous MR=0.7 test with single diamond-packed crevice (estimates from the analysis of bulk samples; NaCl-05).	121
Figure 133. Total Na mass variation in crevice with Na exposure for two tests: NaOH-03 and NaCl-05 with a Na-to-Cl molar ratio of 0.7.	122
Figure 134. Crevice temperatures as a function of time for the magnetite-packed crevice and secondary water chemistry at Na-to-Cl molar ratio of 0.7 (NaCl-06).	124
Figure 135. Normalized crevice temperatures as a function of time for the magnetite-packed crevice and secondary water chemistry at Na-to-Cl molar ratio of 0.7 (NaCl-06).	125
Figure 136. Bulk conductivity as a function of time for the magnetite-packed crevice and secondary water chemistry at Na-to-Cl molar ratio of 0.7 (NaCl-06).	126
Figure 137. Crevice and bulk conductivities as a function of time for the magnetite-packed crevice and secondary water chemistry at Na-to-Cl molar ratio of 0.7 (NaCl-06).	127
Figure 138. Normalized bulk conductivity variation as a function of ΔT for the magnetite-packed crevice and secondary water chemistry at Na-to-Cl molar ratio of 0.7 (NaCl-06).	128

Figure 139. Bulk conductivity variation for the magnetite-packed crevice in comparison of that for the diamond-packed crevice.....	128
Figure 140. W/WO _x potentials measured at bulk and crevice as a function of time for the magnetite-packed crevice and secondary water chemistry at Na-to-Cl molar ratio of 0.7 (NaCl-06). .	130
Figure 141. Tungsten potential difference variations as a function of ΔT in seawater addition testing (from Baum). ³⁹	131
Figure 142. W/WO _x potentials measured at bulk and crevice after the MB shut-down (NaCl-06).....	131
Figure 143. Pt potentials measured at bulk and crevice as a function of time for the magnetite-packed crevice and secondary water chemistry at Na-to-Cl molar ratio of 0.7 (NaCl-06).....	132
Figure 144. Ta potentials measured at bulk and crevice as a function of time for the magnetite-packed crevice and secondary water chemistry at Na-to-Cl molar ratio of 0.7 (NaCl-06).....	133
Figure 145. Alloy 600 potentials measured at crevice as a function of time for the magnetite-packed crevice and secondary water chemistry at Na-to-Cl molar ratio of 0.7 (NaCl-06).....	133
Figure 146. Crevice electrode potentials in comparison of the crevice temperature at the magnetite-packed crevice with the Na-to-Cl molar ratio of 0.7 (NaCl-06).....	134
Figure 147. Crevice tungsten potentials measured at the magnetite-packed crevice compared with crevice tungsten potentials at the diamond-packed crevice with the same Na-to-Cl molar ratio of 0.7 (NaCl-06).....	135
Figure 148. Top area of crevice assembly exposed to the test solution with MR=0.7 for 720 hours at 500°F (260°C).....	136
Figure 149. Top area of crevice assembly after removal of a top retainer exposed to the test solution with MR=0.7 for 720 hours at 500°F (260°C).	136
Figure 150. Crevice mouth after removal of a foam mesh showing that magnetite powder remains in place.	137
Figure 151. Magnetite powder clinging to the alloy 690 tubing surfaces after removal of the crevice ring.	137
Figure 152. Hard scale formed on alloy 690 tube surface exposed to the NaCl-06 test solution with MR=0.7 and magnetite packing for 720 hours at 500°F (260°C) (crevice top: left; crevice bottom: right).....	138
Figure 153. Pitted tube surface exposed to the test solution of NaCl-05 with MR=0.7 for 700 hours at 500°F (260°C) and diamond-packed crevice (crevice top: left; crevice bottom: right).	138
Figure 154. Dye penetrant test results in the same area as shown in Figure 152 (crevice top: left; crevice bottom: right).....	139

Figure 155. Tungsten potentials in bulk and crevice as a function of pH calculated from solution sample analysis with and without Fe and Ni (NaCl-06).	141
Figure 156. Measured tungsten potentials in the NaCl-06 test in comparison with the previously measured tungsten potentials in a W-H ₂ O phase diagram predicted by the thermodynamic code HSC Chemistry.	142
Figure 157. Total mass of Na and Cl accumulated in the crevice as a function of time based on the results of bulk solution analysis (NaCl-06).	143
Figure 158. Total moles of Na and Cl accumulated in the crevice as a function of time based on the results of bulk solution analysis (NaCl-06).	144
Figure 159. Total mass of Na and Cl accumulated in the crevice as a function of exposure based on the results of bulk solution analysis (NaCl-06).	145
Figure 160. Total moles of Na and Cl accumulated in the crevice as a function of molal exposure based on the results of bulk solution analysis (NaCl-06).	145
Figure 161. Na-to-Cl molar ratio variation of bulk samples and estimated crevice concentration from bulk chemical analysis (NaCl-06).	146
Figure 162. Integrated-volume average Na concentration variations with exposure for NaCl-05 and NaCl-06 tests.	147
Figure 163. Integrated-volume average Cl concentration variations with exposure for NaCl-05 and NaCl-06 tests.	148
Figure 164. Permeability of single-crevice tests for diamond- and magnetite-packed crevices predicted by Carman-Kozeny equation ($1 \text{ Darcy} = 9.86923 \times 10^{-13} \text{ m}^2$).	149
Figure 165. Potential-pH diagram of Fe-Cl-Na-H ₂ O system at 260 °C (500 °F) predicted by the thermodynamic code HSC Chemistry.	150
Figure 166. Total Na mass in crevice as a function time with two bulk Na concentrations: 20 ppm Na for upper figure and 2 ppm Na for lower figure. Test conditions are as follows: constant heat flux, diamond packed (52 % porosity), $T_{\text{sat}}=280^{\circ}\text{C}$. ⁴¹	154
Figure 167. Comparison of 20 ppm NaOH ([Na]=11.3 ppm) test results with available NaOH test data from Lumsden's earlier work ⁴¹ (Note: Lumsden's data are the same as shown in Figure 166).	155
Figure 168. Comparison of NaCl hideout mass as a function of Cl exposure determined by Mann and Castle ² and our test results for molar ratios of 1.0 (NaCl-02) and 0.7 (NaCl-05 and -06).	156
Figure 169. Comparison of the steady-state NaCl mass in the crevice as a function of ΔT from NaCl-05 and -06 tests and tests by Mann and Castle. ²	156

Figure 170. Comparison of NaCl hideout mass as a function of Cl exposure in the corroded carbon-fiber packed crevice of Mann and Castle ² and in the magnetite-packed crevice of NaCl-06.....	157
Figure 171. Crevice ECP after exposure to NaCl solution for 48 hours when the molar ratios of bulk solution was (a) [Na]/[Cl]=1.0 and (b) [Na]/[Cl]=0.2. ⁴¹	158
Figure 172. Pt electrode potential variations in bulk and crevice with the molar ratio of 1.0 (NaCl-02 test).	159
Figure 173. Calculated crevice pH by MULTEQ as a function of boiling point elevation in comparison to the measured crevice pH based on the crevice tungsten potential data in the NaOH-03 test (nominal [Na]=11.3 ppm and [Cl] =0.6 ppm).	160
Figure 174. Calculated crevice pH by MULTEQ as a function of boiling point elevation at MR=1.0... 161	
Figure 175. Crevice pH calculated by MULTEQ as a function of boiling point elevation compared to the measured crevice pH based on the crevice tungsten potential data in the NaCl-05 test (MR=0.7).....	162
Figure 176. Crevice pH and ion concentration as a function of concentration factor calculated by MULTEQ assuming the “steam retained” condition and MR=0.7.	163
Figure 177. Crevice pH and ion concentration as a function of concentration factor calculated by MULTEQ assuming the “steam removed” condition and MR=0.7.	163
Figure 178. Measured crevice pH based on the crevice tungsten potential data in the NaCl-06 test in comparison with the NaCl-05 test and calculated pH by MULTEQ.....	164
Figure 179. Calculated crevice pH by MULTEQ as a function of boiling point elevation in comparison with measured crevice pH based on the crevice tungsten potential data in the NaCl-03 test.	165
Figure 180. Initial Na and Cl hideout rates as a function of the temperature difference between primary and secondary saturation temperatures (NaCl-06).	168
Figure 181. Schematic of Na and Cl hideout mass variations as a function of time in a crevice where the porosity and secondary impurity level are assumed to be similar to those in actual SGs. ...	168
Figure 182. Molar ratio in crevice sample as a function of the molar ratio in the bulk sample for a diamond-packed crevice.....	170
Figure 183. Molar ratio in crevice sample as a function of the molar ratio in the bulk sample for a magnetite-packed crevice.	170
Figure 184. Normalized bulk conductivity variations with time from the beginning of each test at $\Delta T=40^{\circ}F$	171
Figure A1. Primary water ($T_p=600^{\circ}F$) and crevice temperature variations with time in 10-mil gap crevice packed with diamond powder during series 1 of NaOH-01 test.	A2

Figure A2. Crevice temperature variations with time in 20-mil gap crevice packed with diamond powder during series 1 of NaOH-01 test.....	A2
Figure A3. Primary water and crevice temperature variations with time in the 10-mil gap crevice packed with diamond powder during series 2 of NaOH-01 test.....	A3
Figure A4. Crevice temperature variations with time in the 20-mil gap crevice packed with diamond powder during series 2 of NaOH-01 test.....	A3
Figure A5. Crevice temperature variation with time in the 10-mil gap crevice packed with diamond powder during series 3 and 4 of NaOH-01 test.....	A5
Figure A6. Crevice temperature variation with time in the 20-mil gap crevice packed with diamond powder during series 3 and 4 of NaOH-01 test.....	A5
Figure A7. Photograph of torn nickel membrane on the 20-mil gap crevice and the absence of diamond packing in the crevice.....	A6
Figure A8. Photograph of 20-mil gap crevice and the absence of diamond packing in the crevice.....	A6
Figure A9. Photograph of 10-mil gap crevice with intact nickel membrane.....	A7
Figure A10. Photograph of 10-mil gap crevice with diamond packing.....	A7
Figure A11. Photograph of gouging in tube wall in the vicinity of the 10-mil gap crevice.....	A8
Figure A12. Crevice temperature variation with time in the 10-mil gap crevice packed with diamond powder for NaOH-02 test.....	A10
Figure A13. Crevice temperature variation with time in the 20-mil gap crevice packed with diamond powder for NaOH-02 test.....	A10
Figure A14. Cooling fan speed and resistance of lower and upper level sensors with time for NaOH-02 test.....	A11
Figure A15. Photo indicating repeated bubble generation and release at the crevice exit due to an SG SCC flow in the packed-crevice region for 10-mil gap.....	A12
Figure A16. Low-pressure bubble test of MB crevice flaw at 0.34 MPa (50 psi) showing bubbles at several sites along an \approx 10-mm (0.4-in.)-long axial SCC located in the bottom half of the crevice.....	A12
Figure A17. Crevice SCC flaw photographed using dye penetrant to enhance visualization. The flaw is longer than 18 mm (0.71 in.).....	A13
Figure A18. C-scan of MB tube MB1 using +Point probe at 300 kHz. Four axial ODSCCs are evident.....	A14
Figure A19. Eddy current profile for the primary axial ODSCC MB1-1.....	A15

Figure A20. Eddy current profile for the axial ODSCC MB1-2.....	A15
Figure A21. Eddy current profile for the axial ODSCC MB1-3.....	A16
Figure A22. Eddy current profile for the axial ODSCC MB1-4.....	A16
Figure A23. Photograph of crevice SCC OD flaw MB1-1 after leak testing at 8.3 MPa (1200 psi).....	A17
Figure A24. Photograph of crevice SCC OD flaw MB1-2 after leak testing at 8.3 MPa (1200 psi).....	A18
Figure A25. Photograph of crevice SCC OD flaw MB1-3 after leak testing at 8.3 MPa (1200 psi).....	A18
Figure A26. Photograph of MB crevice SCC OD flaw MB1-4 after leak testing at 8.3 MPa (1200 psi).A18	
Figure B1. Theoretically predicted conductivity as a function of Na concentration assuming that Na-to-Cl molar ratio is 0.7.....	B4
Figure B2. Na and Cl concentration variation estimated from bulk conductivity.....	B4
Figure B3. Normalized bulk concentration variation as a function of time at $\Delta T=40^{\circ}\text{F}$	B5
Figure B4. Normalized bulk concentration variation as a function of time at $\Delta T=60^{\circ}\text{F}$	B5
Figure B5. Normalized bulk concentration variation as a function of time at $\Delta T=80^{\circ}\text{F}$	B6
Figure B6. Time constant G_i variation as a function of ΔT	B6

This page is intentionally left blank.

Tables

Table 1.	Summary of earlier studies involving laboratory-scaled crevice experiments focused on the crevice chemistry measurement.	7
Table 2.	Physical properties of diamond and magnetite at room temperature and high temperature. ³⁴	24
Table 3.	Test matrix of MB tests with packed crevice conditions.....	27
Table 4.	Chemical compositions for the deposit formed in 10- and 20-mil gap crevices after the NaCl-03 and -04 tests determined by ICP/OES.	78
Table 5.	Summary of monitoring parameters and each corresponding time indicating leakage from primary to secondary side.....	101
Table 6.	Test conditions and dwell times for each test period of the NaCl-06 test.	123
Table 7.	Na and Cl concentration results for crevice samples and adjusted Fe and Ni concentrations in the same crevice samples.	140
Table A1.	Maximum +Point voltage, length, and estimated through-wall length for the four prominent axial ODSCC flaws in tube MB1.	A14

This page is intentionally left blank.

Executive Summary

One of the main tasks in the NRC-sponsored steam generator (SG) tube integrity program (TIP-3) was to evaluate models that predict potential degradation modes of SG tubes of pressurized water reactors (PWRs). One type of degradation that occurred in SG tubes involves impurity concentration in the narrow gap between SG tubes and supporting structures or sludge piles (“crevices”). An understanding of the chemistries in these crevices is needed for models to predict potential degradation modes of SG tubes. The chemistries vary depending on the solubility, volatility, and adsorptivity of impurities in bulk water. A thermodynamic equilibrium code, such as, MULTEQ[®] can predict solubility-limited cases, but in the presence of volatile species, the calculations show a wide pH variation. Therefore, volatility and adsorptivity effects of impurities have been experimentally evaluated. Earlier studies have examined the kinetics of impurity concentration and resultant crevice chemistry change in a packed crevice. However, the results are limited because the crevice pH was not monitored and prototypic thermal conditions in the crevice were not achieved in most cases. The objective of this study was to evaluate crevice chemistry evolution at a given bulk chemistry of varying Na-to-Cl molar ratio (MR) as a function of packing type with an appropriate pH sensor and a test configuration that provides prototypic thermal conditions. Since the chloride is the critical species most likely affected by volatility, this study mainly focused on the effects of chloride volatility.

A model boiler (MB) system has been developed to simulate prototypic thermal hydraulics and bulk chemistry conditions of the secondary side of SGs in PWRs. For the MB system, an instrumented crevice simulator has been developed and successfully operated. A tungsten/tungsten oxide electrode was used as a pH electrode in bulk water. The pH electrode potentials showed good linearity within the pH range of 4-8 under sodium chloride (NaCl) or sodium hydroxide (NaOH) water chemistry while the pH electrode in acidic crevices appeared relatively insensitive to pH change. Two packing materials were evaluated in this work: diamond and magnetite. Diamond packed crevices are easier to instrument, but diamond powder has very high thermal conductivity as compared with magnetite, which can enhance the boiling rate and lead to an overestimate of the impurity accumulation rate in the crevice. To simulate actual SG crevices, a magnetite-packed crevice having lower permeability is more appropriate than a diamond-packed crevice.

A tightly packed crevice with magnetite powder developed a radial chemistry gradient, consistent with earlier experimental work. The crevice chemistry tends to vary actively near the tube wall because the volatility effect of Cl becomes significant at the heated tube wall where boiling occurs. Initially, the crevice pH near the tube wall appears to be alkaline. But, as the impurity concentration progresses, the crevice pH becomes neutralized and even acidic because the reduced boiling rate near the tube wall caused by the development of Na-rich liquid film results in delayed preferential Cl concentration. Based on the test results, the chemistry variation in actual SG crevice deposits near the tube wall was projected. Unless some impurities remain and accumulate in the crevice after each fuel cycle, during a typical fuel cycle, the crevice chemistry would be in a transient rather than a steady-state condition mainly because of the low bulk impurity concentration. It is likely that the volatility effect of Cl in diamond-packed crevices becomes significant as the MR decreases from 1.0. Limited data are available for magnetite-packed crevices, but it is less likely that the volatility effect of Cl will be much influenced by bulk MR variation. Since our test results suggest that the transient behavior is more important in actual SG crevice deposits, the kinetic data for the crevice chemistry evolution with low bulk impurity concentration (~1 ppm) will be helpful for estimating actual SG crevice chemistry where the predictions of thermodynamic equilibrium codes have limited applicability.

This page is intentionally left blank.

Acknowledgments

The authors thank John Oras, Jeffrey Franklin, and Chuck Vulyak for their technical support to the experimental effort; and Ken Natesan and D. R. Diercks for their management and administrative support; Denise Moores for her administrative assistance. The authors also thank James Davis, Joseph Muscara, Todd Mintz, Eric Reichelt, Kenneth Karwoski, and Margaret Stambaugh for their NRC support and program management. The authors are grateful to Allen Baum for many helpful discussions; Al Mcilree of Electric Power Research Institute for providing alloy 690 TT tubing. This work is sponsored by the Office of Nuclear Regulatory Research, U.S. Nuclear Regulatory Commission, under Job Code Y6588; Program Manager: Margaret Stambaugh.

This page is intentionally left blank.

Acronyms and Abbreviations

BPE	Boiling Point Elevation
ECP	Electrochemical Potential
IC	Ion Chromatography
ICP/OES	Inductively Coupled Plasma/Optical Emission Spectroscopy
ID	Inner Diameter
IGA	Inter-Granular Attack
ISE	Ion Selective Electrode
MA	Mill Annealed
MB	Model Boiler
MR	Molar Ratio
NRC	Nuclear Regulatory Commission
OD	Outer Diameter
PWR	Pressurized Water Reactor
SCC	Stress Corrosion Cracking (or Crack)
SG	Steam Generator
SHE	Standard Hydrogen Electrode
SS	Stainless Steel
TC	Thermocouple
TSP	Tube Support Plate
TT	Thermally Treated

This page is intentionally left blank.

Symbols

A_i	Parameter defined in Eq. (B8)
a_{H^+}	Activity of hydrogen ion
c	Impurity concentration in crevice
c_i	Molar concentration of ion species in solution
c_o	Impurity concentration in bulk solution
c_o^o	Initial impurity concentration in bulk solution
D	Steam generator tube diameter
D_p	Particle diameter
E	Cell potential
E^o	Standard cell potential
e^-	Electron
F	Faraday's constant
G_i	Parameter defined in Eq. (B8)
H^+	Hydrogen ion
H_2O	Water
h_{fg}	Heat of vaporization
K_f	Parameter defined in Eq. (B2)
k	Permeability
L	Crevice depth
M	Metal
MO	Metal oxide
\dot{m}_i	Mass flow rate of liquid into the crevice
\dot{m}_o	Mass flow rate of liquid out of the crevice
q''	Heat flux from the tube surface in the crevice
R	Universal gas constant
T	Absolute temperature
u_i	Ionic mobility
V	Total volume in crevice
V_o	Total volume of bulk water
z_i	Charge on the species
α	Fraction of wetted length in the crevice
β'	Parameter defined in Eq. (B4)
ΔT	Primary-to-secondary saturation temperature difference
ε	Porosity in crevice
γ	Liquid-vapor distribution coefficient
Γ	Mass transfer coefficient for diffusion
κ	Conductivity of electrolyte
λ_i	Ionic molar conductivity

ρ	Density of matter
ρ_f	Density of liquid in crevice
ρ_0	Density of bulk water
τ	Tortuosity

This page is intentionally left blank.

1 Introduction

Argonne National Laboratory has participated in the Steam Generator Tube Integrity Program-3 (SG TIP-3) since 2002, which is sponsored by the U.S. Nuclear Regulatory Commission (NRC). Two of the main objectives of this program are to evaluate and experimentally validate models that predict potential degradation of steam generator (SG) tubes under normal plant operating conditions and to provide data for conducting operational assessments. The prediction models use various input data: temperature, stress distribution of SG tubes, material characteristics, chemical conditions surrounding tubes, etc. Although plant programs have been effective of managing the degradation, various corrosion phenomena have been observed in an SG of a pressurized water reactor (PWR).¹ Cracking, which is a main tube degradation phenomenon occurring in operating SG tubes, is difficult to predict mainly because these input data have too much uncertainty. Some corrosion and degradation phenomena of SG tubes involve high uncertainty for the chemical conditions.

In a locally constricted geometry on the outer-diameter (OD) side of SG tubing, trace impurities in the secondary water can concentrate to extreme pH values due to boiling. If a solution containing a solute impurity boils in a flow-restricted region, the steam phase may escape more easily from that region than any remaining liquid phase. As such boiling proceeds, the impurity concentration in the remaining liquid phase dramatically increases to a degree depending on the extent of the restriction. This impurity concentration process in a flow-restricted region is sometimes called “impurity hideout.” The impurity hideout raises the boiling point of the solution by lowering the vaporization pressure and can accompany an extreme chemical condition (strong caustic or acidic). This concentration process occurs mainly at three locations in SGs: the tube-to-tube support plate (TSP) crevice, the tube-to-tubesheet crevice, and the tube-to-sludge pile crevice on the top of the tubesheet. The narrow and tight gap between the SG tube and supporting structure or sludge piles is called a “crevice.” To distinguish it from other types of crevices, it is often called the “heated crevice” because inside the crevice water boiling occurs by heat transfer from the primary to secondary sides of SG tubes. At locations with concentrated solutions, OD stress corrosion cracking/intergranular attack (ODSCC/IGA) may then develop. ODSCC/IGA is one of the major tube degradation modes in SGs even though there is a gap in understanding the mechanism for the degradation mode. In heated crevices, the chemical conditions are not well understood due to the complexity of crevice concentration phenomenon, which increases the uncertainty of model predictions. To reduce this uncertainty and to mitigate ODSCC/IGA in the restricted area, research aimed at gaining a basic understanding of the concentration phenomena in heated crevices has been pursued for many years.

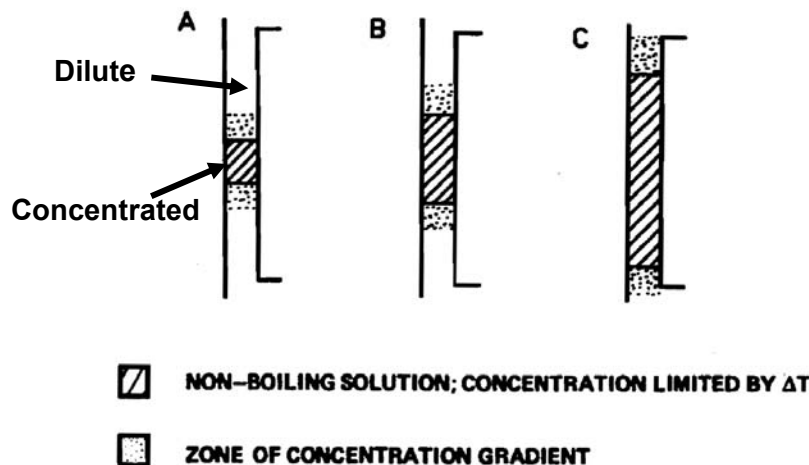
1.1 Model Development

To better understand the impurity hideout in heated crevices, two conceptual crevice models are discussed. Mann and Castle² proposed an impurity hideout model based on crevice experiments with NaCl bulk water chemistry. Figure 1 shows the Mann’s model of impurity hideout in a heated, loosely packed crevice. The authors proposed that impurities initially concentrate deep within the crevice (see Figure 1 A). Diffusion and convection of impurities is very slow, and continued boiling leads to a more concentrated solution (see Figure 1 B). As impurities continue to “hide out,” the boundary between the dilute and the concentrated solution approaches the mouth of the crevice (see Figure 1 C). At this stage, a small increase in the amount of the accumulated impurity leads to a rapid rise in the outward transport owing to diffusion and convection; eventually, equilibrium is established. Figure 2 shows the Mann’s impurity hideout model for a crevice tightly packed with corrosion product. Such a tightly packed crevice is likely to be blanketed in steam (see Figure 2 A). Since there is no liquid access to the steam-filled region, solute concentration will occur initially at the top and bottom of the steam blanket (see Figure 2

B). As impurities accumulate, concentrated solutions will penetrate into the steam-filled region by capillary attraction until the whole crevice is again full of concentrate (see Figure 2 C).

Mann's hideout model is appropriate to explain the concentration behavior of highly soluble chemicals like NaOH, but it is too simple to apply to the hideout process in operating PWR SG crevices. For example, it is difficult to apply this model to less soluble species, like phosphates or sulfates, which are present in the secondary water of SGs. Also, the model does not consider possible effects of volatile species like chlorides on crevice hideout. When boiling occurs, volatile species are distributed to steam and liquid phases so that the hideout in the liquid phase is less effective than non-volatile species, which is called "volatility effect." Chlorine anions form soluble HCl and this soluble HCl in the liquid phase should be in equilibrium with gaseous HCl in the steam phase. Therefore, as HCl is distributed more in the steam phase, the concentration of chlorine anion becomes lower. The adsorption of sulfates and chlorides to magnetite deposits also should be considered. In a tightly packed crevice, Mann's model considers only the axial chemical gradient, but the radial gradient needs to be considered to explain hideout behavior, which has been observed by Baum's experiments³ and Albertin et al.'s examination of the crevice section of pulled tubes.⁴ Albertin et al. found that in a TSP crevice the porosity was reduced immediately at the tube surface by the precipitation of bulk contaminants, and that such a low-porosity region forms in the corrosion layer associated with the TSP, leaving a central region with relatively high porosity.⁴

Baum and Evans⁵ proposed an impurity hideout model in a tightly packed crevice based on Baum's experimental work and the pulled-tube examination results. This model considered the volatility effect and the radial chemistry gradient that Mann's model did not consider. Figure 3 is a schematic of the model. The crevice solutions are formed by concentrating bulk contaminants as a result of boiling at the peripheral regions of the crevice. The concentration continues until the solution precipitates or volatilizes, or until boiling terminates because of an increased solution boiling temperature. Under the latter circumstances, the concentrated solution migrates deeper into the crevice by capillary action, into regions that would otherwise be dried out.



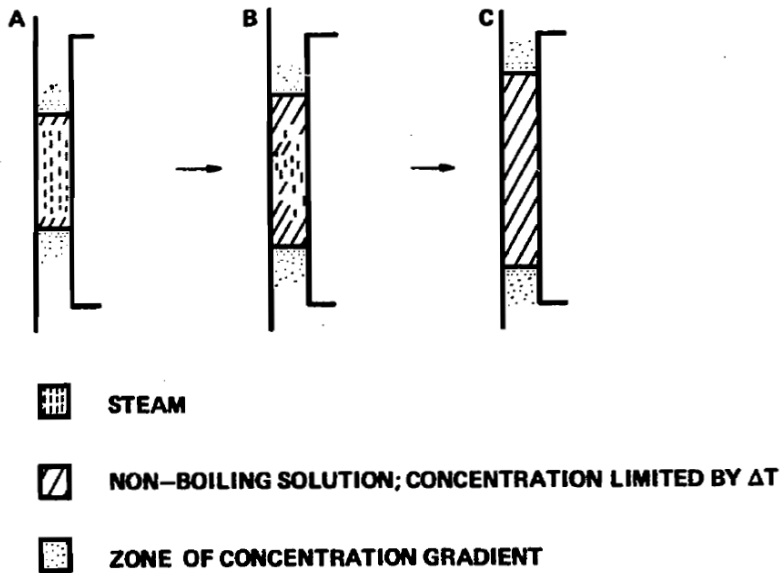


Figure 2.
Mann's model of impurity hideout
in a heated, highly packed crevice
(reprinted from Figure 4-4 of EPRI
Report NP-5015).²

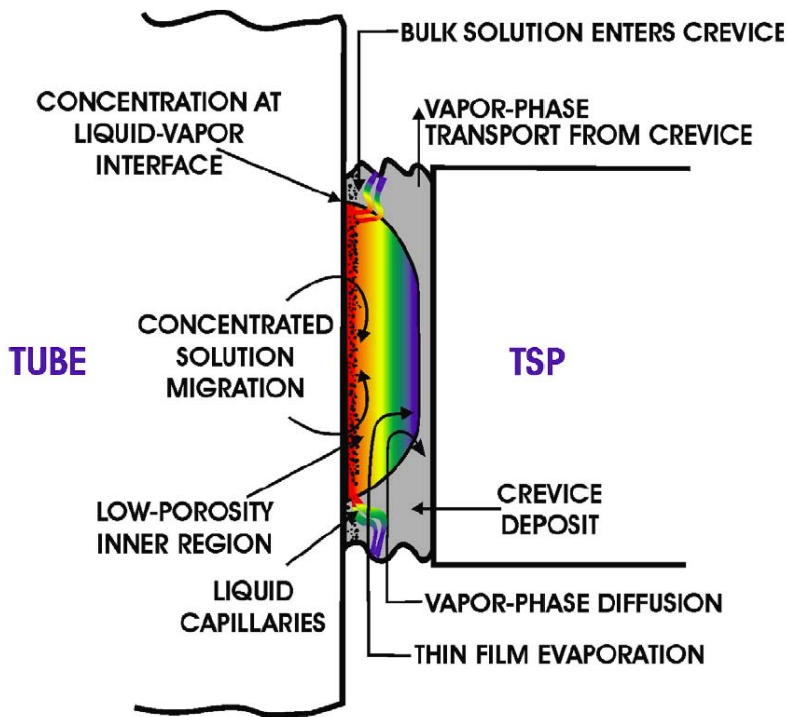


Figure 3.
Schematic showing crevice
solution transport processes.⁵

The concentrated solution near the tube wall plays an important role in tube degradation; therefore it is important to know the chemical conditions of the concentrated solution and its evolution over time. Hideout and crevice conditions depend on the solubility, volatility, and adsorptivity of bulk impurities. Thermodynamic equilibrium codes like MULTEQ[®] can predict solubility-limited cases, for example, the case that the impurity in the secondary water is only NaOH. In the presence of volatile species, however,

the calculation by thermodynamic equilibrium codes results in a wide pH variation because the extent of volatile species in the liquid phase depends on their concentration, the temperature, and the crevice deposit morphology. The current tools for predicting the crevice chemistry, using plant hideout return data as input, can only predict an average crevice pH. Furthermore, without a mass-balance model, the present thermodynamic equilibrium codes cannot handle adsorptivity effects. Therefore, to improve our understanding of crevice condition, the current tests would need to be updated to include the effects of both the volatility and adsorptivity of bulk impurities.

1.2 Literature Review

Much work has performed into crevice studies and they were reviewed in earlier literatures⁶⁻⁸. Some earlier work focused on thermal-hydraulic characteristics of unpacked and packed crevices and some of them evaluated chemical and electrochemical evolution. Numerical modeling including thermal-hydraulic, chemical, and electrochemical reactions has been developed. The key issues that have been pursued in earlier work but are not completely resolved yet are how much and how fast various impurities hideout can occur in packed crevices and how they determine the crevice chemistry like pH by interacting with each other and deposits.

1.2.1 Laboratory Heated Crevice Testing

Early studies into SG crevice effects were primarily focused on crevice thermal-hydraulic characteristics as reviewed by Baum⁶, while studies in recent years have focused on chemical and/or electrochemical evolution in crevices. Table 1 summarizes earlier work involving laboratory-scale crevice experiments focused on crevice chemistry.

Hermer et al.⁹ developed a technique to study electrochemical phenomena in crevices that simulate the TSP geometry in SGs. The electrochemical potential (ECP) was measured in a TSP crevice geometry with chemical conditions causing caustic SCC. The ECP of alloy 600 was measured versus Ag/AgCl (0.01 M KCl) reference electrodes and results indicated the formation of caustic crevice by Na hideout. Even though they tried to simulate an actual SG crevice by introducing simulated plant sludge, impurities studied in this work are limited; only Na effect was studied. Other species like chloride or sulfate should be considered to simulate actual SG crevice chemistries.

In electrochemical studies by Damien,¹⁰ electrochemical impedance spectroscopy and potential measurements were conducted in eccentric and concentric TSP crevices that were instrumented with platinum electrodes. The electrochemical impedance spectroscopy indicated the concentration of Na and boron but it appears difficult to correlate impedance spectroscopic results with actual impurity concentration. Since the crevice was not packed with magnetite or sludge, the application of test results are limited. In our work, the electrochemical impedance spectroscopy was not used due to the calibration difficulty.

Brennenstuhl et al.¹¹ evaluated the electrochemical noise monitoring technique in a refreshed autoclave system for corrosion monitoring in SGs. The system arrangement was designed to simulate a magnetite-fouled SG tube/tubesheet crevice. The results showed a change in the noise activity with change in operating chemistry. The sulfate and the chloride caused alloy 800 tube materials to be anodic relative to a 410 stainless steel (SS) tubesheet, for the entire depth of the crevice, while the caustic environment resulted in the tube becoming the cathode. Exposure to the sulfate environment appeared to cause the highest level of electrochemical noise. The electrochemical noise data, however, need to be carefully interpreted because bubble agitation and boiling affect the noise signal. If the electrochemical

noise signal can be distinguished from the non-electrochemical noise, this method should be a powerful method for investigating the materials degradation under a concentrated crevice environment. Due to the prematurity of the technique, the electrochemical noise monitoring was not used in our work.

Lumsden et al.^{12,13} constructed an experimental system to simulate SG thermal conditions. The system was designed such that *in situ* measurements could be made for the ECP of the tube crevice, the ECP of the free span, and the temperature profile in the crevice. The measurements were obtained for the average boiling point elevation in the crevice, the composition of the extracted crevice solutions, and the ECP of the alloy 600 tubes in the crevice and free span. After equilibrium was attained, the measured values agreed well with MULTEQ[®] predictions. The hideout kinetics data in this test also showed good agreement with the prediction by numerical modeling. Lumsden et al. determined the influence of the Na-to-Cl molar ratio (MR) on the ECP in the crevice for alloy 600, without a crevice pH electrode. The ECP of alloy 600 may give qualitative information on crevice pH, but an independent pH electrode, like a tungsten/tungsten oxide electrode, can monitor the crevice pH quantitatively. Only diamond powder was used as crevice packing materials in these tests. In our work, synthetic magnetite powder was used as packing materials, as well as diamond powder. The differences of two packing materials in terms of crevice hideout kinetics are experimentally shown and discussed in this report. They used an electric heater as a heating source instead of high-temperature water, which might cause non-prototypic thermal conditions inside the crevice. In our work, a test facility was designed to provide prototypic thermal conditions by introducing high-temperature water as a heating source.

Kawamura et al.¹⁴ estimated the NaOH and H₂SO₄ concentration factor in a TSP crevice by monitoring the ECP variation of alloy 600 tubes. The ECP data clearly showed the concentration of impurities and they were converted to actual concentration data by using a calibration curve. However, the crevice was unpacked and impurity hideout behavior in unpacked crevices can be completely different from that in magnetite-packed crevices, especially for sulfuric acid because of its adsorption effect.

Kawamura and Hirano¹⁵ estimated the sodium hydroxide concentration factor in a TSP crevice by using an *in situ* technique for high-temperature conductivity measurement. The concentration factor was about 2000 in the range of the heat flux that can establish a dry and wet condition. As reported in previous literature by the authors, the crevice was not packed with magnetite or sludge. Therefore, the application of this data is limited.

Baum^{3,16} measured the temperature, impedance, and pH in a magnetite-packed TSP crevice. The experiments showed large concentration gradients between the tube and TSP sides of the crevice. The tested crevice gap size of 0.6 mm was relatively wide compared with other literature. Therefore, similar experiments having a narrower gap crevice could provide additional insights. The experiment showed that strong bases concentrated more effectively on the tube wall than strong acids because of the volatility of Cl. The crevice pH on the tube wall, when exposed to sodium and chloride mixtures, increased with increasing superheat and decreasing bulk concentration. It was proposed that Cl tends to evaporate more easily on the tube wall at larger differences between the primary and secondary saturation temperatures, ΔT . Baum also showed that sulfates were adsorbed to the magnetite particles, so that the crevice impedance and pH data did not vary significantly as the test progressed. The volatility effect of Cl and the adsorptivity of sulfate were also examined in a magnetite-packed crevice by Balakrishnan and Strati.¹⁷

Bahn et al.¹⁸ measured the ECP in a tubesheet-type crevice packed with synthetic magnetite powder. They used a water loop with high flow rate as a heating source. Na concentration and resultant ECP variation with and without magnetite were compared. However, only NaOH was tested as an impurity and a pH electrode was not used.

Most of earlier studies measured the ECP of alloy 600 or Pt, but to determine the crevice pH, tungsten/tungsten oxide electrode style pH electrode was needed. Simulating prototypic thermal conditions is also an important factor, which was not achieved successfully in many cases of earlier work, for example, using an electric heater. In our work, a test facility is designed such that it provides prototypic thermal conditions in the crevice. As mentioned earlier, impurities hideout in packed crevice and their effect on the crevice chemistry are still not completely understood. Earlier work indicates that the bulk [Na]/[Cl] molar ratio may have an effect on the volatility and adsorptivity of Cl. Therefore, an examination of Na and Cl hideout behaviors in a magnetite-packed crevice by using a pH electrode under prototypic thermal conditions was conducted.

1.2.2 Crevice Numerical Modeling

A detailed model of the transport processes that produce concentrated solutions locally in PWR SGs was developed by Millett and Fenton.^{19,20} The model describes the heat, mass, and momentum transfer processes that occur in porous deposits such as those found in the TSP and the tubesheet crevices and in the sludge pile on the top of the tubesheet. This model was used to predict the total amount of NaCl in the crevice solution, and the model predictions have been compared to available experimental data by Mann and Castle². The model is in excellent agreement with experimental data obtained with carbon-fiber-packed crevices. However, with the given total impurity amount, this model cannot determine the crevice chemical conditions like electrochemical potential or pH because Millett's model is based on thermal-hydraulic relations and does not consider the chemical and electrochemical properties.

A new model for describing transport processes in PWR SG tube/TSP crevices has been developed by Engelhard et al.^{21,22} Based on Millett's model, this model includes the influence of convective transport, diffusion, and electromigration of species in the crevice on the evolution of crevice properties. Another localized electrochemical model has been developed by Fauchon.²³ The model considers a two-phase countercurrent flow of water and steam within a porous deposit, driven by capillary forces. Convection and diffusion processes are taken into account. Several homogeneous reactions are considered as well as electrochemical reactions. The model predicts that the crevice is initially steam blanketed and slowly becomes wetted as a concentrated liquid with a higher boiling point migrates into the steam-blanketed region. Engelhardt's and Fauchon's models consider a few chemical reactions and species, including Fe^{2+} , FeOH^+ , Na^+ , Cl^- , H^+ , and OH^- .

MULTEQ[®] is an interactive computer program that calculates the composition, pH, and electrochemical potential of an aqueous solution under a thermodynamic equilibrium at an elevated temperature and pressure.²⁴ MULTEQ[®] is primarily designed to be used by PWR plant chemists concerned about corrosion of SGs, but it also can be used for other applications. The code is designed to calculate the changing composition of a solution in a SG crevice or under corrosion product deposits as it undergoes concentration due to local boiling. MULTEQ[®] assumes that the liquid, vapor, and solid phases in the crevice are always in thermodynamic equilibrium. Since MULTEQ[®] is a thermodynamic equilibrium code, it cannot model realistic situations where steady state is established by two-phase flow balance or where a transient effect exists. By coupling MULTEQ[®] with thermal-hydraulic models and transient models, it could describe the evolution of crevice chemistry.

Table 1. Summary of earlier studies involving laboratory-scaled crevice experiments focused on the crevice chemistry measurement.

Author	Experiment	Pressure, MPa (psia)	Crevice Geometry	Packing	Heating Method	Control Method*
Hermer et al. ⁹	A600 ECP measurement by using 0.01 M KCl Ag/AgCl	5.5 (800)	TSP	Sludge packed	Flowing water	ΔT
Feron ¹⁰	Sodium & boric acid hideout with electrochemical impedance spectroscopy	6.4 (930)	TSP	Unpacked	Flowing water	ΔT
Brennenstuhl et al. ¹¹	Electrochemical noise measurement to monitor the effects of chemical excursions on the corrosion response of A800	5.5 (800)	Tubesheet	Magnetite packed	Electric heater	ΔT
Lumsden et al. ^{12,13}	NaOH & NaCl hideout studies with ECP & temperature measurement	6.4 (930)	TSP	Diamond packed	Electric heater	ΔT & q''
Kawamura et al. ¹⁴	NaOH & sulfuric acid hideout studies with ECP measurements	5.5 (800)	TSP	Unpacked	Electric heater	q''
Kawamura et al. ¹⁵	Na concentration factor measurement with high temperature conductivity cell	5.5-6.4 (800-930)	TSP	Unpacked	Flowing water	ΔT
Baum ^{3,16}	Crevice chemistry evaluation by measuring temperature, impedance, and pH difference	3.2 (468)	TSP	Magnetite packed	Flowing water	ΔT
Bahn et al. ¹⁸	NaOH hideout studies with ECP measurements	5.5 (800)	Tubesheet	Magnetite packed	Flowing water	ΔT

* ΔT means the temperature difference between primary and secondary sides are controlled, q'' means the heat flux from primary to secondary sides are controlled.

1.3 Objectives & Approach

One of the objectives of this study is to characterize the chemical conditions in a crevice for a given bulk chemistry of varying Na-to-Cl MR as a function of packing type with an appropriate pH sensor and a test configuration that provides prototypic SG thermal conditions. The generated information can then be used to evaluate the corrosion performance of SG tubing materials in isothermal autoclave-type tests and to improve modeling efforts on the degradation of SG tubes. The long-term goal is to provide the tools for quantifying volatility and adsorptivity effects on the crevice chemistry. This study focuses on the volatility effect of chloride. Of the chemical species judged to significantly affect the crevice chemistry, the chloride concentration is the most likely to be affected by volatility. The dependency of the volatility effect of Cl on the Na-to-Cl MR is also explored.

A model boiler (MB) system simulating a crevice under prototypic SG thermal conditions has been constructed for this study. The crevice is instrumented with thermocouples, ECP and pH electrodes, conductivity probes, and solution sampling lines. Bulk solution chemistry is monitored with the same instruments as used in the crevice. At first, an unpacked crevice test was performed as a reference. Then, diamond-packed crevices were tested under NaOH or NaCl bulk water chemistry. To simulate actual SG crevice conditions, magnetite-packed crevices were also tested under NaCl bulk water chemistry.

2 Experimental

2.1 Model Boiler

An MB system has been constructed at Argonne National Laboratory to simulate actual SG crevice conditions. It provides more prototypic conditions than those obtained in an isothermal autoclave or electrically heated crevice test system. The MB is designed to match prototypic conditions with regard to both the tube wall temperature and crevice heat flux. Design/operation information and shakedown test data for the MB system are presented in a previous NRC report.²⁵ The MB system is briefly described below.

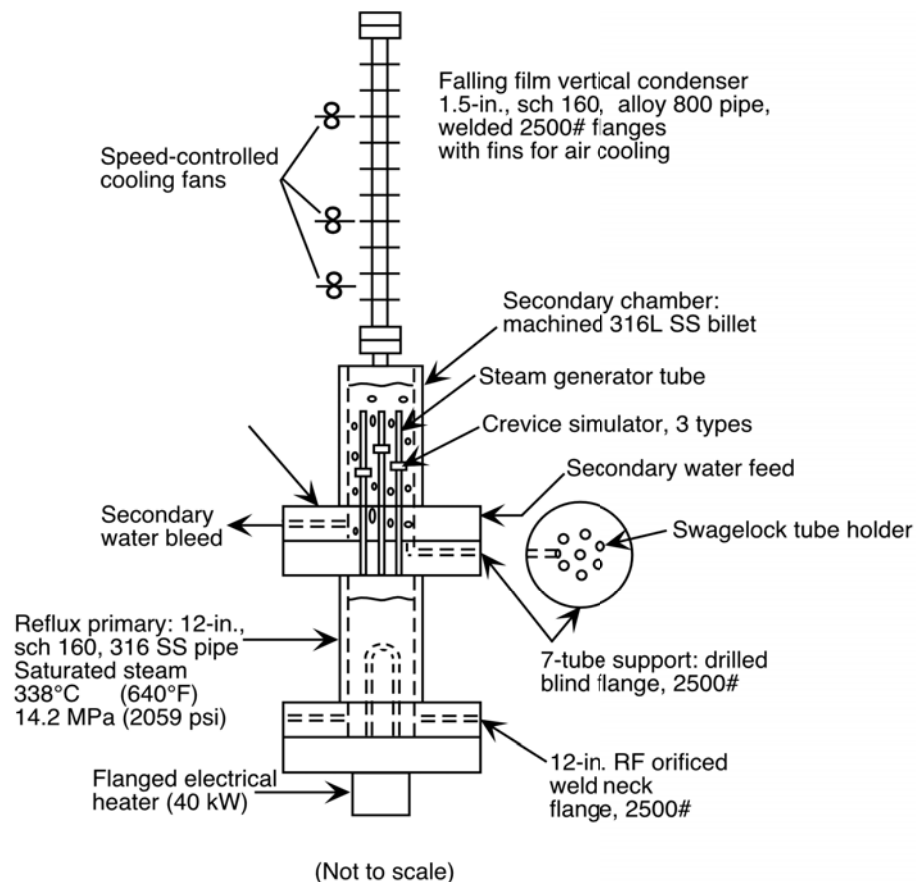


Figure 4.
Schematic of Argonne
model boiler system.²⁵

Figure 4 is a schematic of the MB system. The pressure vessel consists of a lower primary reflux boiler chamber, where steam is generated, and a secondary upper chamber, where boiling occurs on the outside of multiple SG tubes capped on the top and open on the bottom to the steam generated in the lower primary chamber. The MB design is simplified by introducing a static pressure vessel that is used for the secondary chamber as well as the primary chamber. The primary steam condenses on the inner walls of the tubes, creating a boundary condition of high heat flux. Primary electrical heaters (40 kW) are submerged in the primary water to provide prototypical heat fluxes. The outsides of the primary and secondary pressure vessels are surrounded by six zones of combined insulation blankets and trace electrical heaters. A thermocouple in the secondary water and a variable-speed drive fan are used to maintain the temperature and pressure on the secondary side by controlling heat rejection to the ambient air from a finned, fan-cooled steam condenser pipe. As safety features, a pressure-protection system that

uses a rupture disc is introduced in the primary and secondary chambers. The discharge lines of the rupture discs are connected to a collection tank. The MB system is surrounded by concrete protective barriers. A dedicated computer data acquisition system is used to control and monitor experimental parameters during the testing. Figure 5 shows the MB equipped with insulation and instrumentation. The discharge collection tank is located at the right side of the MB.



Figure 5.
Photograph showing the MB equipped with insulation and instrumentation and a discharge collection tank.

2.2 Secondary Water Control & Instrumentations

2.2.1 Water Chemistry Control

The Na-to-Cl molar ratio of the secondary test solution is controlled by mixing reagent-grade sodium chloride (NaCl) powders (Fisher Scientific, >99 % purity), concentrated hydrochloric acid (HCl) solution (Fisher Scientific, 37.4 wt%), and deionized water. In some tests, only sodium hydroxide (NaOH) powders (Fisher Scientific, 97.8 %) are used to prepare the secondary solution.

A high-pressure injector metering pump is used to control the secondary bulk water chemistry. Figure 6 shows a schematic of the injection system for the secondary bulk solution. A concentrated NaCl (or NaOH) solution is filled in a 304L SS 500-mL reservoir and deaerated with high purity Ar gas for 20-30 min before being connected to the injection line. A concentrated feed solution is delivered to the secondary chamber through a micro-bore injector tube (1/16-in. OD, 0.010-in. ID 316 SS) with the tip located at the middle of the chamber. Due to intense SG tube boiling, mixing of the secondary chamber bulk fluid is rapid and efficient. Two level sensors in the secondary chamber are used to ensure that the chamber fill level is maintained within the correct range during the pumping of new chemicals or sampling of the bulk solution. For safety, a check valve and a pressure relief valve are installed at the high pressure side of the injection pump. In addition, a manual isolation valve is installed on the injection line just before entering the MB in case the injector pump system malfunctions during a test and must be repaired. The system also has a pressure transducer for monitoring the delivery pressure and a flow meter for determining the rate of delivery. Figure 7 shows the injection pump system for controlling the bulk water chemistry in the secondary chamber. Figure 8 shows the MB high-pressure manifold access for the bulk solution feed/sampling lines in the secondary chamber, overpressure safety rupture disc, pressure transducer, and filling/drain line.

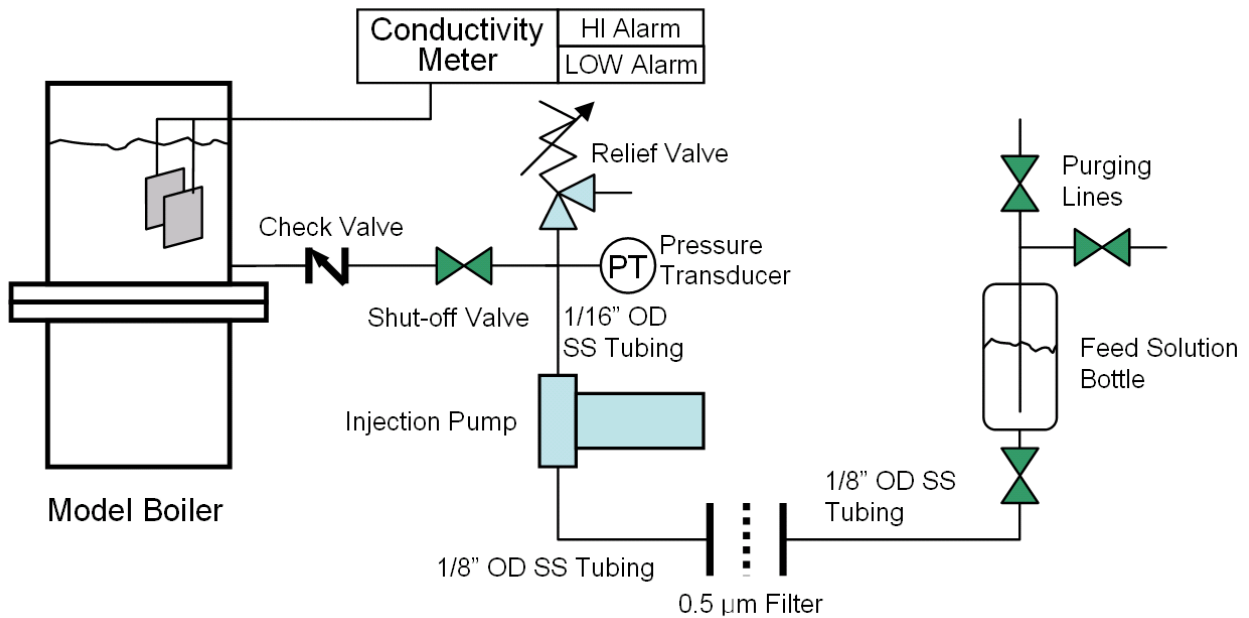


Figure 6. Schematic of injection pump system for secondary bulk solution.



Figure 7.
Photograph of the injection pump system for controlling/changing secondary bulk water chemistry (cart on right side).

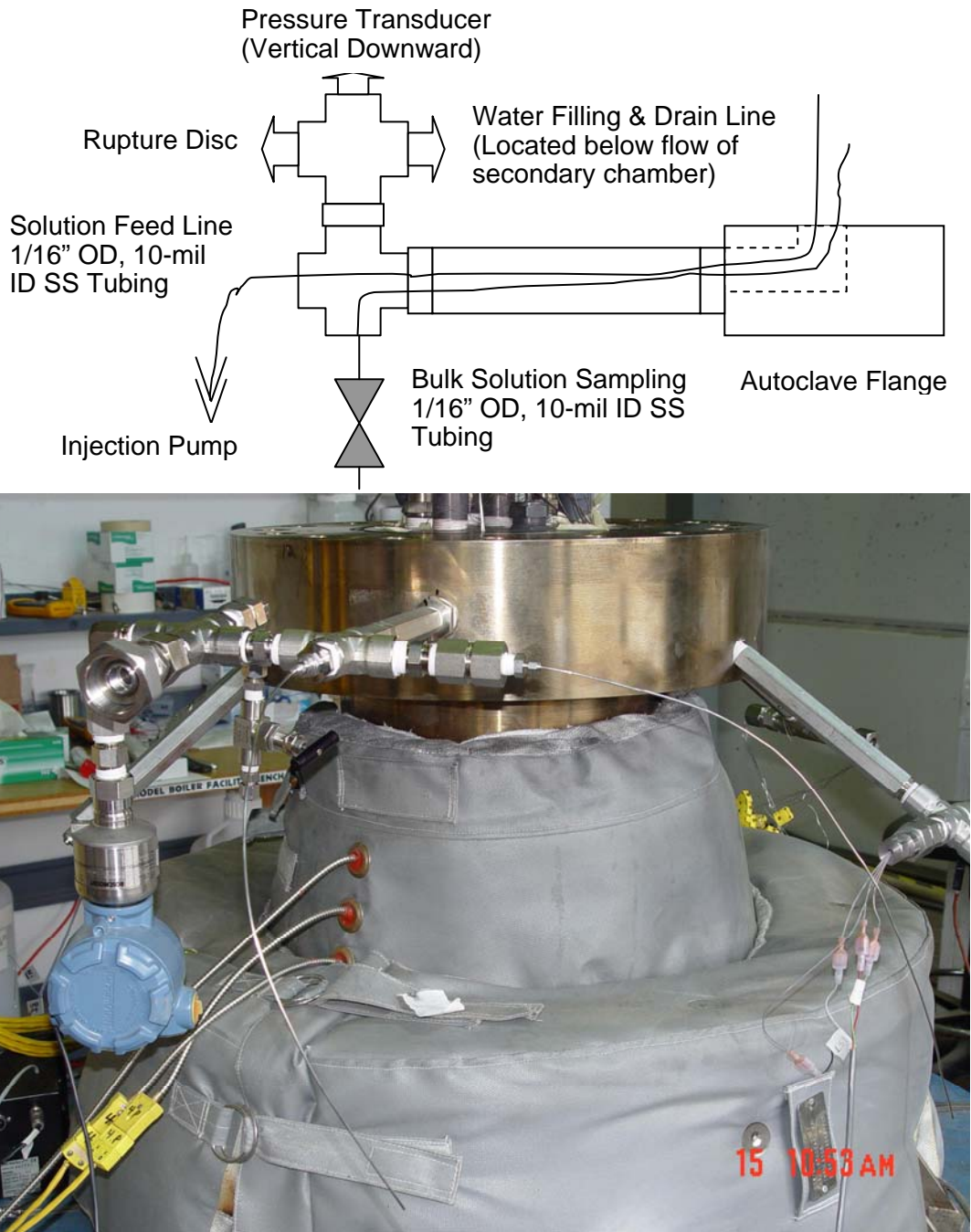


Figure 8. Photograph (bottom) and schematic (top) of the MB high-pressure manifold (upper left) access for secondary-chamber bulk-solution feed/sampling lines, overpressure safety rupture disc, pressure transducer, and filling/drain line.

2.2.2 Instrumentation

Figure 9 shows the MB internal components. To simulate SG tubes, six tubes with 7/8-in. OD are used for heat transfer, and crevice assemblies are mounted on two of them. Two on/off type level sensors are installed to monitor the secondary water level. During normal operation, the water level is located between lower and upper level sensors so that the lower one is always on and the upper one is off. If the lower level sensor indicates loss of water level, the only way to explain such loss of water level could be leaking of the secondary system. If the upper level sensor indicates high water level, that could be explained by a leak from the primary to secondary systems. Therefore, two water level sensors can also be used as a system leak indicator. To measure the bulk environment change *in situ*, various environmental parameters are monitored: temperature, ECP, pH, conductivity, and impurity concentration as determined by solution sampling.

Temperature

The secondary bulk water temperature is monitored with thermocouples located at different levels inside the secondary chamber to ensure temperature uniformity.

ECP, pH, and Conductivity

The thermodynamic stability of a metal or alloy in aqueous solution is primarily controlled by the ECP and pH of the solution. The thermodynamically stable phases of a certain metal or alloy are typically indicated on an ECP versus pH diagram. It is known that the SCC resistance of alloy 600 tubing in SGs depends on ECP and pH. In these tests, the ECPs of platinum (Pt), nickel (Ni), and alloy 600 are monitored with respect to an Ag/AgCl reference electrode. The solution pH can be monitored with various electrochemical tools. In these tests, metal-to-metal oxide electrodes are introduced. The general equation for the reduction of a metal having a charge valence number of 2, and at a certain temperature T, can be written as:



The electric cell potential of the reaction in Eq. (1), E is described by a form of the Nernst equation for the cell:²⁶

$$\begin{aligned} E &= E^o - \frac{RT}{2F} \ln \frac{a_M a_{\text{H}_2\text{O}}}{a_{\text{MO}} a_{\text{H}^+}^2} \\ &= E^o + \frac{RT}{F} \ln a_{\text{H}^+} \quad , \\ &= E^o - 2.303 \frac{RT}{F} \text{pH} \end{aligned} \quad (2)$$

where R , F , and a_{H^+} represent the universal gas constant, Faraday constant, and the activity of the hydrogen ion, respectively. Based on Eq. (2), the metal-to-metal oxide electrode potential is linearly proportional to pH at a given temperature. This relationship enables us to estimate crevice and bulk pH changes from the measured electrode potentials. The slope representing the dependency of the electrode potential on pH $-2.303RT/F$ is called the “Nernstian slope,” which is only dependent on temperature and is -106 mV/pH at 500°F.

Figure 10 shows the bulk ECP electrode assembly and the tip of a pressure-balanced external Ag/AgCl (0.01M KCl) reference electrode. Initially, the bulk ECP electrode assembly was composed of 20-mil (0.5-mm) diameter Pt (99.9 % purity), Ni (99.98 % purity), and two alloy 600 wires. For the later tests, tungsten (W, 0.5-mm dia, 99.95 % purity) and tantalum (Ta, 0.5-mm dia, 99.9+ % purity) wires replaced the two alloy 600 wires for monitoring the bulk pH. Figure 11 is a close-up photograph of the ECP electrode assembly and its electrode wires used for measurement of bulk water chemistry. All wires are covered with heat-shrinkable Teflon tubing for the electric insulation, except the tip length of 5 mm. Teflon is not expected to have creep issues at testing temperature of 260°C (500°F). Four Teflon-sheathed wires are assembled into a Teflon-sealed compression fitting. The Pt electrode provides oxidation/reduction potentials. The Ni and alloy 600 wires are used to measure their own ECP in the secondary test environment. The W and Ta wires are used to measure the bulk solution pH. A tungsten/tungsten oxide (W/WO_x) electrode has been studied and used as a pH electrode at room temperature^{27,28} and high temperature (up to 300°C).²⁹ The tungsten/tungsten oxide electrode showed a Nernstian pH response within the pH range of 2 to 11 at temperatures from 200 to 300°C.²⁹ Based on this reported high-temperature performance, the tungsten electrode was selected as a pH electrode. The tantalum/tantalum oxide (Ta/TaO_x) electrode was introduced as a pH electrode in later tests, but the W/WO_x electrode was used as a main pH sensor. Following earlier work²⁹, a 0.5-mm (20-mil) dia tungsten wire was oxidized in air with a propane torch for 1-2 min. The Ta/TaO_x electrode preparation procedures are the same as for the W/WO_x electrode. White Ta oxide film is formed easily on the Ta wire tip as soon as exposed to a propane torch. A relatively thick oxide layer is formed. By comparing the results of two electrodes, we are able to evaluate if there is any problem in the W/WO_x electrode itself. The design of the external pressure-balanced Ag/AgCl (0.01 M KCl) reference electrode is based on earlier work.^{30,31} The calibration curve of the reference electrode at high temperature is taken from the earlier experimental data of Macdonald et al.³⁰

Electrolytic solutions obey Ohm's law accurately once the effect of the electrolysis products is eliminated by using high-frequency alternating current.³² If direct current is applied continuously, two electrodes used for conductivity measurement become anode and cathode, respectively. Certain chemical products can be formed by oxidation and reduction reactions at each electrode surface which may affect the conductivity measurement (for example, hydrogen and oxygen for electrolysis of water). The conductivity of a solution can be composed of separate contributions from each ion; this is known as Kohlrausch's law of the independent migration of ions.³² The conductivity of a mixture of several electrolytes is

$$\kappa = \sum_i c_i \lambda_i, \quad (3)$$

where c_i is the molar concentration of each ion, and the ionic molar conductivity $\lambda_i = z_i F u_i$, in which F is Faraday's constant, and z_i and u_i are charge number and ionic mobility, respectively. The ionic mobility depends on temperature, ion concentration, and each ion characteristic. Therefore, as shown in Eq. (3), the solution conductivity is dependent on concentration, temperature, and ion species in the solution.

The secondary water conductivity is monitored with Pt parallel plates. The lead wires of two parallel plates are connected to a conductivity meter (MYLON L Company, Model #: 750II). The secondary fluid conductivity probe, which is mounted near the inner wall of the secondary chamber, is shown in Figure 12. Because of its greater surface area than exposed wires, the conductivity probe has a greater sensitivity in tracking changes in bulk water chemistry. The probe was explored as a means for tracking the movement of chemicals into and out of the bulk solution, as an indirect indicator of crevice

behavior. Comparing conductivity changes in the bulk and crevices allows one to monitor the movement of chemicals from the bulk solution to the crevices.

Solution Sampling

The bulk secondary fluid is sampled by use of a micro-bore tube (1/16-in. OD, 0.010-in. ID 316 SS) with the inlet positioned at the mid-fluid level in the secondary chamber, as shown in Figure 13. At the end of the sampling tube, a micro-control valve is adjusted to sample bulk solution. The volume of the bulk samples is typically about 1000 μL , which is much larger than the dead volume of the bulk-solution sampling line of about 90 μL . The impurity concentrations of the samples are analyzed by inductively coupled plasma/optical emission spectroscopy (ICP/OES) and ion chromatography (IC) for Na and Cl, respectively. If desired, the concentrations of Fe, Ni, and Cr can also be analyzed by ICP/OES. The chemical forms of impurities in samples might change during cooling. However, since ICP/OES analyze total concentration of each element regardless of chemical forms unless impurity forms significant precipitates, total concentration of each element should be conserved even after cooling. Some samples are additionally analyzed by a Na ion selective electrode (Accumet, Model #13-620-503) and a Cl ion selective electrode (Orion: Thermo Electron Corp., Model #9617BN).

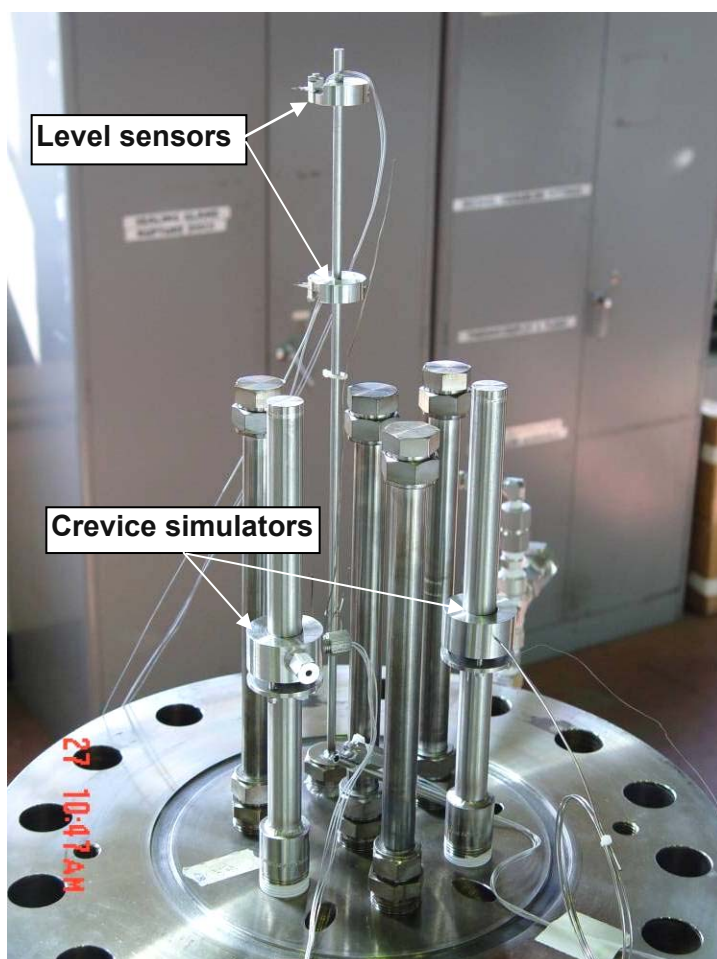


Figure 9.
Photograph of internal model boiler.

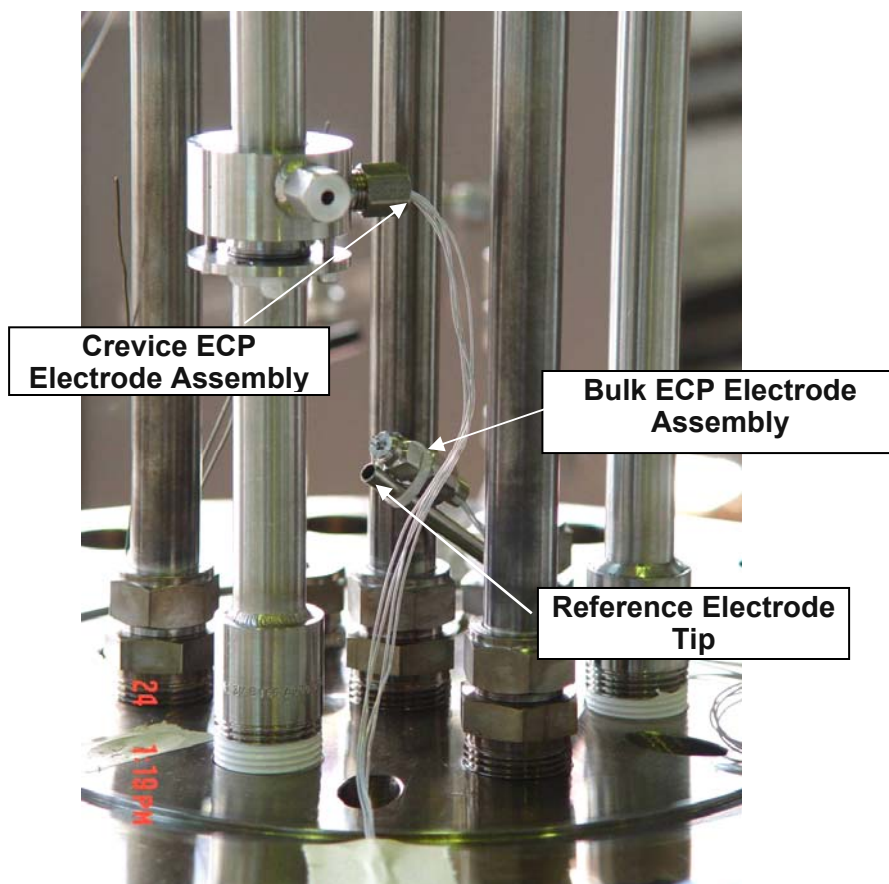


Figure 10. Photograph showing bulk ECP electrode assembly and the tip of the external pressure-balanced Ag/AgCl (0.01M KCl) reference electrode.



Figure 11. Close-up photograph of an ECP electrode assembly for bulk water chemistry measurement.



Figure 12.
Secondary chamber parallel-plate
fluid conductivity probe for
measuring changes in bulk water
chemistry of MB.

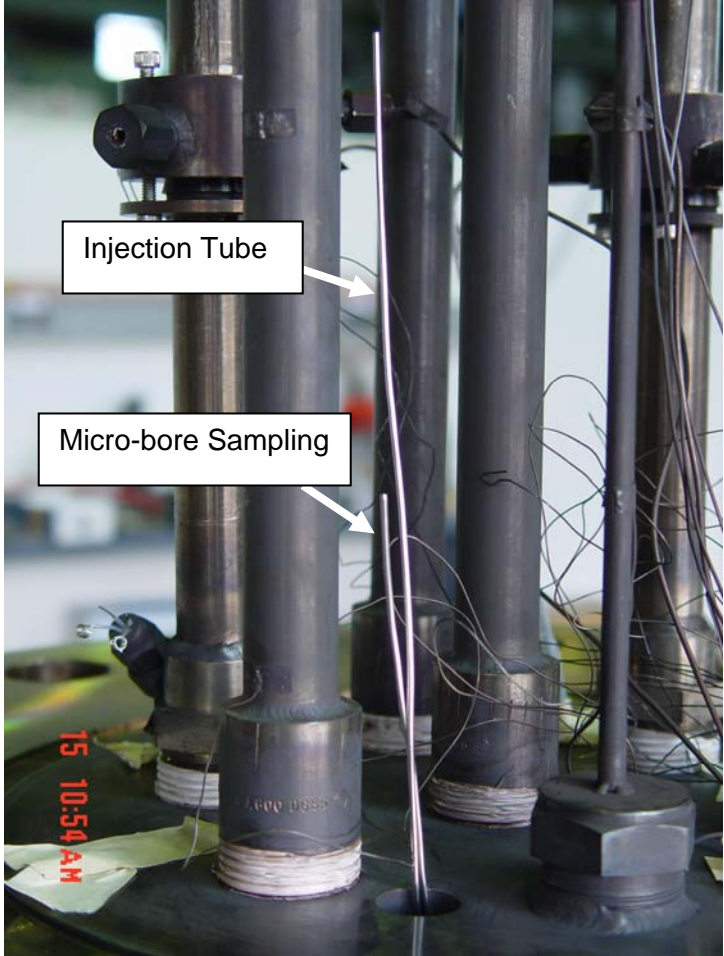


Figure 13.
Photograph of bulk secondary micro-bore
sampling (shorter 1/16-in. OD tubing at
center) and injection tube (longer 1/16-in.
OD tubing at center).

2.3 Crevice Simulator

2.3.1 Design

The MB has two crevice simulators with radial gaps of 0.25 and 0.51 mm (10 and 20 mil). The crevice is open on the top and closed on the bottom and is nominally 7/8-in. deep. Figure 14 shows a schematic of the crevice simulator design. A crevice ring is machined so that the crevice simulator has a radial gap size of 10 or 20 mil. The crevice ring is mounted on the SG tube by a 316 SS cone ring and a 316 SS back ferrule. The SS cone ring is used to seal the bottom of the crevice and hold the simulator on the tube. It resulted in occasional SCC of the SG tubing and, along with the packing, made it difficult to remove the crevice simulator from the tube. Hence, the SS cone ring was replaced with a Teflon seal cone ring to reduce SG tube stressing and facilitate crevice simulator removal, as shown in Figure 15. Because the Teflon is not as robust in holding the simulator on the tube as the 316 SS, especially at elevated temperatures, three narrow 316 SS straps were spot welded on the simulator and extended downward onto the SG tube and welded, as shown in Figure 15. The post-test investigation confirmed the water tightness of the Teflon cone ring.

A nickel foam mesh having 43 pores/cm (110 pores/in.) is located on the top of the crevice mouth to retain the diamond or magnetite powder filling the crevice. A cover plate is placed on the top of the nickel foam mesh and tightened to the crevice simulator by three screws. Inspection of the crevices upon completing acidic tests showed that the nickel foam had been badly corroded by the acidic environment having Na-to-Cl MR of less than one. After that, a Ni-Cr-Mo alloy foam mesh was introduced because it is more inert to acidic bulk water than Ni.

To ensure concentricity of the crevice ring mounted on the SG tubes, three wire shims equally spaced around the circumference are spot welded on the top of the crevice ring. Alloy 600 tubing (Sandvik Heat No. NX8527) was mill-annealed for 3 min at 940°C.³³ Since the carbon concentration in this tubing is 0.023-0.025 wt%, this tubing can be considered to have been mill-annealed at low temperature. Generally, low-temperature mill-annealed alloy 600 has less resistance to corrosion than thermally treated (TT) alloy 600. The alloy 600 SG tubes were replaced with 7/8-in. OD alloy 690 TT (Sumitomo Metal Industries, Heat No. D1A1801) because post-test investigations revealed that the alloy 600 tube surfaces were gouged and cracks were developed in the crevice region. Alloy 690 TT is usually known to be more corrosion resistant than mill-annealed alloy 600.

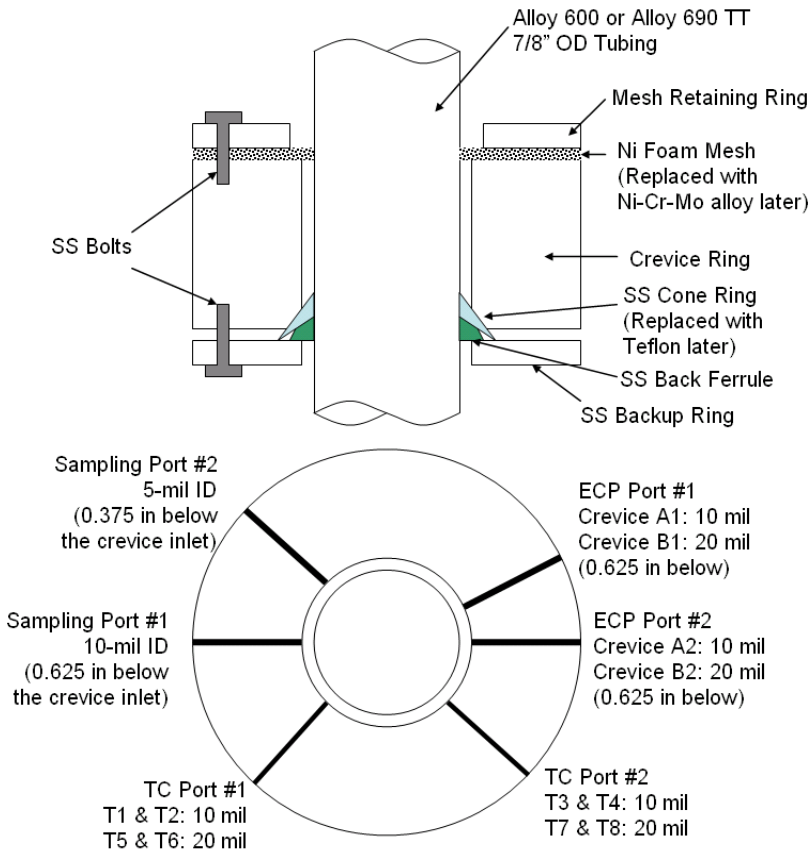


Figure 14. Schematic of crevice simulator design.

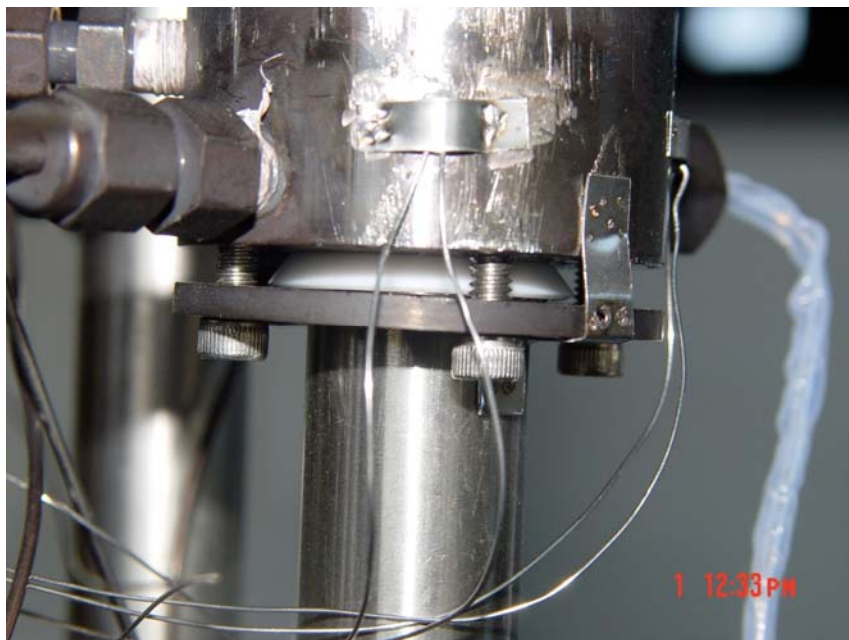


Figure 15. Close-up of 10-mil gap crevice showing new Teflon seal ring on bottom of crevice to reduce SG tube stressing and facilitate crevice removal.

2.3.2 Instrumentation

To measure the crevice environment change *in situ*, various environmental parameters are monitored: temperature, ECP, pH, conductivity, and impurity concentration as determined by solution sampling. Figure 16 shows the crevice simulator with various instrumentation ports. Figure 17 shows a fully assembled crevice simulator having two ECP electrode assemblies, thermocouples, and sampling lines.

Temperature

Each crevice simulator has four radial ports for crevice thermocouples, which are located at two circumferential locations, 90 degrees apart, as shown in Figure 16. The top and the bottom thermocouples are located 0.442-in. and 0.567-in. below the crevice inlet, respectively. The radial position of the thermocouples is adjusted to be at the mid-radial gap. As shown in Figure 16, thermocouples in the 10-mil gap crevice simulator are named T1, T2, T3, and T4. In the 20-mil gap crevice simulator, thermocouples located at the same positions as those of the 10-mil gap crevice simulator are named T5, T6, T7, and T8, respectively. However, since post-test examination revealed that crevice thermocouples have slipped during the test, high-pressure fittings were welded outside of the crevice ring, and the thermocouples were swaged and fixed by soft Teflon ferrules to prevent the thermocouple slippage. Only two thermocouples were installed through the radial holes in the crevice ring; T2 and T4 are located 0.57-in. below the crevice top opening. Due to the welded fittings, the radial holes for T1 and T3 were not available. In some tests, one more thermocouple was installed touching the tube wall labeled "TW." This thermocouple is not shown in Figure 14 but it is located at the opposite direction of 'TC port #1.' In later tests a 20-mil OD thermocouple sheathed with alloy 600 was introduced as the crevice electrode assembly to measure the electrode tip temperature.

The measured crevice solution temperature can be related to the concentration of impurities in the crevice if the identity of the impurities is known. The boiling point of a solution elevates as the concentration of impurities increases at constant pressure.⁶ If the solution is dilute in all solutes, the crevice impurity concentration is linearly proportional to the temperature difference between the measured and bulk saturation temperature, i.e. the boiling point elevation (BPE). The proportionality constant of each species depends on temperature and concentration. The BPE as a function of impurity concentrations can be predicted by MULTEQ.

ECP, pH, and Conductivity

Each crevice has two ECP ports, but in some tests only one ECP port is used. The ports are located at the same elevation in the crevice but are separated by 30 degrees. The ECP port is located 0.625-in. below the crevice inlet, which is the lowest level that facilitates the welding of a compression fitting. The crevice ECP electrode assembly is composed of four 20-mil dia wires. Initially, like the bulk ECP electrode assembly, Pt, Ni, and alloy 600 wires are used, but later W and Ta wires replaced alloy 600 wires as pH electrodes. Like the bulk ECP electrode assembly, all wires are covered with heat-shrinkable Teflon tubing for electric insulation, except the tip length of 1-2 mm. Four Teflon-sheathed wires are assembled into a Teflon-sealed compression fitting. The preparation procedures for W/WO_x and Ta/TaO_x electrodes are the same as those of the bulk ECP electrode assembly, described in Section 2.2.2. For ECP measurements, an electrochemical interface system (Solartron 1287) and a multiplexer with 8 channels (Solartron 1281) are used. Platinum and alloy 600 wires are connected to a crevice conductivity meter (MYLON L Company, Model #750 II). In some tests, two alloy 600 wires are used as the crevice

conductivity probes. As discussed before, one alloy 600-sheathed thermocouple is installed in a crevice ECP electrode assembly, which is used to act as an alloy 600 electrode.

Sampling

There are two sampling lines for the crevice solution: 5- and 10-mil inner dia (ID) 316 SS tubes. The two sampling lines are located 0.375- and 0.625-in. below the crevice inlet, respectively. In most tests, the 10-mil dia sampling line was used for the crevice solution extraction because the 5-mil dia sampling line was clogged. Both crevices have the micro-bore solution extraction lines with a micro-bleed valve used to meter the samples on a two- or three-drop basis, which is roughly varied at 40-90 μL . The crevice sampling frequency is varied over time. In earlier tests, the crevice solution was extracted once or twice a day for analysis. However, after crevice sample analysis showed a time-delay effect due to the dead volume of the sampling lines, the crevice samples were taken only before changing the temperature. Since the dead volume of the solution sampling line, 90 μL , is comparable to the crevice sample's volume, a crevice sample taken at a certain time does not really represent the actual crevice chemistry at the sampling time. Instead, it represents the crevice chemistry at the previous sampling time. Crevice sample analysis should be analyzed considering this time-delay effect.

The samples were analyzed by ICP/OES and IC for Na and Cl concentrations, respectively. Like bulk samples, Fe, Ni, and Cr concentrations were also analyzed, if desired, by ICP/OES. To prevent the diamond or magnetite powders from plugging the entrances of the sampling tubes, an SS porous frit disc is mounted on the entrance of each of the sampling tubes, as shown in Figure 18.

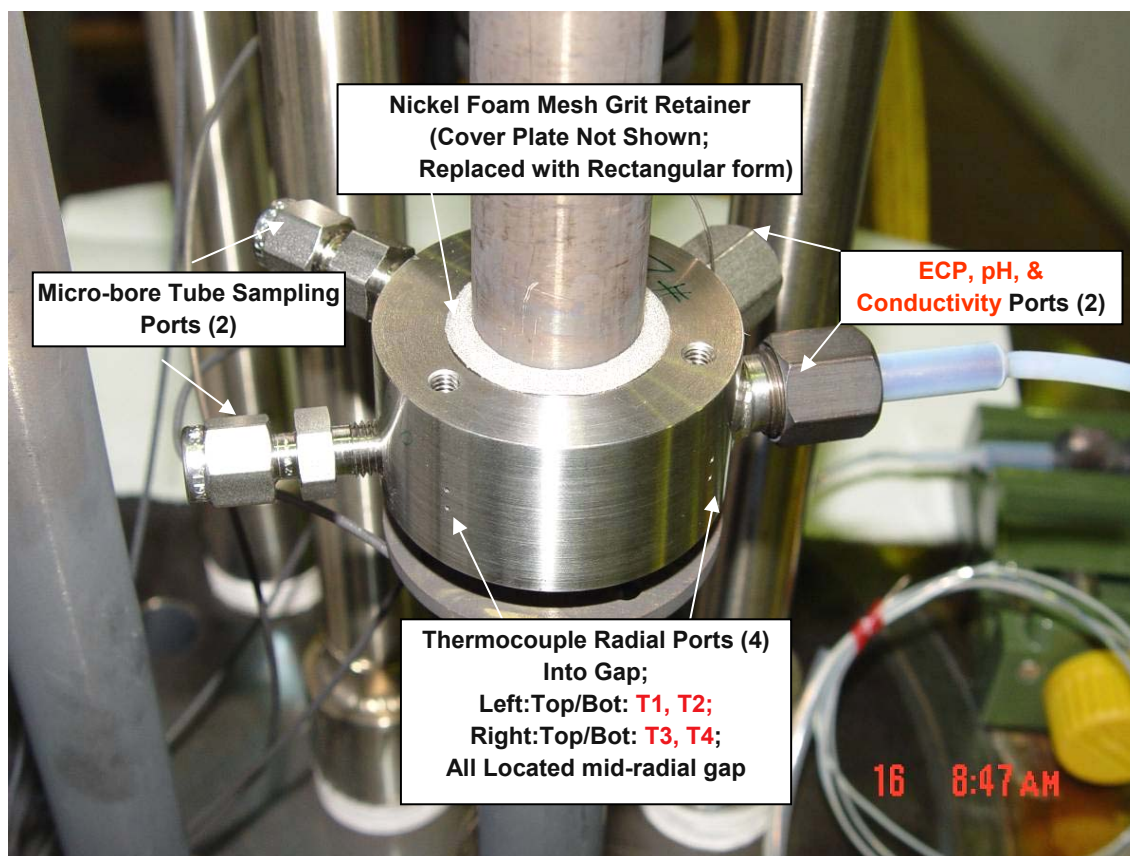


Figure 16. Photograph of 10-mil gap crevice simulator showing various instrumentation ports.



Figure 17. Assembled diamond-packed crevice with 0.010-in. radial gap. Photograph shows two ECP electrode probes (right), four installed mid-crevice gap thermocouples, and Ni-Cr-Mo alloy porous foam mesh for retaining packing.

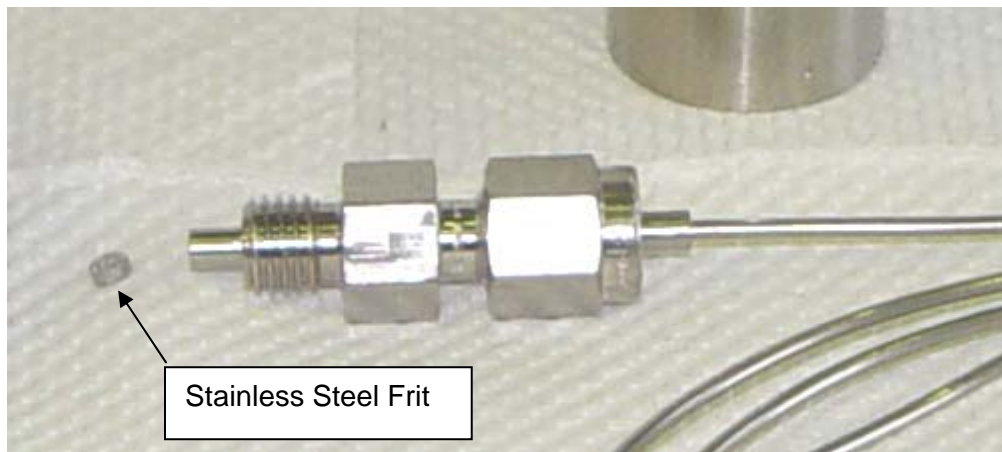


Figure 18. Micro-bore crevice sampling tube assembly and SS frit used to prevent plugging of the tube.

2.3.3 Packing Materials

As packing materials, synthetic diamond powders are introduced first. Diamond is known to be chemically inert even at acidic or caustic environments, and this means diamond itself will not react with the crevice chemistry. Since the effect of packing materials on the crevice chemistry can be excluded, chemically inert diamond is a convenient packing material. However, since magnetite is known as the main deposit in actual SG crevices of nuclear power plants, magnetite powders are also used in later tests. Table 2 shows the thermal conductivity and density of diamond and magnetite. As compared with magnetite, diamond has around 600 times higher thermal conductivity at room temperature, which may drastically change the heat transfer characteristics in a packed crevice. The test results with diamond powder should be carefully evaluated by considering the higher thermal conductivity of diamond compared with magnetite.

Table 2. Physical properties of diamond and magnetite at room temperature and high temperature.³⁴

Properties	Diamond		Magnetite	
	27 °C	127 °C	Room Temp.	260 °C (500 °F)
Thermal Conductivity (W/m-K)	2320 (IIA)	1540 (IIA)	3.8 ³⁵	3.5 ³⁵
Density (10 ³ kg/m ³)	3.51	-	5.17	-

Some crevices were packed with diamond grit ranging in size from 127 to 165 μm (Diamond Innovations, Model #MBG-660). To increase packing density, two sizes of diamond powders were used: 127-165 μm and 75-97 μm . However, no significant change in packing density was observed. Packing density which is inversely related to porosity for each crevice was estimated from the weight of the diamond powder used and the estimated total crevice volume. The highest packing density possible for filling space by stacking equal-sized hard spheres is 74 % regardless of the diameter of the sphere.³⁶ The measured values were close to the ideal packing density, considering that the diamond powders are non-spherical and vary in size. In one test, the crevice porosity was significantly lower than other tests. The post-test investigation revealed that one idle ECP port had not been completely plugged, and this condition created an unexpected crevice volume. In some tests, the crevices were packed with magnetite (Fe_3O_4) powder (Alfa Aesar, 99.997 % purity). Even though fine magnetite particles were used as packing materials and were expected to provide tight packing, the measured packing porosity was very high in the first use. In the next magnetite-packed crevice test, a highly packed crevice was achieved by pushing down powders with a thin metal plate shim. The magnetite is not inert to the hideout chemicals like diamond. It can become involved in chemical reactions, but this represents more realistic crevice environments than diamond-packed crevices. Figure 19 shows the top of a crevice ring packed with diamond powder. It also shows three equally spaced wire shims, the micro-bore sampling tubes, the thermocouples, and the ECP electrode assembly port. Figure 20 shows the top of a crevice ring packed with magnetite powders. The introduction of magnetite allows an initial assessment of the influence of the two types of packing on hideout.

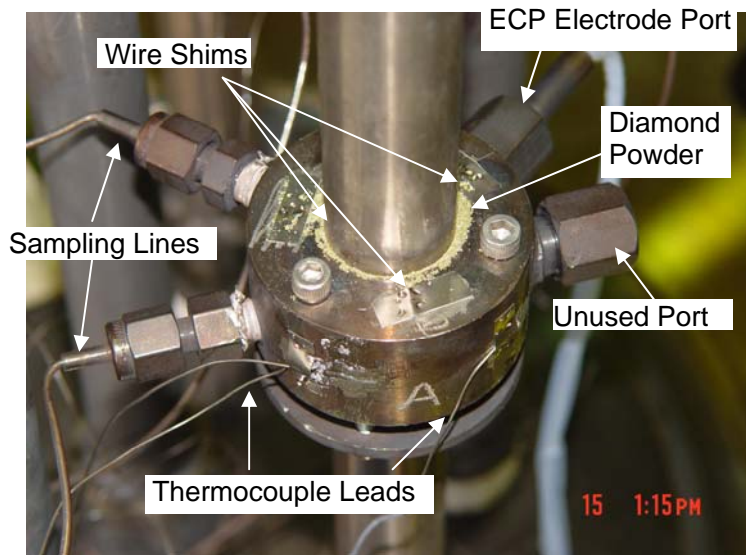


Figure 19. Photograph of crevice A (0.010-in. radial gap) showing diamond grit packing, three equally spaced wire shims, two micro-bore sampling lines, ECP electrodes connections, thermocouple leads, and an unused crevice port (right).



Figure 20.
Photograph of crevice B (0.020-in. radial gap) showing magnetite packing and equally spaced wire shims.

2.4 Test Procedures

The secondary chamber was closed and cleaned by flushing it with pure water several times until the effluent had conductivity $< 1 \mu\text{S}/\text{cm}$. Then, the secondary chamber was loaded with 39 lb (17.7 L at room temperature) of high purity water and began heat-up to the desired initial primary/secondary test temperatures, for example, 282/260°C (540/500°F). During the heat-up, when the MB primary and secondary chambers reached 149°C (300°F), non-condensables were purged from each chamber by venting steam. The heating was then continued to the desired temperatures. Between test inspections we discovered that the SG tube initially built with a Swagelok fitting on its upper end for filling the primary heater chamber and also for purging non-condensable gases during test startup would not seal tightly. This SG tube was replaced with a tube having a welded cap into which was welded a high-pressure SS tube for bleeding gases from the primary chamber. The bleed tube exits from the pressure vessel for purging primary non-condensable gases during the start of a test without having to open the secondary chamber. Figure 21 shows the primary chamber bleed line and valve exiting from the pressure vessel. Figure 21 also shows two high-pressure fitting ports used for two crevice ECP electrode assemblies. This arrangement has greatly facilitated the bleed/gas-purge operation and also allows monitoring of the purging process of the non-condensable gases in the primary-side water. The valve on the bleed line was opened with the primary chamber heated to 149°C (300°F). The flow rate through the bleed line was slow and steam was cooled easily to the ambient temperature so that no steam reached the tube at the exit. Thus only water or air exited the tube. At the early stages of non-condensable gas purge from the primary chamber with the tube immersed in a beaker of water, mainly air bubbles purged. Later in the purge no air bubbles were evident, and the purging was complete.

The temperature of the MB secondary chamber for all tests was kept at 260°C (500°F), while the primary-side temperature was varied from 282°C (540°F) to 327°C (620°F). In earlier tests, the primary-to-secondary temperature difference, ΔT was 100 or 120°F but in later tests, three ΔT conditions (40, 60, and 80°F) were used. For each test, reference data were generated for the primary/secondary temperatures of 540/500°F with only high purity water in the secondary chamber. The generated reference data allowed us to compare crevice thermal distributions for the case of no hideout with that for hideout after a chemical was added, as well as for a packed and unpacked crevice. After achieving steady state and obtaining the pure water data, we injected a solution with impurities into the secondary chamber using a

high-pressure metering pump. Changes in crevice temperatures and secondary bulk and crevice chemistry conditions were tracked by ECP electrodes and micro-bore sampling lines as hideout occurred. In earlier tests where the high-pressure metering pump was not used, a chemically adjusted secondary test solution was injected by a pump before heat-up. For each test we allowed several days for the crevices and bulk solution to adjust and allowed hideout to develop in response to the temperature or chemical changes. Sometimes, after crevice and bulk thermal and chemical stability were achieved, the solution on the secondary side was altered to match the initial test conditions and assess its influence on crevice behavior.



Figure 21.
Primary chamber bleed line and valve which exits the pressure vessel and purges primary non-condensable gases.

2.5 Test Matrix

In the initial crevice tests, reference data were obtained for unpacked conditions with NaOH bulk water chemistry. Then, packed crevice tests were conducted. Table 3 shows the test matrix of the MB tests with packed crevices, which is listed chronologically. Each test has its own ID, as shown in Table 3. For simplicity of the bulk water chemistry, NaOH solution was introduced first (NaOH-01 and NaOH-02). Two diamond-packed crevices were installed and tested simultaneously. The NaOH tests were followed by the tests with NaCl bulk water chemistry having an MR of 1.0 (NaCl-01 and NaCl-02). To evaluate the effect of MR on the crevice hideout behavior, the bulk solution's MR was changed from 1.0 to 0.3 (NaCl-03) and then 0.7 (NaCl-04). Packing materials were not changed between the NaCl-03 and the NaCl-04 but the secondary system was flushed with high purity water. When lowering the bulk MR, the larger gap crevice was packed with magnetite powders. The pH electrodes at the crevice and bulk and a crevice conductivity probe were introduced from the NaCl-03 test. The crevice hideout tests with two crevices provided a large amount of data in a short time, but it was difficult to analyze the partition of the bulk impurity hideouts between each crevice. Therefore, to simplify the test conditions and maximize the use of bulk solution data for the evaluation of crevice chemistry, a single crevice was introduced instead of double crevices. Another NaOH test, NaOH-03, was conducted before the single-crevice tests with NaCl bulk water chemistry (NaCl-05 and NaCl-06) in order to confirm the functionality of the crevice instrumentation under relatively simple bulk water chemistry. Then, the effect of packing materials on the

crevice hideout was explored in NaCl-05 and -06 tests. As shown in Table 3, for each crevice test, ΔT stays constant or varies stepwise. The minimum and the maximum ΔT are 40°F and 120°F, respectively. The actual ΔT at normal operating SG conditions is plant-specific but would be close to 60°F.

Table 3. Test matrix of MB tests with packed crevice conditions.

Test ID	Bulk Water Chemistry	ΔT Variation (°F)	Measuring Parameters	Crevice A (10-mil)		Crevice B (20-mil)	
				Packing Materials	Porosity	Packing Materials	Porosity
NaOH-01	20 ppm NaOH	100	Sampling, Temperature	Diamond	30 %	Diamond	30 %
NaOH-02	20 ppm NaOH	100	Sampling, Temperature	Diamond	40 %	Diamond	29 %
NaCl-01	10 ppm Cl (MR=1.0)	100→120	Sampling, Temperature, Bulk Conductivity	Diamond	3 % ^{a)}	Diamond	32 %
NaCl-02 ^{b)}	10 ppm Cl (MR=1.0)	100 →60 →80 →40	Sampling, Temperature, Bulk Conductivity, ECP	Diamond	3 % ^{a)}	Diamond	32 %
NaCl-03	10 ppm Cl (MR=0.3)	40 →60 →80 →40	Sampling, Temperature, Bulk & Crevice Conductivity, ECP, pH	Diamond	33 %	Magnetite	78 %
NaCl-04 ^{c)}	10 ppm Cl (MR=0.7)	40 →60 →80 →60 →40	Sampling, Temperature, Bulk & Crevice Conductivity, ECP, pH	Diamond	33 %	Magnetite	78 %
NaOH-03	20 ppm NaOH	40 →60 → 100	Sampling, Temperature, Bulk & Crevice Conductivity, ECP, pH	Diamond	35 %	Open	100 %
NaCl-05	10 ppm Cl (MR=0.7)	40 →60 →80 →50 →40	Sampling, Temperature, Bulk & Crevice Conductivity, ECP, pH	Diamond	40 %	Crevice Ring Removed	N/A
NaCl-06	10 ppm Cl (MR=0.7)	40 →60 →80	Sampling, Temperature, Bulk & Crevice Conductivity, ECP, pH	Magnetite	54 %	Crevice Ring Removed	N/A

a) Since one idle electrode port was not completely plugged, actual crevice porosity should be higher than this value.

b) This test was continued after NaCl-01 without opening the MB.

c) This test was continued after NaCl-03 without opening the MB.

This page is intentionally left blank.

3. Preliminary Crevice Tests

3.1 Unpacked Crevice Tests

Unpacked crevice hideout tests were conducted as a reference. The tests were performed on three unpacked crevice simulators having a closed bottom and open top and drilled symmetric holes and having 0.25-, 0.38- and 0.51-mm (0.010-, 0.015-, and 0.020-in.) radial gaps. In later tests the crevice having a 0.38-mm radial gap was not used any more. The primary bulk temperature was 316°C (600°F) but, in one test, it was increased to 329°C (625°F) to examine the effect of the primary-to-secondary temperature difference. The secondary bulk temperature was maintained at 260°C (500°F). The depth of the crevices was nominally 21.6 mm (0.85 in.). The secondary chamber was filled with 11.5 ppm Na solution (20 ppm as NaOH) having a conductivity of 113.8 $\mu\text{S}/\text{cm}$ at 22.1°C (71.8°F).

Crevice hideout was determined from samples drawn periodically by using micro-bore sampling tubes. The micro-bore-extracted fluid samples from the crevices were analyzed by ICP/OES. Concentration factors are plotted as a function of time in Figures 22 and 23 for most of the tests. The concentration factor was defined by the crevice-to-bulk Na concentration ratio. The hideout concentration for these crevices varies with time, gap size, and ΔT , and the maximum concentration factor was around 30. The largest concentration occurred for the smallest radial gap crevice of 0.25 mm (0.010 in.) in a test with $\Delta T=56^\circ\text{C}$ (100°F). This test was repeated as a check on experimental reproducibility, and similar concentration behavior was obtained, as shown in Figures 22 and 23. When the smallest gap crevice was tested under $\Delta T=69^\circ\text{C}$ (125°F), the concentration factor was only 3. The maximum concentration factors were 3.6 and 7 for the 0.5- and 0.38-mm (0.020- and 0.015-in.) radial gap crevices under the 56°C (100°F) temperature difference, respectively. For all tests, a steady-state crevice concentration buildup was reached within 2-3 days. The smallest gap crevice of 0.25 mm (0.010 in.) exhibited the highest concentration, which is compatible with greater flow resistance in the smaller crevice gap that retards the boiling-induced expulsion and ingress of fluid. For some crevice gaps smaller than the current tested sizes, the flow resistance to boiling-induced fluid expulsion out of the crevice and ingress of bulk refreshing liquid will increase to a level that is conducive to higher hideout.

The crevice thermocouples for these tests showed no increase of superheat in the crevice. The crevice temperature elevation from the secondary bulk temperature of 260°C (500°F) was within 0.28°C (0.5°F), which suggests no significant Na hideout in the crevice. This observation is also supported by the very low Na concentration observed in the crevice samples. No significant large-amplitude oscillations in crevice temperature were detected. These observations imply that, for the range of geometries and thermal conditions tested, the crevices do not undergo intermittent periods of steam blanketing that would cause transient hot spots. Thus, for these unpacked crevices, the mixing between crevice and bulk appears to be so active that significant hideout does not occur, and the hideout is kinetically limited. The boiling occurring in the crevices, which creates an expulsion and ingress of fresh bulk fluid, is robust enough to limit hideout. The 0.25-mm (10-mil) gap crevice also shows that merely increasing ΔT , in this case from 56 to 69°C (100 to 125°F), does not necessarily increase hideout. Our data showed the concentration factor to be reduced from 30 to 3. The liquid penetration depth, i.e., how deep the liquid phase can penetrate into a heated crevice, decreases with the increase of heat flux or ΔT . Because of higher ΔT and resultant shorter liquid penetration depth, the area around the sampling line in the crevice became a steam-dominant region. The sampling solution picked up more steam rather than concentrated liquid. If crevices are not filled with deposits and the gap size is larger than 0.25-mm (10 mil), the impurity hideout in the crevice can be limited. However, in actual SGs, crevices tend to be packed with magnetite and less

soluble precipitates, except for new SGs. Crevice hideout studies with packed crevices will permit evaluating and estimating the actual crevice conditions in SGs.

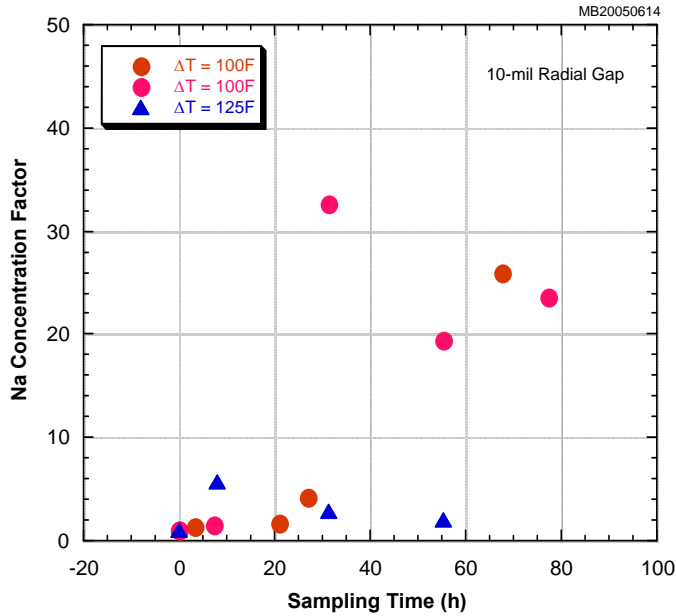


Figure 22. Concentration factors vs. time for 0.25-mm (0.010-in.) radial gap unpacked crevice and primary-to-secondary temperature differences of 56°C and 69°C (100°F and 125°F).

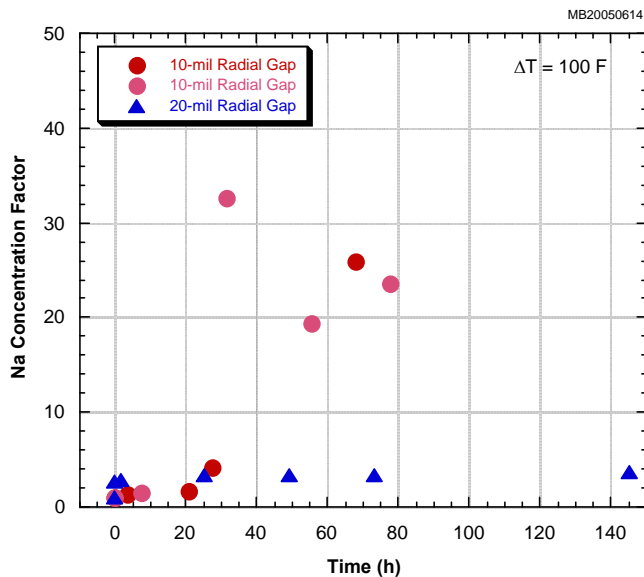


Figure 23. Concentration factors vs. time for 0.25- and 0.51-mm (0.010- and 0.020-in.) radial gap unpacked crevice and a 56°C (100°F) primary-to-secondary temperature difference.

3.2 Packed Crevice Test with NaOH

Two packed crevice tests (NaOH-01 and NaOH-02) were conducted for two crevice simulators with radial gap sizes of 0.25 mm (10 mil) and 0.51 mm (20 mil). Each crevice was filled with synthetic diamond powders. The secondary bulk solution was 11.5-ppm Na solution as NaOH, the same as for the unpacked crevice test. Two NaOH tests were basically conducted under the same chemical and thermal-hydraulic conditions, and the NaOH-02 was a duplicate test of the NaOH-01. The NaOH-01 had longer

test duration than the NaOH-02 because the NaOH-02 had to be shut down due to a leak. More details on the test results and analysis for the preliminary packed crevice tests with NaOH are described in Appendix A.

3.2.1 Packed Crevice Test: NaOH-01

Four initial series of tests were conducted. The first test involved about 2 days of testing, after which the MB was shut down and allowed to cool over a weekend. The second test involved 4.5 days of testing and was performed as a check on the reproducibility of test data from the first test and the possibility of achieving increased concentration with longer time. The third test extended for 14 days to explore the ultimate crevice concentration achievable. The fourth test involved, without interrupting the third test, raising the primary temperature from 316 to 329°C (600 to 625°F), as was done for the unpacked crevices, to see if crevice hideout increases or decreases.

Inspection of the two crevices revealed that most of the diamond packing in the 0.51-mm (20-mil) radial gap crevice was blown out because a tear in the nickel foam membrane placed over the crevice exit had resulted in a failure to seal the gap. For the 0.25-mm (10-mil) radial gap crevice, the nickel membrane was intact, and the crevice retained its packing. This explained why substantial crevice superheating, approaching 27°C (49°F), was observed in the 0.25-mm (10-mil) crevice while only minor superheat occurred in the 0.51-mm (20-mil) gap crevice, similar to our previous result for the unpacked crevice of the same radial gap size. The inspection also showed that the tube wall for the 0.25-mm (10-mil) radial gap crevice had undergone considerable outer-wall gouging of the tube at the end of NaOH-01, as shown in Figure 24. Gouging means that the depth of the dimple is comparable to the diameter of the dimple or less, i.e., a roughening of the surface. This crevice exhibited a NaOH hideout factor approaching 8,600, and the total time under these conditions was 490 hours. The gouging seems to be developed by the strong caustic chemistry. Considering that the diamond particles might vibrate or be agitated by the boiling on the tube surfaces, the abrasion of hard diamond particles may enhance this gouging. Based on the IGA growth rate data for mill-annealed (MA) alloy 600 at the crevice pH of 11 and temperature of 315°C,³⁷ the estimated IGA attack depth during the 490-hour exposure is around 25 µm (1 mil). The actual depth of gouging was not measured but the order of magnitude seems to be comparable with the prediction result. No gouging/pitting occurred on the larger 0.51-mm (20-mil) gap crevice where the hideout factor is only 5 and where the packed diamond powders were blown out of the crevice.

An estimate of crevice hideout using the MULTEQ code predicts a maximum concentration factor of 45,000 and pH of 11.07, with the neutral pH being 4.88 at the maximum available superheat of 100°F. The estimated concentration factor at the observed maximum boiling point elevation of 49°F is 43,000. The observed maximum concentration factor of 8,600 among crevice samples is less than the MULTEQ predicted value by a factor of five. This discrepancy may be attributed to that the crevice samples were mixed and diluted by the secondary solution during the sampling process which resulted in less concentrated crevice samples. The MULTEQ code cannot account the kinetic effect like mixing between crevice and secondary solution.



Figure 24.
Photograph of gouging in
tube wall in the vicinity of
the 0.25-mm (0.010-in.)
radial gap crevice.

3.2.2 Packed Crevice Test: NaOH-02

After the NaOH-01 test, the two crevices were repacked, and new nickel-foam grit retention membranes were installed. The 0.25-mm (10-mil) radial gap crevice was packed with 50:50 mixture of two mesh sizes of diamond grit (127-165 μm and 75-97 μm), and the 0.51-mm (20-mil) radial gap crevice was packed with the same grit size (127-165 μm) as used in the NaOH-01 test to obtain data for this grit and crevice size that were not obtained previously because grit was blown out of the crevice through a faulty retention membrane. The estimated crevice porosity was 40 % and 29 % for 0.25-mm (10-mil) and 0.51-mm (20-mil) gap crevices, respectively.

Under the primary and secondary chamber test temperatures of 316°C and 260°C (600°F and 500°F), respectively, the pressure differential across the tube was 5.7 MPa (827 psi). The alloy 600 tube of the 0.25-mm (10-mil) gap crevice failed after about 590 hours of testing accumulated over the two consecutive series of diamond-packed crevice testing during which the crevice hideout factors reached 8,600. The post-test investigation revealed that axial through-wall cracks developed in the 0.25-mm (10-mil) gap crevice. The bulk Na concentration for all tests was initially 11.5 ppm Na (20 ppm as NaOH) in deionized water, but it decreased to 4.2 ppm. Since sodium ion usually does not adsorb on oxide surface and there is no other heat-transfer surfaces than the two crevices, Na ions that left the bulk are expected to hide out in the crevices. Considering the SCC growth rate data of alloy 600 MA under the crevice pH of 11 at 315°C³⁷, the estimated crack length during the 590-hour exposure is about 67 mils, which is comparable to the tube wall thickness of 50 mils. Because the flaw was very tight, dye penetrant was applied to allow it to be seen and photographed. As shown in Figure 25, the OD axial SCC flaw developed from the bottom to top of the crevice region.

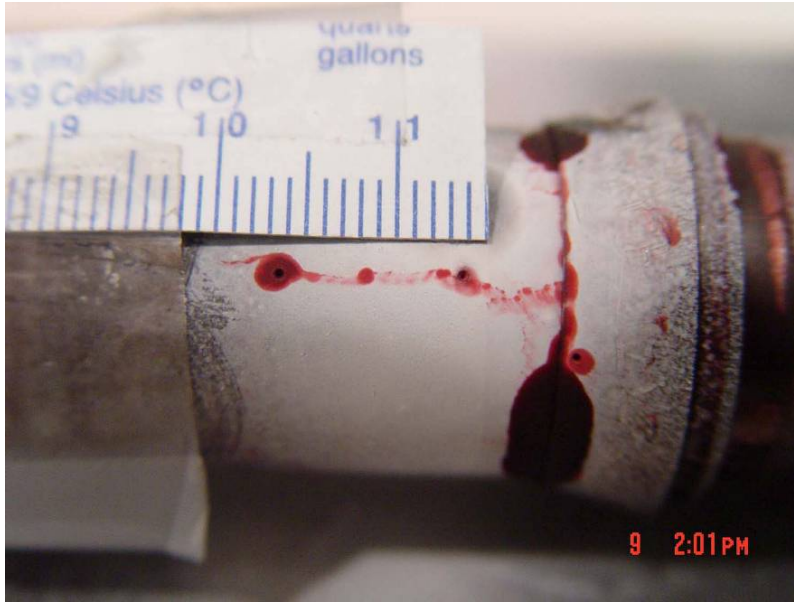


Figure 25.
Crevice SCC flaw photographed using dye penetrant to enhance visualization. The flaw is longer than 18 mm (0.71 in.).

The MB not only appears to be a good facility for studying chemical hideout induced by heat transfer in a prototypic SG tube crevice, but also determining, in a reasonable length of time, the actual cracking potential for various types of hideout chemicals as a function of crevice geometry, thermal hydraulics, and tube materials. There is the possibility that, in the presence of corrosive chemicals concentrated by crevice hideout, the vigorous nucleate boiling at an SG tube outer surface accelerates the growth of SCC above that which takes place in the absence of heat transfer and nucleate boiling.

This page is intentionally left blank.

4. Sodium Chloride Tests with Two Crevices

Based on the preliminary crevice test results with the NaOH solution, crevice hideout tests with NaCl solutions were conducted. The Na-to-Cl MR was varied at each test to determine the effect of the molar ratio on the crevice hideout and chemistry changes. All tests described in this section had two crevices with radial gaps of 10 mils and 20 mils. Each crevice was packed with diamond or magnetite powder.

4.1 NaCl-01: NaCl (MR=1.0) Test

4.1.1 Test Conditions

The first crevice hideout test was conducted with 10-ppm Cl solution as NaCl and MR=1.0. Both crevices were packed with a mixture of two sizes of diamond grit (127-165 μm and 75-97 μm). The estimated porosities for the 10- and 20-mil gap crevices are 3 % and 32 %, respectively. While 32 % is very similar to that in the NaOH-02 test, 3 % cannot be a real value. From the post-test examination, we discovered that one unused ECP port had not been completely plugged, which resulted in unexpected space in the crevice. Based on previous test experiences, the actual crevice porosity for the 10-mil gap crevice should be similar to that of the 20-mil gap crevice. Prepared test solution is injected through a pump before heating up the MB.

4.1.2 High Purity Water Test

As a reference, a test was performed in high purity water first. Five and four thermocouples were installed at the 10- and 20-mil gap crevice, respectively. Their locations are described in Section 2.3.2. Figure 26 shows the normalized temperature variation for the 10-mil crevice gap. To normalize the temperature, the temperature difference between the crevice temperature and secondary saturation temperature are divided by the primary-to-secondary temperature difference. Temperature remained constant for the test period except for the initial heatup and stabilization period. There was no indication of a temperature rise by impurity hideout. The thermocouple labeled "TW" showed a higher value than others because it was installed to touch the outer wall of the alloy 600 tubing. Figure 27 shows the bulk conductivity variation with time. The bulk conductivity value kept constant except for the initial heat-up period.

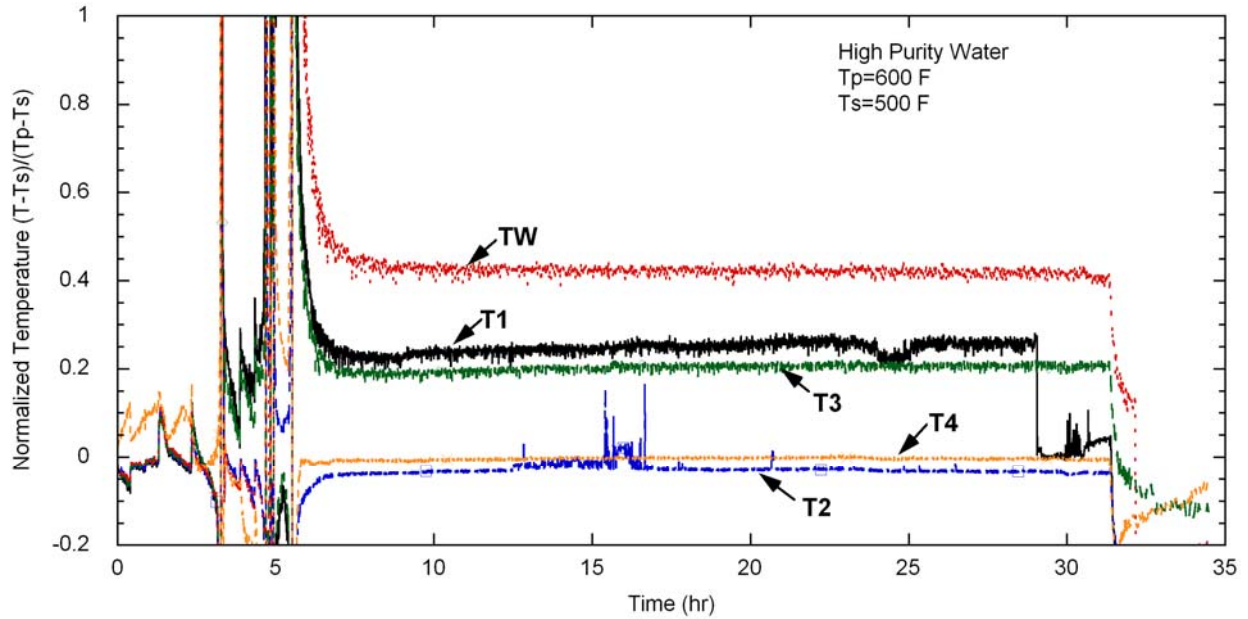


Figure 26. Normalized temperature variation at 10-mil-gap crevice with high purity water in the bulk (NaCl-01).

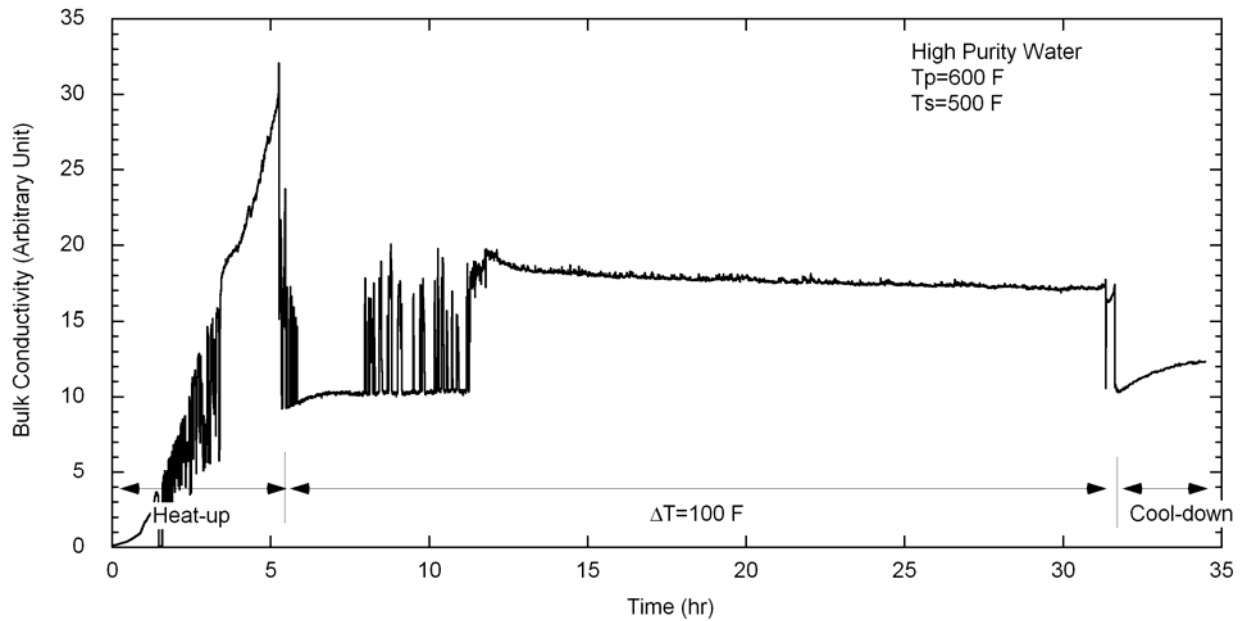


Figure 27. Bulk conductivity variation with time in high purity water (NaCl-01).

4.1.3 Temperature and Conductivity

Figure 28 shows the crevice temperature variation with time in the 10-mil gap crevice packed with diamond powder. The temperature varied with the location of thermocouples and hideout processes. For the 10-mil gap crevice, temperatures increased gradually for the initial test period, followed by stabilization after about 80 hours. The gradual temperature increase over a few tenths of hours is

interpreted as meaning that the Na and Cl ions accumulate in the crevice, causing the boiling point elevation. Since the primary water temperature stabilized within a few hours, the gradual crevice temperature increase cannot be attributed to the primary water temperature variation. The temperature labeled “TW” decreased instead, probably because this thermocouple touched the wall of the alloy 600 tubing. As shown in Figure 28, the amplitude and time constant of the boiling point elevation for each thermocouple varied, mainly because of the different radial distances from the wall of the primary tubing. Based on this interpretation, T4 appears to be the farthest from the wall. After increasing the primary temperature from 600 to 625°F, additional boiling point elevation was not observed at any thermocouple location. NaCl would remain in a dissolved state until its concentration reaches the solubility limit. Since a boiling point elevation is related to the dissolved impurity concentrations, the boiling point elevation equivalent to the NaCl solubility limit under crevice conditions can be predicted thermodynamically. Based on MULTEQ[®] prediction, the maximum boiling point elevation with NaCl is 46°F; the NaCl precipitation would start if measured temperature is higher than 546°F. At $\Delta T=125^\circ\text{F}$ NaCl precipitation probably occurred over almost the entire crevice except the location labeled T4 where the measured boiling point elevation was lower than 46 °F. Figure 29 shows the normalized temperature variation in the 10-mil gap crevice. The initial temperature behavior is the same as that in Figure 28, but the normalized temperatures did not change after the increase of ΔT . This finding means that the conduction heat transfer is dominant in the crevice rather than boiling heat transfer before and after the ΔT change. It appears that the boiling rate was decreased by the boiling point elevation and NaCl precipitation.

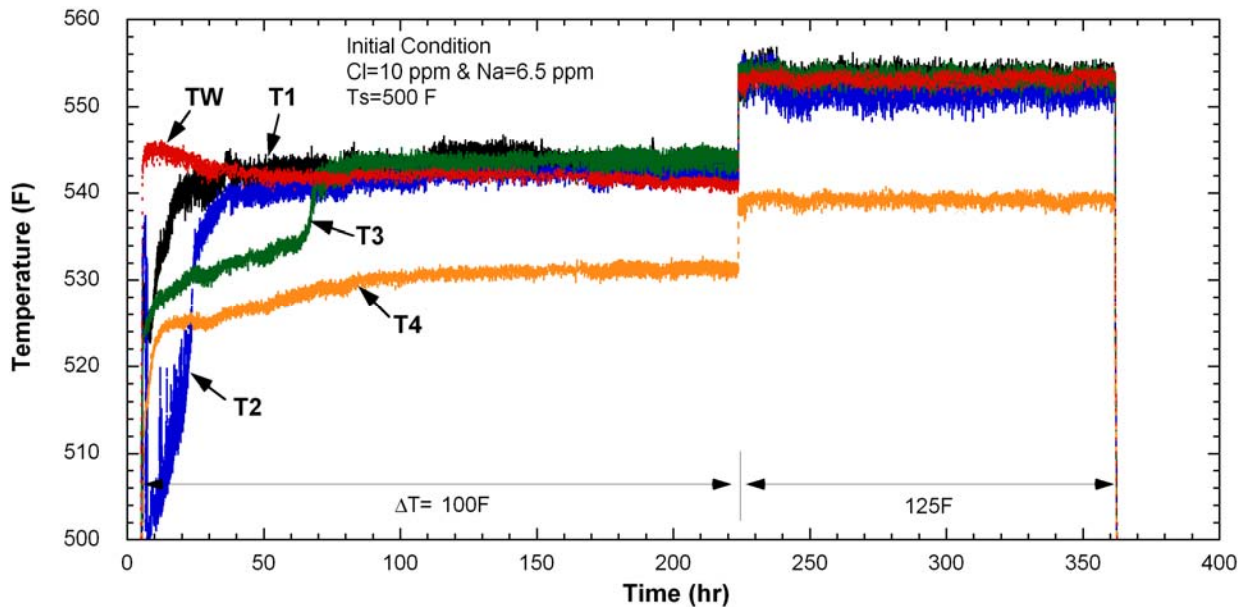


Figure 28. Crevice temperature variation with time in the 10-mil radial gap crevice packed with diamond powder and with NaCl in the bulk solution (NaCl-01).

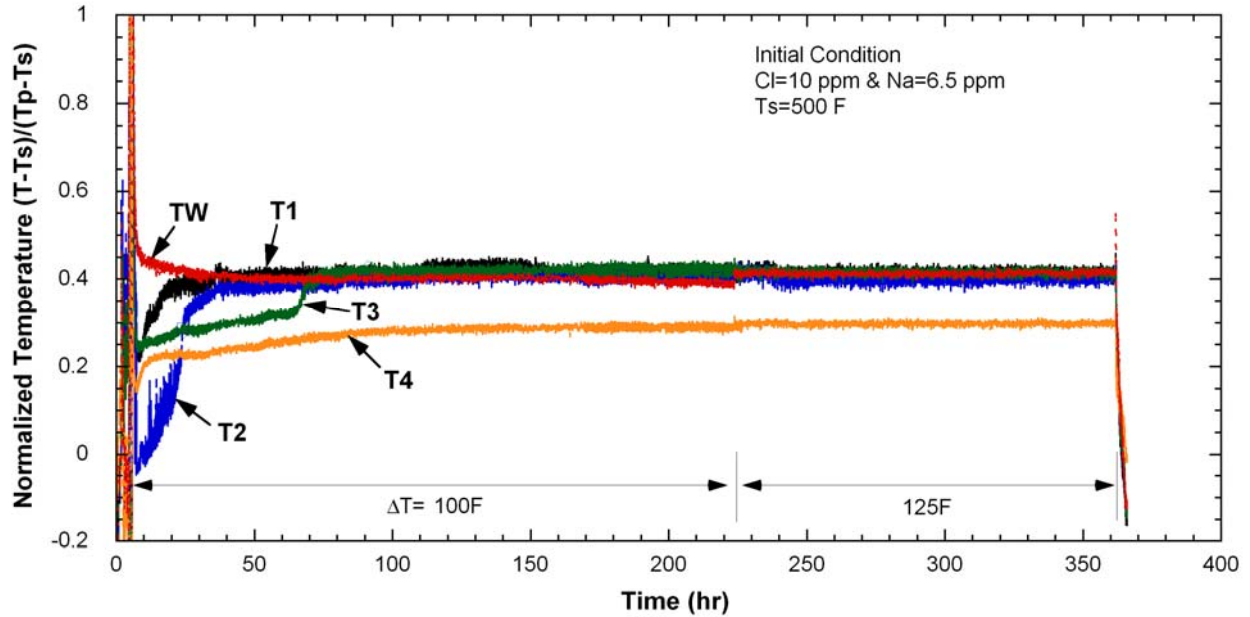


Figure 29. Normalized temperature variation at the 10-mil gap crevice with NaCl in the bulk solution (NaCl-01).

Figure 30 shows the crevice temperature variation in the 20-mil gap crevice. The crevice temperatures varied depending on the thermocouple locations, and the temperature was much lower than that in the 10-mil gap crevice, except for the thermocouple labeled T7, which might be closer to the alloy 600 tubing wall than the others. The noisy temperature signal appears to indicate boiling heat transfer in the crevice as well as conduction. The alternation of a liquid film and dry spot can cause such a temperature oscillation, as described in earlier work⁶. Gradual boiling point elevation was not significant as compared with the 10-mil gap crevice. T6 and T5 appear to indicate a slow boiling point elevation by impurity hideout after the ΔT increase from 100 to 125°F, but the value is less than 6°F. Figure 31 shows the normalized temperature variation as a function of time and thermocouple location. If overall heat transfer coefficient is the same at each ΔT , the normalized temperature should remain constant regardless of ΔT . However, the normalized temperatures showed a shift immediately after the ΔT change, which might indicate that overall heat transfer coefficient became less.

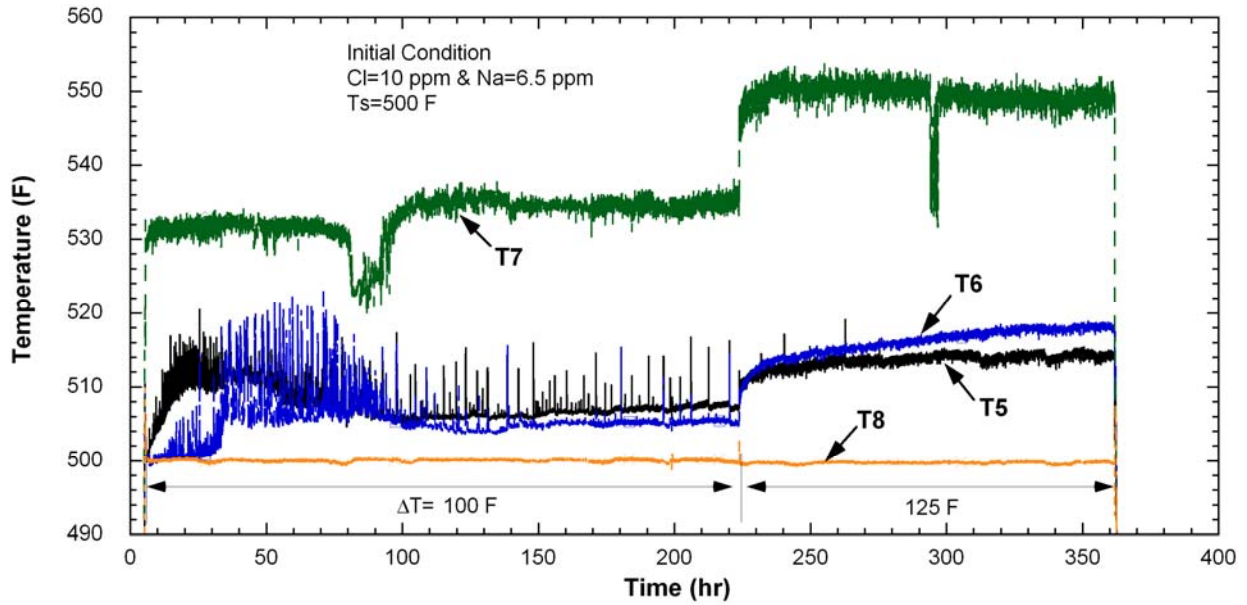


Figure 30. Crevice temperature variation with time in the 20-mil radial gap crevice packed with diamond powder (NaCl-01).

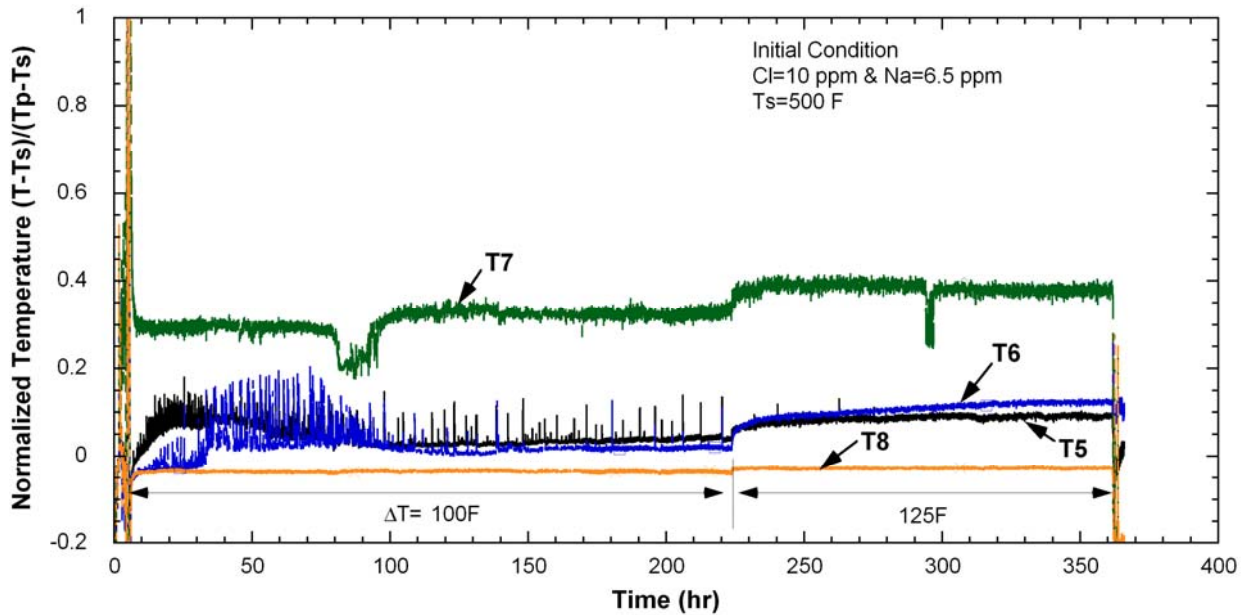


Figure 31. Normalized temperature variation at 20-mil gap crevice (NaCl-01).

Figure 32 shows the bulk conductivity variation and Cl ion concentration in bulk water samples measured by an ion selective electrode (ISE). The bulk conductivity started to decrease right after the primary temperature stabilization. The reduction rate in the bulk conductivity was not much changed after the ΔT increase from 100 to 125°F. At the end of the test, bulk conductivity decreased to 10 % of the initial value, indicating very significant impurity hideout in the crevice. Quick hideout return was observed after the primary temperature reduction. It is hypothesized that the diamond powder packing was not so restrictive that the impurities in the crevice could easily return to the bulk solution. This is also evidence that mixing between crevice and secondary solutions can be significant. Reduced ΔT allowed

liquid penetration into the crevice and dissolution of the precipitated NaCl. The bulk conductivity decrease after the shut-down is attributed to the temperature decrease. The measured Cl ion concentrations in bulk samples were consistent with the bulk conductivity data before the change of ΔT . However, even though the measured data points are limited, the Cl ion concentration did not appear to change significantly after the change of ΔT . The Na ion concentration was also measured by the ISE, but the uncertainty of the measurements was too large to be of value. In the next tests, the bulk and the crevice samples were analyzed by analytical equipment in addition to the ISE to obtain more accurate ion concentrations.

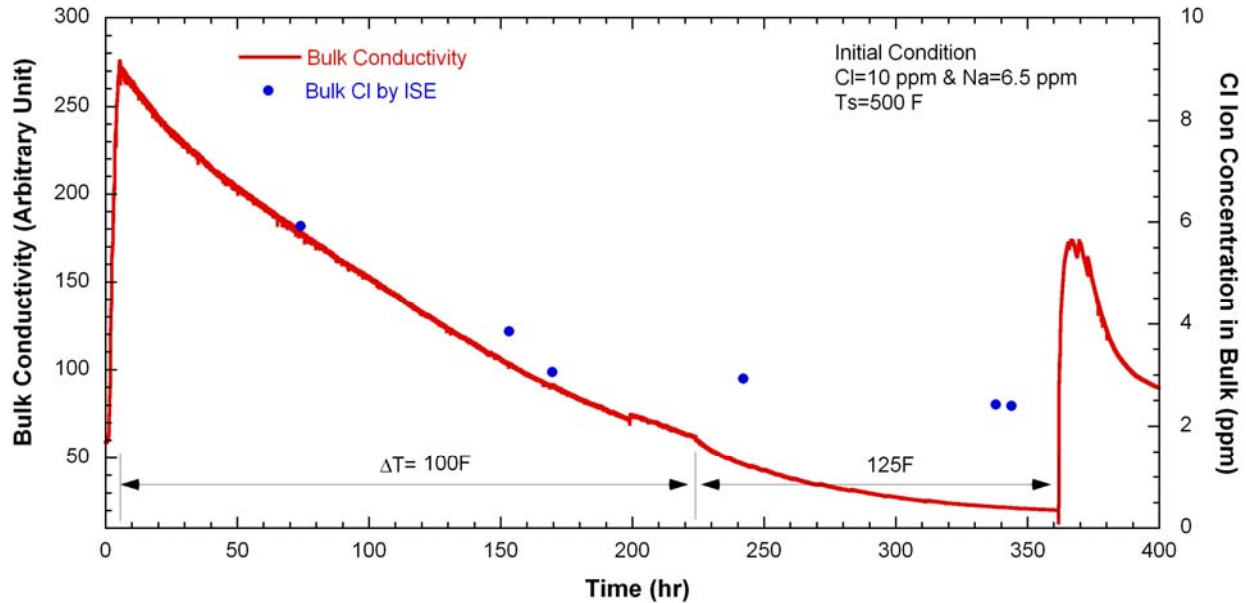


Figure 32. Bulk conductivity variation and Cl ion concentration versus time in bulk water samples measured by an ISE (NaCl-01).

4.1.4 ECP Measurement

Figure 33 shows the variation in Ni electrode potential in the crevice with respect to the Ag/AgCl (0.01 N KCl) reference electrode in the bulk solution. Because of the potentiometer problem, other ECP data are not available. Assuming that the Ni electrode serves as a hydrogen electrode in deaerated alkaline and neutral environments, rough estimation for crevice pH variation may be possible from Figure 33. This assumption may be reasonable because Kawamura et al.¹⁴ experimentally showed that the ECP versus pH slope of alloy 600 was close to that of hydrogen electrode at high temperature and pH ranging 3-10. The Ni ECP initially decreased and stabilized at -650 mV over the first 20 hours. However, the Ni ECP started increasing and stabilized at -610 mV at $\Delta T=100^\circ\text{F}$. If the ECP decreases, that correlates to an increasing pH or hydrogen fugacity in crevice, but hydrogen is not supposed to concentrate in the crevice. A pH variation can be a result of the variation of Na and Cl concentrations in the crevice. The initial decrease of the Ni ECP indicates the crevice pH increased as a result of preferential Na concentration and a Cl volatility effect. The following Ni ECP increase and stabilization at $\Delta T=100^\circ\text{F}$ might be interpreted as a crevice pH decrease caused by preferential Cl hideout following the initial preferential Na hideout. The delayed Cl hideout is discussed and experimentally supported in single crevice tests (NaCl-05 & -06).

At $\Delta T=125^\circ\text{F}$, the Ni ECP gradually decreased. This decrease might indicate an increased Cl volatility effect caused by the increased boiling rate at higher ΔT . Note that the crevice temperature data indicated NaCl precipitation at $\Delta T=125^\circ\text{F}$ so that the ECP might not be measurable under the

precipitation condition. Therefore, the tip of the Ni electrode appears to be located far enough from the tube wall not to be dry. The measured Ni ECP may represent the chemistry far from the tube wall rather than the chemistry near the tube wall. The effects of the radial location of the electrode tip are discussed in Section 4.2.3. The Ni ECP variation from the beginning of a test at constant ΔT , as shown in Figure 33, is typical ECP behavior under NaCl bulk water chemistry. In other NaCl tests, where a tungsten electrode was used as a pH electrode, the electrode potentials are similar.

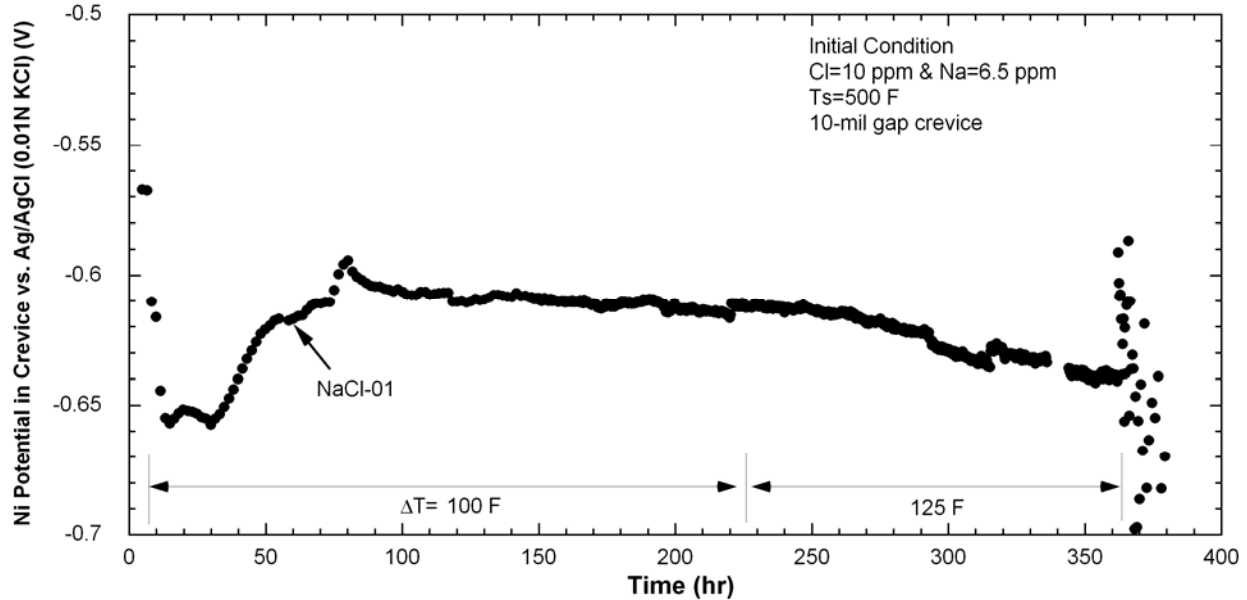


Figure 33. Ni electrode potential variation in crevice with respect to Ag/AgCl (0.01 N KCl) reference electrode in bulk (NaCl-01).

4.2 NaCl-02: NaCl (MR=1.0) Test

After the NaCl-01 test, the MB was heated up again without opening the secondary chamber and changing the bulk solution. This next test was done to evaluate the reproducibility of the NaCl-01 test results. The secondary-side temperature was kept at 260°C (500°F), while the primary-side temperature was set at 282, 293, 304, and 316°C (540, 560, 580, and 600°F) because $\Delta T=100$ or 120°F is higher than the normal operating differential temperature between the primary and secondary sides in actual SGs. The NaCl-02 test results are summarized as below.

4.2.1 Temperature Data

The NaCl-02 test was performed with the primary superheat variation ranging from 40 to 100 °F. The secondary test solution contained 10 ppm Cl as NaCl. Figure 34 shows the crevice temperature variation measured at various crevice locations in a 10-mil gap crevice. As observed in the NaCl-01 test, the amplitude and time constant for the temperature increase caused by impurity hideout depended on the location of each thermocouple at $\Delta T=100^\circ\text{F}$. The crevice temperatures decreased instantaneously after decreasing ΔT from 100 to 60°F. After increasing ΔT again from 60 to 80°F, the crevice temperatures started to increase gradually. The TW thermocouple touching the tube wall showed the highest temperature elevation. From this observation, we concluded that impurity hideout kinetics is fastest at the tube wall, and the resultant temperature elevation is the most sensitive on the tube wall at least when ΔT is 60°F or 80°F. When ΔT dropped to 40°F, crevice temperatures decreased instantaneously and did not

show any temperature elevation. But TW indicated a small temperature elevation of about 6°F. The tests at $\Delta T=60^\circ\text{F}$ and 40°F followed the tests at 100°F and 80°F , respectively. The transition from higher to lower ΔT resulted in the impurity movement out of the crevice, a dilution by drawing in the secondary solution to the crevice, and possible dissolution of the precipitated NaCl. These are the reasons why temperature elevation was not observed at $\Delta T=60^\circ\text{F}$ and 40°F . With decreasing ΔT , the crevice would reach a new steady-state condition at lower ΔT in a short time due to relatively fast diffusion in the diamond powder pack. Figure 35 shows the normalized crevice temperatures as a function of time. As shown in Figure 35, the crevice temperature appears to be relatively independent of the primary superheat ΔT . However, the temperature increased at the beginning of the test with the primary superheat of 100°F . The normalized temperatures labeled as T2 and T3 increased when ΔT was decreased from 100°F to 60°F and from 80°F to 40°F , while the tube wall temperature labeled TW decreased when the ΔT was decreased. It is concluded from the normalized temperature variation that the concentrated solution on the tube wall is diluted when ΔT decreases but the area away from the tube wall is affected by NaCl precipitates formed at higher ΔT so that the nucleate boiling rate is reduced because of the concentrated solution formation by the dissolution of NaCl precipitates at that area when ΔT decreases.

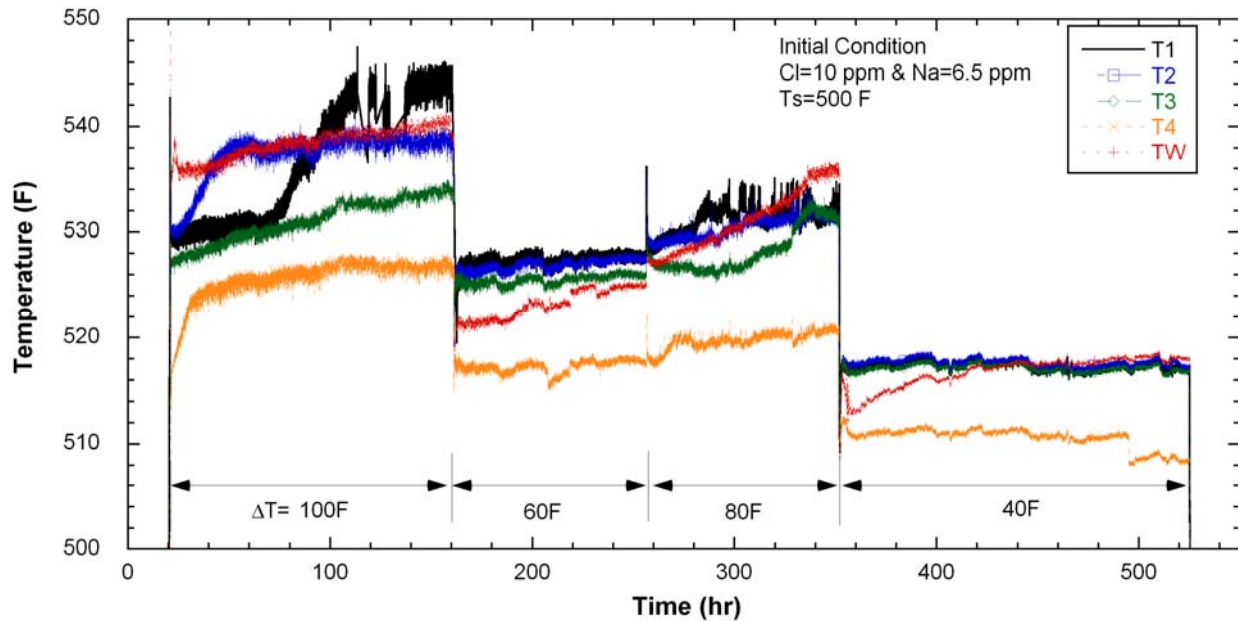


Figure 34. Crevice temperature variation with time and ΔT in a 10-mil radial gap crevice packed with diamond powder (NaCl-02).

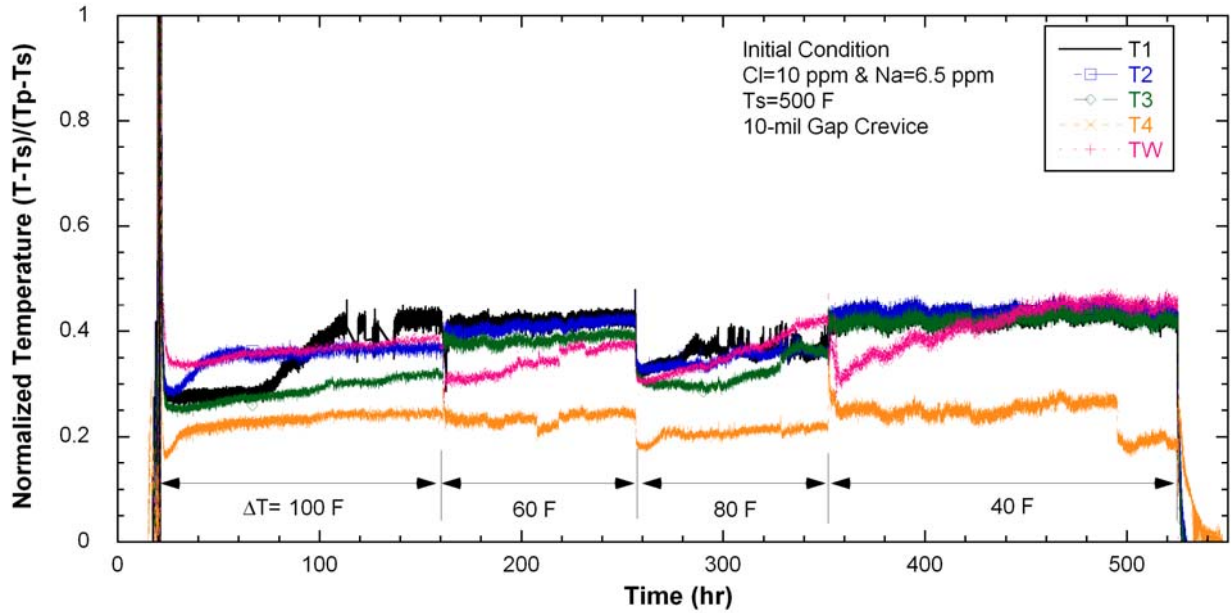


Figure 35. Normalized temperature variation at 10-mil gap crevice (NaCl-02).

Figure 36 shows the crevice temperatures in the 20-mil radial gap crevice. As observed in the NaCl-01 test and shown in Figure 30, the temperature elevation is not significant except at T7. Some noisy temperature signals might indicate presence of both steam and liquid phases in near the thermocouple. As shown in Figure 37, the normalized temperature is relatively independent of ΔT except at T7; this finding is interpreted as the effect of the thermocouple's location. As compared with the temperature data in 10-mil gap crevice, the normalized temperatures in the 20-mil gap crevice are lower. In the wider gap crevice, liquid penetration into the crevice and mixing between bulk and crevice appear to be easier, and this condition causes a higher heat transfer coefficient and lower normalized crevice temperatures.

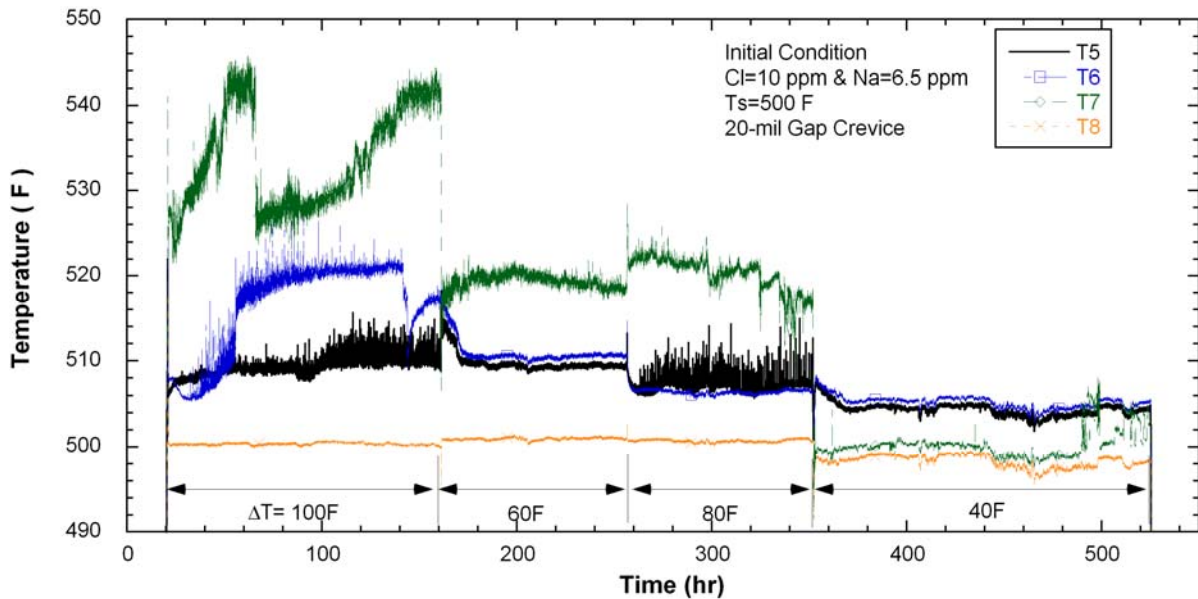


Figure 36. Crevice temperature variation with time and ΔT in a 20-mil radial gap crevice packed with diamond powder (NaCl-02).

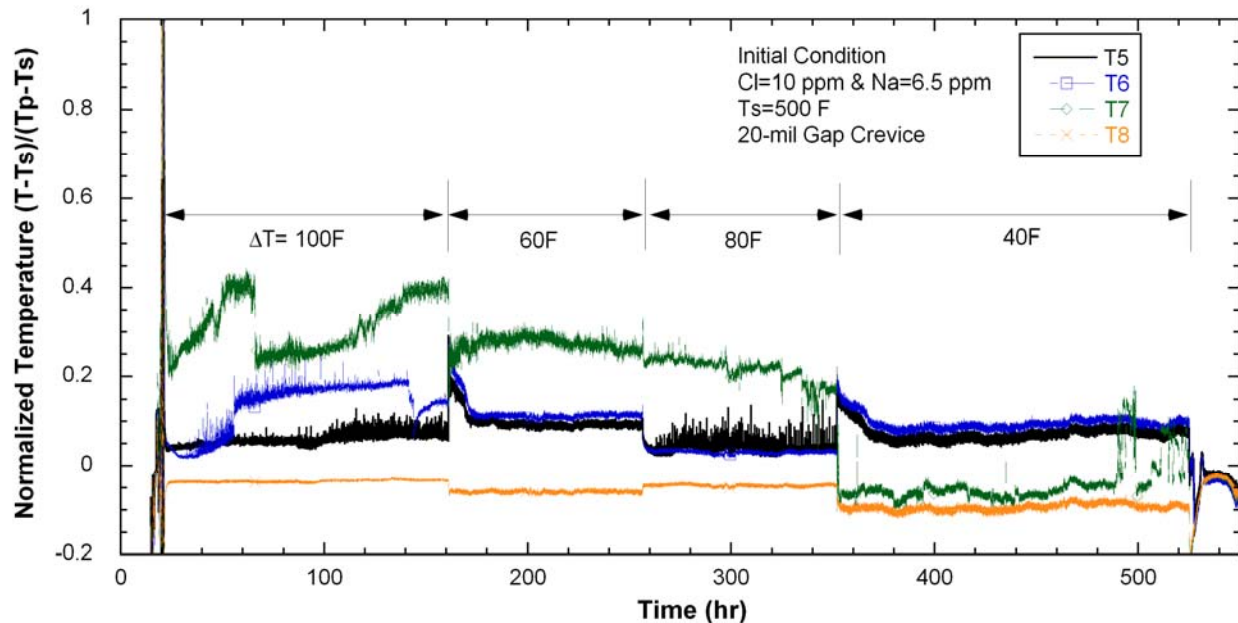


Figure 37. Normalized temperature variation at 20-mil gap crevice (NaCl-02).

4.2.2 Bulk and Crevice Chemistry

Figure 38 shows the bulk conductivity and the bulk impurity concentration measured by solution sampling. The bulk conductivity reduced gradually, but the conductivity reduction rate was dependent on ΔT . Hideout return was observed after ΔT decreased from 100°F to 60°F and from 80°F to 40°F. The Cl and Na concentrations measured by IC and ICP/OES are consistent with the bulk conductivity variations. The Na data determined by ICP/OES at 400 hours deviate from the general trend. The large fluctuation of Na ion concentration at $\Delta T=40^\circ\text{F}$ is unexpected because the Cl ion concentration and bulk conductivity kept nearly constant over that time period. This Na data at 400 hrs could be measurement error. The Cl concentration determined by ISE did not correspond to the value determined by IC, but the overall trend seems to be consistent with the bulk conductivity data at least during the first two ΔT periods. These findings verify that the ISE analysis method for Cl determination is appropriate for evaluating the overall trend but not for accurate measurements. The Na concentration determined by the ISE is not reliable because the sampling solution volume of about 1-1.5 mL was too small for the Na ISE.

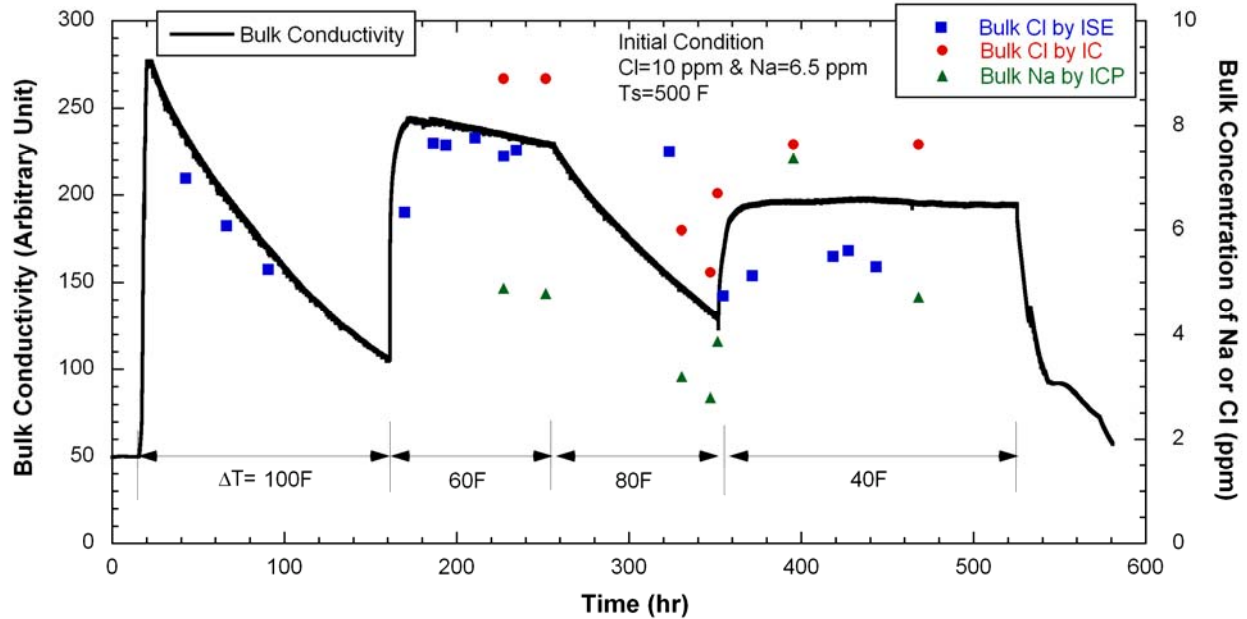


Figure 38. Comparison of bulk conductivity and measured bulk impurity concentration determined by solution sampling (NaCl-02).

The bulk conductivity from the NaCl-02 test was compared with that from the NaCl-01 test over the first 150 hours at $\Delta T=100^{\circ}\text{F}$, as shown in Figure 39. The conductivity excursions showed very similar behavior. Since the experimental conditions for the two tests were exactly the same, this comparison confirmed the data reproducibility at $\Delta T=100^{\circ}\text{F}$. The slopes for bulk conductivity reduction are strongly dependent on the superheat changes, as shown in Figure 40. To remove the dependency on bulk concentration itself, the bulk conductivity data were normalized with the initial bulk conductivity at each ΔT . There is a drastic change in the rate of bulk conductivity reduction between $\Delta T=60^{\circ}\text{F}$ and $\Delta T=80^{\circ}\text{F}$. As discussed earlier, ΔT was not increased monotonically from 40°F to 100°F . In evaluating the data, it should be noted that the excessive hideout occurred before changing ΔT from 100°F to 60°F and from 80°F to 40°F . Because of this excessive amount of hideout prior to decreasing the ΔT , the force to drive ions out of the crevice was large immediately after the decrease of ΔT . Then driving forces to move ions into and out of the crevice were balanced and, at $\Delta T=60^{\circ}\text{F}$, the driving force to move ions into the crevice became dominant because the diffusion flux of ions out of the crevice became negligible. At $\Delta T=40^{\circ}\text{F}$ steady state was achieved based on the data for bulk conductivity and Cl ion concentration. We expect that if ΔT is increased monotonically from 40°F to higher value, the rate of bulk conductivity reduction at $\Delta T=40^{\circ}\text{F}$ and 60°F will be much higher than those in Figure 40 and possibly even close to the rates at $\Delta T=80^{\circ}\text{F}$ and 100°F . This assumption is supported by the test results for a single-diamond-packed crevice test, NaCl-05, discussed in Section 5.3.3.

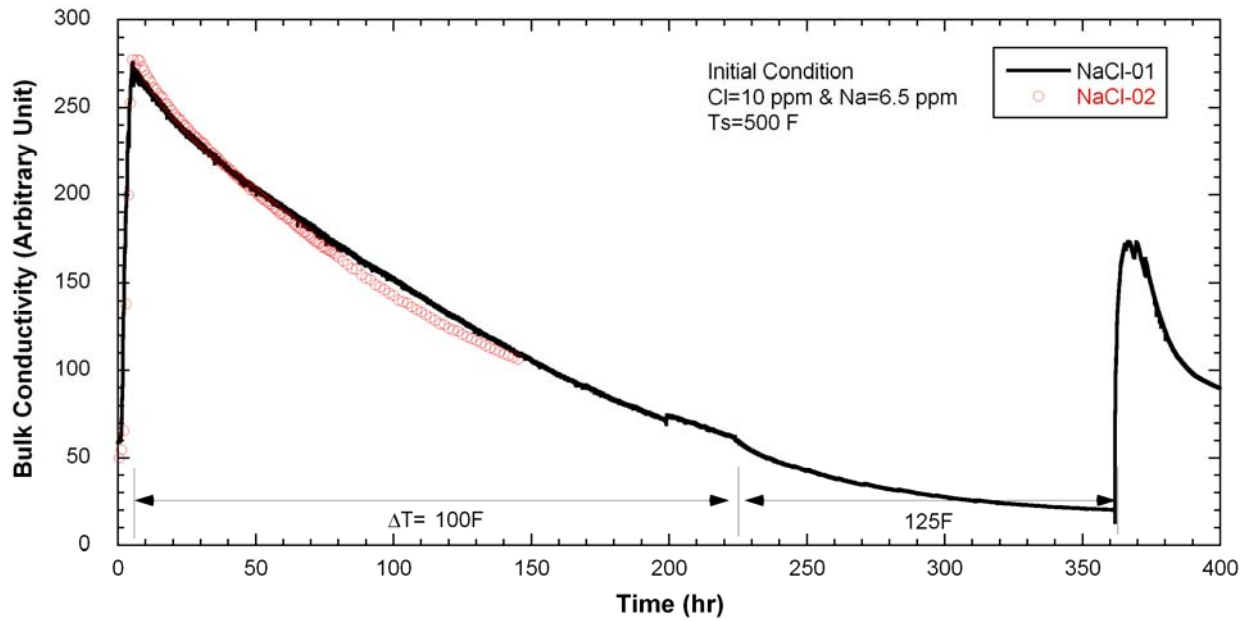


Figure 39. Comparison of measured bulk conductivity in the NaCl-01 test and NaCl-02 test.

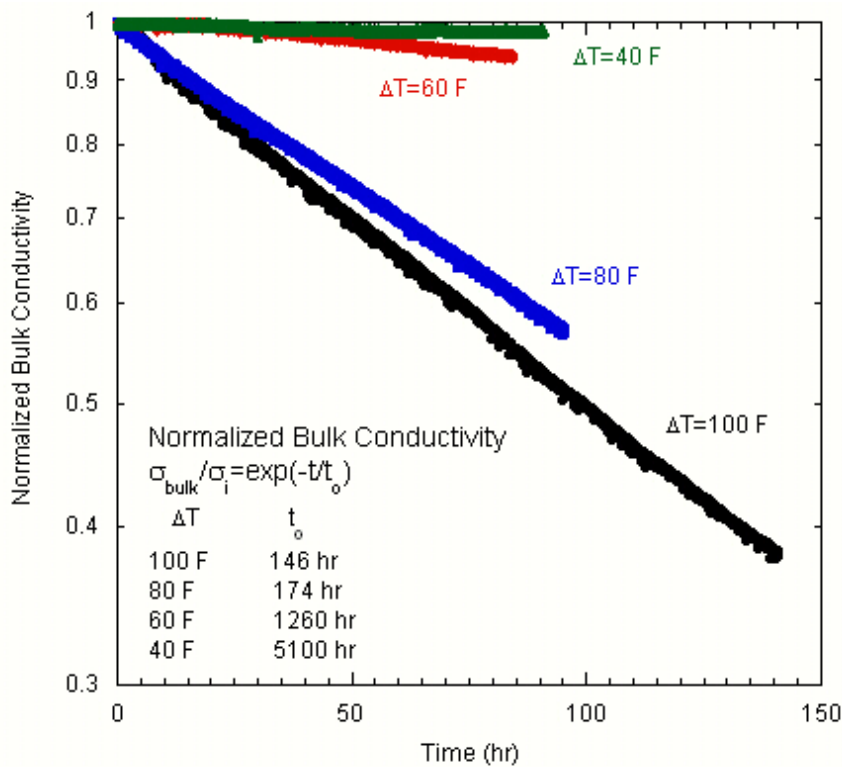


Figure 40. Normalized bulk conductivity variation as a function of ΔT in the NaCl-02 test comparing the bulk conductivity decreasing rates.

Figure 41 shows the results for crevice-solution analysis by IC for Cl and ICP/OES for Na, as well as some results by ISE. When the $\Delta T=80$ or 100°F , the crevice samples did not show hideout, but significant impurity concentrations were observed at lower ΔT . It is likely that higher ΔT resulted in NaCl

precipitation on the tube surface, and mainly steam is condensed and sampled out of the crevice. However, at $\Delta T=40^\circ\text{F}$, the precipitated NaCl dissolved at the beginning of the test, and this dissolution caused the highest concentration in the earliest crevice sample, followed by a gradual decrease and stabilization. In Figure 41, Na and Cl concentrations determined by ISE are shown to be similar to those obtained by IC or ICP/OES. The ISE analysis has better accuracy at higher concentration in the crevice samples compared with the accuracy at lower concentration in the bulk samples shown in Figure 38.

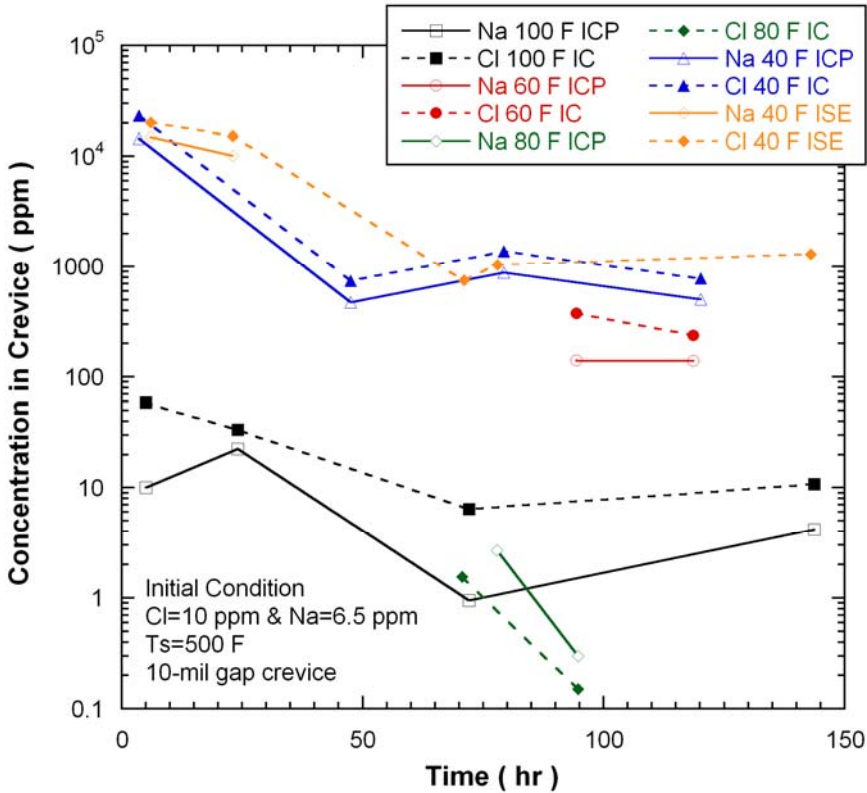


Figure 41. Concentrations from crevice-solution sample analysis as functions of time and ΔT in the NaCl-02 test.

Figure 42 shows the Na-to-Cl molar ratio ($[\text{Na}]/[\text{Cl}]$) in a crevice compared with that in the bulk as a function of ΔT for the 10-mil and 20-mil gaps. For the 10-mil gap crevice, as ΔT decreases, $[\text{Na}]/[\text{Cl}]$ in the crevice increases. This trend indicates that mainly steam is condensed and extracted from the sampling line at higher ΔT , and actual concentrated liquid is extracted at lower ΔT . The variations of the crevice molar ratio at $\Delta T=100^\circ\text{F}$ is also attributed to the variations of the extracted amount of steam. As compared with the $[\text{Na}]/[\text{Cl}]$ in the crevice, the variation of $[\text{Na}]/[\text{Cl}]$ in the bulk is not as large but slightly increases with ΔT . This result appears to indicate a dependence of Cl volatility on ΔT . Since $[\text{Na}]/[\text{Cl}]$ in the bulk is less than unity, the crevice solution should have higher $[\text{Na}]/[\text{Cl}]$ than unity. However, only crevice samples at $\Delta T=40^\circ\text{F}$ tend to have $[\text{Na}]/[\text{Cl}]$ ratios that are higher or close to unity, because at $\Delta T=40^\circ\text{F}$ concentrated liquid from NaCl dissolution minimized the steam extraction. For the 20-mil gap crevice, as compared with 10-mil gap crevice, $[\text{Na}]/[\text{Cl}]$ in the crevice is closer to the bulk value. It appears that fluid mixing between the crevice and bulk is easier in the 20-mil gap than in the 10-mil gap.

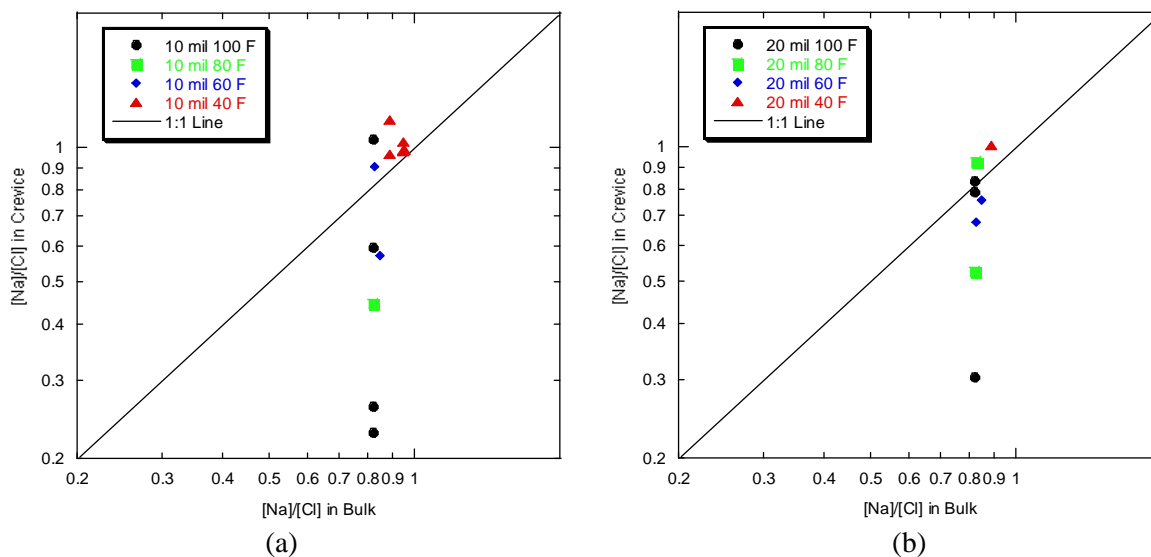


Figure 42. [Na]/[Cl] ratios in crevice versus bulk as a function of ΔT for (a) 10-mil gap and (b) 20-mil gap crevices in the NaCl-02 test.

4.2.3 ECP Measurement

Figure 43 shows the ECP variation of various electrodes installed in the crevice and the bulk solution with respect to the Ag/AgCl (0.01 N KCl) reference electrode. The bulk Pt electrode potential increased gradually and independently of the primary superheat. If the bulk Pt change was caused by the drift of the Ag/AgCl reference electrode, potential should change toward a negative direction. Assuming the Pt electrode behaves as a pH electrode under the deaerated condition, it is assumed that the bulk pH would gradually move to the acidic direction because of the high volatility of Cl and resultant preferential hideout of Na. Precise bulk chemistry analyses by IC and ICP/OES indicated that the [Na]/[Cl] molar ratio in the bulk solution was always less than unity, a finding that supports the measured bulk Pt potential variation. Figure 44 shows the solution pH variation with molar ratio and ion concentration at 260°C (500°F). For the 10-ppm Cl concentration, the MR change from 1.0 to 0.9 can lower the solution pH by almost one pH unit. However, reduced ion concentration itself can make the solution pH higher. Consideration should be given to both effects when evaluating the bulk solution pH with ion concentration data. Based on the MULTEQ calculations in Figure 44, it is difficult to explain the initial decrease of bulk Pt ECP. The Pt electrode might be affected by residual oxygen, but the Pt ECP decrease suggests that eventually the oxygen becomes consumed by the oxidation of metals. As shown in Figure 43, Ni and alloy 600 electrodes in bulk water show similar behavior to bulk Pt electrode.

Figure 45 shows the electrode potential difference between the crevice and bulk for Pt, Ni, and alloy 600 electrodes. If all conditions are the same for the crevice and bulk, the potential difference should be zero. Assuming Pt behaves as a hydrogen electrode and hydrogen activity in the crevice and bulk are the same or the difference of hydrogen activity between the bulk and crevice is negligible, the potential difference can be interpreted as related to a pH difference. Based on this assumption, it was concluded that the crevice was acidified gradually during the first 50 hours. The crevice solution analysis at $\Delta T=100^\circ\text{F}$, as shown in Figure 42, indicated that the crevice sample was acidic. Since the potential difference decreased with time, the crevice pH was gradually increasing. After the primary superheat change from 80°F to 40°F, the Pt potential difference was drastically changed in the alkaline direction. The molar ratio in bulk solution at $\Delta T=80^\circ\text{F}$ was less than unity, which means Na was preferentially concentrated in the crevice. Preferential Na concentration should make the crevice more alkaline than the

bulk, but the measured Pt ECP in the crevice was higher than that of the bulk Pt. This discrepancy can be resolved with the assumption that at higher ΔT (80°F or 100°F) NaCl precipitation occurred at the tube surface of the deeper crevice region, and around the Pt electrode tip, the steam phase was dominant. The condensed steam would cause the slightly acidic pH signal of the Pt ECP. The drastic change of crevice Pt potential when lowering ΔT is attributed to the fact that the formerly present NaCl precipitation near the tube surface was mixed with penetrating liquid caused by the reduced ΔT , and then the mixed liquid touched the Pt electrode tip. The Pt potential difference slowly came back to near neutral condition, which is caused by the mixing between bulk and crevice solution. The return of excessive Na from the crevice was confirmed by the bulk solution analysis, indicating the molar ratio had become larger and close to unity.

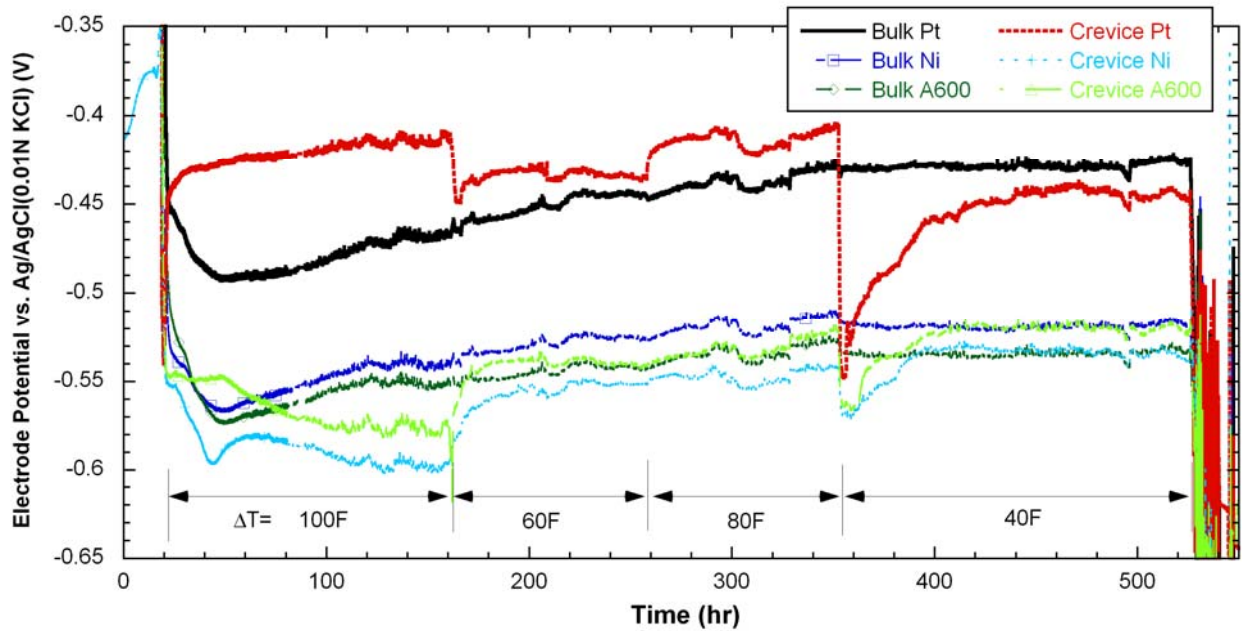


Figure 43. Electrode potential variation with respect to Ag/AgCl (0.01N KCl) (NaCl-02).

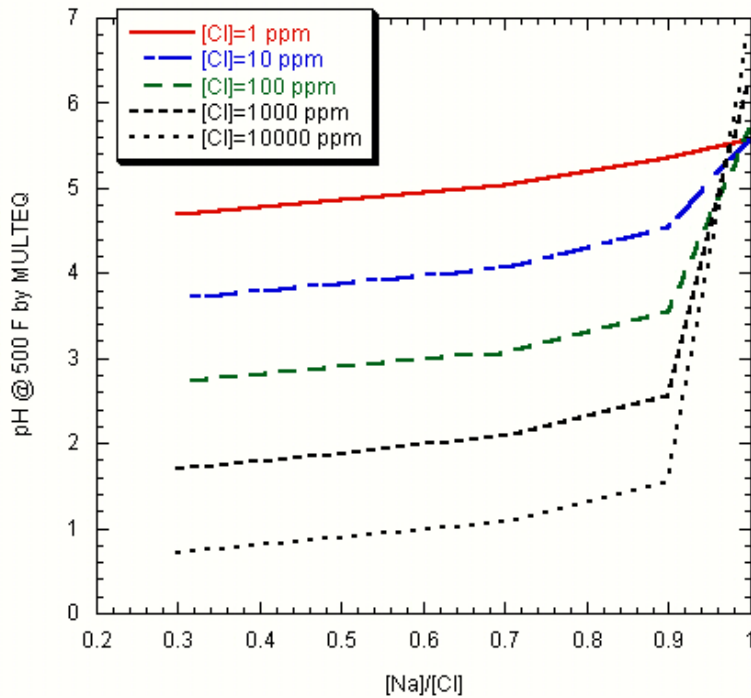


Figure 44. Predictions of solution pH variation at 260°C (500°F) with Na-to-Cl molar ratio and ion concentration.

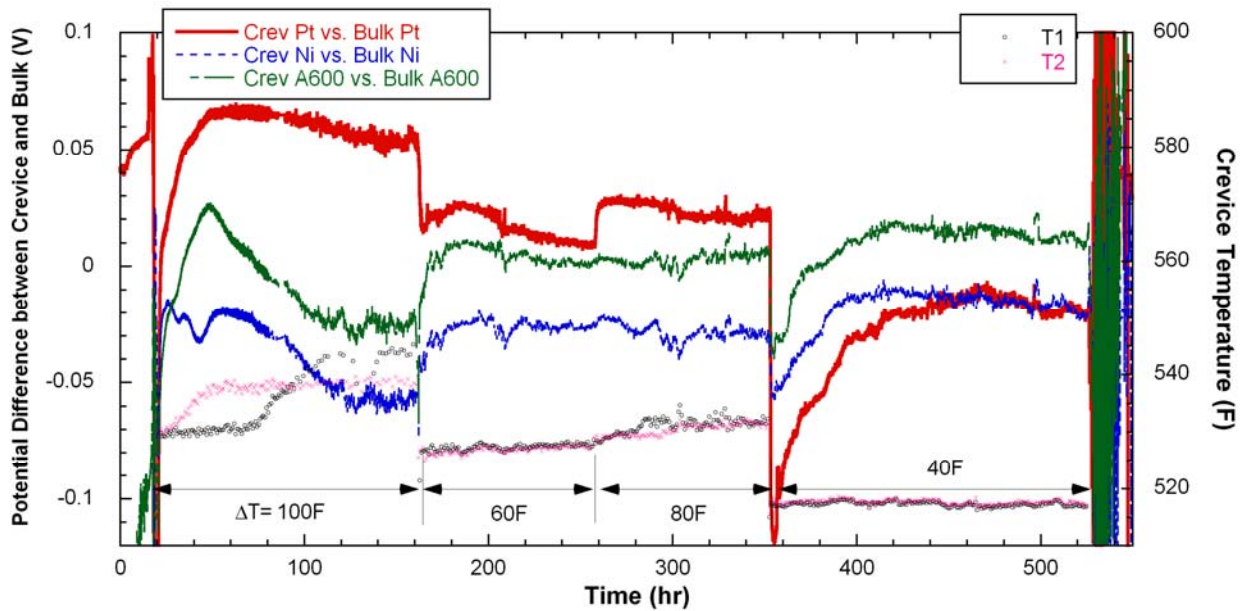


Figure 45. Electrode potential difference between crevice and bulk (NaCl-02).

As shown in Figure 46, the crevice Ni electrode potential of the NaCl-02 test was compared with that of the NaCl-01 test. In general, the NaCl-02 results indicated higher potential. The initial potential decrease was not significant in the NaCl-02 test, probably because the precipitated NaCl in the NaCl-01 test, which might not have been completely dissolved out, affected the crevice Ni electrode potential in the subsequent test, NaCl-02. The potential difference between the two NaCl tests was around 10 mV after 150 hours, which is an acceptable reproducibility for high-temperature ECP measurements.

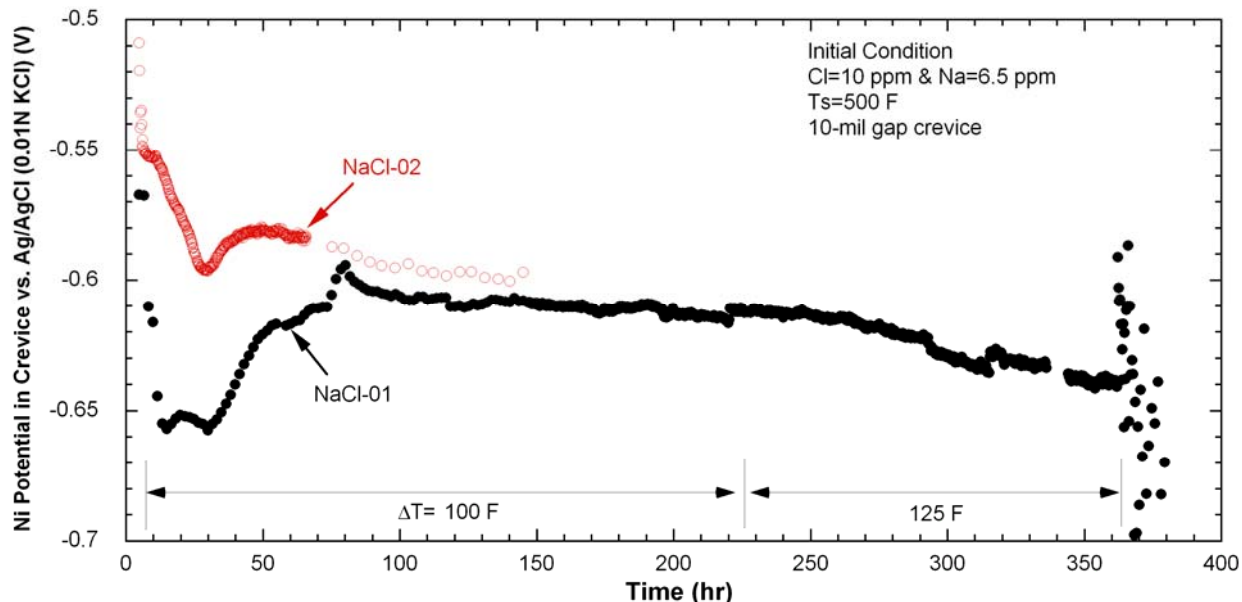


Figure 46. Measured Ni electrode potential in crevice in the NaCl-01 and NaCl-02 tests.

Figure 47 shows the Pt potential difference between the crevice and bulk as a function of pH difference. The sample pH was calculated by MULTEQ, and Pt potential data corresponding to the sampling time were used. If the Pt electrode reaction follows the Nernstian equation, the potential slope with respect to pH should be -106 mV/pH at 260°C (500°F), but the measured slope was only -18 mV/pH . The calculated pH data based on the extracted sample composition predict a larger pH difference between crevice and bulk compared with measured Pt potential. For example, the maximum potential difference is about -120 mV , corresponding to one pH unit difference, but the calculated pH difference was around 5. It is likely that the crevice samples might have been diluted or affected so that they did not fully represent the actual Na and Cl concentrations in crevice. The post-test examination for the tube surfaces in the crevice region revealed no gouging in the 10- or 20-mil gap crevice. Even though the crevice sample indicated the caustic chemistry in a short-time period at $\Delta T=40^\circ\text{F}$, the post-test examination suggests that the crevice chemistry was near neutral during the NaCl-01 and -02 tests. Keeping the bulk water chemistry neutral and having the $\text{MR}=1.0$ helped the crevice chemistry stay near neutral.

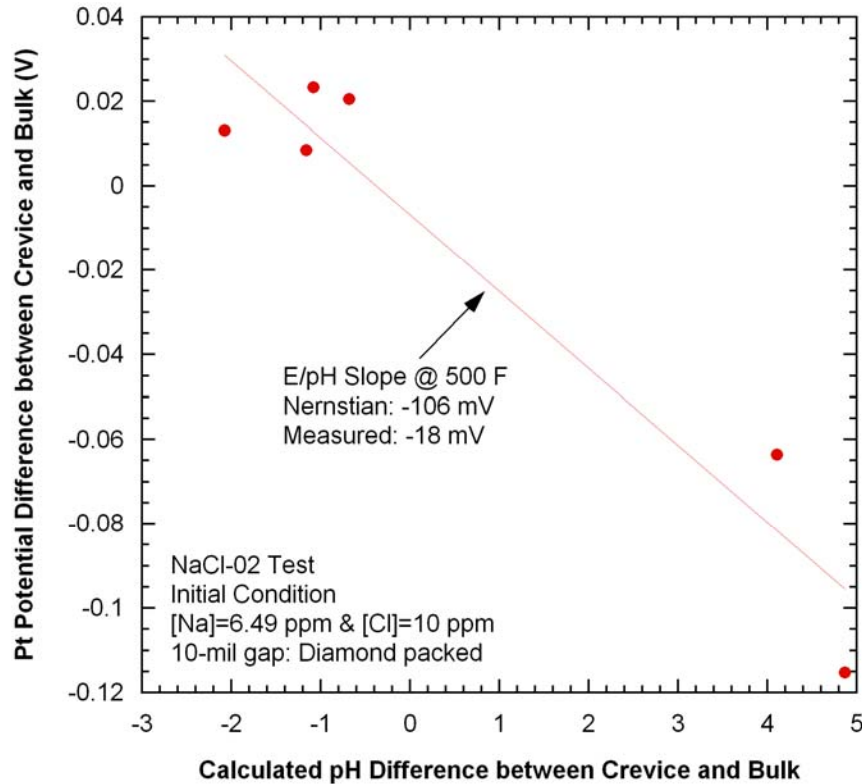


Figure 47.
Pt potential difference between crevice and bulk as a function of pH difference calculated by MULTEQ (NaCl-02).

4.2.4 Summary

Figure 48 illustrates the precipitation and concentrated phenomena in the crevice for (a) higher ΔT and (b) lower ΔT . The gap is filled with diamond powder, and a small pocket exists for signal wires, as shown in Figure 48. For higher ΔT , liquid film that condensed from the steam would exist around the signal wire, which tends to generate signals for acidic condition. On the tube surface there would be NaCl precipitation and/or Na-rich concentrated liquid film. By lowering of ΔT from 100°F to 60°F and from 80°F to 40°F, the bulk liquid would penetrate into the crevice and be mixed with the Na-rich liquid film present. The formerly precipitated NaCl at higher ΔT would be dissolved. Then, the concentrated liquid would touch the signal wire, which makes an alkaline or near neutral crevice signal. Note that this interpretation for crevice hideout phenomena with ΔT is limited to this NaCl-02 test. If ΔT increases monotonically from 40°F to 100°F, the crevice hideout phenomena as a function of ΔT will be different. Nonetheless, the NaCl-02 test has shown the MB to be a good vehicle for studying chemical hideout induced by heat transfer in prototypic SG tubes. Temperature and potential variation with time and experimental conditions were successfully monitored. The effects of crevice gap size and primary-to-secondary temperature differences were explored. The extracted solution samples from both the crevice and bulk solutions were analyzed, and the results were reasonably consistent with the potential data. However, an advanced crevice sampling method and installation of a pH electrode instead of the Pt electrode might provide a better representation of actual crevice chemistry.

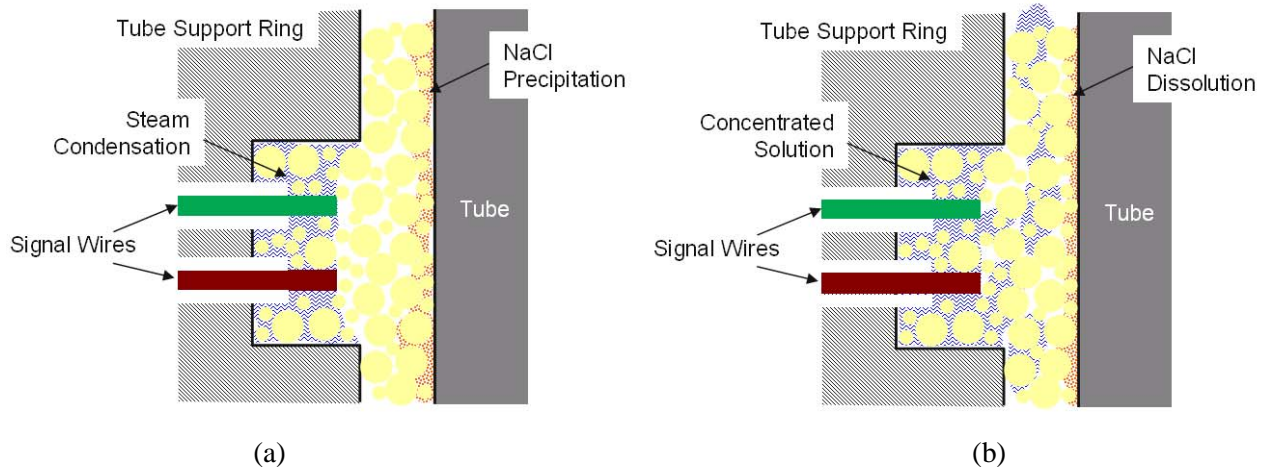


Figure 48. Schematics of the precipitation and concentration phenomena in the crevice for (a) higher ΔT (80°F and 100°F) and (b) lower ΔT (40°F and 60°F).

4.3 NaCl-03: NaCl (MR=0.3) Test

The influence of $[Na]/[Cl]$ MR on the hideout behavior and Cl volatility was investigated in tests NaCl-03 (MR=0.3) and NaCl-04 (MR=0.7) with 10 ppm Cl. The crevice hideout for MR=1.0 was investigated in NaCl-01 and -02. For the NaCl-03 and NaCl-04 tests, there were major system upgrades and test condition changes: use of magnetite (Fe_3O_4) as packing material, use of tungsten/tungsten oxide electrode as a pH sensor, and installation of a high-pressure injection pump. The experimental setup is described in Sections 2.2 and 2.3. The crevice with a radial gap of 10 mil was packed with diamond grit (127-165 μm -dia), and the crevice with a radial gap of 20 mil was packed with magnetite powder. The measured packing porosities for the 10- and 20-mil gap crevices were 33 % and 78 %, respectively. Only the 10-mil radial gap crevice had ECP electrodes due to the limitation of potential measurement system.

4.3.1 Temperature Data

Figure 49 shows the crevice temperature variation with time in the 10-mil gap crevice packed with diamond powders. Before the first solution injection, all thermocouples indicated about 10°F higher temperatures than the secondary saturation temperature of 500°F. This difference appears to be caused by the diamond powder with its extremely high thermal conductivity surrounding the thermocouple tip area. After the NaCl solution injection, all crevice temperatures started to rise gradually. At $\Delta T=60^\circ F$ and $80^\circ F$, the temperature elevation was not significant as compared with that at $\Delta T=40^\circ F$. The reference temperature data at these ΔT 's with high purity water will permit evaluating the temperature elevation induced by the chemical hideout, but unfortunately only reference data at $\Delta T=40^\circ F$ were available. As shown in Figure 49, the second NaCl solution injection to make up depleted bulk ion concentration did not affect the crevice temperatures. Normalized temperatures in the 10-mil gap crevice are plotted in Figure 50 as a function of time. The temperature difference between each crevice temperature and the bulk secondary saturation temperature was divided by the difference between the primary and secondary temperatures. The normalized crevice temperatures show that for $\Delta T=60^\circ F$ and $80^\circ F$ the increase in crevice temperatures was mainly due to the increase in the primary temperature and the temperature difference across the SG tubes; this behavior indicates that the conduction heat transfer by diamond powder is dominant at $\Delta T=60^\circ F$ and $80^\circ F$ as compared with the boiling heat transfer. However, the

normalized crevice temperature data at $\Delta T=40^\circ\text{F}$ show a different behavior from those of the two higher ΔT cases; hideout is partially responsible for the temperature elevation above the secondary saturation temperature of 500°F .

Figure 51 shows the temperature variation in the 20-mil gap crevice packed with magnetite powder. With high purity water the crevice temperatures are much closer to the secondary saturation temperature as compared with the 10-mil gap crevice, even though T8 shows higher temperature, which appears to be caused by the tip location of the thermocouple. The lower crevice temperature in high purity water with magnetite powder is attributed to the low thermal conductivity of magnetite. After the first NaCl solution injection, all thermocouples indicated a gradual temperature elevation. As observed in the 10-mil gap crevice, the significant temperature elevation did not occur at $\Delta T=60^\circ\text{F}$ and 80°F compared with that at $\Delta T=40^\circ\text{F}$. When decreasing ΔT from 80°F to 40°F , the temperatures returned to the final values of the initial $\Delta T=40^\circ\text{F}$ test. Figure 52 shows the normalized crevice temperatures in the 20-mil gap crevice packed with magnetite powder. As observed in Figure 50, the normalized temperatures did not vary with time except for $\Delta T=40^\circ\text{F}$.

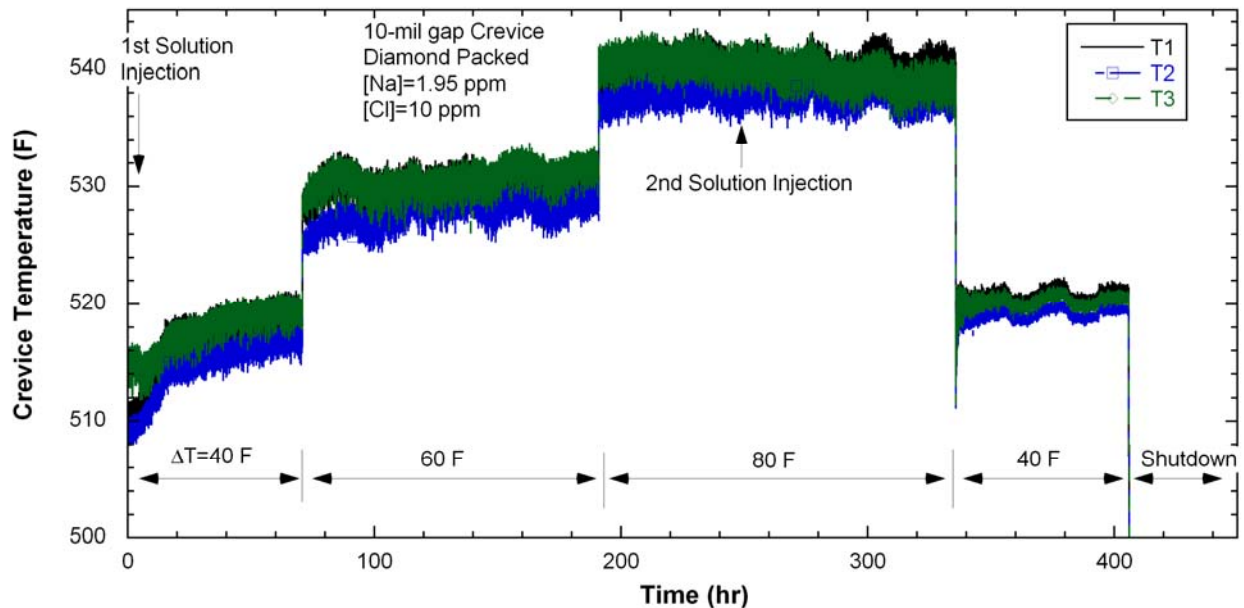


Figure 49. Crevice temperature variation with time in a 10-mil gap crevice packed with diamond powder (NaCl-03).

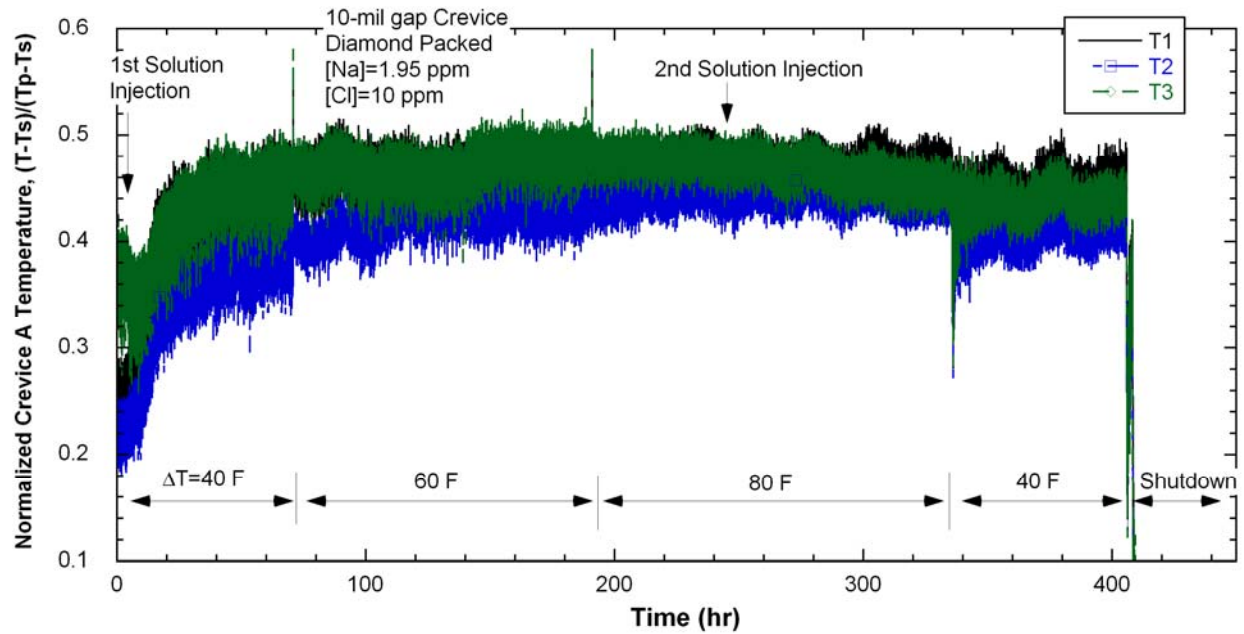


Figure 50. Normalized crevice temperature variation with time in a 10-mil gap crevice packed with diamond powder (NaCl-03).

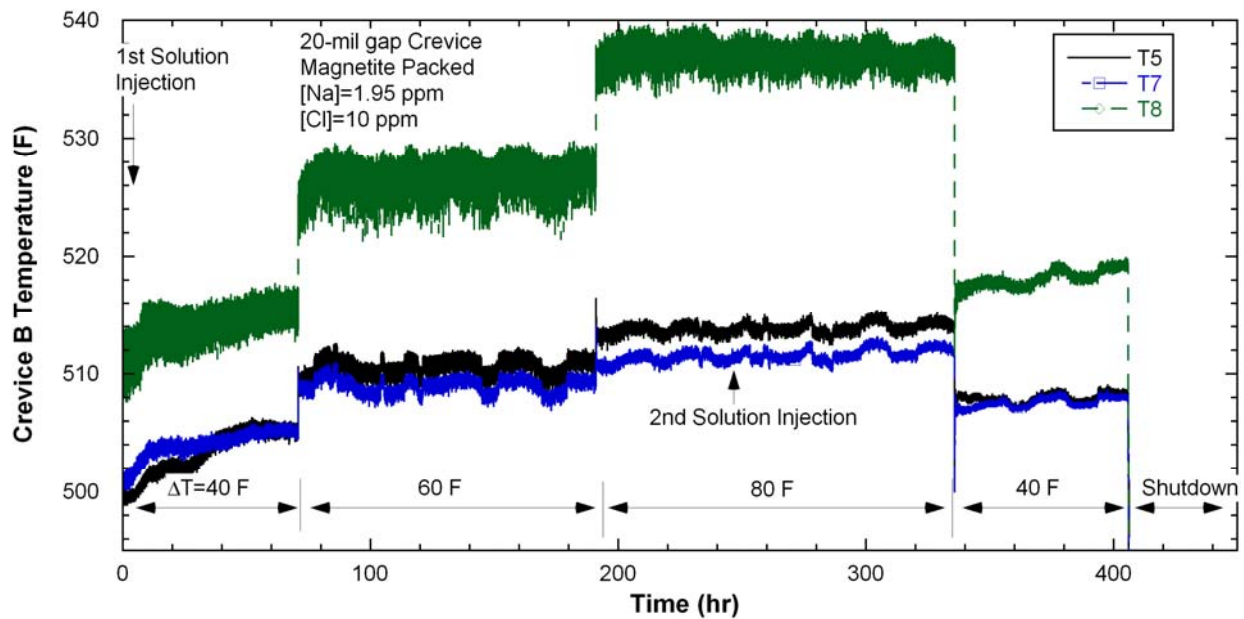


Figure 51. Crevice temperature variation with time in a 20-mil gap crevice packed with magnetite powder (NaCl-03).

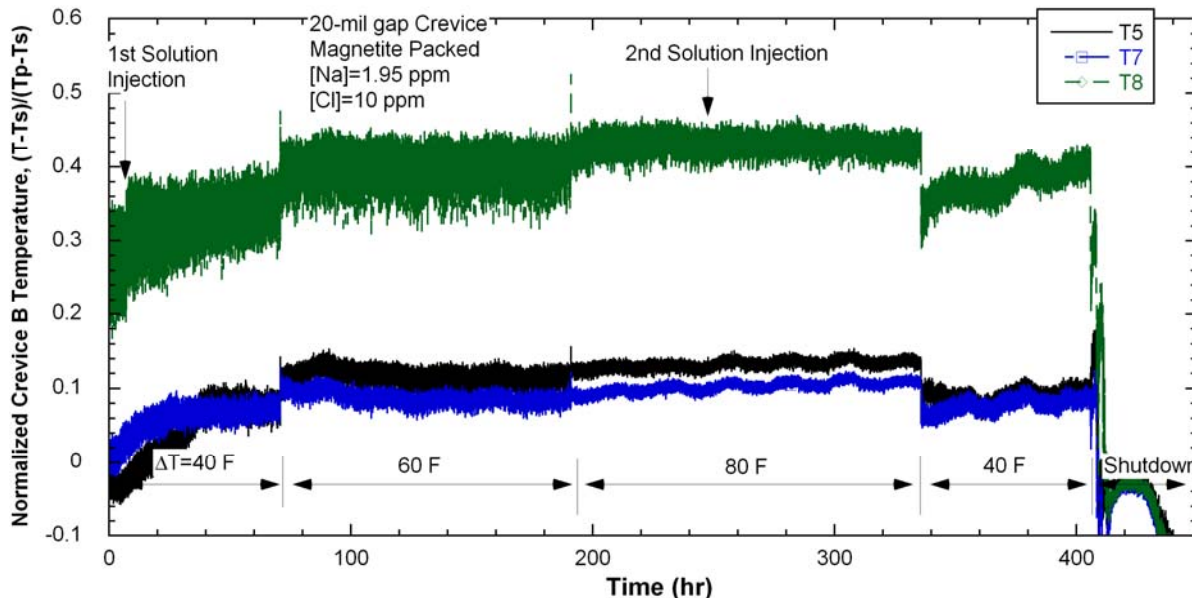


Figure 52. Normalized crevice temperature variation with time in a 20-mil gap crevice packed with magnetite powder (NaCl-03).

4.3.2 Bulk & Crevice Chemistry

The variations in bulk conductivity and the ion concentrations for bulk samples are plotted in Figure 53. The bulk conductivity responded quickly to the change of the bulk solution chemistry. At $\Delta T=40^{\circ}\text{F}$, large hideout was indicated by the bulk conductivity change, which is much greater than that of the previous test NaCl-02 with $\text{MR}=1.0$, but in the NaCl-02 test, $\Delta T=80^{\circ}\text{F}$ was followed by $\Delta T=40^{\circ}\text{F}$. The IC analysis for Cl showed better fit to the bulk conductivity variation than the ISE results. The ISE tends to underestimate the Cl concentration. The plateau that occurred after the second NaCl solution injection is attributed to the bulk conductivity exceeding the upper limit of the conductivity meter. The accumulated impurity mass or concentration in crevices can be estimated from the bulk solution analysis. This is discussed in Section 4.3.4.

Figure 54 shows crevice conductivity versus bulk conductivity for the 10-mil gap crevice. The crevice conductivity started to show hideout 40 hrs after introducing the NaCl. We attribute this effect to the fact that, as impurity concentration in the crevice proceeded, the pore between the two conductivity probes became filled with concentrated liquid rather than steam, which caused the conductivity signal to start increasing. The additional increase in crevice conductivity after the ΔT increased from 40°F to 60°F was attributed to the increase of the impurity concentration in the crevice. The plateau of the crevice conductivity at $\Delta T=60^{\circ}\text{F}$ (from 90 to 140 hours in Figure 54) occurred because the actual conductivity exceeded the upper limit of the measurement of the conductivity meter. The drop and sudden recovery of crevice conductivity at 120 hours occurred because, at this time, the steam phase was located between the two conductivity probes, which blocked the electric path. The gradual decrease of conductivity at $\Delta T=60^{\circ}\text{F}$ could be attributed to several causes. In general crevice conductivity can vary in three ways: a liquid-to-vapor ratio change between the two conductivity probes, an ion composition/concentration change, and salt precipitation. At $\Delta T=60^{\circ}\text{F}$, based on the temperature data, it is not likely that NaCl precipitation occurred because the measured superheat was less than that for the NaCl solubility limit, 46°F . The ion composition and concentration might have changed; metal cations were released by corrosion of alloy 600 tubing and Na diffused out of the crevice, which is called electromigration effect

and is discussed again in Section 6.3.6. The crevice chemistry change at that time is supported by the increase in bulk Na concentration and post-test tube surface examination revealing heavy gouging. After changing ΔT from 60 to 80°F, the crevice conductivity decreased more, which is interpreted as the result of all three possible causes. Precipitation of NaCl might have occurred on the tube surface, and steam phase might have become dominant. But a change in liquid-to-vapor ratio is more likely because higher ΔT brings a higher boiling rate and more steam phase. However, the crevice conductivity variation and scattering after the 2nd solution injection is difficult to be explained by three ways. After the decrease of ΔT from 80°F to 40°F, the conductivity signal becomes noisy again and fluctuates presumably because of the residual chemistry developed during $\Delta T=80^\circ\text{F}$ test.

Figure 55 shows the analysis results for crevice solution samples. The ICP and IC analyses for the 10-mil gap crevice packed with diamond showed higher Na and Cl concentrations at $\Delta T=40^\circ\text{F}$ and 60°F than that at $\Delta T=80^\circ\text{F}$, probably because at a higher ΔT the steam phase was more dominant so that more steam was extracted from the solution line. For the 20-mil gap crevice packed with magnetite, the Cl ion concentration was much higher than the Na ion concentration, and the molar ratio was less than 0.2 in most samples based on the IC results. These findings suggest that either Cl is preferentially concentrated in the magnetite-packed crevice or the steam phase is more dominant at the same ΔT as compared with a diamond-packed crevice. The absolute concentration of Na and Cl in the magnetite-packed crevice was much lower than that in the diamond-packed crevice. This result suggests that it takes much longer for impurities to be concentrated in the magnetite-packed crevice than in the diamond-packed crevice, and the wider gap results in a higher mixing tendency between crevice and bulk solutions and leads to lower concentration. The ISE ion concentration results are also plotted in Figure 55. The ISE tends to have better accuracy for higher concentration (>100 ppm). At lower concentration, the ISE underestimates the Cl concentration, and the ISE is not consistent with ICP analysis results for Na especially at lower concentrations (<100 ppm).

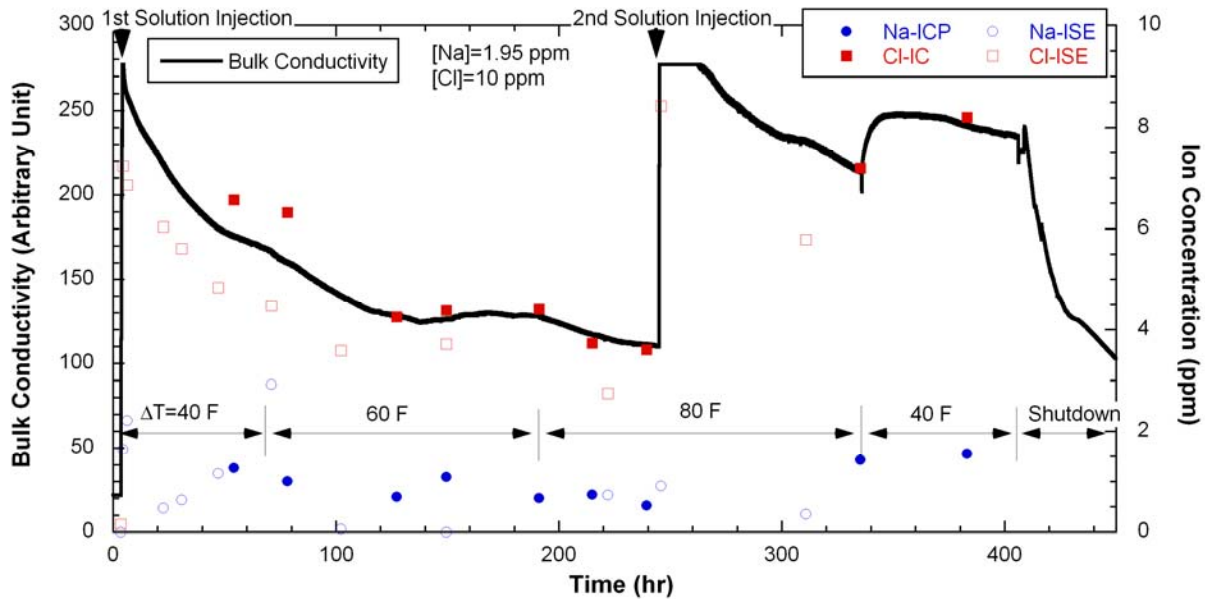


Figure 53. Variation in bulk conductivity and ion concentration with time (NaCl-03).

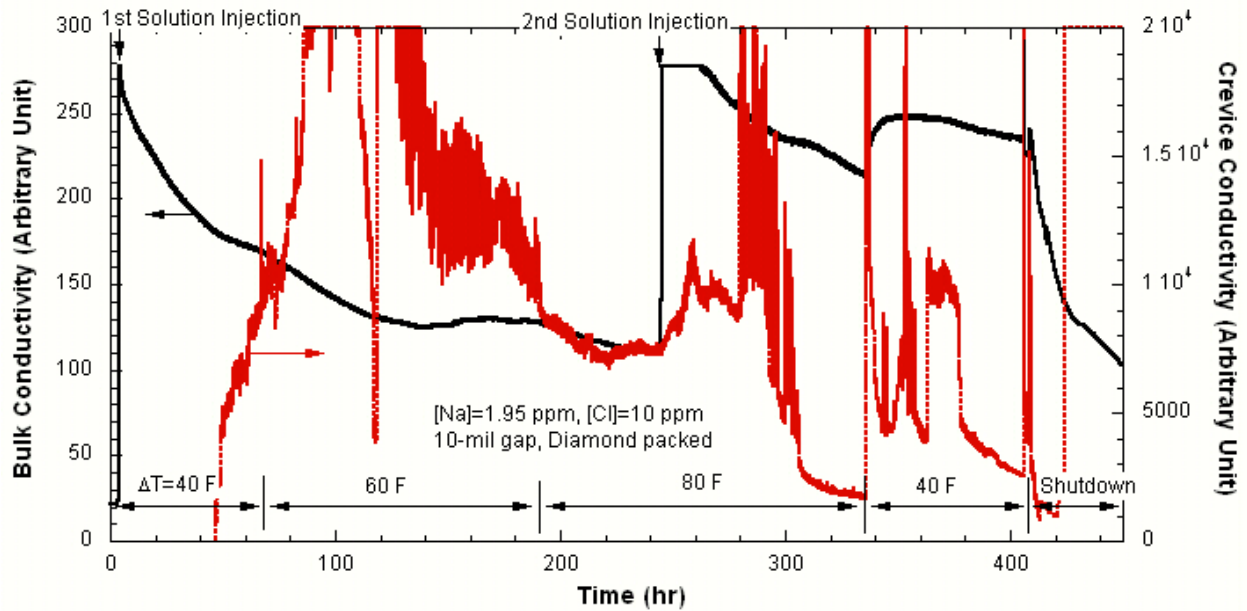


Figure 54. Variation in bulk and crevice conductivity with time in a 10-mil gap crevice packed with diamond powder (NaCl-03).

The sudden drop of crevice concentration in the sample taken at 120 hours was followed by the recovery of concentrations for both Na and Cl. To better understand this unexpected crevice concentration drop and recovery, the crevice concentrations in solution samples were compared with the crevice conductivity variation shown in Figure 56. Taking into consideration the time delay in the crevice solution samples, we concluded that when the sudden crevice conductivity dropped is close to when the crevice ion concentration dropped. The crevice temperature data did not show any significant change at that time, but this result suggests that crevice instability possibly happens for short periods.

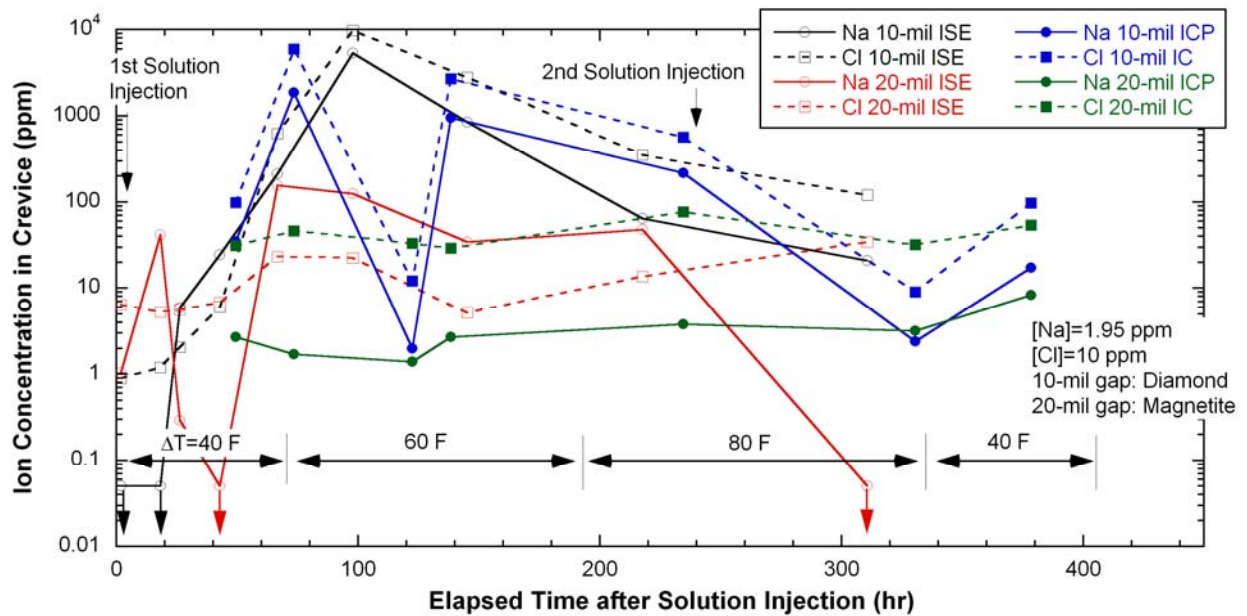


Figure 55. Concentration results for crevice solution samples by using ICP/OES for Na, IC for Cl, and ISE for Na and Cl (NaCl-03).

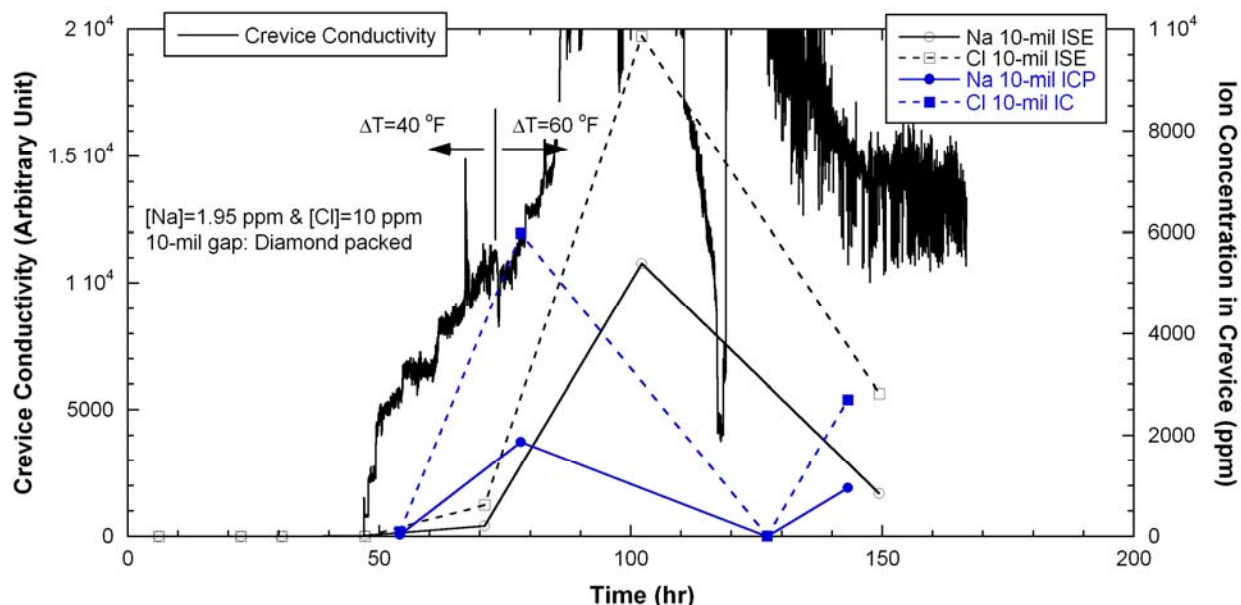


Figure 56. Crevice conductivity variation with time in the 10-mil gap crevice packed with diamond along with analysis results of crevice samples (NaCl-03).

4.3.3 ECP Measurement

The Pt electrode potentials in the bulk and the 10-mil crevice are plotted in Figure 57. Right after the first injection of MR=0.3 NaCl solution, the bulk and the crevice potentials increased because the MR=0.3 NaCl solution is more acidic than pure water. After this test, NaCl-03, the Pt electrode was not used to estimate the solution pH. The crevice Pt potential did not significantly vary with ΔT except for an initial transient period. The oscillation of the Pt bulk electrode potential for the initial 20 hours may be attributed to the dissolved oxygen that originated from the injected solution, which might not have been sufficiently purged. After the second NaCl solution injection, the bulk and crevice potentials increased. Based on the rapid response of the crevice potential to the bulk chemistry change, it is likely that the 10-mil gap crevice was mixed well with the bulk water due to the highly permeable diamond packing. Figure 58 shows the Ni electrode potential variation with time. As was observed in the Pt electrode potential, the Ni electrode potentials in the bulk water and crevice responded quickly to the bulk chemistry change. The crevice Ni potential gradually decreased, probably because Na was preferentially concentrated, and this decrease led to the increase of crevice pH. However, to estimate the crevice pH, the tungsten electrode potentials should be used. The Ni electrodes in the bulk solution and the crevice showed as quick a response to the second NaCl solution injection as the Pt electrodes.

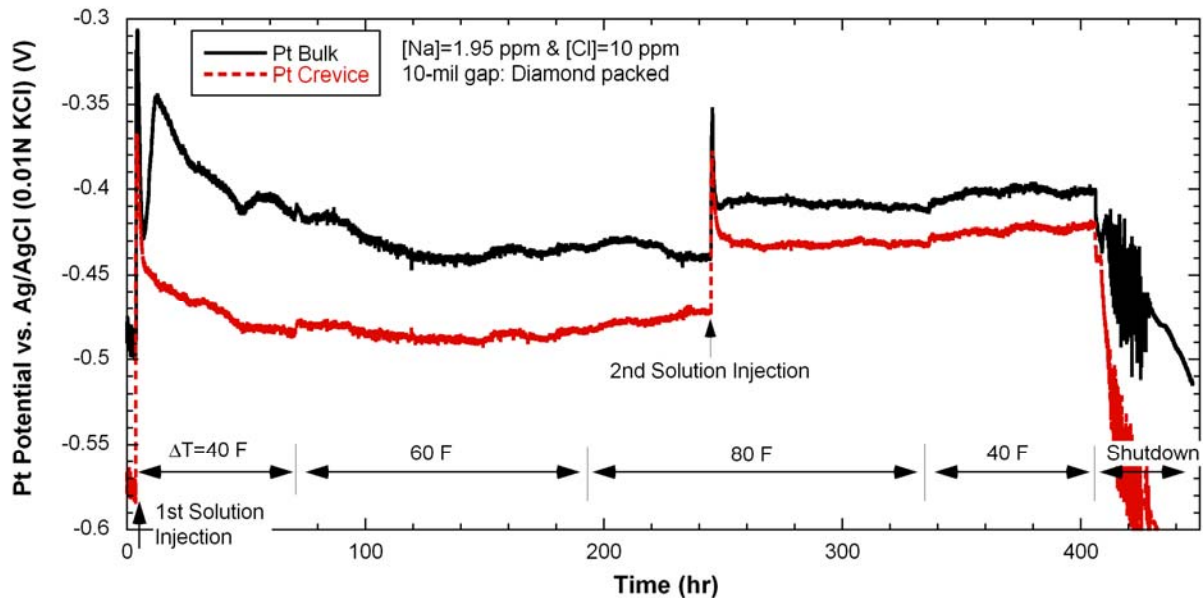


Figure 57. Variations in Pt electrode potential with time in bulk and 10-mil gap crevice packed with diamond (NaCl-03).

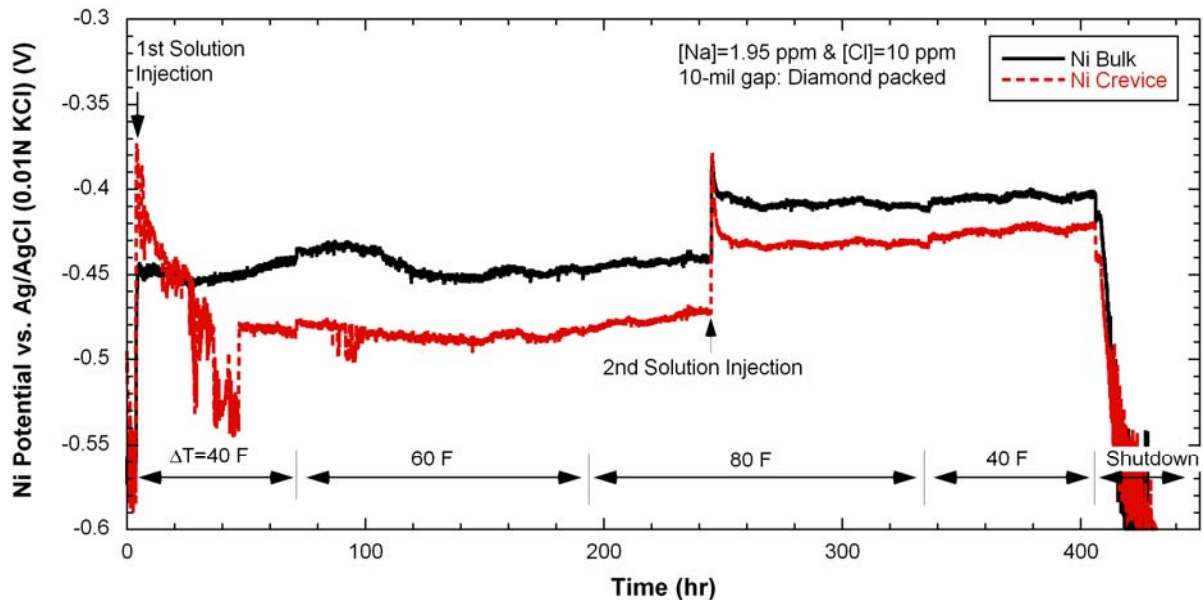


Figure 58. Variations in Ni electrode potential with time in bulk and 10-mil gap crevice packed with diamond (NaCl-03).

The tungsten potentials measured in the 10-mil gap crevice and the bulk solution are plotted in Figure 59. These potentials increased after the first NaCl solution injection because the bulk solution was acidified by the test solution injection from a neutral condition of high purity water. Then, the crevice tungsten potential dropped quickly, followed by a more gradual decrease. This finding might be interpreted as meaning that because of the volatility effect of Cl, less volatile Na was preferentially concentrated. The crevice pH increase associated with the crevice tungsten potential decrease was expected with the increase of ΔT because the volatility effect of Cl becomes more significant at higher boiling rate. However, the crevice tungsten potential slowly moved in a positive direction until the end of

the test even though ΔT was increased, which does not support the expected volatility effect of Cl with ΔT variation. The measured crevice pH based on tungsten electrode potentials tends to reflect the decrease of crevice pH with ΔT . This observation may be attributed to the location of the tungsten electrode tip. As reported by Baum,³ Na is expected to be preferentially concentrated right on the tube surface. If the tungsten electrode tip is located away from the tube surface, volatilized Cl from the surface would be present around the tungsten tip area and might become dominant with the increase of ΔT .

The bulk tungsten potential showed a gradual decrease with time until the second solution injection. This potential decrease may be interpreted as a bulk solution pH increase. But it should be noted that, as discussed earlier with regard to Figure 44, bulk solution pH can be increased by the dilution of ion concentration itself, even if the Na-to-Cl molar ratio is constant. After the second solution injection, the bulk tungsten potential increased. It was intended to bring the bulk potential to the initial value after the first injection, but the potential value was slightly higher than that because more Cl ion was injected than needed. The potential difference between the bulk and crevice appears to be consistent even after the second solution injection, which is evident in Figure 60. After the ΔT was decreased from 80°F to 40°F, the bulk tungsten potential increased due to the return of Cl and Na to the bulk solution, and it then stabilized. After the MB shut-down, the potential difference between the bulk and crevice increased, and this result might indicate that the crevice had become more acidic during this test.

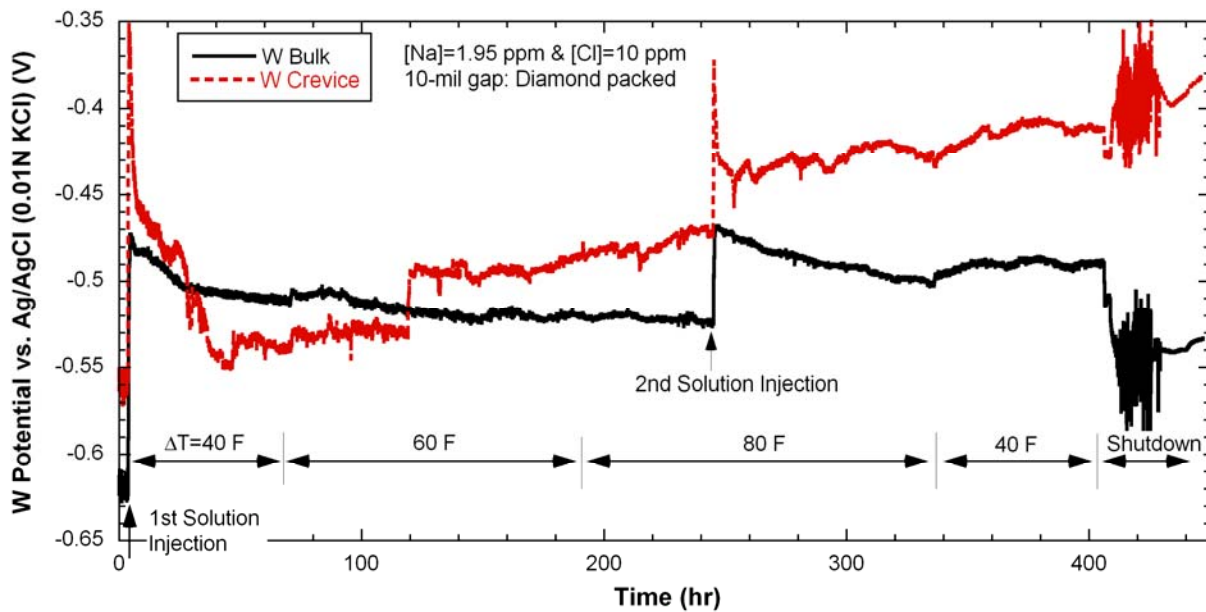


Figure 59. Tungsten electrode potential variations with time in bulk and 10-mil gap crevice packed with diamond (NaCl-03).

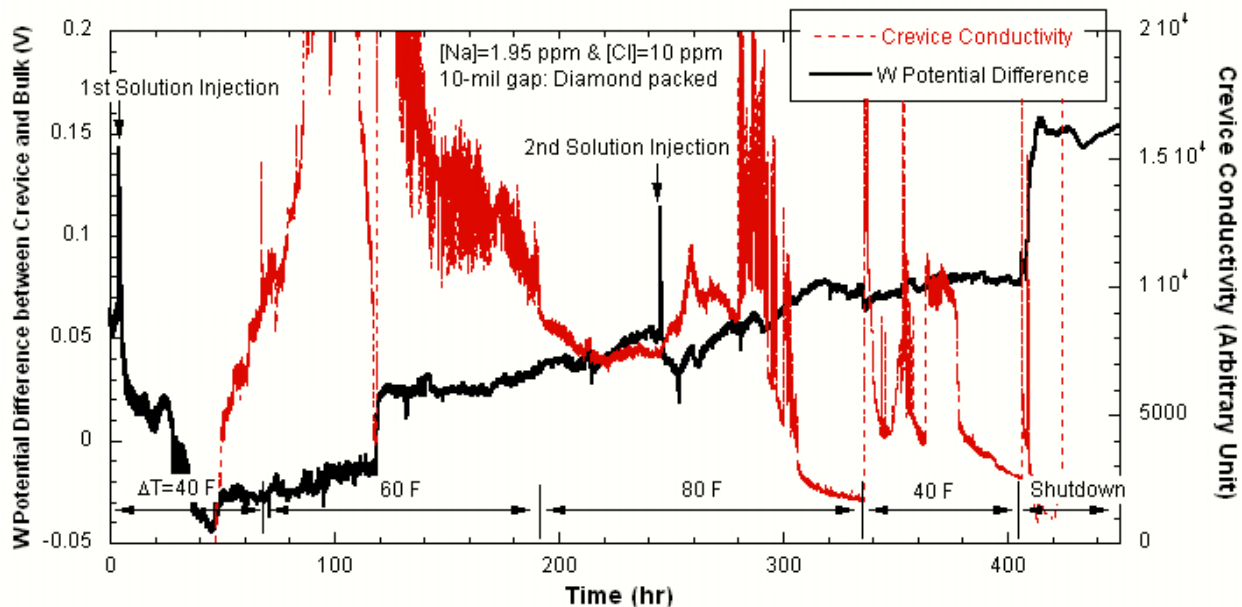


Figure 60. Tungsten potential difference between crevice and bulk compared with crevice conductivity variation in 10-mil gap crevice packed with diamond (NaCl-03).

Figure 60 shows the variations in the tungsten potential difference between the crevice and bulk, as well as the variations in crevice conductivity. The crevice was more alkaline than the bulk during the period of 30-120 hours. The time when the crevice conductivity dropped exactly corresponds to the time when the crevice tungsten potential suddenly jumped. At 120 hours, it is possible that steam was generated near the crevice conductivity probes and this steam also affected the crevice tungsten potential. The higher ΔT and resultant increased steam phase might maintain the increased crevice tungsten potential. The tungsten potential difference did not change significantly after the second NaCl solution injection. The potential difference did not return to the previous value after decreasing ΔT from 80°F to 40°F but maintained a similar value. Since the second $\Delta T=40^\circ\text{F}$ test had a different operating history from the first one, the tungsten potential difference is not supposed to be the same. Formerly precipitated NaCl or the chemistry that developed at $\Delta T=80^\circ\text{F}$ would affect the chemistry when the ΔT returned to 40°F.

4.3.4 Discussion

Potentials and pH Analysis

Figure 61 shows the tungsten potential difference as a function of the pH difference between the bulk and 10-mil crevice samples. The sample pH was calculated by using the MULTEQ code based on the solution sample analysis. The tungsten potentials measured at the time when the crevice and bulk samples were taken are used in this figure. The calculated pH difference data indicate that the crevice pH is always lower than the bulk pH. The tungsten potential difference data agreed with the calculated pH difference, except for two data points suggesting that the crevice was more alkaline than the bulk. A trend is not apparent from the data shown in Figure 61. The data in Figure 47 showed at least a linear relationship, even though the slope was far from ideal behavior. Because of the data scattering in Figure 61, the crevice and bulk data were plotted independently. The tungsten potentials measured in the crevice and the bulk are plotted as a function of predicted pH by MULTEQ in Figure 62. The bulk data show

good linear behavior, while the crevice data still do not show any linearity between tungsten potential and solution pH. The measured ECP/pH slope for bulk solution data is -88 mV/pH, which is close to the Nernstian value of -106 mV at 260°C (500°F). The bulk data in Figure 62 confirm that the tungsten electrode can be used as a precise pH electrode at high temperature and in a slightly acidic environment. The data scattering of the crevice data can be attributed to several factors: possible problems during the electrode preparation, the location of the tungsten electrode tip with respect to the tube surface, the total exposed area of the tungsten electrode tip, the accuracy of the MULTEQ calculation, and the representativeness of the crevice solution samples. The bulk and crevice tungsten electrodes were prepared with the same materials and procedures, so that the electrode preparation appears appropriate. The location of the crevice tungsten electrode tip might be far from the tube surface so that the tungsten potentials did not represent the actual crevice pH variation well. The total exposed area of the tungsten electrode tip may be a problem. The bulk electrode has an exposed wire tip that is about 6-7 mm long, but the crevice tungsten electrode has an exposed tip that is only about 1 or 2-mm long, which might decrease the electrode sensitivity. However, the crevice electrode tip cannot be exposed too much if we want to measure the narrow-gap crevice chemistry. The MULTEQ-predicted pH appears to have a reasonable accuracy because the bulk tungsten potentials are well fitted to the bulk sample pH calculated by MULTEQ. The dilution of crevice samples is possible since the crevice and bulk solution interact, but it is difficult to quantitatively evaluate the dilution effect of crevice samples.

One possible correction for the crevice samples data is to consider the time delay effect determined by the dead volume of the sample extraction line and valve, as mentioned in Section 3.2.2. The total dead volume of the extraction line and valve is 90 μ L, and the volume of crevice sample varied from 50 to 100 μ L. For a simple correction, if the volume of crevice sample is equivalent to that of the dead volume of the extraction line, a crevice sample taken at certain time represents the chemical condition at the time when the very last sample was taken. Crevice tungsten potentials were corrected based on the time delay effect, as shown in Figure 63. Crevice data still show scattering but at least appear to roughly show a decreasing trend with pH. The bulk data did not have to be corrected because there was enough sample volume. The bulk ECP/pH slope after including one more data point measured before chemical injection is much closer to the Nernstian value compared with the data in Figure 62. As discussed in the post-test examination, severe gouging was observed on the tube surface. Therefore, the crevice pH estimation from the crevice samples appears to represent the corrosive crevice chemistry developed in this test.

Figure 64 shows the MR variations as a function of time in the bulk and 10- and 20-mil gap crevices. The MR in the 10-mil gap crevice is always higher than that in the bulk. The MR data cannot specify the solution pH but can suggest the preferential Na concentration in the diamond-packed crevice. The bulk MR was varied within the range of 0.2-0.3, except for one point at 150 hours. At that time the analysis results for bulk samples indicated the return of Na ion from crevices, which increased the bulk MR. The reason for the Na return from crevices is given in Section 4.4.5, but briefly, metal cations generated by the tube corrosion could be driving Na ions out of the crevice. The MR in the 20-mil gap crevice tends to follow the bulk MR variation tendency, and this trend suggests that the extracted sample from the 20-mil gap crevice might contain a significant amount of bulk solution.

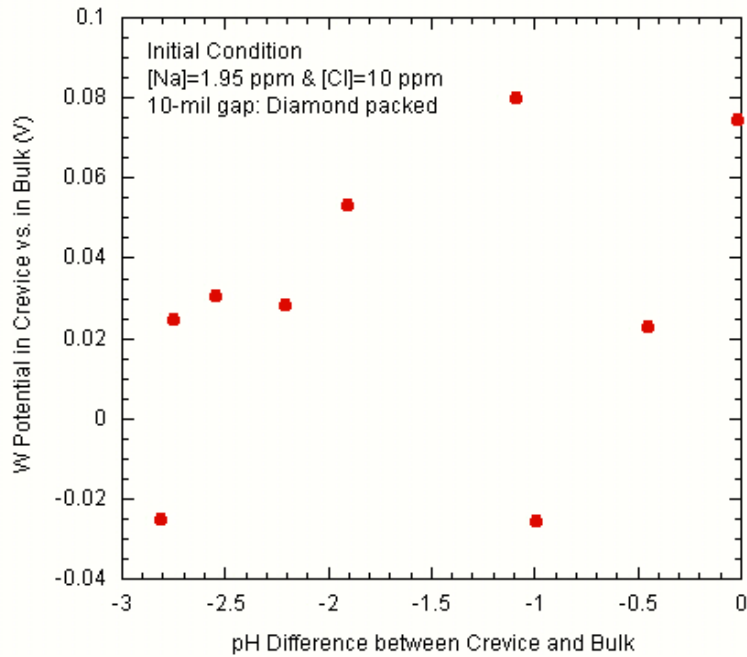


Figure 61.
Plot of MULTEQ-predicted pH difference and tungsten potential difference between bulk and 10-mil gap crevice packed with diamond (NaCl-03).

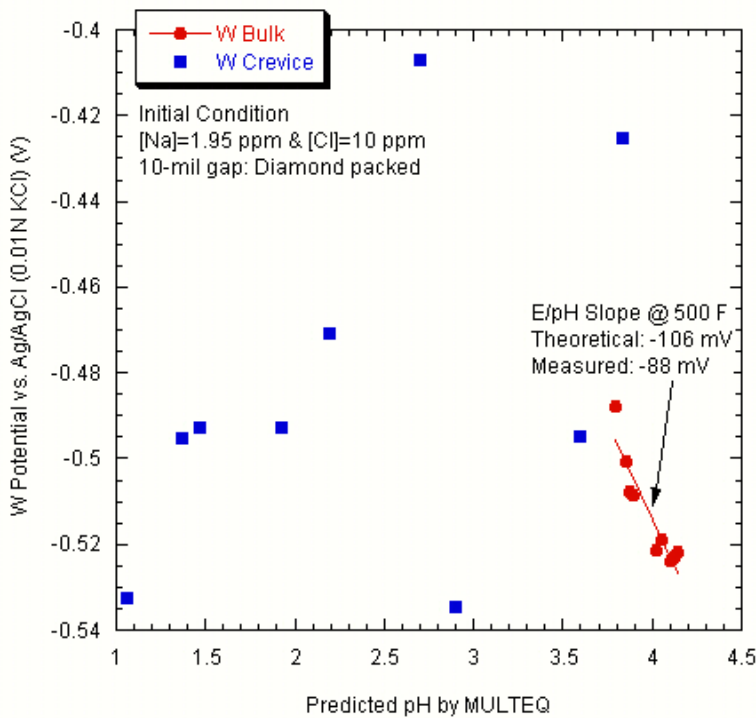


Figure 62.
Tungsten potential measured in crevice and bulk as a function of predicted pH by MULTEQ (initial [Na]/[Cl]=0.3; NaCl-03).

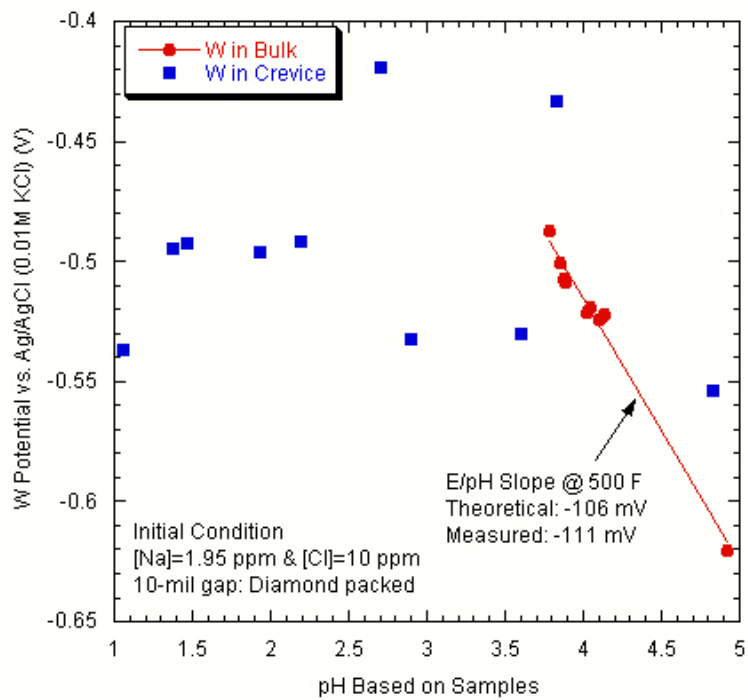


Figure 63. Tungsten potentials as a function of the calculated pH based on solution samples from crevice and bulk (NaCl-03).

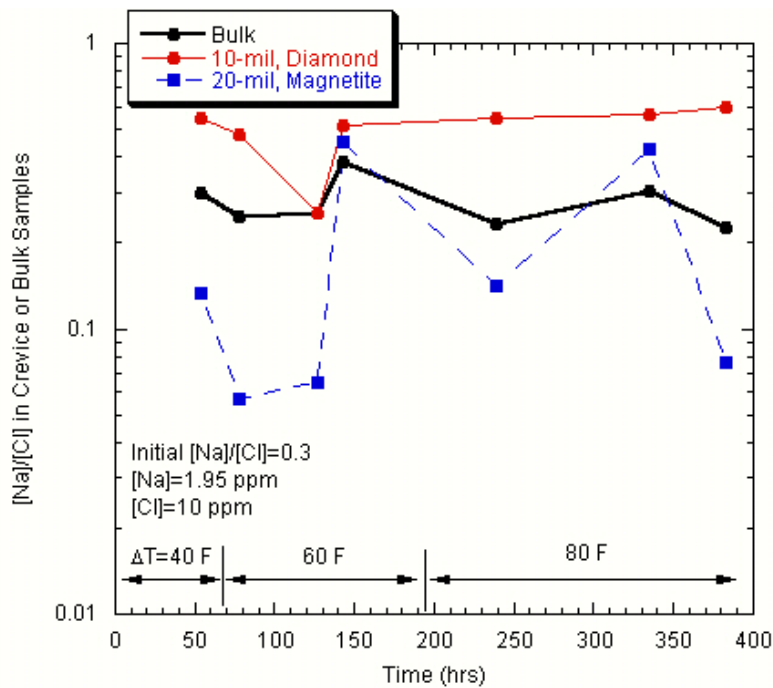


Figure 64. Molar ratio variations as a function of time in bulk and crevices (NaCl-03).

Mass Balance Analysis

Since the Argonne MB is a closed system, the crevice impurity accumulation can be calculated from the bulk chemical analysis data over time. Figure 65 shows the total accumulated moles of Na and Cl in the crevices as a function of time. The loss of impurity mass by crevice and bulk solution sampling was also considered in calculating the mass balance. The data measured before additional NaCl impurities were injected into the bulk at the elapsed time of 240 hrs were used. Since the atomic weights of Na and Cl are different, a molar unit was used instead of a mass unit. The MR for total accumulated Na and Cl does not correspond to any MR in either diamond- or magnetite-packed crevices. Its value is between the MRs of the diamond-packed crevice and bulk. It appears that Na concentrates preferentially in a diamond-packed crevice and Cl concentrates preferentially in a magnetite-packed crevice. Since, with bulk chemistry data, we cannot distinguish how much impurity hides out in diamond- and magnetite-packed crevices, respectively, a single- rather than a double-crevice test would be more appropriate for the crevice estimation with the bulk data in a closed system like the Argonne MB. As shown in Figure 65, Cl concentration tends to reach a steady state at each ΔT , while the Na concentration does not. The hideout rate into a crevice usually depends on the bulk concentration. Since the MR of the test solution is 0.3, the bulk concentration of Na is much less than that of Cl, and it thus takes longer to reach a steady state. The Na and Cl moles in the crevice vs. ion exposure is shown in Figure 66. The “exposure” is defined by the integration of the variation in bulk concentration with time. We can compare each ion’s hideout rate with the exposure unit regardless of the bulk concentration. As shown in Figure 66, the hideout rates of Na and Cl appear to be similar. But, when interpreting these hideout rates, one should note the two different crevice packings used in this test. It is likely that the preferential Na hideout in the diamond-packed crevice and the preferential Cl hideout in the magnetite-packed crevice made a similar contribution to the bulk impurity change. A single crevice test is recommended for estimation of the precise crevice hideout.

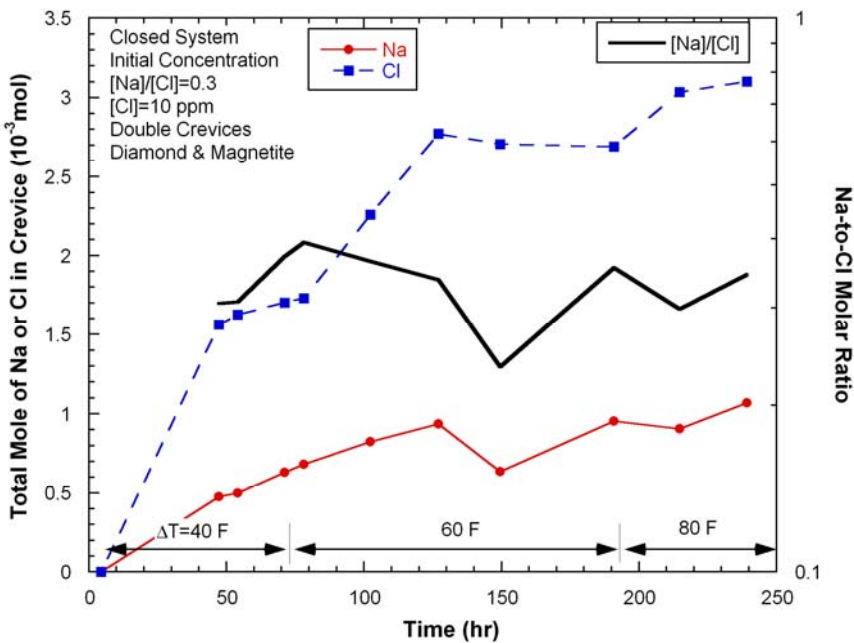


Figure 65.
Total accumulated moles of Na and Cl in crevices as a function of time (NaCl-03).

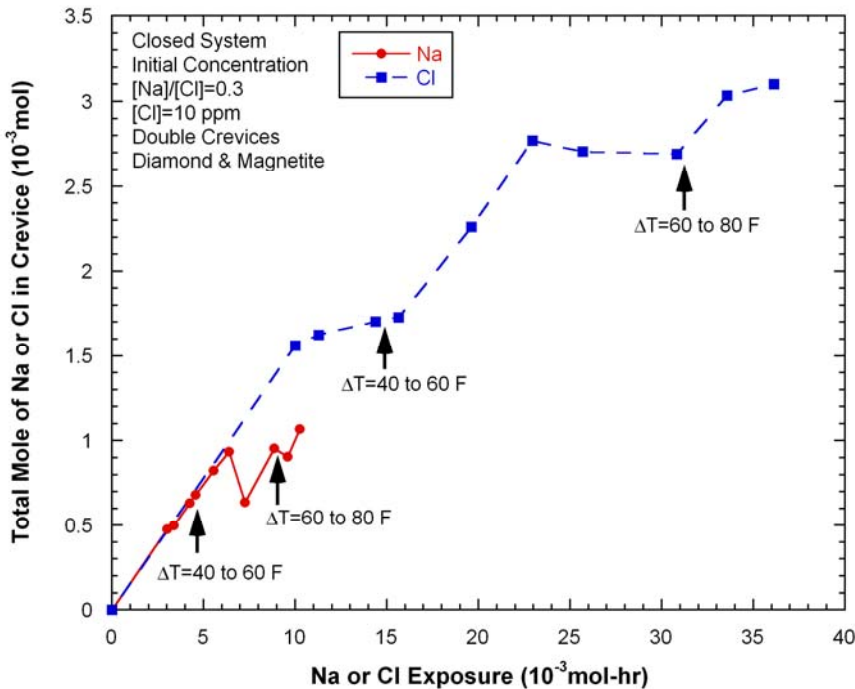


Figure 66. Total accumulated moles of Na and Cl in crevices as a function of exposure (NaCl-03).

4.3.5 Summary

We introduced W/WO_x electrodes as pH electrodes in the crevice and the bulk water chemistry. In the bulk water chemistry with MR=0.3, the W/WO_x electrode showed a good linearity with respect to the pH variation, and the ECP/pH slope was close to the Nernstian value. The crevice tungsten potential indicated that the crevice was initially alkalinized due to the volatility of Cl, followed by its gradual acidification with time and ΔT . Crevice samples and the post-test examination, which are discussed in Section 4.4.5, indicated that a strongly acidic crevice packed with diamond had developed during the NaCl-03 test. Bulk conductivity variation and bulk samples indicated that Na ions were driven out of the crevice at $\Delta T=60$ °F. This behavior might be caused by the accumulation of metal cations and resultant Na ion's migration to conserve charge neutrality. Molar ratio analysis for crevices and bulk samples showed that the MR in the diamond-packed crevice was always higher than that in the bulk. For the magnetite-packed crevice, Cl appears to be preferentially concentrated as compared with the diamond-packed crevice, probably because of adsorption of Cl to magnetite. In double crevice tests, it is difficult to estimate how much impurity is concentrated at each crevice from bulk concentration data.

4.4 NaCl-04: NaCl (MR=0.7) Test

The NaCl-04 test followed the NaCl-03 test without opening of the MB. The secondary chamber was cleaned with high purity water several times to remove possible residual Na and Cl ions. The test water was prepared with NaCl powders and concentrated HCl solution. The test solution was injected by means of a high-pressure injection pump when the primary and secondary temperatures became stabilized with high purity water. The crevice packing and configurations are the same as those for the NaCl-03 test. The detail test system and instrumentation are described in Sections 2.2 and 2.3.

4.4.1 Temperature Data

The temperature variations with time in the 10-mil gap crevice are plotted for NaCl-04 in Figure 67. The temperature increased gradually after the solution injection and stabilized after 20 hours. After changing ΔT from 40 to 60°F and from 60 to 80°F, the time-dependent temperature increase was not observed, but the crevice temperature remained nearly constant. As compared with the NaCl-03 test, the crevice temperatures with high purity water were higher. This observation suggests that the NaCl from the previous test, NaCl-03, was not completely returned to bulk water, and the crevice still had some impurities. The steady-state crevice temperatures at each ΔT were almost the same as those in the previous test, shown in Figure 49. Figure 68 shows the variations in normalized crevice temperature with time in the 10-mil gap crevice packed with diamond powder. The crevice temperature elevation is clear at $\Delta T=40^\circ\text{F}$. The normalized temperatures do not significantly change after increasing ΔT , indicating that conduction heat transfer is dominant in the crevice. As shown in Figures 67 and 68, the T2 thermocouple read 4-5°F lower temperature than it did in the previous test. This thermocouple was probably not fixed rigidly enough, and its position might have moved slightly out from the tube surface during cool-down or heat-up.

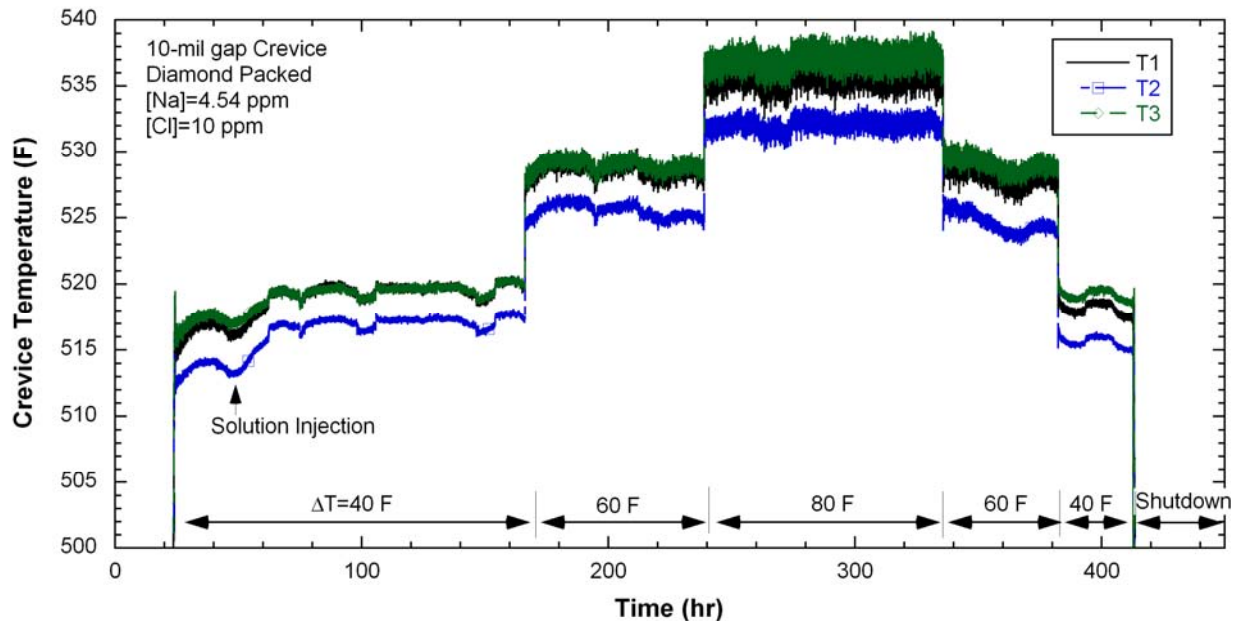


Figure 67. Temperature variation in 10-mil gap crevice with time and locations of TCs (initial $[\text{Na}]/[\text{Cl}]=0.7$; NaCl-04).

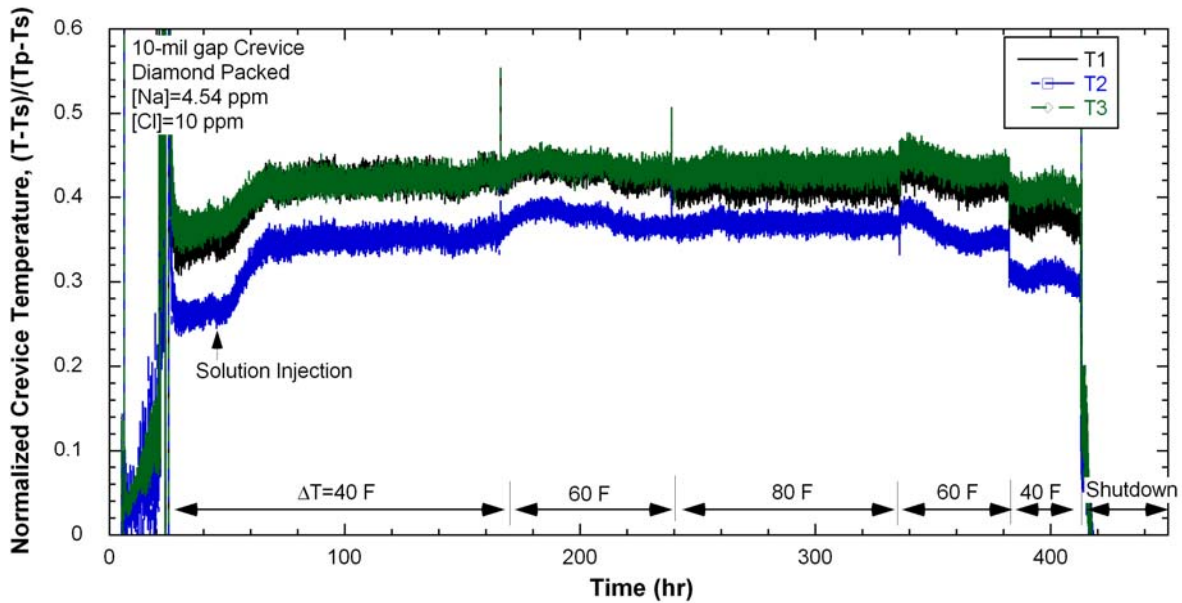


Figure 68. Normalized temperature variation in 10-mil gap crevice (initial [Na]/[Cl]=0.7; NaCl-04).

In Figure 69, the crevice temperature variations with time in the 20-mil gap crevice are plotted. The temperature at T5 only increased after the solution injection and dropped suddenly during $\Delta T=80^\circ\text{F}$. However, the other two thermocouples did not show any temperature increase, as they did in the previous test, NaCl-03. Some magnetite powder may have been dislodged from the crevice after the NaCl-03 test. At $\Delta T=80^\circ\text{F}$, T5 suddenly dropped to the bulk solution temperature, indicating that the boiling phenomenon in the magnetite-packed crevice is not stable or that the magnetite powder moved around in the crevice. Normalized temperatures in the 20-mil gap crevice are plotted as a function of time in Figure 70. The normalized temperature was relatively independent of the change in ΔT . This behavior indicates that conduction heat transfer is dominant in both the 20- and 10-mil gap crevice.

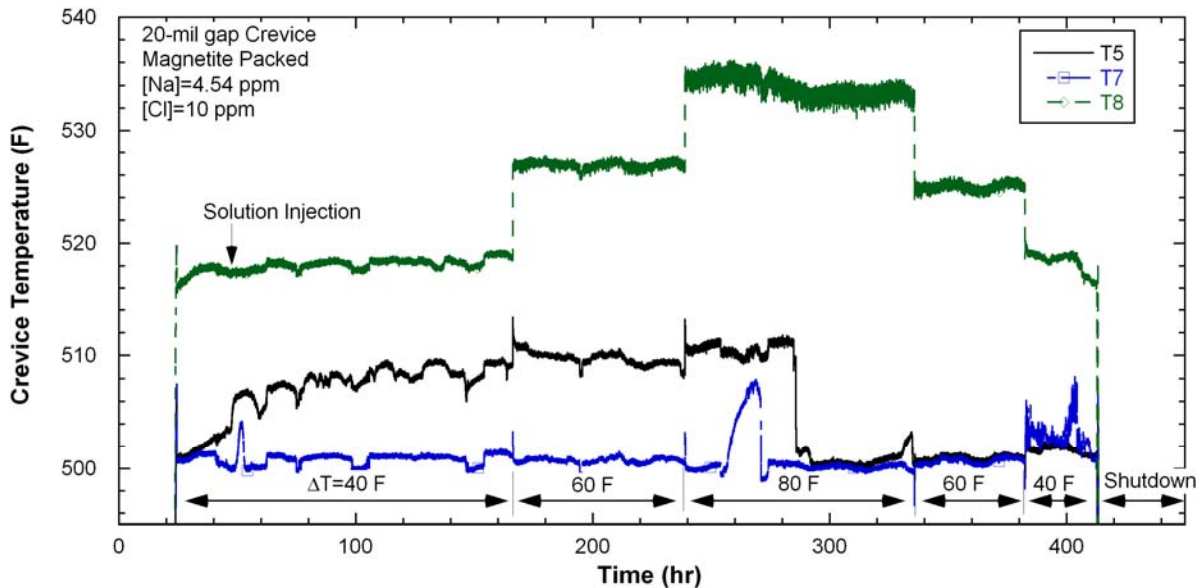


Figure 69. Temperature variation in 20-mil gap crevice with time and locations of TCs (initial [Na]/[Cl]=0.7; NaCl-04).

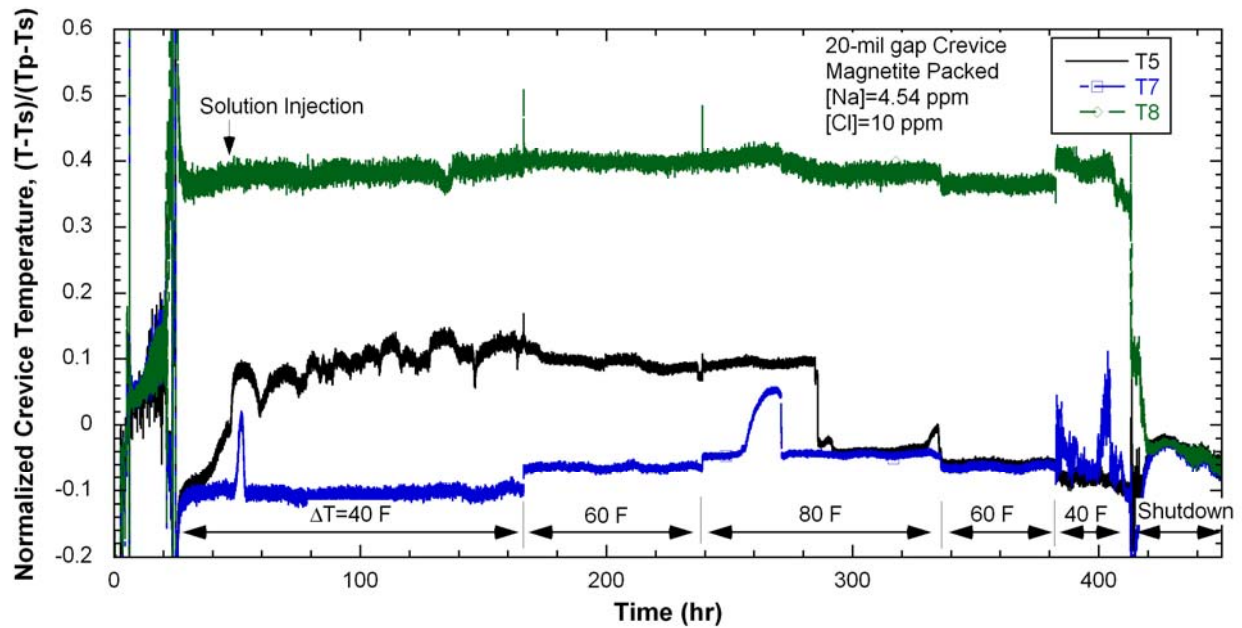


Figure 70. Normalized temperature variation in 20-mil gap crevice (initial [Na]/[Cl]=0.7; NaCl-04).

4.4.2 Bulk & Crevice Chemistry

The variations in the bulk conductivity and the bulk solution analysis are plotted as a function of time in Figure 71,. The ion concentrations are consistent with the measured bulk conductivity. The bulk conductivity did not reach a steady state and increased with decreasing ΔT . In Figure 72, the crevice conductivity in the 10-mil gap crevice packed with diamond is plotted as a function of time. The crevice conductivity increased quickly after the solution injection, but it started to decrease 20 hours later. When increasing ΔT from 40°F to 60°F, the crevice conductivity variation was similar. At $\Delta T=80^\circ\text{F}$, the crevice conductivity stabilized at a low value (nearly the same as in high purity water), which means that the steam phase is dominant in the crevice at higher temperature and that possible NaCl precipitation occurred on the tube surface. However, the crevice conductivity did not increase after changing ΔT from 80°F to 60°F and from 60°F to 40°F. After the decrease of ΔT from 80°F to 60°F, the crevice conductivity quickly increased, but it subsided and stabilized at a similar level to that at $\Delta T=80^\circ\text{F}$. After the shut-down the crevice conductivity quickly increased then slowly decreased, indicating the hideout return of impurities from the crevice.

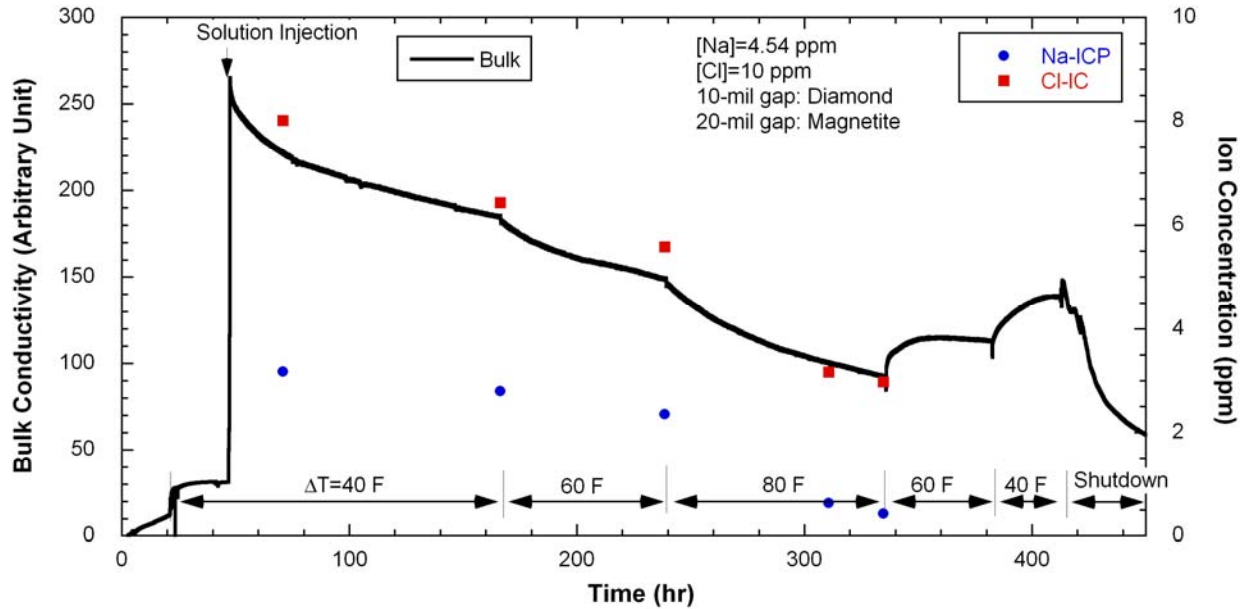


Figure 71. Bulk conductivity variation and measured Na and Cl concentrations in bulk water samples (NaCl-04).

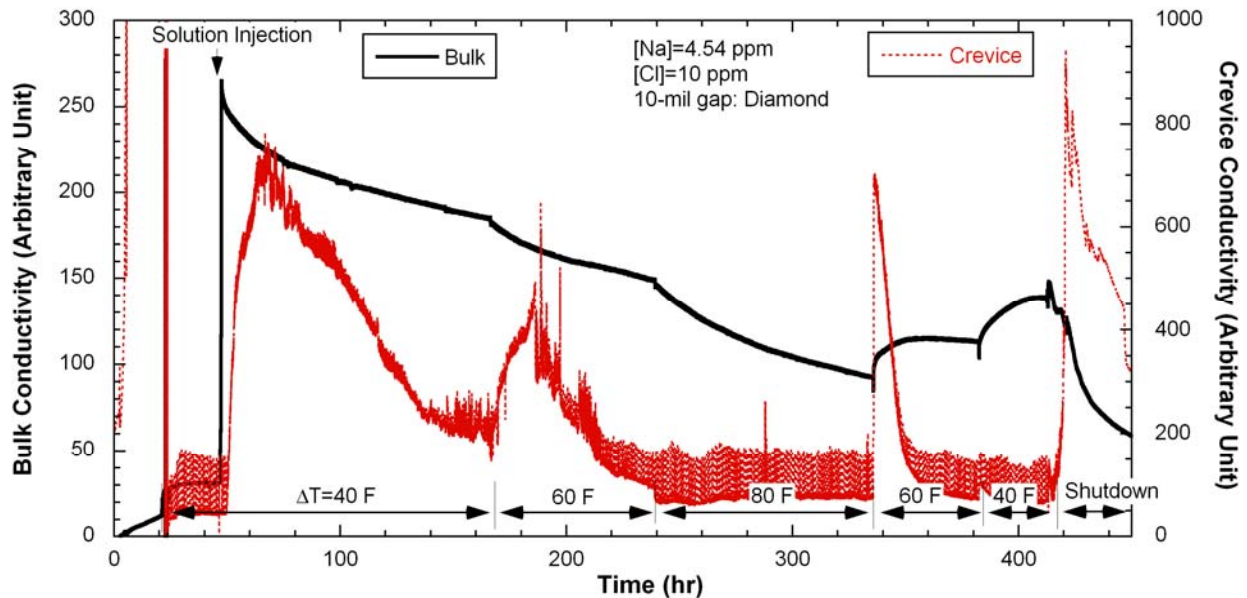


Figure 72. Crevice conductivity variation with time in the 10-mil gap crevice packed with diamond powder (NaCl-04).

Figure 73 shows the chemical analysis results for crevice samples taken from the 10- and 20-mil gap crevices. For the 10-mil gap crevice, the concentration levels are much lower than those in the previous test, NaCl-03 with MR=0.3, as shown in Figure 55. The 20-mil gap crevice packed with magnetite appears to show similar concentration levels to the NaCl-03 test results. One sample taken before the NaCl solution injection had high Cl concentration. This finding indicates that even after flushing the MB several times with high purity water, Cl ions are difficult to remove, possibly because of

the adsorption characteristics on the MB internal surfaces. The low ion concentration level in the diamond-packed crevice appears to be caused by the fact that NaCl-04 followed NaCl-03. Some quantity of precipitates or deposits might not be completely removed from the crevice and might remain in the crevice. This hypothesis is discussed again in the post-test examinations (Section 4.4.5).

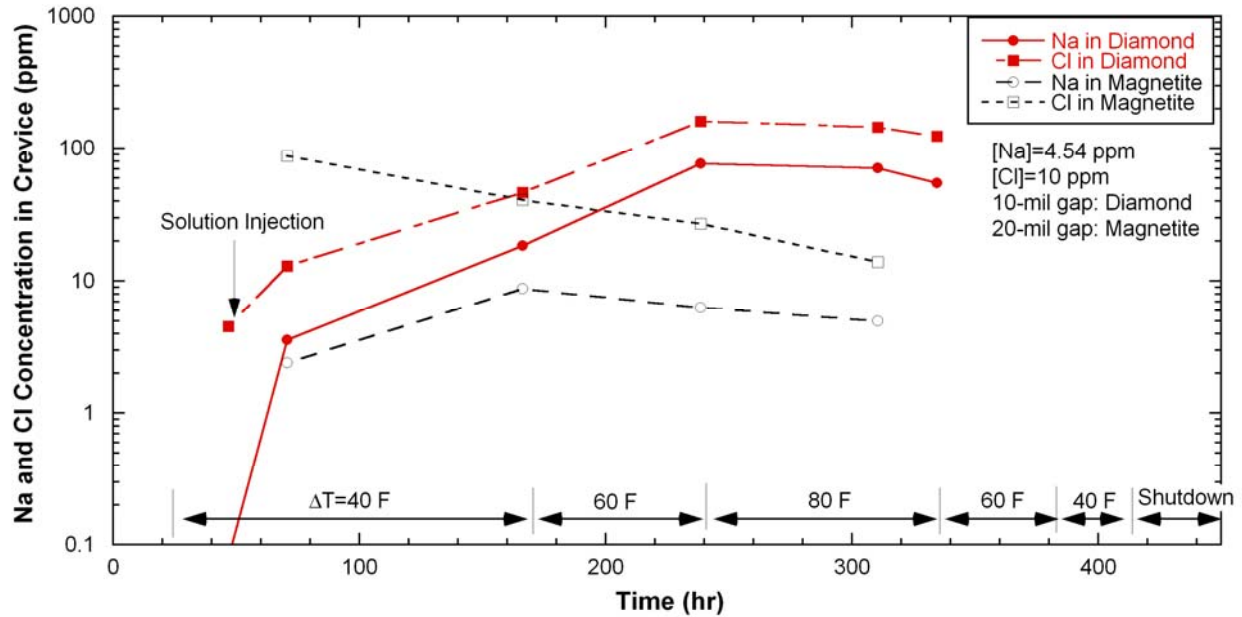


Figure 73. Chemical analysis results for crevice samples from 10-mil gap crevice packed with diamond and 20-mil gap crevice packed with magnetite (NaCl-04).

4.4.3 ECP Measurement

Figure 74 shows the Pt electrode potential variations in bulk and 10-mil gap crevice packed with diamond powder. Bulk and crevice Pt potentials are almost constant regardless of the ΔT . Figure 75 shows the Ni electrode potentials in the bulk and the 10-mil gap crevice packed with diamond. As shown in Figure 74, the bulk Ni electrode potential was almost constant. The tungsten electrode for the crevice and bulk responded quickly to the solution injection, as shown in Figure 76. The crevice tungsten potential before the NaCl solution injection was 140 mV higher than the bulk tungsten potential. It appears that high Cl concentration, as shown in Figure 73, caused the crevice to become acidic and resulted in a higher potential than in the bulk solution. The bulk tungsten potential slowly decreased with the increase of ΔT but seems to have stabilized after the decrease of ΔT because of hideout return from the crevice. The crevice tungsten potential quickly dropped and became stabilized before ΔT was changed from 40°F to 60°F. The initial big spike after the solution injection, which was also observed in the previous test, was caused by the crevice acidification from high purity water followed by the increase in the impurity level. As shown in Figure 44, the solution pH can be decreased by an increase in the ion concentration level, even though the MR remains constant. The tungsten potential in the crevice seems relatively independent of ΔT . The crevice tungsten potentials observed in this test appears to represent actual crevice chemistry, but the crevice tungsten electrode tip might be located too far from the tube surface, such that it might not represent the actual crevice pH change. This issue is discussed further in later sections.

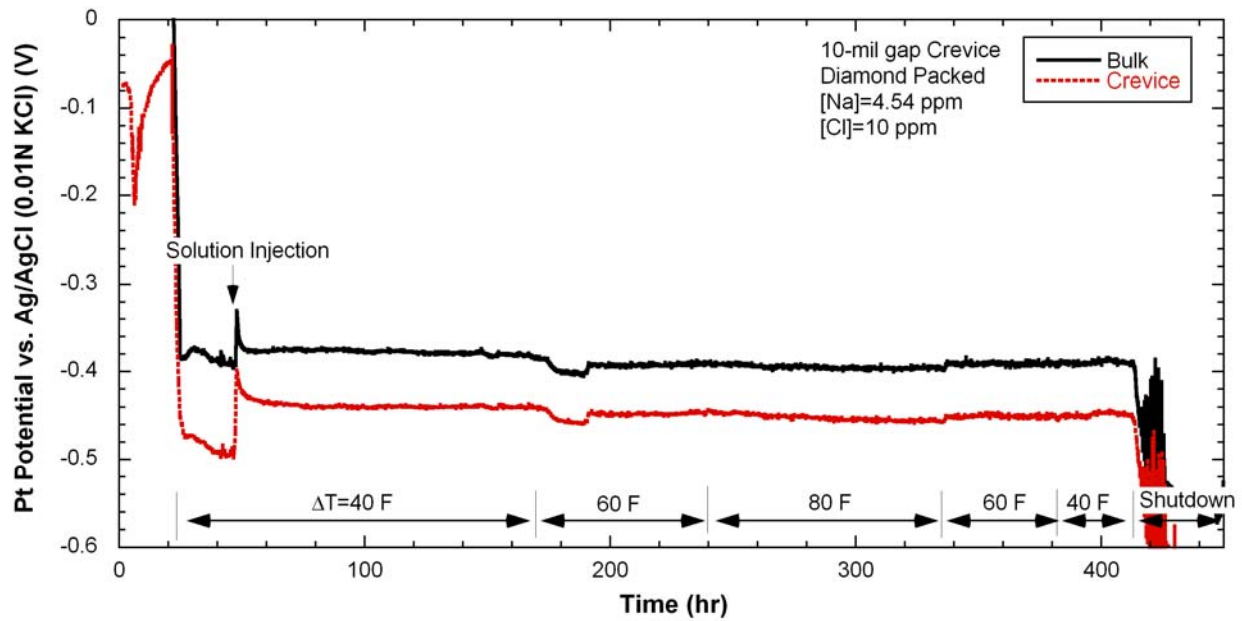


Figure 74. Variations of Pt electrode potential in bulk and 10-mil gap crevice packed with diamond (NaCl-04).

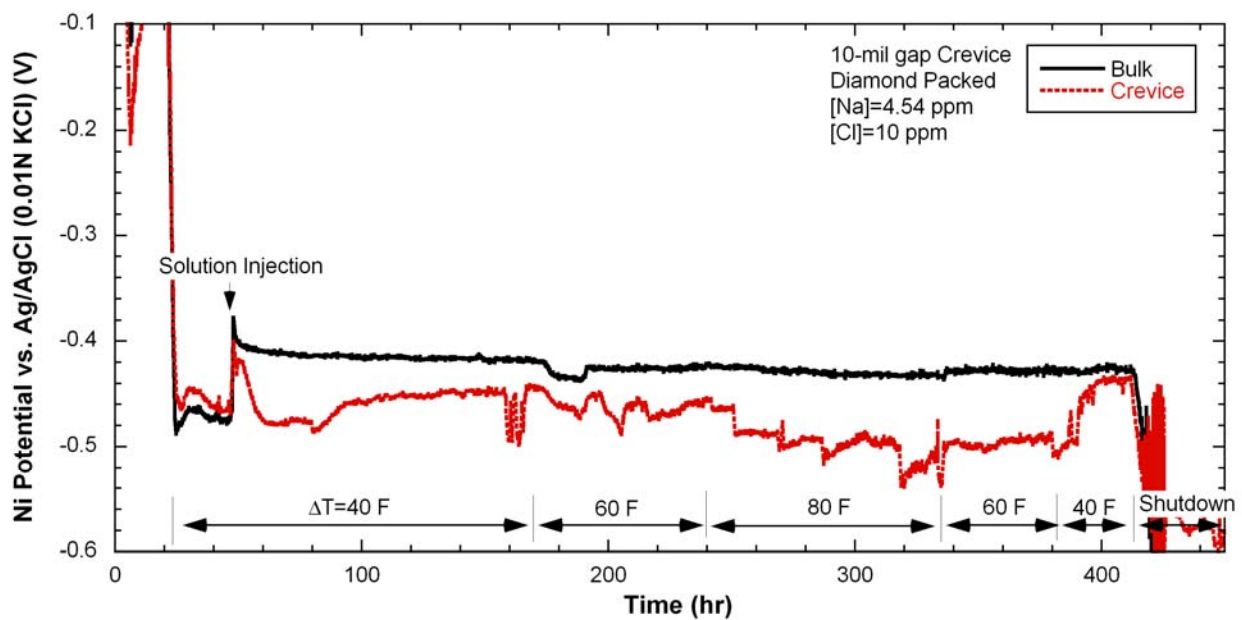


Figure 75. Variations in Ni electrode potential in bulk and 10-mil gap crevice packed with diamond (NaCl-04).

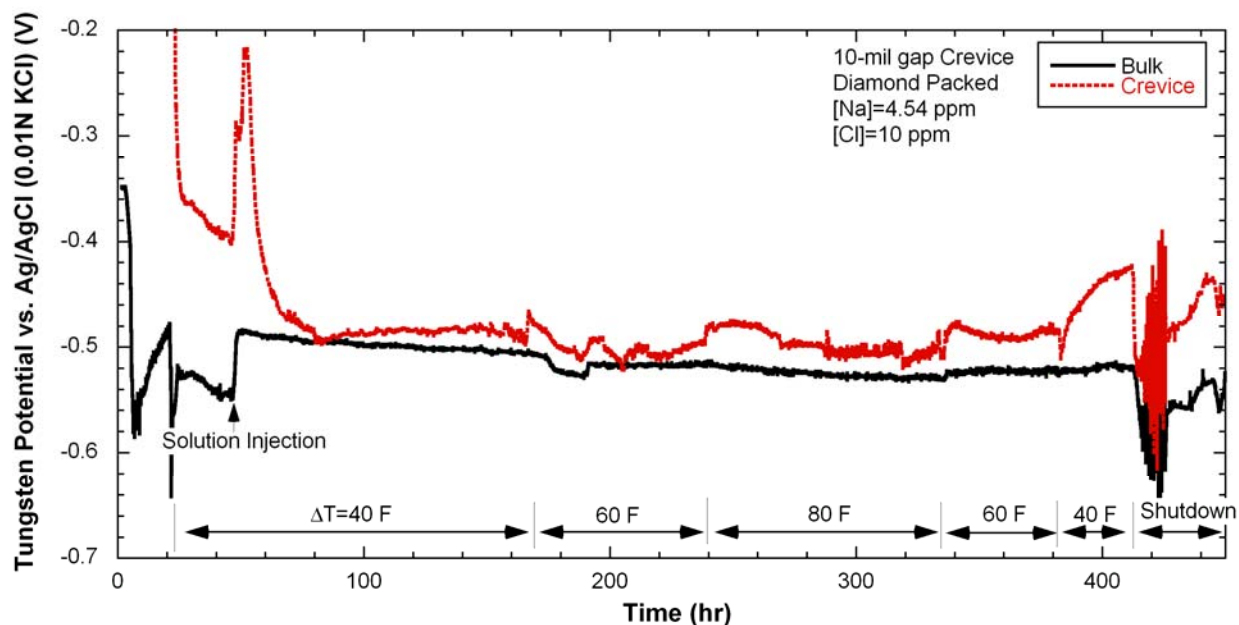


Figure 76. Variations in tungsten electrode potential in bulk and 10-mil gap crevice packed with diamond (NaCl-04).

4.4.4 Discussion of ECP and Solution Analysis

Figure 77 shows the tungsten potential difference between the crevice and the bulk with respect to the pH difference between the 10-mil gap crevice and the bulk. The pH was calculated by using MULTEQ with input from the solution sample analysis. The calculated pH indicates that the crevice pH is always lower than the bulk pH, which agrees with the measured tungsten potential difference except for one data point (indicated by a circle in Figure 77). However, even if the one data point is excluded, the potential slope with respect to pH is much lower than the Nernstian slope of -106 mV/pH at 260°C (500°F). Figure 78 shows the tungsten potential measured in the crevice and bulk as a function of the sample pH calculated by MULTEQ. The data shown in Figure 78 were corrected by considering the delay effect discussed in Section 4.3.5. The tungsten potential for the bulk solution responded in a linear fashion to the pH variation, but the crevice data did not. As observed in the NaCl-03 test, the bulk tungsten electrode behaved as a pH electrode in NaCl solution having $\text{MR}=0.7$.

Figure 79 shows the Na-to-Cl MR variations with time in the bulk and crevices. The MR was calculated from the bulk and crevice sample analyses. The bulk MR was stable but decreased after increasing ΔT from 60°F to 80°F . This finding indicates that Na was preferentially concentrated in crevices at $\Delta T=80^\circ\text{F}$. The MR for the two crevices gradually increases with increasing ΔT . The MR increase for the magnetite-packed crevice at $\Delta T=80^\circ\text{F}$ appears to correspond with preferential Na concentration in the crevice at $\Delta T=80^\circ\text{F}$, but the Na concentration level in the magnetite-packed crevice, as shown in Figure 73, is too small to explain the bulk MR decrease. The crevice samples from the magnetite-packed crevice do not appear to represent the actual crevice chemistry because of the dominant steam phase in the crevice. The initial MR data for the crevices are lower than for the bulk, which indicates that some residual Cl ions from the previous test were present in the crevice. Conditions from the previous test may have affected the results of the NaCl-04 test.

From the bulk concentration data, the total accumulated moles of Na and Cl in crevices were calculated, as shown in Figure 80. Neither the Na nor Cl concentration appears to saturate at any of the ΔT 's. As was expected from Figure 79, the crevice MR increased after the increase in ΔT from 60°F to 80°F. To compare the hideout rate of Na and Cl, the accumulated moles of Na and Cl in crevices were estimated with respect to each ion's exposure using the bulk concentration data, as shown in Figure 81. The initial hideout rate was almost the same for Na and Cl ions, and the rates were relatively constant until the ΔT was increased from 60°F to 80°F. From the results in Figure 81, we can expect that if the test starts with $\Delta T=80^\circ\text{F}$, the preferential Na concentration in the crevice would be observed from the beginning of the test.

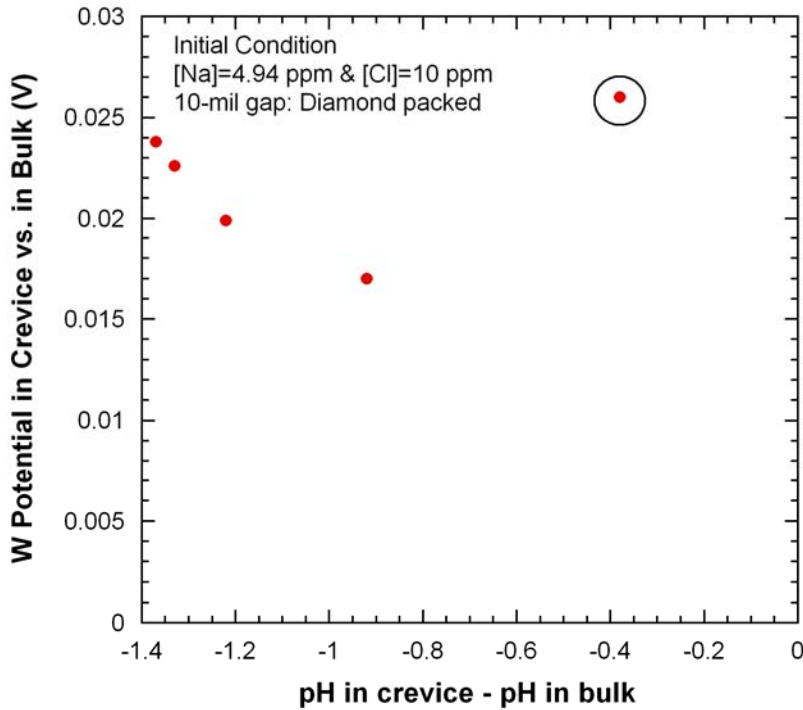


Figure 77.
 Calculated pH and tungsten potential difference between the 10-mil gap crevice and bulk (NaCl-04).

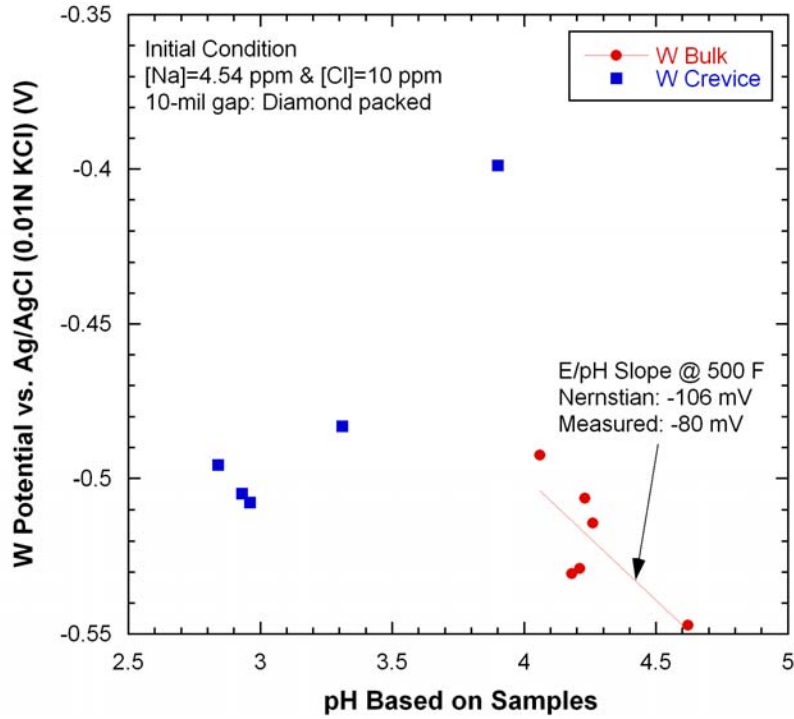


Figure 78. Tungsten potential measured in bulk and 10-mil gap crevice as a function of calculated pH for the samples taken at the same time when tungsten potentials were measured (NaCl-04).

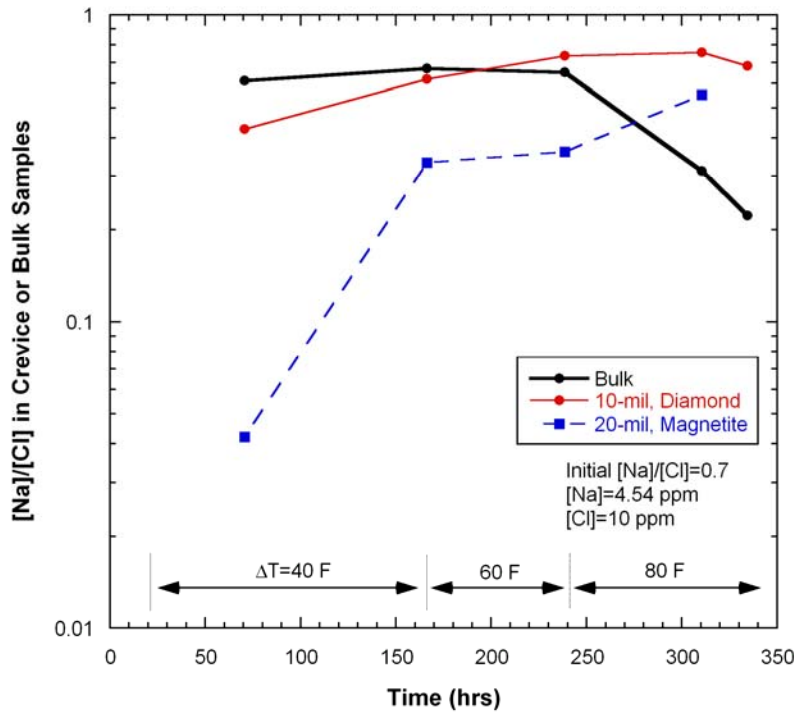


Figure 79. Na-to-Cl molar ratio variations with time in bulk and crevices (NaCl-04).

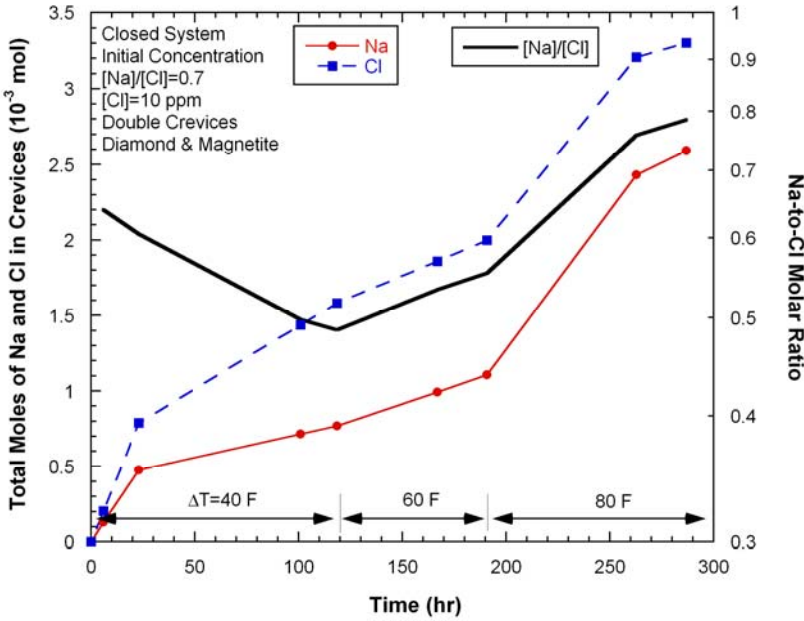


Figure 80. Total accumulated moles of Na and Cl in crevices and their molar ratio as a function of time after the solution injection (NaCl-04).

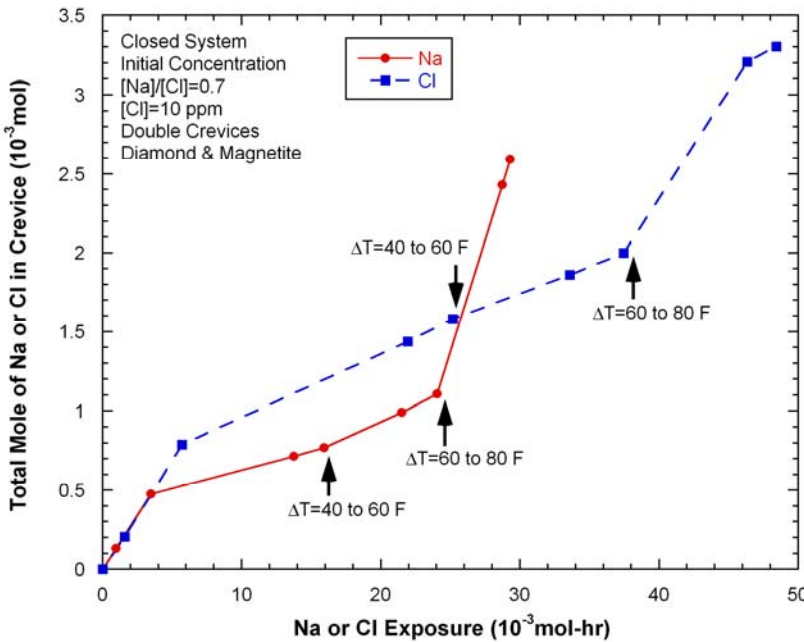


Figure 81. Total accumulated moles of Na and Cl in crevices as a function of exposure after the solution injection (NaCl-04).

4.4.5 Post-test Examination

The post-test inspections were conducted after the NaCl-03 and -04 tests. Figure 82 shows the disintegrated Ni foam on the 10-mil gap crevice assembly. The Ni foam became thinner than its original thickness and became brittle, which was not observed in the previous two tests, NaCl-01 and -02 having an MR of 1.0. The Ni foam apparently was dissolved in the relatively acidic bulk water. Figure 83 shows that a green deposit appeared at the bottom area of the 10-mil gap crevice packed with diamond. The small particles at the upper crevice region are residual diamond particles that appeared after removal of

the crevice assembly ring. The ICP/OES analysis indicated that the main elements in the green deposit were Ni, Fe, and Cr, as shown in Table 4. Since the color of NiO and Cr₂O₃ is green, we inferred that the deposit is mainly composed of NiO and Cr₂O₃ as well as iron oxide or a nickel-chromium-iron oxide mixture. The bare tube surfaces after removal of the deposits and diamond powders are shown in Figure 84. Severe gouging was observed at the upper half, but not in the green deposit area. This gouging seems to have developed as a result of the crevice chemistry being strongly acidic and might have been enhanced by abrasion of diamond particles, as discussed in Section 3.2.1. Considering that no gouging was observed after the NaCl-01 and -02 tests having MR=1.0, the abrasion of diamond particles alone does not likely cause the gouging without severe chemical excursion. A dye penetrant test was performed to permit visual identification of any surface cracks, but no visible cracks were detected on the surface of the 10-mil gap crevice tube. Under acidic environments, alloy 600 tubing can be severely gouged, but stress corrosion cracks do not appear to easily develop as compared to caustic environments, such as in the NaOH-01 and -02 tests.

As shown in Figure 85, magnetite powder still appeared in the 20-mil gap crevice after the series of tests. A green and red deposit was observed at the upper part of the 20-mil gap crevice, as shown in Figure 86. Analysis results by ICP/OES indicated that the green and red deposit was composed of Ni and Fe oxides. The black powder observed in the 20-mil gap crevice was mainly composed of Fe, indicating magnetite, as was expected. The chemical compositions for the deposits in the 10- and 20-mil gap crevices are summarized in Table 4. After removal of the deposit in the 20-mil gap crevice, no gouging was detected on the bare tube surfaces, as shown in Figure 87.

Table 4. Chemical compositions for the deposit formed in 10- and 20-mil gap crevices after the NaCl-03 and -04 tests determined by ICP/OES.

Powder Description	Chemical Composition (wt%)*				
	Fe	Ni	Cr	Cu	Na
Green powder in 10-mil gap crevice	9.99	21.0	2.36	<0.4	<0.4
Black powder in 20-mil gap crevice	64.8	1.74	<0.05	<0.05	<0.05
Green and red powder in 20-mil gap crevice	31.3	35.7	<0.2	<0.2	<0.2

* Powder samples were pretreated and dissolved in strong acid before ICP/OES analysis. The weight of the acid is not listed in this table, which should be the balance.

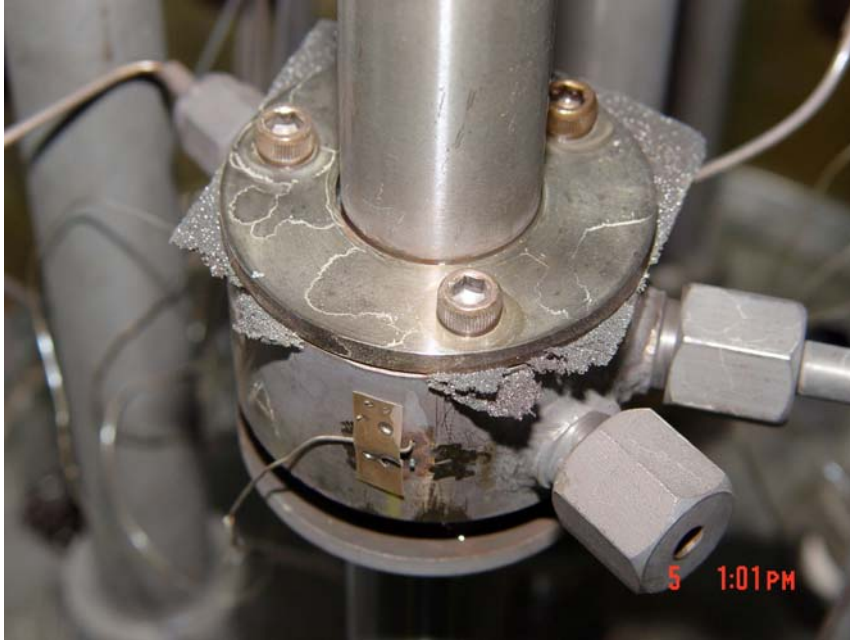


Figure 82.
Photograph of 10-mil gap
crevice assembly after the
NaCl-03 and -04 tests showing
disintegrated Ni foam.



Figure 83.
Tube surfaces in the 10-mil
gap crevice packed with
diamond powder after removal
of the crevice ring.



Figure 84.
Bare tube surfaces in the 10-mil gap crevice after removal of deposits and diamond powders, showing gouges (the same area as shown in Fig. 83).



Figure 85.
Top view of 20-mil gap crevice after removal of Ni foam and retaining ring, showing the magnetite powder in the crevice after the NaCl-03 and -04 tests.



Figure 86.
Tube surfaces of 20-mil gap crevice after removal of the crevice assembly showing the deposit formed on the upper crevice region and magnetite powder.



Figure 87.
Bare tube surfaces in the 20-mil gap crevice after removal of the deposit and magnetite powder, showing neither pitting nor gouges.

Two possible questions about the deposits detected in the crevices include: what is the origin of the Ni-rich deposits, and, why were the deposits located at different axial locations in the crevices having different packing materials. As shown in Figure 82, Ni dissolution occurred during the NaCl-03 and -04 tests as a result of the disintegration of the Ni foam. It is expected that this disintegration mainly occurred during the NaCl-03 test because of its more acidic bulk water. Dissolved Ni ions in the bulk water would be concentrated in the crevices, similar to the Na and Cl ions. Note that significant Cr was detected in the deposit formed in the 10-mil gap crevice. Since Cr usually does not dissolve in slightly acidic water because of the presence of a protective Cr oxide film, the origin of Cr is most likely the alloy 600 tube itself instead of the bulk water. This hypothesis is supported by the gouging shown in Figure 84.

Therefore, the deposits in the 10-mil gap crevice were formed by Ni hideout from the bulk water and gouging of the alloy 600 tubing. The Ni-rich deposits in the 20-mil gap crevice likely originate from the Ni ions in the bulk water as a result of the Ni foam dissolution.

The axial locations of the Ni-rich deposits may be related to the choice of packing material and its characteristics. The depth to which liquid phase can penetrate depends on the packing materials. The highly permeable diamond powder packing used in our tests allows liquid to penetrate deeply into the crevice, but the less permeable magnetite powder packing does not. We expect that Na and Cl hideout in the 10-mil gap crevice occurred mainly at the gouging region, and the region below the gouging region was a liquid and steam mixture. At the liquid and steam region, Ni-rich deposits having low solubility formed. Usually deposits can be formed at an intermediate region between liquid-dominant and dryout regions. For the 20-mil gap crevice, liquid could not penetrate deep enough because of the relatively less permeable magnetite packing. That is the reason that Ni-rich deposits were formed only near the crevice mouth. To verify the possibility of the Ni foam dissolution in bulk water, the Ni solubility was calculated with MULTEQ[®]. The calculated Ni solubility increased with decreasing pH, as shown in Figure 88. Each data set shown in Figure 88 was calculated by assuming constant Cl concentration and adjusting the Na concentration for various values of pH. The Ni solubility increased significantly with even small pH variation. It appears that approximately 10-20 ppm Ni can be dissolved in slightly acidic solutions, like the NaCl-03 test having MR=0.3. To prevent the Ni dissolution in acidic water, a corrosion-resistant metal (like chromium) can be added as an alloying element. After the NaCl-04 test, Ni-Cr-Mo alloy foams were used instead of pure Ni foams.

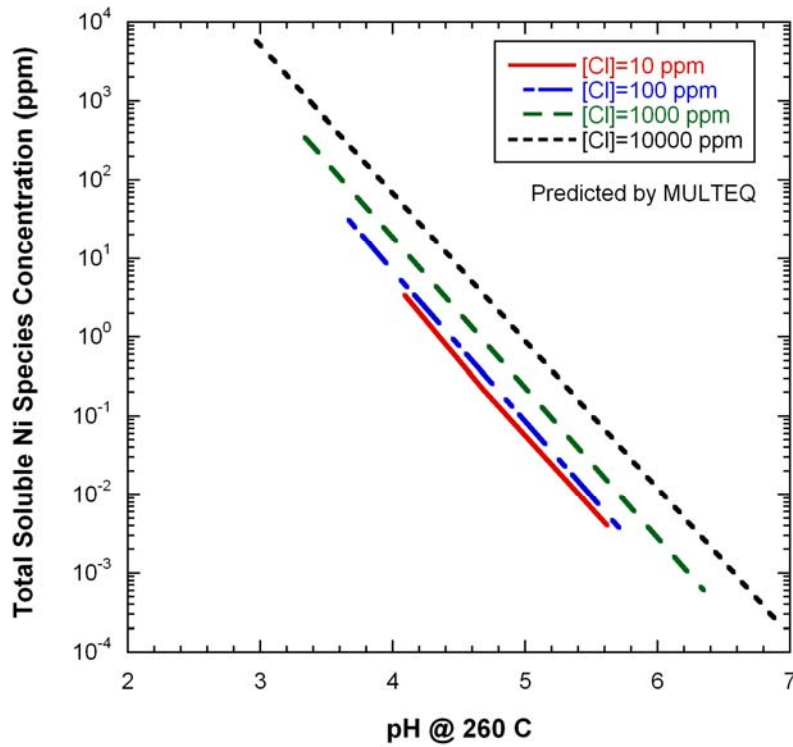


Figure 88.
Ni solubility as a function of pH and Cl concentration.

4.4.6 Comparing the Results for NaCl-02 through -04 Tests

In Figure 89, all Pt potential data collected from the three tests with different molar ratios, NaCl-02 through -04, are plotted versus the pH. The pH was determined using MULTEQ with input from the ICP/OES for Na and IC for Cl. The bulk Pt data closely follow the hydrogen electrode equilibrium line, assuming 1-ppb hydrogen concentration. The data from NaCl-03 with MR=0.3 are closer to the Ni/NiO equilibrium line than the other two data sets; this result can be explained by the dissolution of the Ni foam in the relatively acidic environment, as discussed in the previous section. Unlike the bulk Pt data, the crevice Pt data sets do not follow a linear trend. A Pt electrode usually serves as an oxidation/reduction potential electrode. To determine if other reactions are causing the mixed potential, the Fe/Fe₃O₄ equilibrium line was plotted in the same E-pH domain. The crevice data appear to be mostly located between the Fe/Fe₃O₄ and Ni/NiO lines. The scattering of crevice data might be explained by the mixed potential due to other reactions and the complexity of the heated crevice environment. However, it is still difficult to analyze the crevice potential data quantitatively.

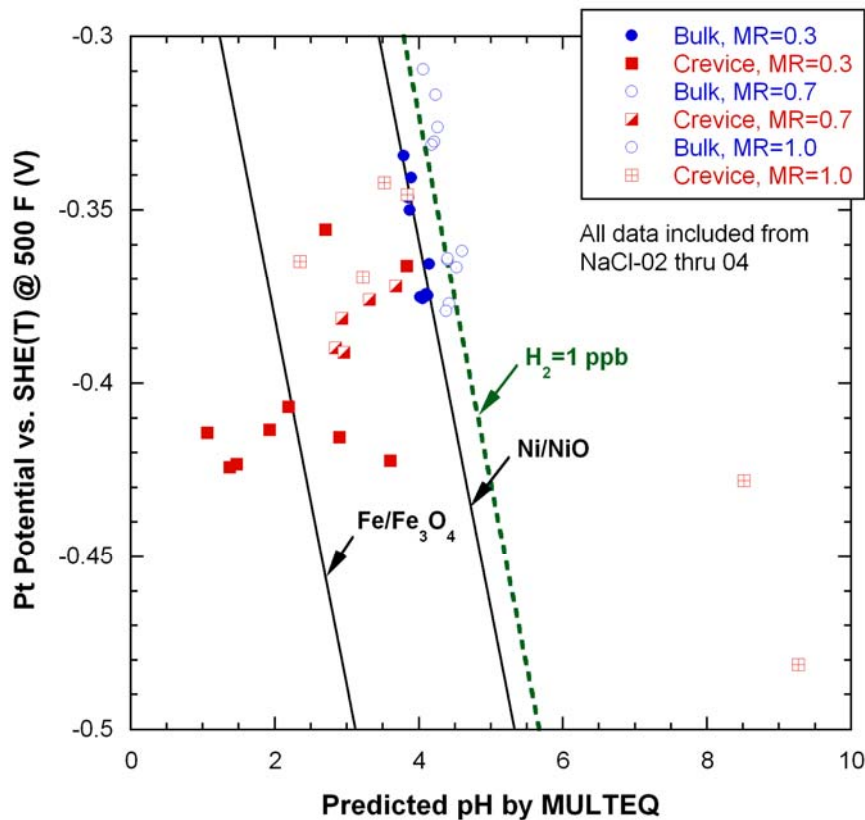


Figure 89.
Pt potential data measured in crevice and bulk water as a function of MULTEQ calculated pH based on solution sample analysis.

Figure 90 shows the tungsten potential measured in the bulk and the 10-mil gap crevice packed with the diamond powder as a function of sample pH taken at the same time as the tungsten potentials were measured. All the data from the NaCl-03 and -04 tests are included. The bulk data show good linearity, and the potential slope with respect to pH is very close to the Nernstian slope. Kriksunov and Macdonald²⁹ investigated the tungsten/tungsten oxide electrode as a pH sensor over the pH range of 2 to 11 at temperatures from 200 °C (392 °F) to 300 °C (572 °F). In Figure 90, the measured potential line by them at 250 °C (482 °F) is plotted. The line is about 50 mV higher than the bulk tungsten data, but this

discrepancy is not that high, considering the test temperature difference of 10 °C. It is not clear whether the crevice data are linear. If the crevice tungsten electrode follows the same tungsten oxidation reaction as the bulk tungsten electrode, the crevice data should fit on a single line.

Note that at least the bulk tungsten data and the earlier literature data are within the same intermediate tungsten oxide region, which is a compound between pentavalent (W_2O_5) and hexavalent (WO_3) forms. Additional data would be needed to confirm whether it is appropriate to use the tungsten electrode as a pH electrode under such a complicated crevice environment. To reduce the chemical complexity in a crevice, a crevice hideout test with highly soluble NaOH water chemistry appears to be an appropriate means to confirm the functionality of the tungsten electrode as a pH electrode under crevice environments.

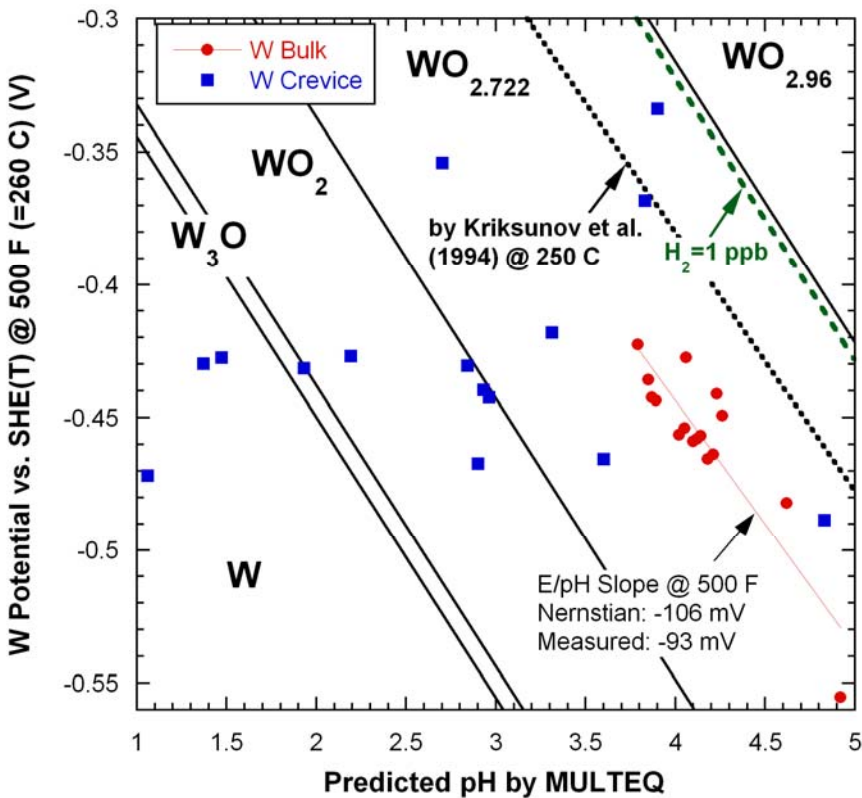


Figure 90. Tungsten potential measured in bulk and crevice as a function of sample pH, including all data from NaCl-03 and -04 tests plotted in a potential-pH diagram of W-H₂O system predicted by the thermodynamic code HSC Chemistry.

4.4.7 Summary

The NaCl-04 test followed the NaCl-03 test without the MB being opened. The NaCl-04 test appears to have been affected by residual chemicals from the NaCl-03 test. In the NaCl-03 and -04 tests, the tungsten electrode behaved as a pH electrode in the bulk water, but the crevice tungsten electrode data did not linearly fit the sample pH data. The crevice tungsten electrode tip appeared to be too far from the tube surface to represent the actual crevice pH variation. The crevice samples in the NaCl-04 test

indicated less acidic pH than those in the NaCl-03 test. The post-test examinations after NaCl-03 and -04 showed that gouging occurred on the alloy 600 tube surfaces in the 10-mil gap crevice packed with diamond, but no cracks were detected. This result indicates strong acid conditions developed during the NaCl-03 and -04 tests, mostly during the NaCl-03 test. The magnetite-packed crevice did not show any corrosion on the tube surfaces. To maximize the advantage of a closed system and evaluate the crevice hideout characteristics from bulk concentration data, a single crevice was tested instead of a double crevice.

This page is intentionally left blank.

5. Single Crevice Test

5.1 Background

As discussed in Section 4, in the double crevice tests having different packing materials, we had difficulty in analyzing the crevice concentration behavior with results from bulk water chemistry analysis. In contrast, use of only one crevice packed with one kind of packing material should make it much easier to analyze the crevice chemistry from bulk chemistry data because the MB is a closed system and there is only one crevice where hideout can occur.

5.2 NaOH-03: NaOH Test

The main objective of the NaOH-03 test is to confirm that the W/WO_x electrode can work as a pH electrode even in complex crevice environments. Since the behavior of the NaOH chemistry is much simpler than the NaCl chemistry, testing with NaOH bulk water is valuable. This testing will furnish a much simpler starting point for developing and confirming the adequacy of our chemical instrumentation. The 10-mil gap crevice was packed with diamond powder, and the 20-mil gap crevice was left unpacked. The estimated porosity of the 10-mil gap crevice was 35 %. This simplified configuration allows us to better model crevice behavior and perform chemical balances accounting for what happens between a single crevice and the bulk water. The bulk water was an 11.5-ppm Na solution as NaOH, which is the same Na level as NaOH-01 and -02 tests.

Leakage from the primary to secondary chamber occurred, and the system was automatically shut down after about 400 hours. Multiple through-wall cracks were detected in the unpacked crevice tubing, which had been used during prior tests. A through-wall crack was found in the packed crevice tubing, which was being used for the first time in the MB. The starting point of the leak was carefully determined, and only test results acquired before the start of the leak were used in the crevice chemistry analysis.

5.2.1 Temperature Data

As shown in Figure 91, all the crevice temperatures in the diamond-packed 10-mil gap crevice started to increase immediately after the injection of the 11.5-ppm Na solution, followed by stabilization 20 hours later. This temperature increase is attributed to Na concentrating in the crevice and resulting in elevation of the boiling point. The temperature increase after solution injection was about 5°F. After increasing the primary temperature from 540°F to 560°F, the crevice temperature increased immediately but did not show any additional temperature increase. The thermocouple labeled T3 indicated temperature instability at $\Delta T=60^\circ\text{F}$ and a noisy signal at $\Delta T=100^\circ\text{F}$, a sign of leakage. The primary temperature was increased to 600°F to evaluate the reproducibility of the NaOH-01 and -02 test results. However, the reproducibility test was shut down due to the leakage. In Figure 92, the temperature in the 20-mil gap crevice did not increase even after NaOH solution injection. The non-packed condition and wider gap induced violent mixing between the crevice and bulk environments, which led to only minor hideout and boiling point elevation. Crevice solution samples for the unpacked crevice also showed only minor Na hideout. Thermocouple T5 indicated temperature fluctuation at $\Delta T=60^\circ\text{F}$. Since through-wall cracks were detected at the open crevice, the noisy temperature signal appears to indicate the start of leakage. Since the primary water temperature is higher than the secondary water temperature, we inferred that as the crack length became longer and the steam leak rate became higher, the upper bound of the noisy temperature became higher.

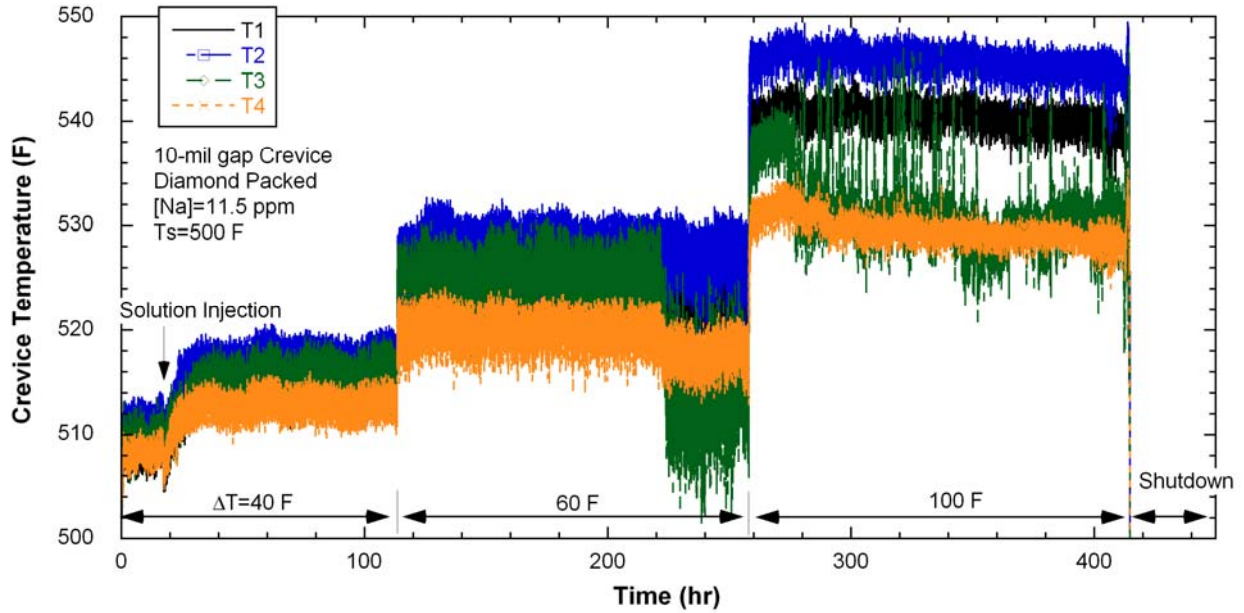


Figure 91. Crevice temperature variation in the 10-mil gap crevice packed with diamond (NaOH-03).

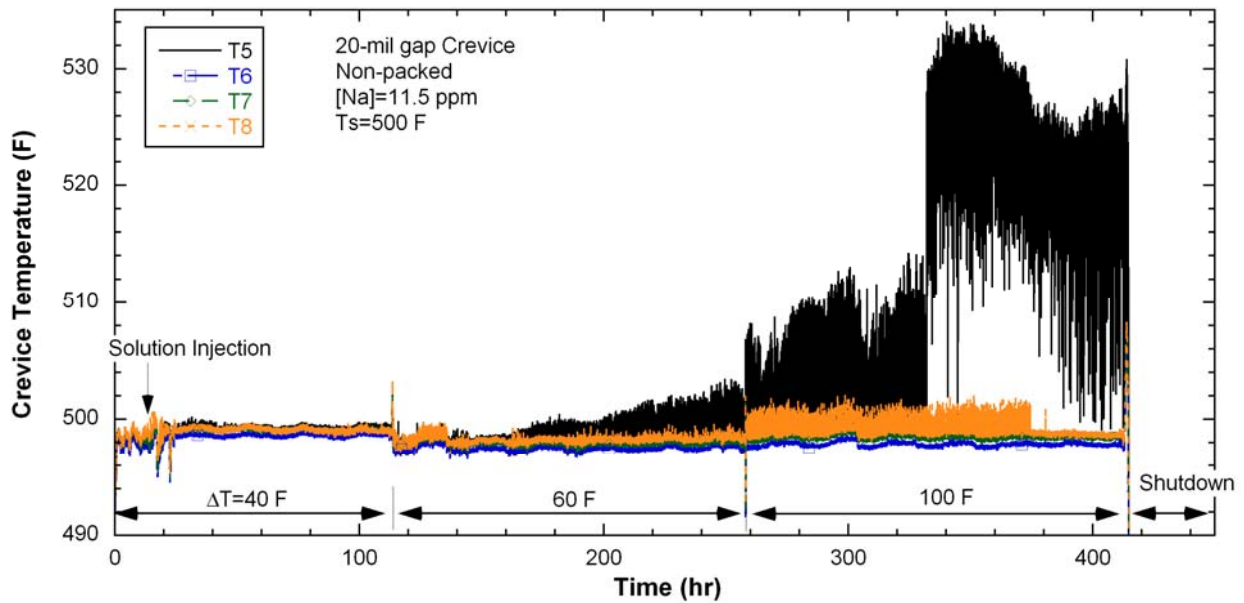


Figure 92. Crevice temperature variation in the 20-mil gap crevice without packing (NaOH-03).

The crevice temperatures were normalized by using the primary and secondary temperatures, as shown in Figure 93. The temperature increase is clear after the solution injection. The normalized temperatures slightly increased after raising the primary temperature from 540°F to 560°F. Temperature fluctuations became smaller after increasing the primary temperature from 560°F to 600°F except for T3. This result indicates that the two-phase mixture zone became smaller at the thermocouples in the crevice, and the steam phase became dominant.

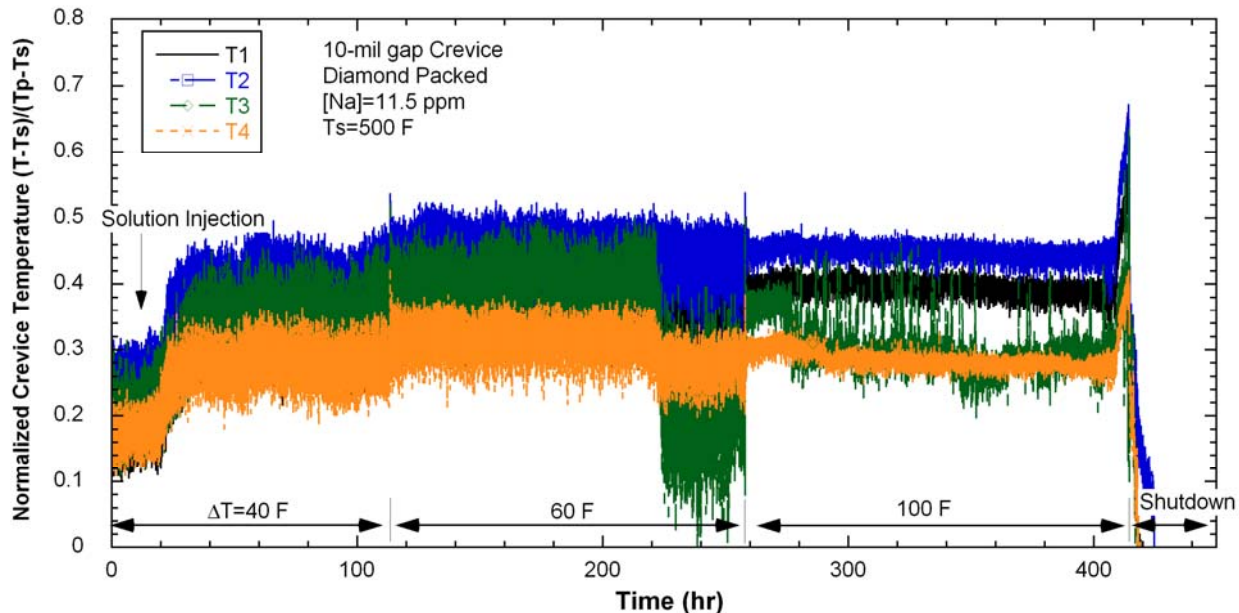


Figure 93. Normalized crevice temperature in the 10-mil gap crevice packed with diamond (NaOH-03).

5.2.2 Bulk & Crevice Chemistry

The bulk conductivity responded very quickly to the solution injection but exceeded the upper limit of the conductivity meter with 20-ppm NaOH solution, as shown in Figure 94. After changing the range module in the conductivity meter, the recording of the bulk conductivity was resumed. Based on the analysis results for bulk samples, the Cl ion concentration was around 0.6 ppm. This test can be considered as having a high Na-to-Cl molar ratio. The source of Cl ions is not clear, but some Cl ions adsorbed on the oxide surface of the secondary chamber during the previous NaCl tests may have been released. The Na concentration decreased continuously, but the Cl concentration remained the same value. After changing ΔT from 60°F to 100°F, the conductivity reduction rate increased more than before. But a certain transition appears before and after a lapse of 280 hours. This transition may be another indication of the start of leakage from the primary to secondary chamber. As compared with the temperature indication for leakage, the bulk conductivity was less sensitive to leakage because the bulk conductivity reduction could be interpreted as Na hideout in the crevice as well as primary-to-secondary leakage.

In Figure 95, crevice conductivity can be seen to increase a few hours after the solution injection. This finding indicates that a certain time is needed for the concentrated solution to penetrate into the bottom region of the crevice and replace the steam phase. Crevice conductivity also exceeded the upper limit of the meter. In the NaOH-03 test, the contribution of the OH⁻ ion to total conductivity became larger than that in the previous NaCl tests, because the total OH⁻ ion concentration is higher and the conductance of the OH⁻ ion is about two times higher than the Na⁺ or Cl⁻ ion at 500°F.³⁸ After replacing the range module, we resumed the crevice conductivity recording. The crevice conductivity at $\Delta T=60^\circ\text{F}$ showed a gradual decrease followed by an increase. At $\Delta T=100^\circ\text{F}$, the conductivity dropped quickly after increasing the primary temperature because the steam phase became dominant in a very short time. Then, the conductivity increased rapidly, which indicates Na hideout. Subsequently, the conductivity started

decreasing again followed by oscillations. The crevice conductivity oscillations appear to be the effect of the steam leakage through a crack.

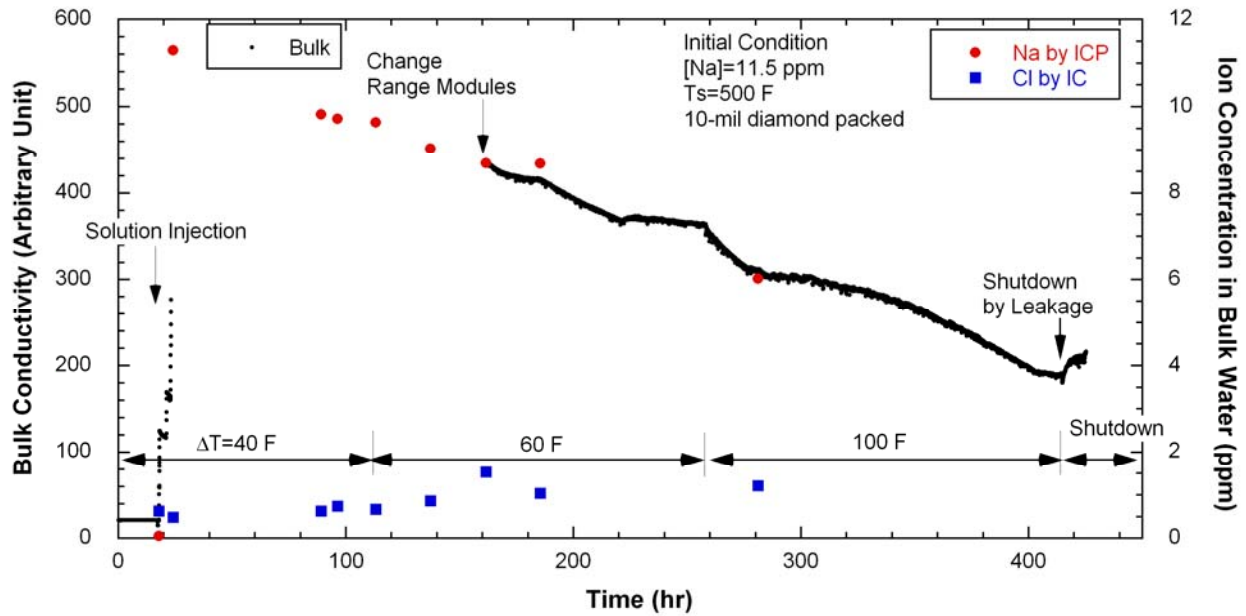


Figure 94. Bulk conductivity variation with time and impurity concentrations in bulk solution (NaOH-03).

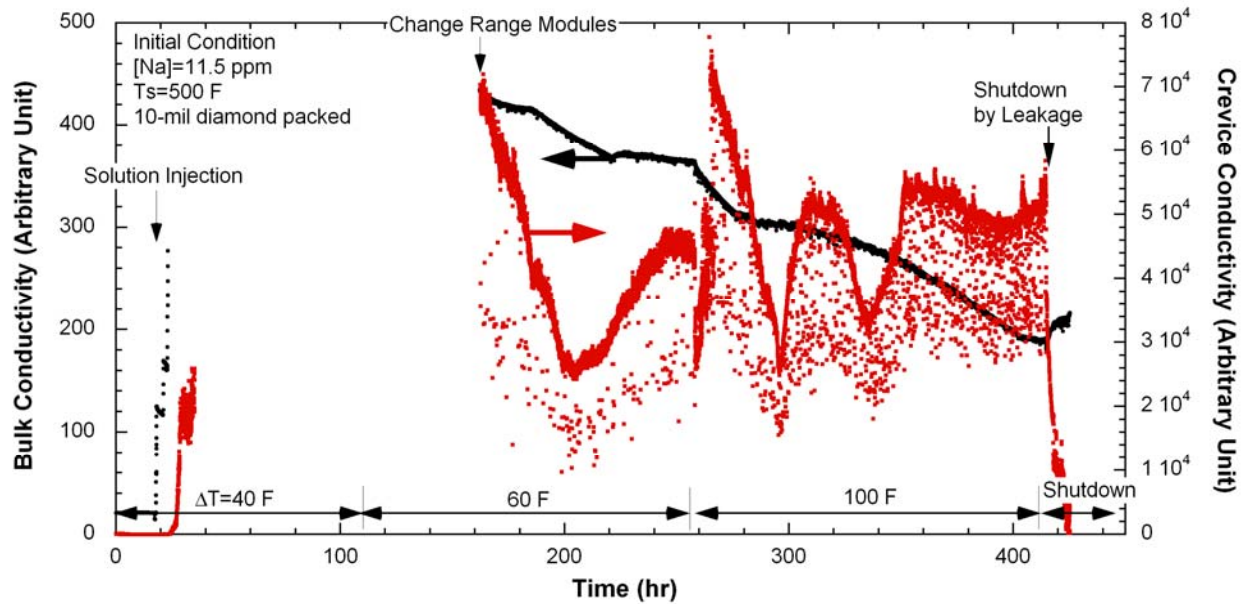


Figure 95. Crevice conductivity variation in the 10-mil gap crevice packed with diamond (NaOH-03).

Solution samples were taken from the 10-mil gap crevice and analyzed by ICP/OES or IC. Figure 96 shows the chemical analysis results for the crevice samples. At $\Delta T=40^\circ\text{F}$ the maximum crevice concentration for Na was 12,500 ppm, as shown in Figure 96. The samples taken just before increasing the ΔT showed low concentration, but they recovered to higher concentration again one day later. At $\Delta T=60^\circ\text{F}$ the maximum crevice concentration for Na was 31,400 ppm. Note that the variation of the Cl concentration in the crevice follows that of the Na ion. The concentration factor for Cl is around 10^3 as

compared with the bulk Cl concentration. This observation suggests that the total ion concentration in a crevice is proportional to the bulk impurity concentration.

A time delay appears to occur between solution samples and actual crevice chemistry. The first sample showing high concentration of Na was taken after a lapse of 100 hours, but the tungsten potential had already decreased indicating a high concentration of Na after about 50 hours elapsed. As discussed before, the volume of the sampling line and valve is about 90 μL , and the sampling volume is usually 50-100 μL , which causes the time delay. We can assume no time delays for bulk samples because we flushed the bulk sampling line before taking samples and the volume of the bulk sample is about 1500 μL . Figure 96 shows ion concentration versus time in the crevice not corrected for the time delay. To make the crevice samples more representative of the actual crevice chemistry, the analyses were corrected for the time delay. We assumed that a solution sample extracted at a certain time represents the crevice chemistry at the previous sampling time. The corrected chemical analyses are shown in Figure 97. Crevice concentration started to decrease after 160 hours for both crevices. For the unpacked crevice, the Na concentration did not exceed 100 ppm, which is consistent with the earlier test results described in Section 3.1. The crevice concentration decrease observed at $\Delta T=60^\circ\text{F}$ is another indication of leakage.

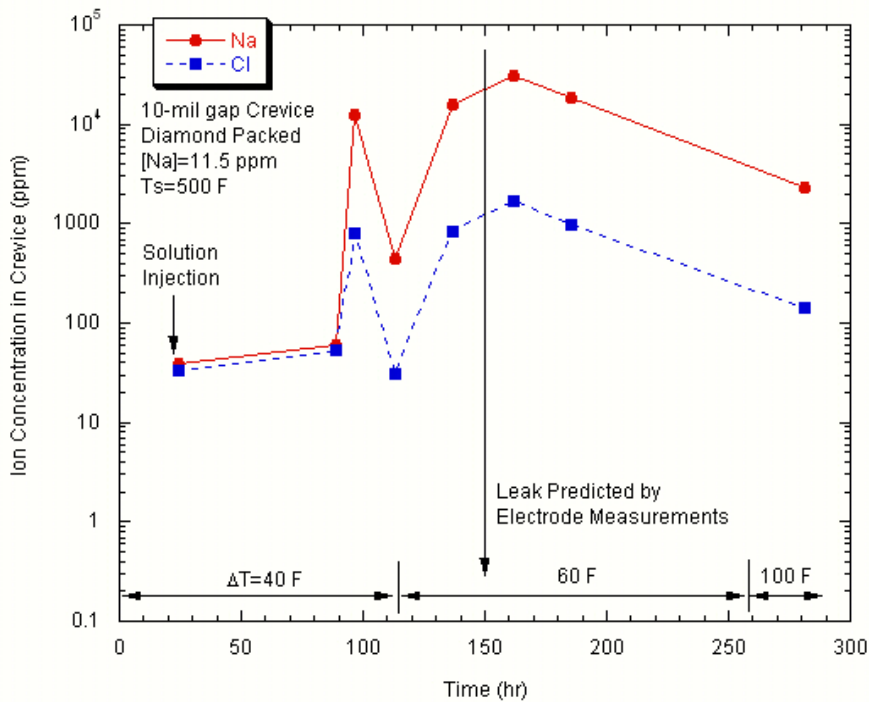


Figure 96. Chemical analyses of the samples taken from the 10-mil gap crevice packed with diamond dust (NaOH-03).

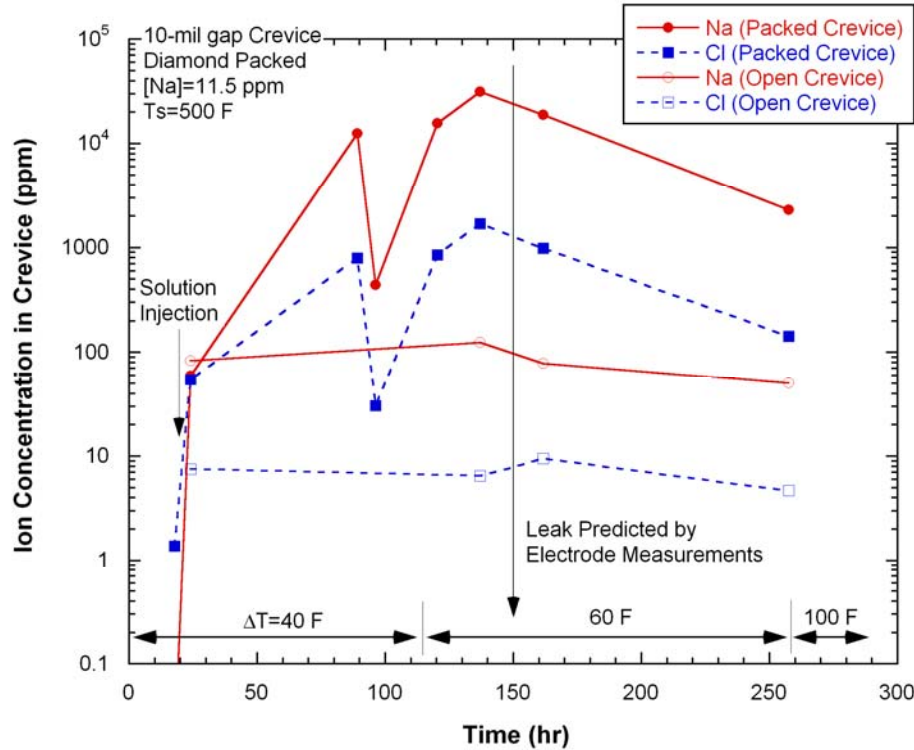


Figure 97. Chemical analyses of crevice samples corrected for sampling time (10-mil gap crevice: diamond packed, 20-mil gap crevice: open crevice).

5.2.3 ECP Measurement

Two tungsten/tungsten oxide electrodes were installed in the 10-mil gap crevice separated by 30 degrees at the same crevice elevation. Before the solution injection, one tungsten electrode exhibited noisy behavior, as shown in Figure 98. The other tungsten electrode was stable before and after the solution injection. After the solution injection, the two tungsten potentials became almost the same, suggesting that there is no significant chemical concentration gradient with circumferential location at $\Delta T=40^\circ\text{F}$. The bulk tungsten potential quickly responded to the NaOH injection, and the decrease of potential indicated an increase of bulk pH. The bulk potential change after the NaOH injection was 263 mV. The pH change calculated by MULTEQ was 3.0 at 500°F . If the tungsten electrode follows the Nernstian potential/pH slope, -106 mV at 500°F , this pH change will cause potential decreases of 318 mV, which is close to the measured bulk tungsten potential change. The crevice tungsten potential changes before and after injection was -588 mV at $\Delta T=40^\circ\text{F}$, and the pH change based on the solution samples was 5.7. If the crevice tungsten electrode follows the Nernstian potential/pH slope, this pH change will cause a potential decrease of 600 mV, which is very close to the measured value, -588 mV. Based on the crevice temperature data, the boiling point elevation at $\Delta T=40^\circ\text{F}$ was 5°F higher in this case than that observed in high purity water. The calculated crevice pH and concentration factor corresponding to this boiling point elevation are 10.33 and 2500, respectively. The measured pH and the maximum concentration factor at $\Delta T=40^\circ\text{F}$ are 10.11 and 1300, respectively. This discrepancy is probably due to an overestimation in the calculation of crevice concentration or dilution of the crevice solution during the sampling. At $\Delta T=60^\circ\text{F}$, the potential spikes were not observed immediately after changing ΔT from 40°F to 60°F , but some spikes were observed 40 hours later. These potential spikes can be considered an indication of leakage. In contrast to the crevice conductivity data shown in Figure 95, oscillations in crevice potential data are not apparent, but a small fluctuation in the tungsten potential denoted as “Crevice A2” appears at $\Delta T=60^\circ\text{F}$ and 100°F .

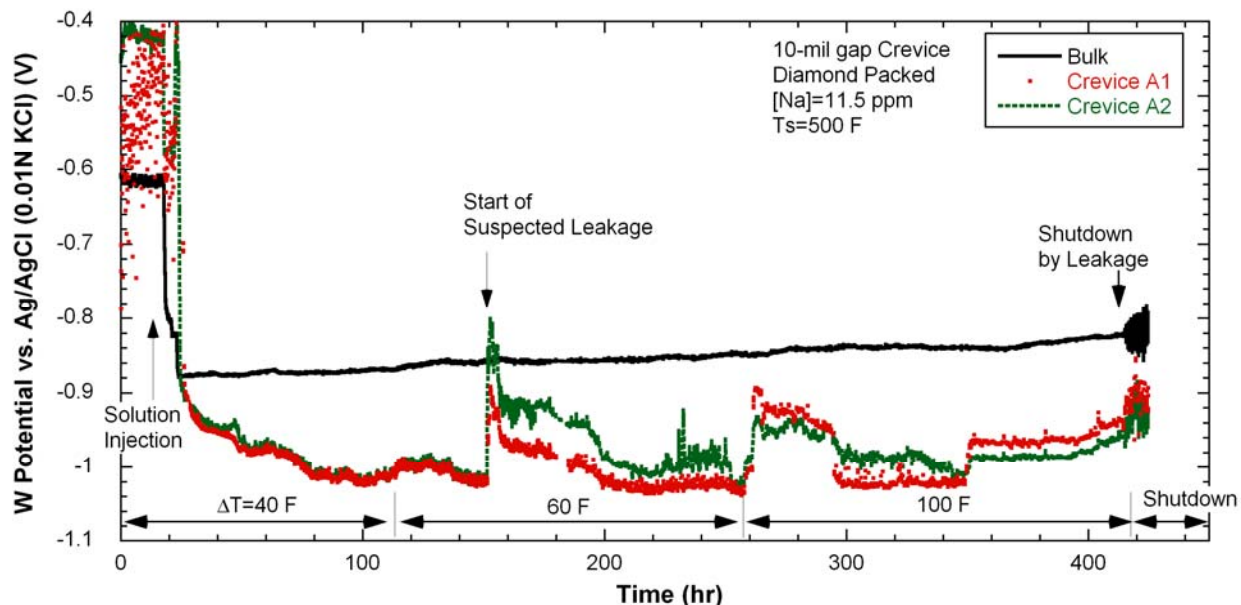


Figure 98. Tungsten potential variation in bulk and 10-mil gap crevice packed with diamond powder (NaOH-03).

Figure 99 shows the variations in Pt electrode potential for the bulk and 10-mil gap crevice packed with diamond powders. The bulk and crevice potentials are almost identical to those of the tungsten electrodes, as shown in Figure 98. The crevice Pt electrode potential shows noisy behavior before the solution injection, suggesting that the steam phase was dominant around the Pt wire electrode due to vigorous boiling. The subsequent stabilization of the potential was caused by Na concentrating in the crevice and the resultant increase in the concentrated liquid phase. Figure 100 shows the alloy 600 electrode potential variations in the bulk and crevice. Alloy 600 electrodes also show identical behavior to the tungsten electrode. Based on these observations, under deaerated NaOH water chemistry, alloy 600 and Pt electrodes can be used as a pH electrode, just as the W/WO_x electrode.

To determine if any relationship exists between conductivity and measured potential in the crevice, data for tungsten and alloy 600 are plotted along with the conductivity in Figure 101. After the solution injection, the potential decreased as the conductivity increased. After a potential spike, the alloy 600 potential in the crevice appears to follow the oscillations of crevice conductivity. If the conductivity depends on ion concentration in the liquid and the alloy 600 electrode behaves as a hydrogen electrode in the crevice, the alloy 600 potential should go in the negative direction when the conductivity increases. However, conductivity also depends on the ratio between steam and liquid phase as well as the liquid concentration, which complicates any simple comparison.

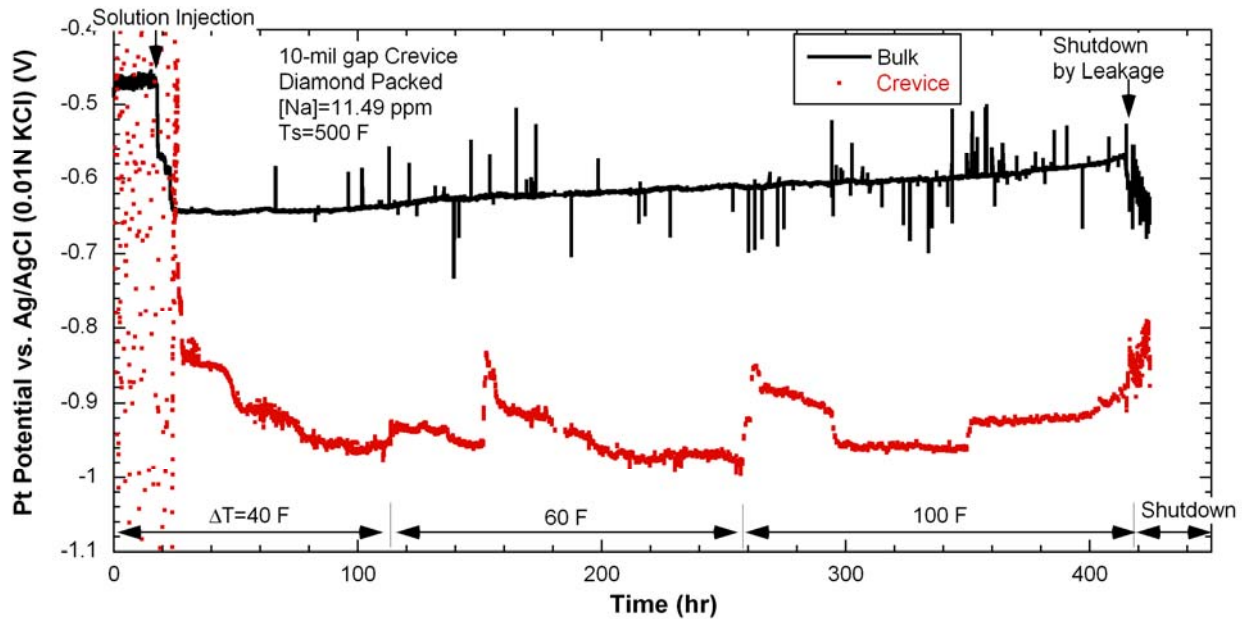


Figure 99. Pt potential variations in bulk and 10-mil gap crevice packed with diamond powder (NaOH-03).

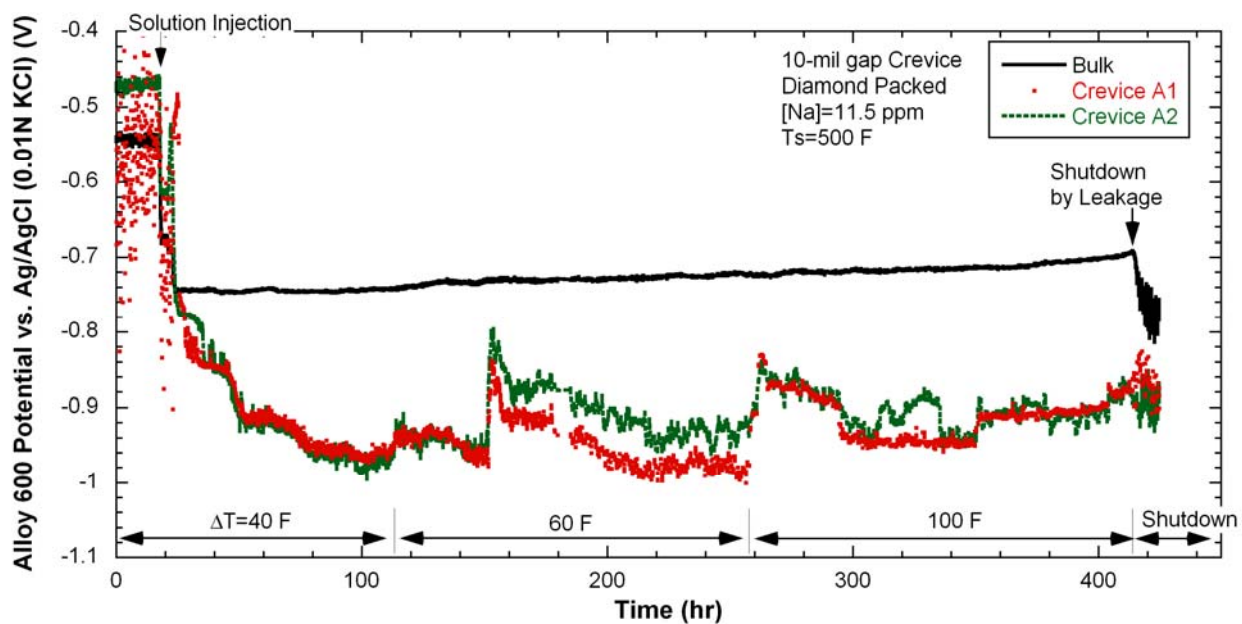


Figure 100. Alloy 600 potential variations in bulk and 10-mil gap crevice packed with diamond powder (NaOH-03).

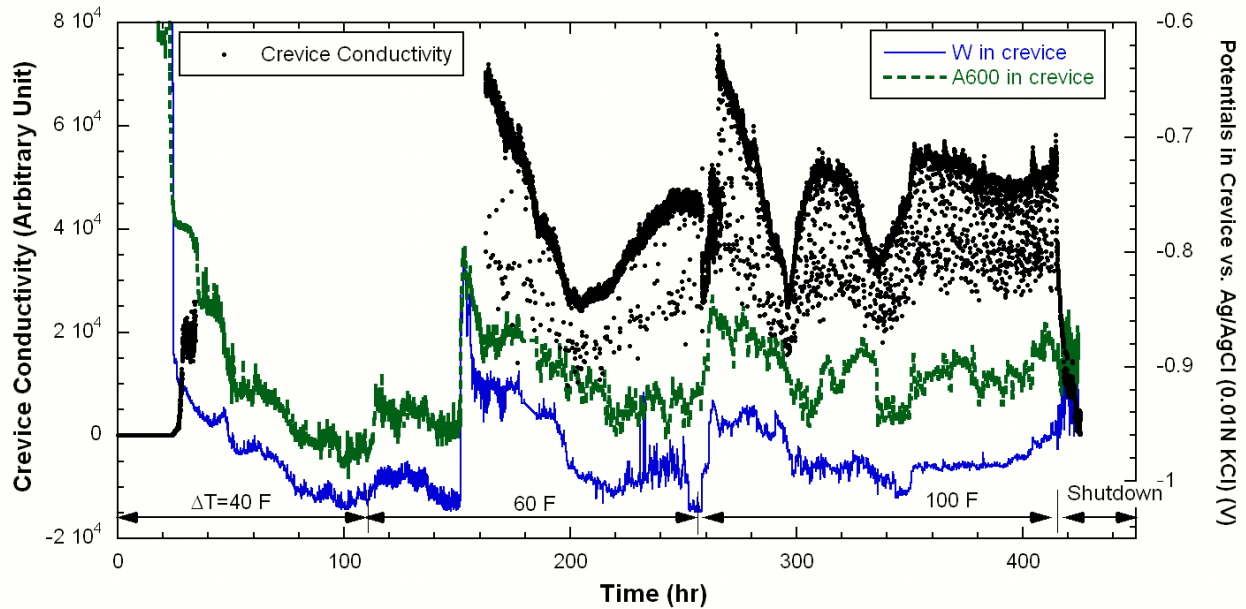


Figure 101. Tungsten and alloy 600 potentials in 10-mil gap crevice packed with diamond as compared with crevice conductivity variation (NaOH-03).

5.2.4 Post-Test Examination

Figure 102 shows the bare surfaces of alloy 600 tubing in the 10-mil crevice region, which indicate severe gouging. The gouging looks similar to that observed after the NaOH-01 and -02 tests shown in Figure 24. As discussed in Section 3.2.1, the gouging may be enhanced by abrasion caused by hard diamond particles. However, the total exposure time before the leakage is much shorter than that of NaOH-01 and -02 tests. In this test the total exposure time was about 160 hours, but in the NaOH-01 and -02 tests the leakage was detected after about 590 hours. The only difference between the two cases is ΔT . A higher ΔT is supposed to result in higher impurity concentration in a crevice. In the NaOH-01 and -02 tests, since the temperature was the only crevice monitoring parameter, the leakage might be detected later than its actual start time. Based on dye penetration test results, the crack depth in the previous NaOH tests appears to be deeper than that in the NaOH-03 test. Figure 103 shows the bubble test result for the packed crevice tubing. The tubing was pressurized up to 350 psig and put in a water bath. A 5-mm-long axial crack was detected where a Teflon cone ring and a stainless steel back ferrule had sat. These results suggest that low-temperature mill-annealed alloy 600 is very weak to cracking under NaOH solution with only operational hoop stress. Figure 104 shows the dye penetration results for the packed crevice tubing. Many axial cracks were detected around the tube surfaces. At the bottom of the crevice, the cracks linked together forming what looked like a circumferential crack.



Figure 102.
Bare surface of alloy 600
tubing showing severe
gouging due to caustic
crevice chemistry.



Figure 103.
Gas bubbles coming out of
a through-wall crack
detected underneath the
Teflon swaging ferrule and
developed inside the 10-mil
gap crevice packed with
diamond dust.

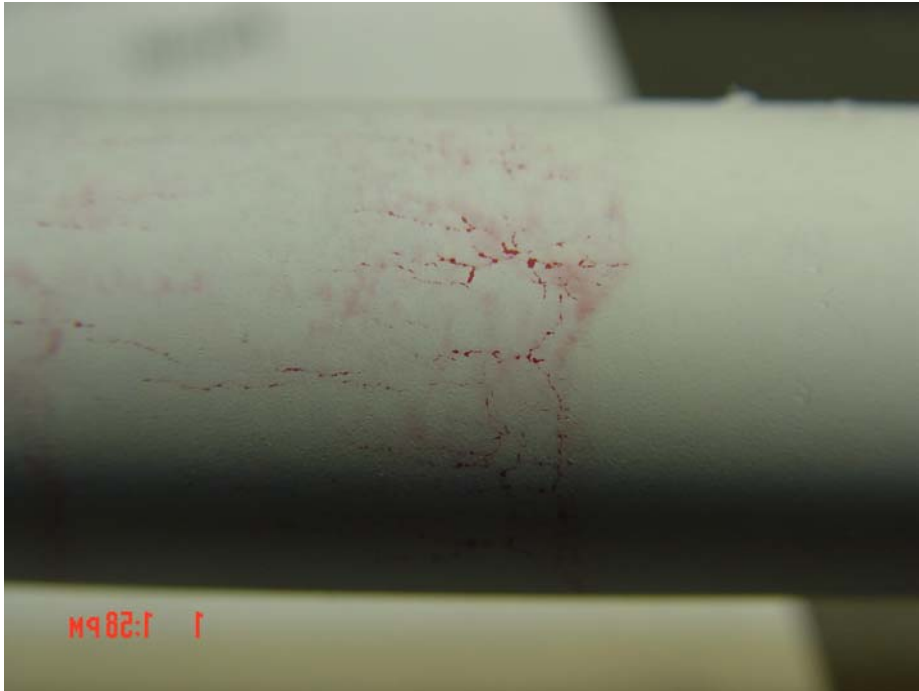


Figure 104.
Axial cracks developed inside the 10-mil gap crevice packed with diamond dust and visually enhanced by dye penetration (left side: crevice top, right side: crevice bottom).

Figure 105 is a photo of a bubble test showing multiple axial cracks developed at the 20-mil gap crevice without packing. In Figure 106 the cracks were visually enhanced by dye penetration. All cracks were detected at the middle or slightly upper region of the crevice, not at the bottom where the impurity concentration is expected to be higher than other areas, and residual stress is supposed to be higher because of a swaging ferrule. The tubing used for the open crevice had been exposed to NaOH or NaCl solution since the beginning of MB tests.

We can discuss two aspects of the through-wall cracks in the 20-mil gap crevice: crack initiation and propagation to the through-wall condition. In the previous series of NaCl tests, magnetite was packed in the 20-mil gap crevice. Since no gouging was observed on the tube surfaces, it is not likely that cracks were initiated during the previous NaCl tests. Cracks appear to have developed during the NaOH-02 tests because the packed diamond powders were blown out of the crevice during the NaOH-01 test. The crack propagation also appears to have occurred mainly during the NaOH-02 and this test, NaOH-03. A gas pressurization test before starting the NaOH-03 test confirmed that there was no through-wall crack. The question is how cracks can propagate under the unpacked condition. The crack itself can be considered as a crevice, which can cause impurity hideout if it is wide and deep enough. As shown in Figure 97, the crevice samples from the unpacked 20-mil gap crevice did not show high hideout. However, if a deep and long crack had developed, impurity hideout might have occurred inside the deep crack, which made the crack grow during this test.

The test results indicate that hideout/cracking can easily occur in Na-concentrated crevices, even with less flow-restrictive packing like diamond powder. A crack growing in a crevice that was cleaned is potentially very important to SG operators. It suggests that cracks or scratches themselves can become hideout crevices. It may be worthwhile to grow 20-40% through-wall cracks and then test them in the MB to determine if they will increase to 100% through-wall without any crevice or packing present.



Figure 105.
Gas bubbles coming out of through-wall cracks developed inside the unpacked crevice region having a 20-mil radial gap.

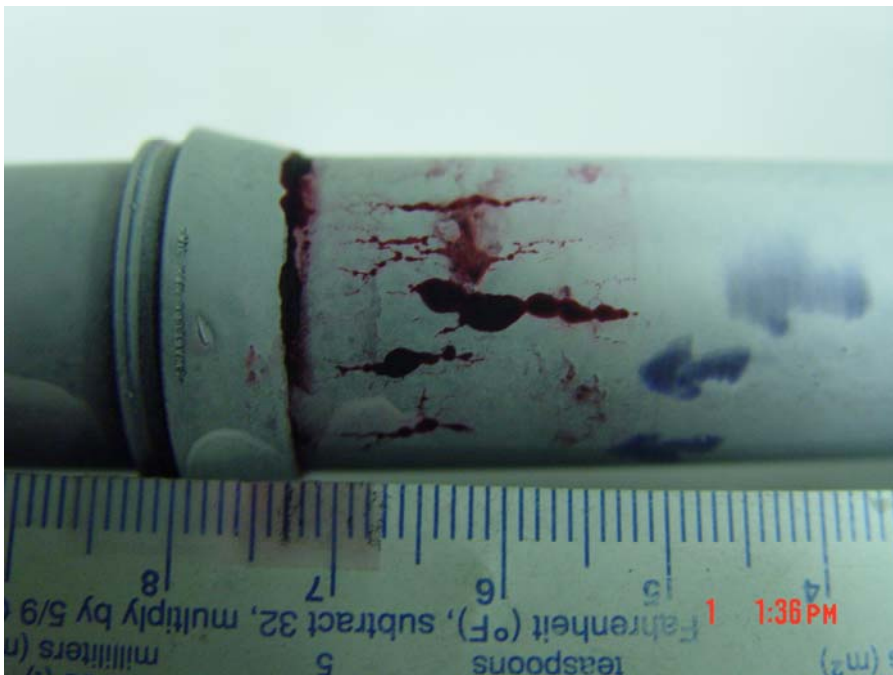


Figure 106.
Axial cracks developed inside the unpacked crevice region and visually enhanced by dye penetration.

5.2.5 Discussion

Starting Point of Leakage

It is important to know when the leakage started from the primary to secondary chamber because leakage could affect the data being analyzed. The primary and secondary water temperatures were plotted as a function of time, as shown in Figure 107. Since the primary and secondary temperatures were well controlled by heater power regulators and a cooling fan, no leakage was evident from the primary and secondary water temperatures. The primary and secondary pressures were also plotted as a function of time, as shown in Figure 108. Again, it was difficult to find any indication of leakage.

The cooling fan speed is plotted as a function of time in Figure 109. Since three rather than two fans were used at $\Delta T=100^\circ\text{F}$, each fan speed was automatically readjusted after the change in ΔT from 60°F to 100°F . Cooling fan speed started to increase gradually at 330 hours, which indicates an increase of the thermal load in the secondary chamber because of leakage from the primary side.

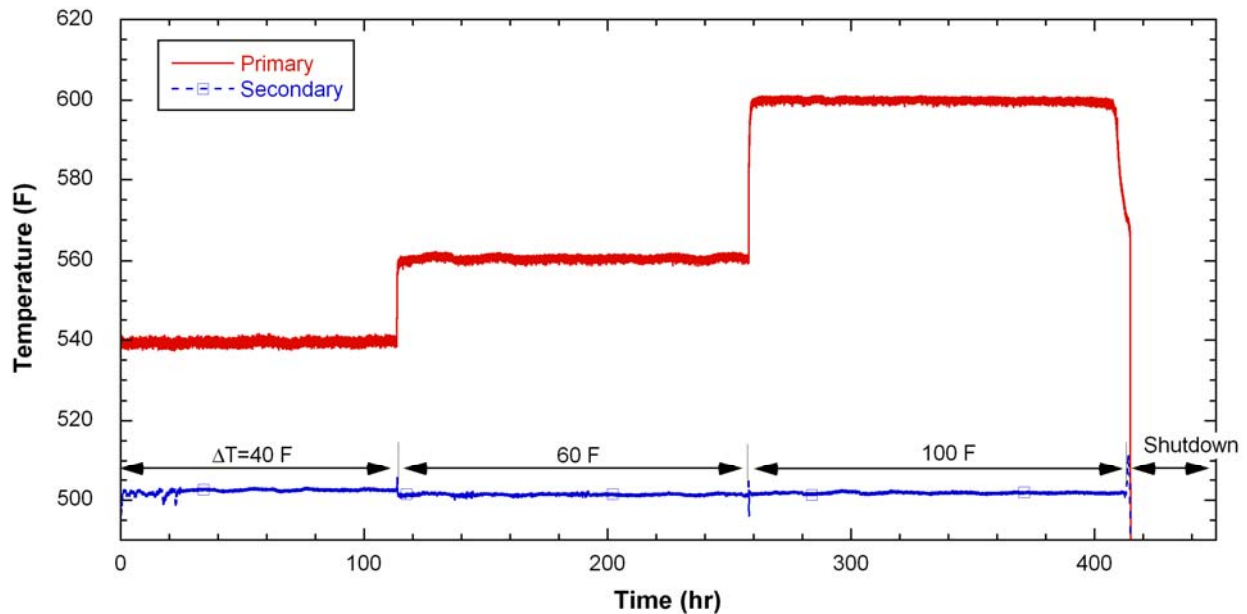


Figure 107. Primary and secondary water temperature variation with time (NaOH-03).

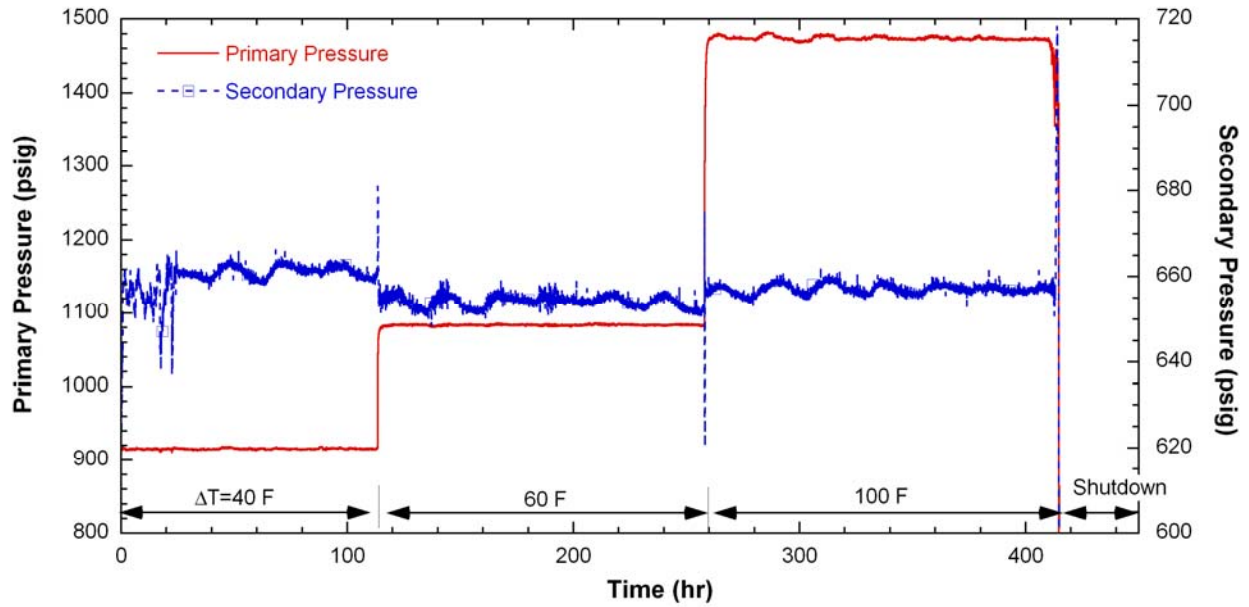


Figure 108. Primary and secondary pressure variation with time (NaOH-03).

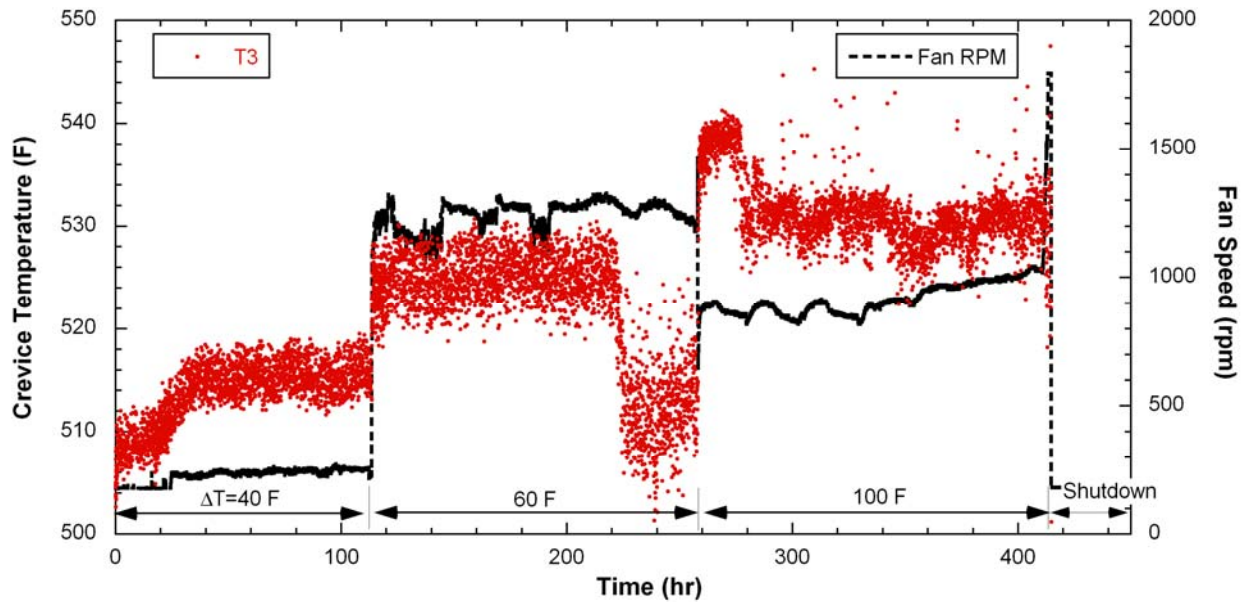


Figure 109. Cooling fan speed and crevice temperature (T3) variations with time (NaOH-03).

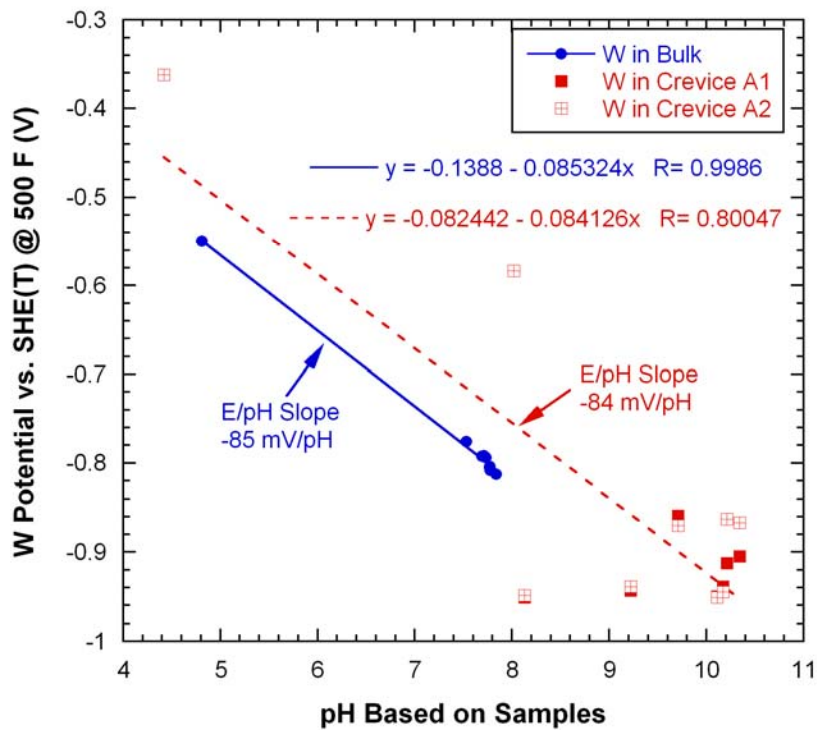
Table 5 summarizes the parameters monitored and the suggested starting time of the leak based on an evaluation of the data. The parameters measured in the bulk water, such as cooling fan speed or bulk conductivity, are less sensitive than the crevice monitoring parameters, as expected.

Table 5. Summary of monitoring parameters and each corresponding time indicating leakage from primary to secondary side.

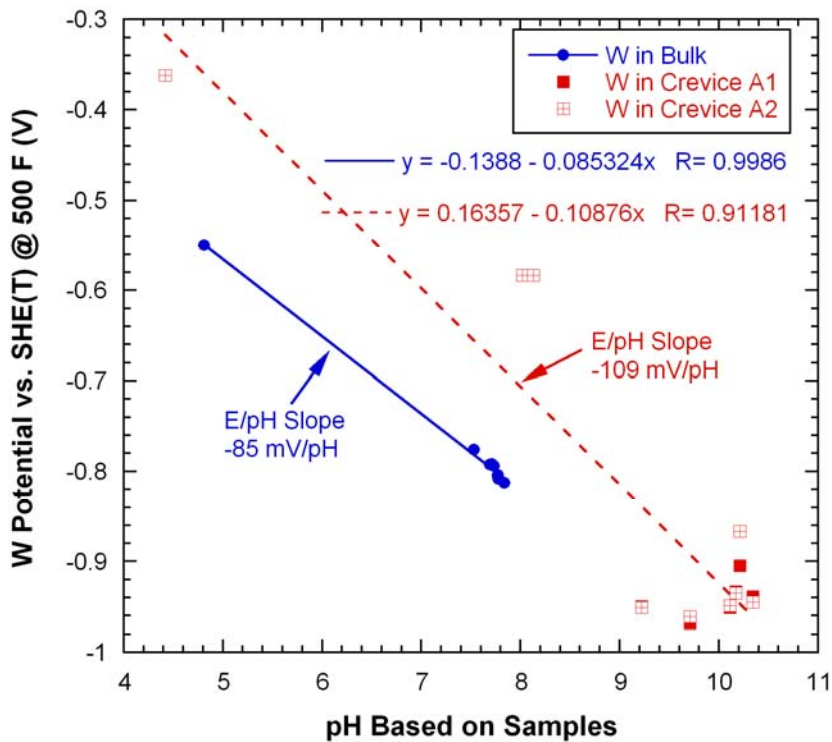
Monitoring Parameter		Time Indicating Leakage	Comments
10-mil Crevice (Packed)	Crevice Temperature	220 hr	Figure 91
	Crevice Conductivity	Earlier than 160 hr	Figure 95
	Crevice Potentials	150 hr	Figure 98
	Crevice Solution Samples	Earlier than 162 hr	Figure 97
20-mil Crevice (Unpacked)	Crevice Temperature (Unpacked Crevice)	160 hr	Figure 92
	Crevice Solution Samples	Earlier than 162 hr	Figure 97
Bulk	Cooling Fan Speed	330 hr	Figure 109
	Bulk Conductivity	280 hr	Figure 94

ECP and pH Data Analysis

In Figure 110, variations in crevice and bulk tungsten potentials are plotted as a function of crevice pH based on sample analysis results. As mentioned with regard to Figure 97, a correction for sampling time was applied. For the bulk water data the correction was not applied because the bulk samples have enough volume to overcome the dead volume of the sampling line. Only the crevice samples taken before the start of leakage were considered in this analysis. As compared with Figure 110(a), the crevice tungsten data after the sampling time correction in Figure 110(b) appear to better fit a single line. The bulk tungsten data show a linear behavior, and their slope is -85 mV/pH , which is less than the Nernstian slope of -106 mV/pH at 500°F , but the slope becomes closer to the Nernstian one when combined with NaCl test data (see Figure 114). The corrected data for crevice tungsten potential and bulk potential were plotted in a potential-pH diagram for the W-H₂O system, shown in Figure 111. The data from the NaCl-03 and -04 tests are plotted in the same figure. The bulk tungsten data in the NaOH test are well fitted to a line with the bulk solution data in NaCl tests, and the slope of the line appears to be close to the theoretical slope, -106 mV . The crevice tungsten data appear to be linear for the overall pH range, but data scatter occurs in the local caustic pH range. As compared with the bulk data, the crevice data in the NaOH test tend to have higher potentials at the same pH level. The oxidation states of the crevice W/WO_x electrode might be different from the bulk water, or the boiling liquid around the crevice tungsten wire tip might affect the potential value. The main purpose of the NaOH-03 test was to confirm the functionality of overall instrumentation. From this point of view, within the pH range of 5-10 at 500°F , the instruments at the crevice and bulk appear to generate reasonable data.



(a) Before sampling time correction



(b) After sampling time correction

Figure 110. Crevice and bulk tungsten potential variation as a function of crevice pH based on samples (NaOH-03).

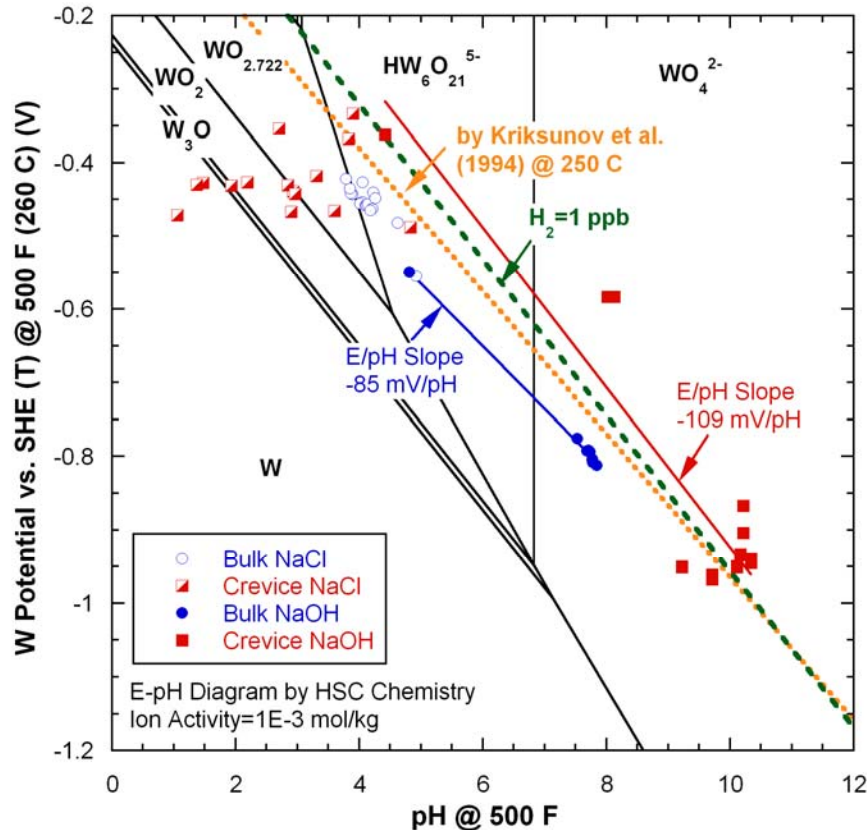


Figure 111. Tungsten potentials in bulk and crevice as a function of pH by sampling results in a potential-pH diagram of W-H₂O system predicted by the thermodynamic code HSC Chemistry.

Crevice Concentration Estimation

Figure 112 shows the variation in integrated-volume averaged crevice Na concentration as a function of time. The crevice Na concentrations were estimated from the data on bulk chemistry, crevice potential, and crevice temperature and compared with concentrations determined from the crevice samples. When estimating the concentration using the bulk samples, we assumed that all of the Na that left the bulk water was concentrated in the 10-mil gap crevice region, which is a credible assumption. The volume-averaged crevice concentration was calculated based on the total Na hideout mass and crevice porosity. The crevice samples showed lower concentrations than the three other estimated values.

The method for estimating the crevice concentration from the crevice temperature is as follows. The boiling point elevation was assumed to be as the temperature difference between the crevice temperature and the secondary saturation temperature of 500°F. As shown in Figure 113, MULTEQ[®] can predict the relationship between crevice concentration and corresponding BPE. The relationship is represented as follows:

$$[Na (ppm)] = \frac{BPE (F) + 0.053497}{0.00019134} \quad (4)$$

In this MULTEQ calculation, a static condition and steam-retained option were selected. By means of Eq. (4), we estimated the Na concentration from the crevice temperature data. The crevice tungsten potential data can also give the Na concentration in the crevice. Before NaOH solution injection, the

crevice tungsten potential and pH were -0.362 V (vs. a standard hydrogen electrode) and 4.42, respectively. If the slope of the line relating potential to pH is determined, the crevice pH can be estimated from the crevice tungsten potential data. As shown in Figure 114, the potential/pH slope for the tungsten/tungsten oxide electrode was determined from the tungsten potential data for the bulk solution. Since we know the tungsten potential/pH slope and we have the pH and corresponding potential for one instant in time in the crevice, a linear equation can be derived for the relationship between crevice tungsten potential and crevice pH. The data in Figure 113 (from MULTEQ[®]) can then be used to relate the crevice pH (determined from the crevice potential) to the Na concentration. Based on the data in Figure 113, the logarithmically fitted equation was derived:

$$[Na(ppm)] = 10^{\frac{pH - 7.3378}{0.67514}} \quad (5)$$

From Eq. (5), the crevice Na concentration was estimated from the crevice tungsten potential data. The estimated Na concentration was similar to the estimated value from the crevice temperature data at $\Delta T = 40^\circ\text{F}$ and slightly lower at $\Delta T = 60^\circ\text{F}$, as shown in Figure 112. If the test had been continued without the leakage at $\Delta T = 60^\circ\text{F}$, the discrepancy between the two data sets might have decreased.

Based on the comparison results shown in Figure 112, the Na concentration determined from the crevice samples tends to follow the same general trend as the Na concentration determined by other methods but they are lower than those estimated using other methods. The crevice samples may be diluted because less concentrated solution from the bulk region is mixed with the solution from the crevice bottom region, even though the sampling line itself is located at the crevice bottom region.

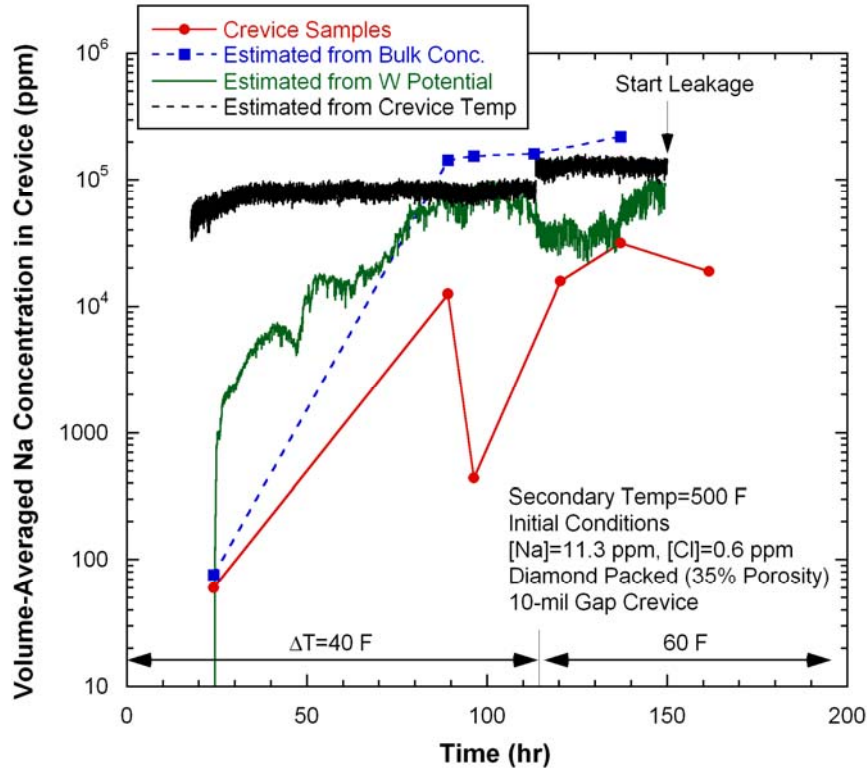


Figure 112. Volume-averaged crevice Na concentration estimated from bulk chemistry data, tungsten potential in crevice, and temperature data in crevice as compared with the analyses for crevice samples (NaOH-03).

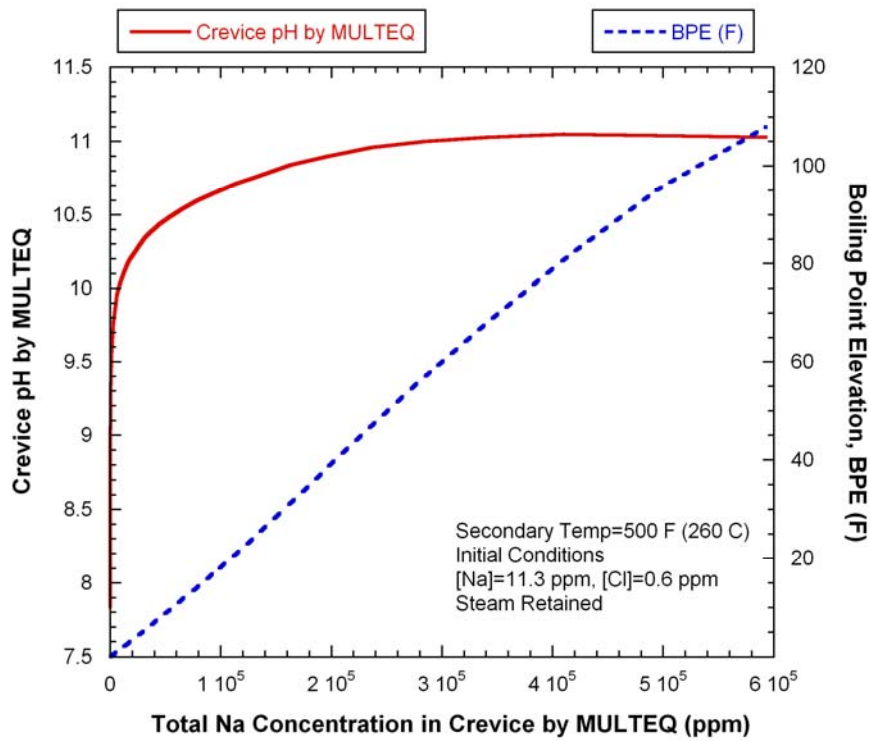


Figure 113. Calculated pH and boiling point elevation variation as a function of total Na concentration in crevice predicted by MULTEQ.

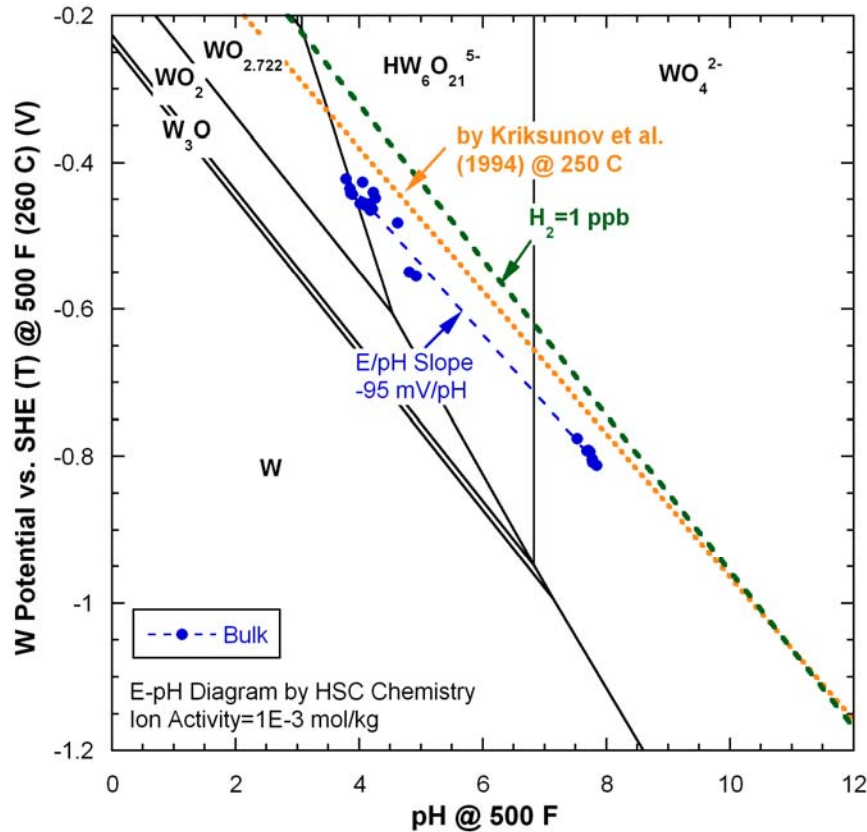


Figure 114. Measured tungsten potentials as a function of pH based on bulk solution samples plotted in a potential-pH diagram of W-H₂O system predicted by the thermodynamic code HSC Chemistry.

5.2.6 Summary

The NaOH-3 test involved a NaOH solution and only one crevice packed with diamond powder. The tungsten potential data for the bulk solution were consistent with the previous data measured in tests with NaCl chemistry. The crevice tungsten potential data showed good linearity within the pH ranges of 5-10, even though data scatter occurred in narrow pH ranges. Based on these results, the crevice chemistry instrumentation itself appears to work properly under the NaOH chemistry. The integrated-volume averaged Na concentrations in the crevice were estimated from the bulk samples analysis results, the crevice temperature, and crevice tungsten potential, and compared with Na concentrations estimated from the crevice solution samples. The estimated crevice concentrations from the bulk samples, the temperature, and tungsten potentials are higher than that by the crevice samples which might be diluted during sampling processes by being mixed with bulk solution, but the three data sets follow similar trends. Through-wall cracks developed in the unpacked crevice during this test. Crack growing in a crevice that was cleaned is potentially very important to SG operators. It may indicate that cracks or scratches themselves can become hideout crevices.

5.3 NaCl-05: NaCl (MR=0.7) Test with Diamond Packing

5.3.1 Background

Since the NaOH-03 test confirmed that the crevice chemistry instrumentation worked properly, the bulk water chemistry was returned to NaCl. Test NaCl-05 involved only one diamond-packed crevice having a radial gap of 10 mils. The crevice was packed with 127-165- μm -dia diamond grit. The estimated crevice porosity was 40 %. This arrangement allowed us to focus more carefully on only one crevice producing hideout for the NaCl chemistry. The initial Na-to-Cl MR in the bulk water was set at 0.7. The previous test with MR=0.7, NaCl-04, followed the NaCl-03 test without opening of the secondary chamber. As discussed in Section 4.4, the NaCl-04 test appeared to be affected by the NaCl-03 test. The NaCl-05 tests will permit verification of the NaCl-04 tests. As a result of the cracking of the alloy 600 tubing in the NaCl-04 test, the SG tubes were replaced with 7/8-in. dia. alloy 690 TT for the NaCl-05 test. An unpacked crevice having 20-mil radial gap was not tested during the NaCl-05 and following tests.

5.3.2 Temperature Data

As shown in Figure 115, the crevice temperature started to increase right after the solution injection in NaCl-05. One thermocouple was installed near the crevice electrode assembly labeled “Near Electrodes” in Figure 115. This reading showed similar behavior to other thermocouples but was about 1°F higher than others at $\Delta T=40^\circ\text{F}$. At $\Delta T=60^\circ\text{F}$, the “Near Electrodes” thermocouple was about 6°F higher than T2. After the increase in ΔT , two of the thermocouples exhibited noisy behavior, followed by stabilization at the secondary saturation temperature. T2 also started to decrease followed by gradual recovery, and T1 recovered its original temperature value when T2 returned to its original value. The “Near Electrodes” thermocouple exhibited a noisy signal and did not come back to the original value. The temperature variation observed at $\Delta T=60^\circ\text{F}$ was not evident in the earlier MR=0.7 test (NaCl-04). After increasing the ΔT from 60 to 80°F, T1 and T2 did not show a noisy signal. The post-test examination indicated that all the diamond powder was secure inside the crevice, but that the thermocouples may have slipped since they were not tightly secured. Therefore, a reasonable explanation for the unexpected temperature oscillation is that the thermocouples slipped during the test and were pushed backward from the tube wall, which led to the decrease of temperature. Then, as concentration proceeded at the thermocouple tip area, the temperature returned to the original value or even higher. The temperature data obtained after the occurrence of instability was not used for further analysis. The “Near Electrodes” thermocouple started to malfunction at 215 hours, probably because the protective alloy 600 sheath failed by corrosion. At $\Delta T=80^\circ\text{F}$, a second solution was injected to confirm that the crevice had become saturated but it is difficult to determine the saturation from the temperature data because of the thermocouple problem. In the next test, a new method of positioning and tightening the thermocouples was used.

In Figure 116, the normalized crevice temperatures are plotted as a function of time. The temperature elevation after the solution injection is clearly evident. The normalized crevice temperature, however, did not change significantly after the increase of ΔT from 40 to 60°F.

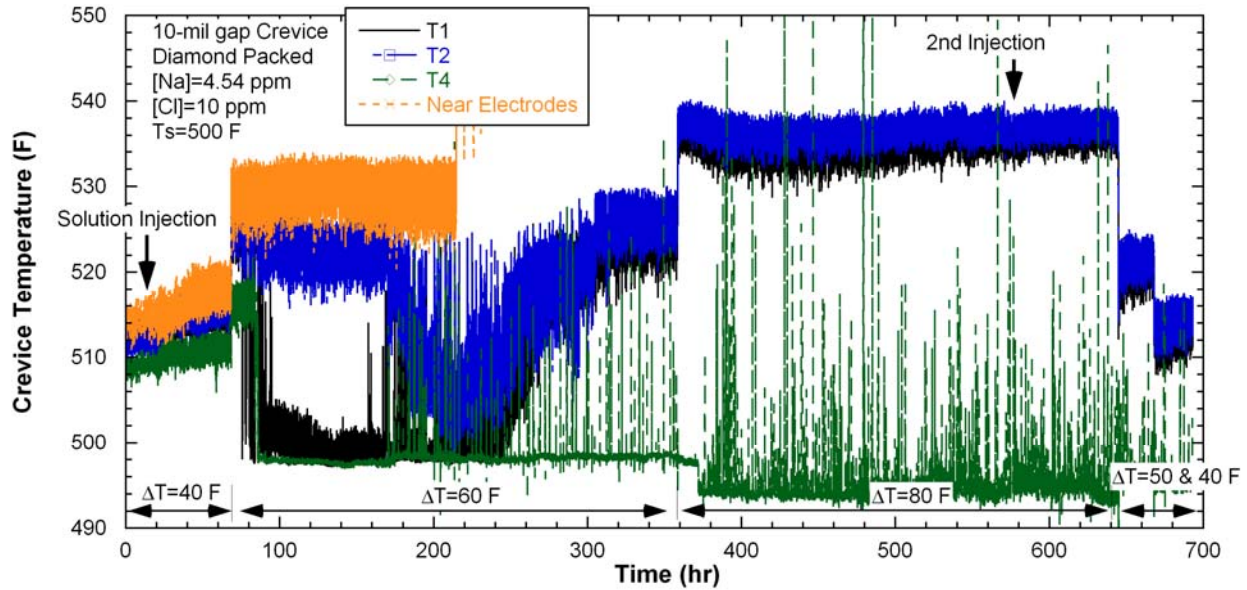


Figure 115. Crevice temperature variation with time in the 10-mil gap crevice packed with diamond powder (initial MR=0.7; NaCl-05).

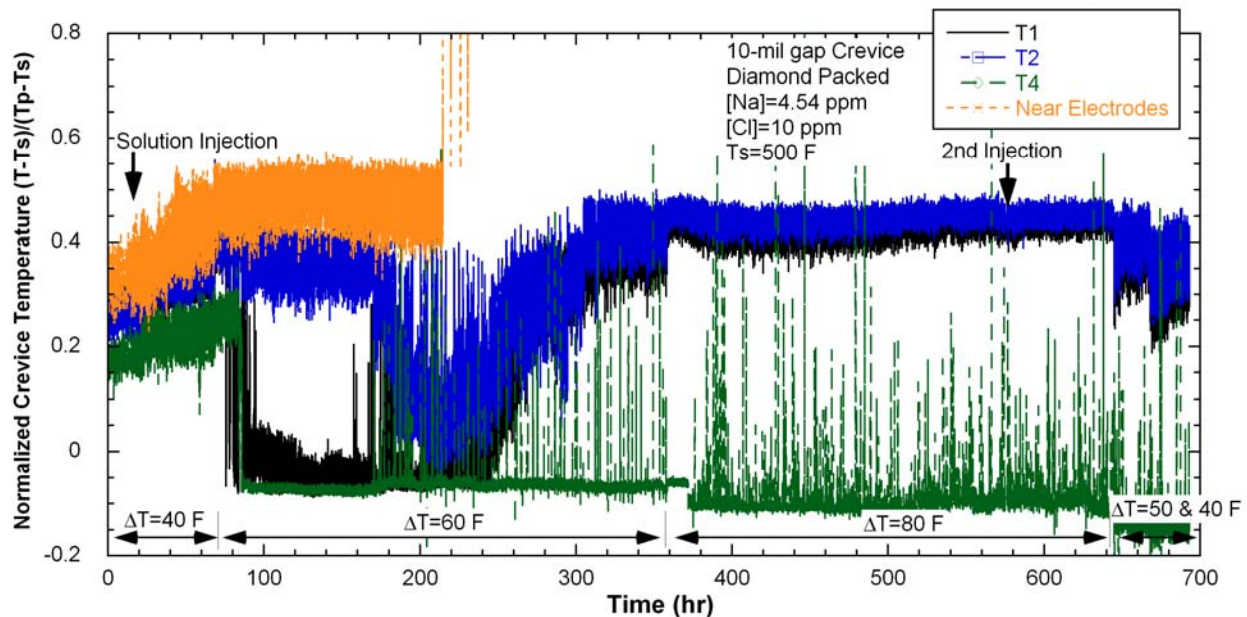


Figure 116. Normalized crevice temperature variation with time (initial MR=0.7; NaCl-05).

5.3.3 Bulk and Crevice Chemistry

Figure 117 shows the conductivity variation with time for the bulk solution in NaCl-05. Most of the bulk conductivity reduction occurred at $\Delta T=60^\circ\text{F}$. Based on the MULTEQ code prediction, NaCl precipitation can occur if the boiling point elevation exceeds 46°F . Therefore, it is likely that the NaCl precipitation occurred inside the crevice and became saturated after about 100-hours operation at $\Delta T=60^\circ\text{F}$. The occurrence of the NaCl precipitation will be verified by a mass balance analysis, discussed

in Section 5.3.6. When increasing ΔT from 60 to 80°F, the bulk conductivity initially decreased but became stabilized in a short time, indicating that most of the NaCl precipitation had already occurred at $\Delta T=60^\circ\text{F}$. The bulk conductivity increased immediately after injecting more MR=0.7 NaCl solution and did not decrease with time, indicating that the crevice is in a fully saturated state. During the test period of 240-320 hours, the Cl concentration decreased while the Na concentration increased slightly. The concentration change is slightly higher than analysis error ($\pm 10\%$) and, considering that the tube surfaces were corroded (based on post-test inspection), electromigration might have occurred during this time period; the dissolved metal cations from the corrosion drove Na^+ out of the crevice and Cl^- into the crevice.

The variation in crevice conductivity with time is plotted in Figure 118. The crevice conductivity increased suddenly a few hours after the first solution injection. It then quickly stabilized at $\Delta T=40^\circ\text{F}$. After the increase of ΔT from 40 to 60°F, crevice conductivity did not change significantly, but about 30 hours later it started to decrease and stabilized at another value. However, the crevice conductivity started to increase again and stabilized at the same value as before. The crevice conductivity variation at $\Delta T=60^\circ\text{F}$ is unexpected and difficult to be explained by simple impurity hideout mechanism. After ΔT was increased from 60 to 80°F, the crevice conductivity slowly increased, followed by a slow decrease. If the NaCl precipitation occurred around the conductivity probes, the crevice conductivity should decrease. Therefore, the conductivity change at $\Delta T=80^\circ\text{F}$ may be attributed to the NaCl precipitation around the conductivity probe.

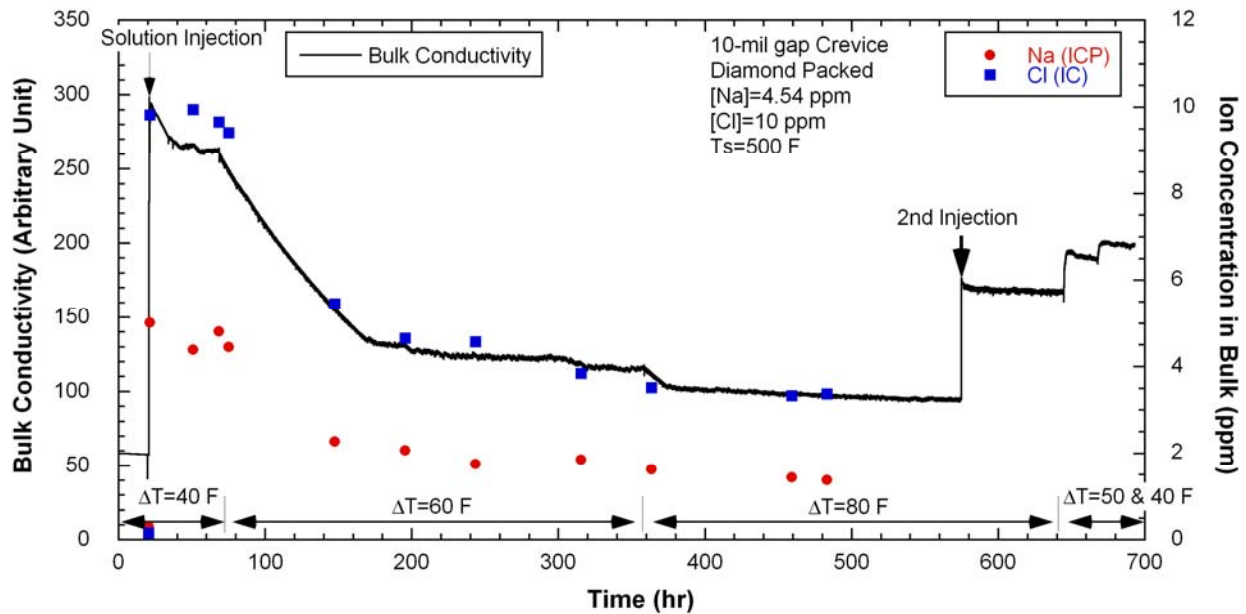


Figure 117. Bulk conductivity variation with time and the chemical analysis results for bulk samples (initial MR=0.7; NaCl-05).

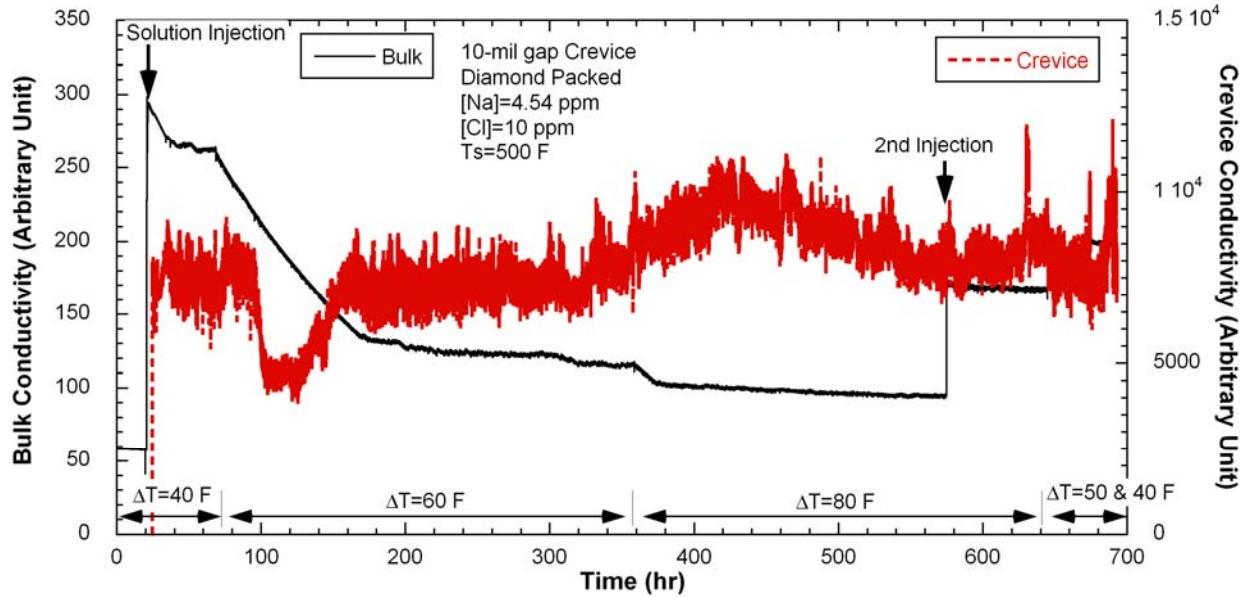


Figure 118. Bulk and crevice conductivity variation with time (initial MR=0.7; NaCl-05).

Figure 119 shows the variation in ion concentration based on the analyses of crevice samples. As discussed earlier, the sampling time correction was applied to minimize the effect of the sampling-line dead volume. The initial ion concentration in the crevice increased rapidly but suddenly dropped to about the bulk concentration before the change in ΔT from 40 to 60°F. About 60 hours later, it recovered to the initial high value. The timing is not exactly consistent with the crevice conductivity drop but, as shown in Figure 118, the crevice conductivity showed similar behavior. These results suggest the possible instability of the crevice hideout. Additional investigations could lead insights on whether or not this crevice instability is generic and repeatable and can occur in a magnetite-packed crevice and in the actual field SG crevice. The Na and Cl concentrations in this test are much higher than those in the NaCl-04 test (Figure 73) at $\Delta T=40$ and 60°F. These results support the earlier observation that the crevice concentrations in the NaCl-04 test were affected by the previous NaCl-03 test.

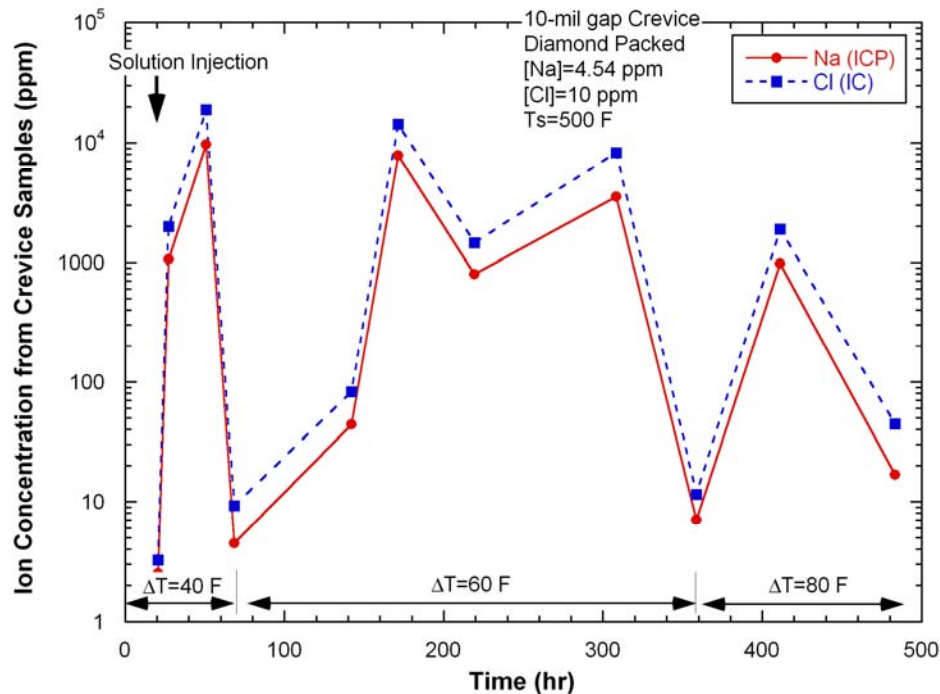


Figure 119. Chemical analyses of the crevice samples (initial MR=0.7; NaCl-05).

5.3.4 ECP Measurements

Figure 120 shows the tungsten potential changes in the bulk and the crevice during NaCl-05. The bulk potential drop after the solution injection is 164 mV. The pH change calculated by MULTEQ using the chemical analyses of the bulk samples is 1.95, which corresponds to a potential change of 185 mV. The calculated potential change is close to the measured bulk potential change. Two tungsten/tungsten oxide electrodes were installed in the 10-mil gap crevice separated by 30 degrees at the same crevice elevation. The two tungsten potentials showed very similar behavior. The bulk tungsten potential gradually decreased during the test period at $\Delta T=60^\circ\text{F}$ and stabilized at $\Delta T=80^\circ\text{F}$. If the Na-to-Cl MR in the bulk water remains at 0.7, the bulk water pH will increase because the absolute amount of H^+ ions needed to maintain charge neutrality will decrease as the absolute Na and Cl amounts decrease in the bulk water. This explanation is supported by the pH calculations for bulk samples, as described in Section 5.3.6. The crevice tungsten potential was almost insensitive to the change in ΔT , except for the initial 20 hours after the first solution injection. The initial increase after the first solution injection was caused by the transition from pure water to the acidic NaCl solution. The following abrupt potential decrease was caused by the volatility effect of Cl, which is supported by the finding that, in the same short time period, bulk tungsten potential slightly increased, indicating preferential Na concentration and resultant acidification of the bulk water. However, the crevice tungsten potentials increased again, and this change suggests that the volatility effect of Cl became less significant. Based on the post-test examination showing the gouging on the tube surfaces, the insensitiveness of the crevice tungsten potential might be due to the crevice tungsten wire tip being too far from the tube surface to represent the active chemical change near the tube surface.

The Ta/TaO_x electrode was introduced for the first time during this test and was expected to serve as a pH electrode, just as the W/WO_x electrode did. As shown in Figure 121, the bulk potential decreased 160 mV after the chemical injection at 20 hours, which is very close to the tungsten potential change of 164 mV. The bulk Ta potential stayed almost the same for the test period; this behavior differs from that

of the bulk tungsten potentials shown in Figure 120. Detailed comparisons between tungsten and Ta electrodes are discussed in Section 5.3.6. There was no advantage observed in using a Ta electrode over a tungsten electrode.

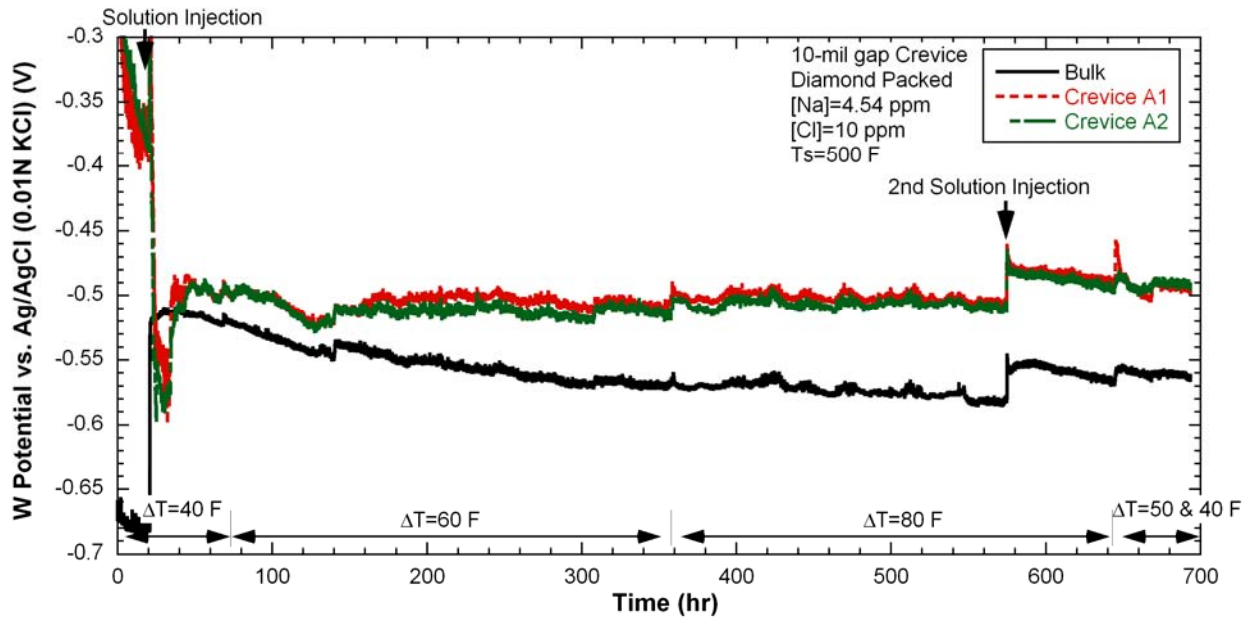


Figure 120. Tungsten potential variation with time in the bulk and 10-mil gap crevice packed with diamond powder (initial MR=0.7; NaCl-05).

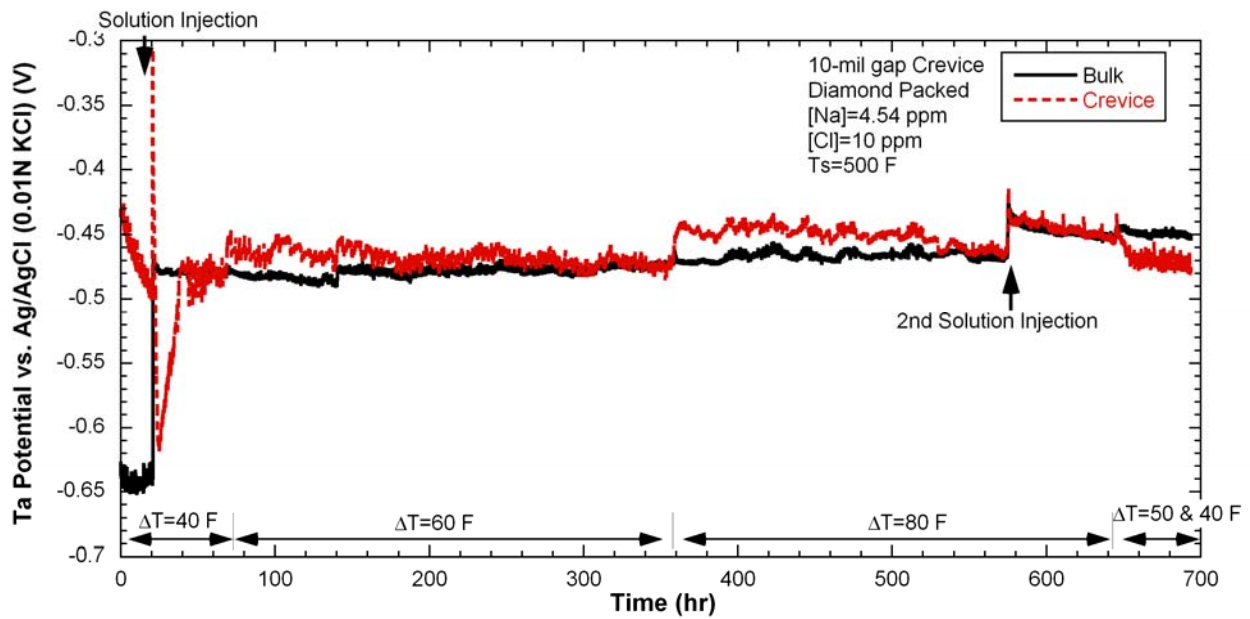


Figure 121. Ta potential variation with time in the bulk and the 10-mil gap crevice packed with diamond powder (initial MR=0.7; NaCl-05).

5.3.5 Post-Test Examination

Figure 122 shows the top of the crevice ring after removal of the Ni-Cr-Mo alloy foam and retaining ring, and shows that the diamond dust was secure inside the crevice. Gouging was apparent over the alloy 690 TT tube surfaces, as shown in Figure 123. The degree of gouging is comparable with that observed on the alloy 600 surfaces after the NaCl-03 and -04 tests, as shown in Figure 84. The corrosion data of alloy 690 TT under strong acid environments are very limited. Based on this gouging observation, the corrosion resistance of alloy 690 TT in a strong acid is comparable with that of alloy 600 MA. The severe gouging on the tube surfaces suggests that a strong acid chemistry developed in the crevice in this test. As discussed in Section 3.2.1, the abrasion of hard diamond particles might enhance this gouging. For this reason and others, a magnetite-packed crevice test similar to NaCl-05 should be conducted and compared with the results of the diamond-packed crevice test. The calculated pH from the crevice samples supports the development of acidic crevice chemistry, but the crevice tungsten potentials, shown in Figure 120, do not support this observation. No evidence suggests the development of strongly alkaline crevice chemistry in this test. Therefore, it is reasonable to try to explain the insensitivity of the crevice tungsten potentials to the changing chemical conditions within the crevice. As mentioned earlier, the crevice tungsten wire tip was probably placed too far from the tube surface to represent the actual chemistry. Assuming the development of an acidic crevice chemistry, the increase of bulk Na concentration and corresponding decrease in bulk Cl concentration can be interpreted as the result of ion migration. Ion migration would take place to maintain charge neutrality after excess metal cations accumulated in the crevice.

To determine if the tube surface cracked, the tubing was removed from the MB, and a dye penetrant test was performed. Figure 124 shows the tube surface area before application of the dye penetrant. To make sure that no crack had formed on the tube, the hard scales were removed, and the dye penetrant was applied, as shown in Figure 125. No cracks had formed underneath the hard scale. The black hard scale shown in Figure 124 seems to be magnetite because it stuck to a magnet. The source of the magnetite is likely the inner surface of the MB secondary chamber made of SS. The solution pH of the current test is slightly acidic, which can enhance the dissolution of magnetite from the SS surfaces and increase the bulk Fe ion concentration.



Figure 122.
Top of the crevice ring after removal of the Inconel foam and retaining ring, which shows the diamond dust was secure inside the crevice.



Figure 123.
Alloy 690 TT tubing surface after removal of the crevice ring and diamond dust showing gouging in the crevice region.



Figure 124.
Bare alloy 690 TT tubing
surface (left: crevice top,
right: crevice bottom).



Figure 125.
Dye penetrant test results
after removal of the hard
scale underneath the SS
back ferrule showing no
visible cracks in the
crevice region.

5.3.6 Discussion

Potential and pH Analysis

In Figure 126, the tungsten and Ta potentials in the crevice and bulk solution are plotted as a function of pH. The pH was estimated from the solution sample chemistry using MULTEQ. The sampling time correction was applied to all data. The tungsten potentials in the bulk solution show very good linearity with respect to pH, but the Ta potentials exhibit scatter in a narrow pH range of 4-5. The potential/pH slope of the tungsten electrode is much less than the Nernstian slope of -106 mV/pH . There is no available data for Fe or Ni ion concentration in the bulk water, but the magnetite deposits observed in the crevice region suggest the presence of significant metal ions in the bulk water, which can increase the solution pH but could not be considered in Figure 126. If Fe and Ni concentration data is available and estimated bulk pH shifts in the alkaline direction by the effect of dissolved metal ions, the potential/pH slope will become steeper and closer to the Nernstian value. The W/WO_x electrode is more appropriate in NaCl solution than the Ta/TaO_x electrode as a pH sensor because the tungsten potential changes more substantially with respect to the bulk pH change. Neither the tungsten nor Ta potentials in the crevice varied significantly which is inconsistent with the pH change estimated from the crevice samples.

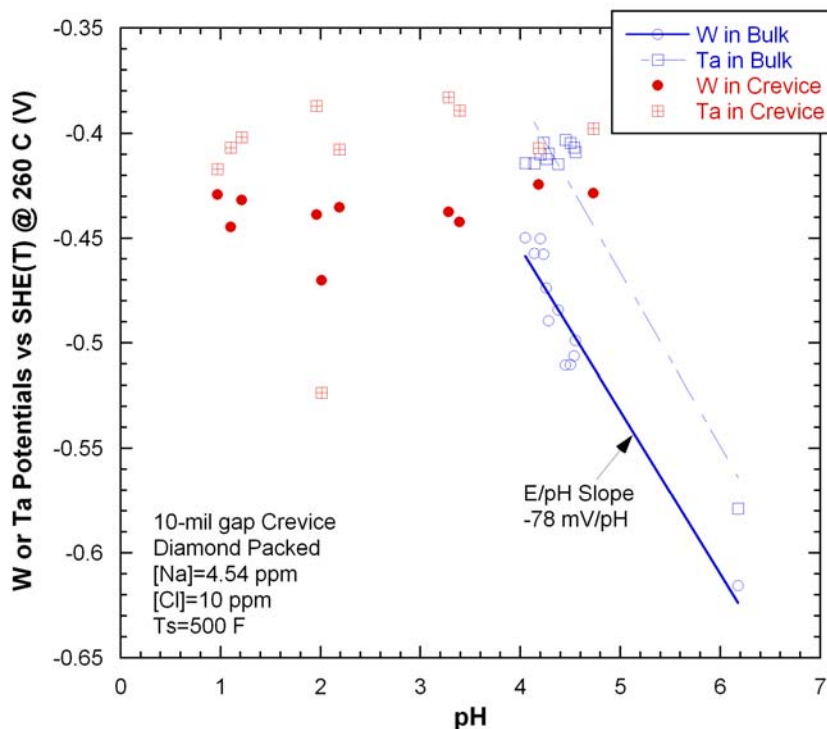


Figure 126.
Tungsten and Ta potentials in bulk and crevice as a function of pH estimated from the solution samples by MULTEQ (initial MR=0.7; NaCl-05).

In Figure 127, the measured data in NaCl-05 are compared with the previous NaCl and NaOH test data. The tungsten potential data for the bulk solution in the present test are consistent with the previous data. The crevice tungsten potential data in this test are within the same range as the previous data, but the crevice potentials are again insensitive to crevice sample pH in this test. As discussed earlier, because the crevice tungsten wire tip was not close enough to the tube surface, the crevice tungsten potentials appear to be insensitive to the pH change and indicate only weakly acidic crevice chemistry. The effect of the crevice tungsten wire tip location is discussed again in the next test (NaCl-06). A dashed line designated

by 'Kriksunov et al.' denotes a measured potential of tungsten oxide electrode as a function of pH at 250°C by Kriksunov and Macdonald²⁹.

Figure 128 shows the MR variation in the bulk and crevice samples with time for NaCl-05. The bulk MR was in the range of 0.6-0.8, and the crevice MR was higher than the bulk MR at most times but still less than unity. At $\Delta T=40^\circ\text{F}$ and 60°F , the bulk and crevice MRs tend to vary in opposite directions, which is an expected result because the model boiler system is a closed one so that mass balance should be maintained between bulk and crevice. But at $\Delta T=80^\circ\text{F}$ the crevice MR follows the bulk MR. These results suggest that at lower ΔT the crevice samples represent actual crevice chemistry, but at higher ΔT the crevice samples are mixed with bulk solution so that the crevice MR becomes similar to the bulk MR.

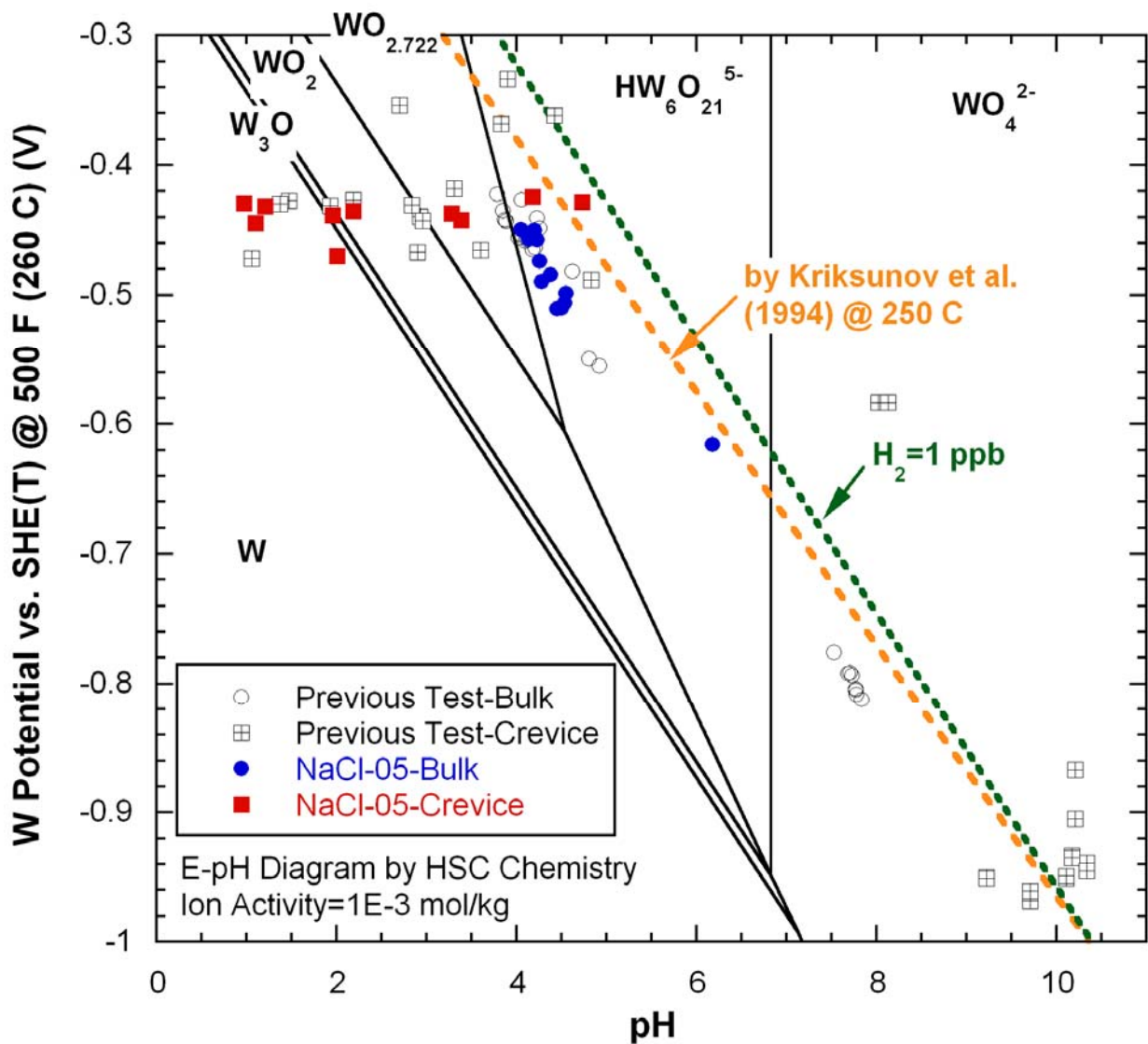


Figure 127. Tungsten potentials measured during NaCl-05 compared to the data from previous tests plotted in a phase diagram of W-H₂O system predicted by the thermodynamic code HSC Chemistry.

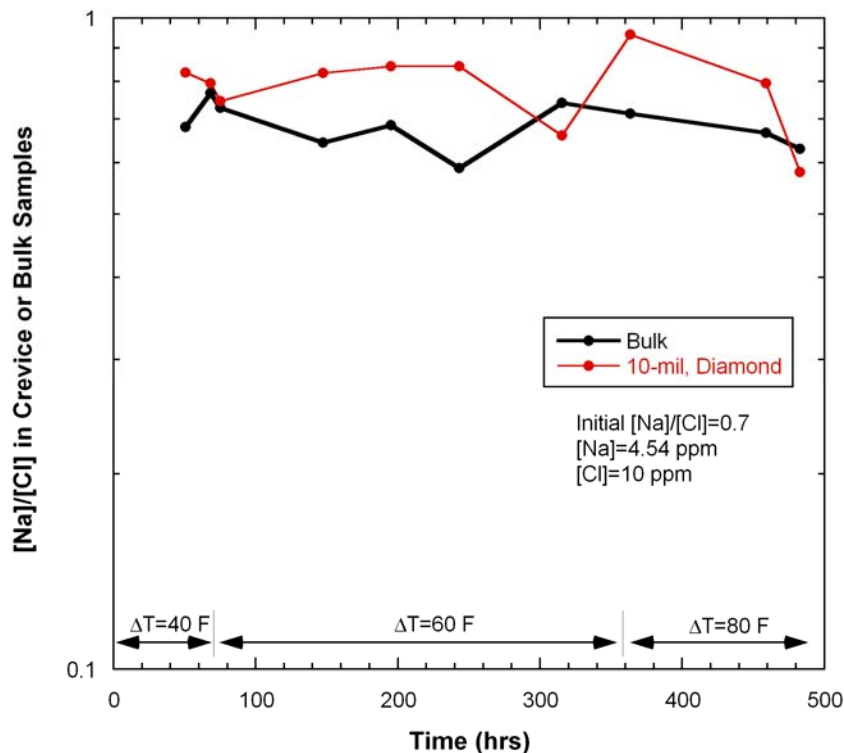


Figure 128. Molar ratio variations in bulk and crevice samples with time (NaCl-05).

Mass Balance Analysis

Figure 129 shows the total mass of Na and Cl in the crevice as a function of time, which is estimated from the analysis results for the bulk samples. As was done in the analysis of the NaOH-03 test data, we considered the mass losses by the crevice and bulk sampling. The Na and Cl masses before the ΔT change from 40 to 60°F are relatively small. At a given ΔT , an impurity concentration limit in the crevice can be determined thermodynamically, which is called a thermodynamic limit. If the thermodynamic limit is larger than a solubility limit, the solubility limit becomes an effective limit. The estimated thermodynamic limit by MULTEQ at $\Delta T=40^\circ\text{F}$ is 28.9 mg for Na and 44.5 mg for Cl, and these limits are much higher than the measured crevice Na and Cl masses. Therefore, the crevice did not reach the thermodynamic limit at $\Delta T=40^\circ\text{F}$. However, after the ΔT was changed from 40°F to 60°F, significant Na and Cl hideout occurred. In Figure 129 the solubility limits of Na and Cl are also plotted. The Na and Cl masses became saturated much above the Na and Cl solubility limit calculated by MULTEQ. At $\Delta T=60^\circ\text{F}$ the precipitated NaCl on the tube surfaces and the concentrated liquid appear to coexist because the hideout masses of Na and Cl exceeded the solubility limit. To determine the variation of the Na-to-Cl molar ratio, the Na and Cl hideout amounts were plotted on a molar basis instead of mass, as shown in Figure 130. Except at $\Delta T=40^\circ\text{F}$ and the early part of $\Delta T=60^\circ\text{F}$, the Na-to-Cl molar ratio was less than one. If the total amounts of Na and Cl in Figure 129 or 130 are used as input values for MULTEQ, the predicted crevice pH is less than 1.0, which means strong acid chemistry developed inside the crevice.

To compare test results obtained from different bulk concentrations, the term “Na or Cl exposure” is introduced, which is defined as the time integration for the variation in bulk concentration. Figure 131 shows the Na and Cl masses as a function of Na and Cl exposures. At $\Delta T=40^\circ\text{F}$ the Na hideout is much

faster than Cl hideout at the same bulk solution exposure, probably because of the volatility effect of Cl. As ΔT increased, Cl hideout became larger. Since Na and Cl have different atomic weights, the comparison with molar quantity is better suited to evaluating the Na or Cl preferential concentration in the crevice. Figure 132 shows the total moles of Na and Cl in the crevice as a function of Na and Cl exposures. The results in Figure 132 still indicate that, at lower ΔT , Na tends to accumulate preferentially in the crevice, but at higher ΔT , Cl hideout becomes more efficient under the diamond-packed crevice condition and $MR=0.7$. At $\Delta T=60^\circ\text{F}$ the Cl hideout rate was almost the same as the Na hideout rate. This finding suggests that the volatility effect of Cl became less significant, probably because the formerly present Na-rich liquid phase caused a boiling point elevation and decreased the boiling rate. As discussed earlier, the results in Figure 129 suggest that the metal cations in the crevice drive Cl^- ions into the crevice at $\Delta T=60^\circ\text{F}$.

In Figure 133, Na mass variations in the crevice obtained from the NaOH-03 test are compared with those from the NaCl-05 test. In the NaCl-05 test, the Na mass before changing ΔT from 40 to 60°F was much lower than the steady state value of the NaOH-03 test at $\Delta T=40^\circ\text{F}$. But at $\Delta T=60^\circ\text{F}$, significant Na hideout occurred in the NaCl-05 test. The discrepancy of Na hideout in the two tests may be interpreted as due to the bulk chemistry difference ($\Delta T=60^\circ\text{F}$) and exposure time difference ($\Delta T=40^\circ\text{F}$). If NaCl has a similar solubility limit to NaOH, the steady-state Na mass at $\Delta T=60^\circ\text{F}$ will be smaller and closer to that of the NaOH-03 test. However, NaCl has a much lower solubility than NaOH, which could result in NaCl precipitation. The crevice at $\Delta T=60^\circ\text{F}$ in the NaCl-05 test appears to be composed of NaCl precipitation and saturated NaCl solution because the Na and Cl hideout mass observed at $\Delta T=60^\circ\text{F}$ exceeded the NaCl solubility limit. Additional tests could confirm whether the low Na mass at $\Delta T=40^\circ\text{F}$ in the NaCl-05 test, as compared with the NaOH-03 test, was caused by the bulk chemistry difference or shorter exposure time. Assuming the whole crevice areas reached the NaCl solubility limit, the maximum Na mass is 33 mg with the given crevice porosity. If unoccupied space in the crevice is completely filled with NaCl precipitation, the maximum Na mass is 94 mg. By using the two limiting values, we estimated how much volume of crevice is filled with NaCl precipitates. At $\Delta T=60^\circ\text{F}$, 40 % of the unoccupied space in the crevice is filled with NaCl precipitates, and 50 % is filled at $\Delta T=80^\circ\text{F}$. The top area of the crevice near the mouth should have lower concentration because of the concentration gradient between the bulk solution and crevice. Therefore, the actual fraction of crevice area filled with NaCl precipitates is larger than the estimated value.

Appendix B presents a mass balance analysis for the NaCl-05 test with a simple analytical method applicable to a closed system like the MB.

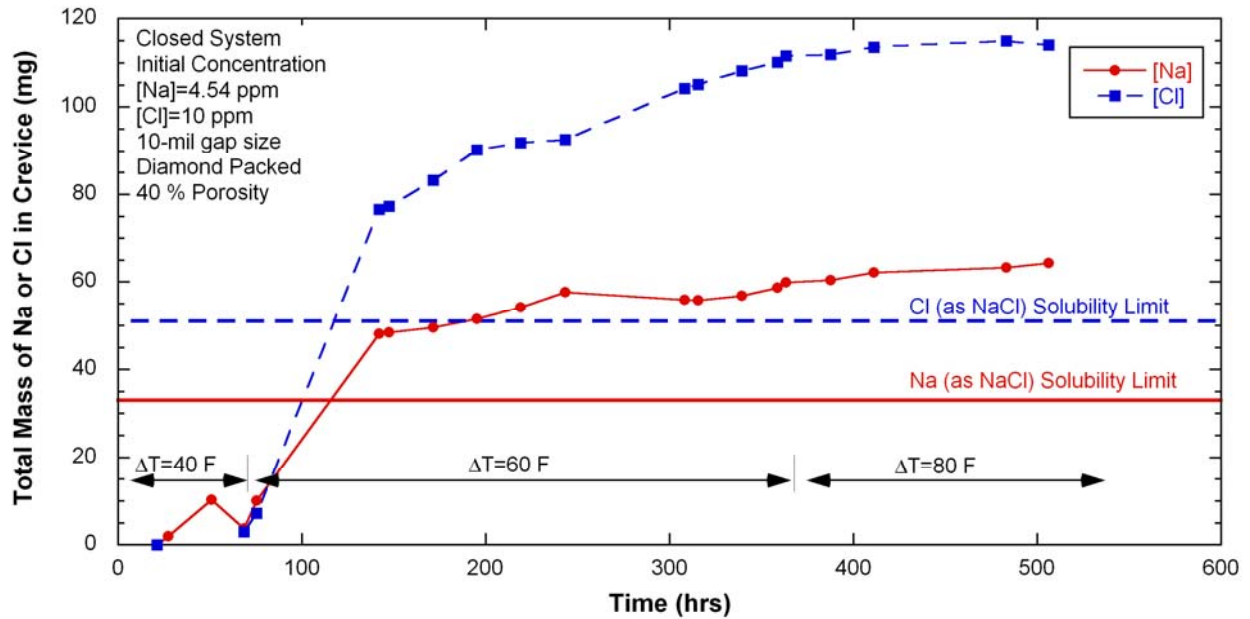


Figure 129. Total mass of Na and Cl in crevice as a function of time for the previous MR=0.7 test with single diamond-packed crevice (estimates from the analysis of bulk samples; NaCl-05).

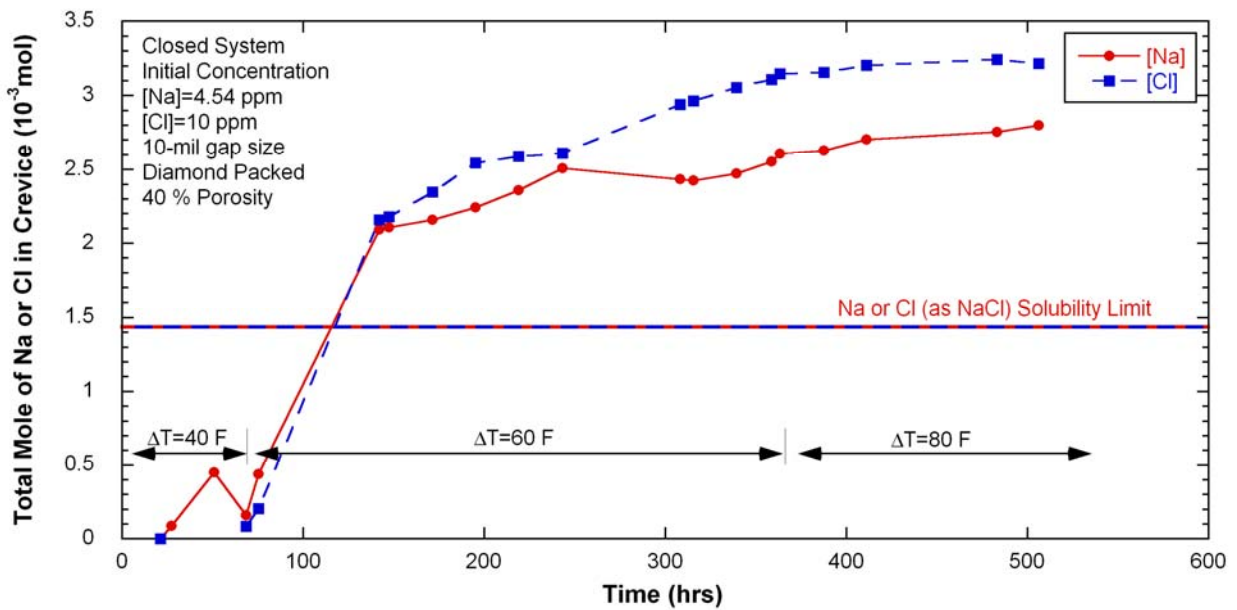


Figure 130. Total moles of Na and Cl in crevice as a function of time for the previous MR=0.7 test with single diamond-packed crevice (estimates from the analysis of bulk samples; NaCl-05).

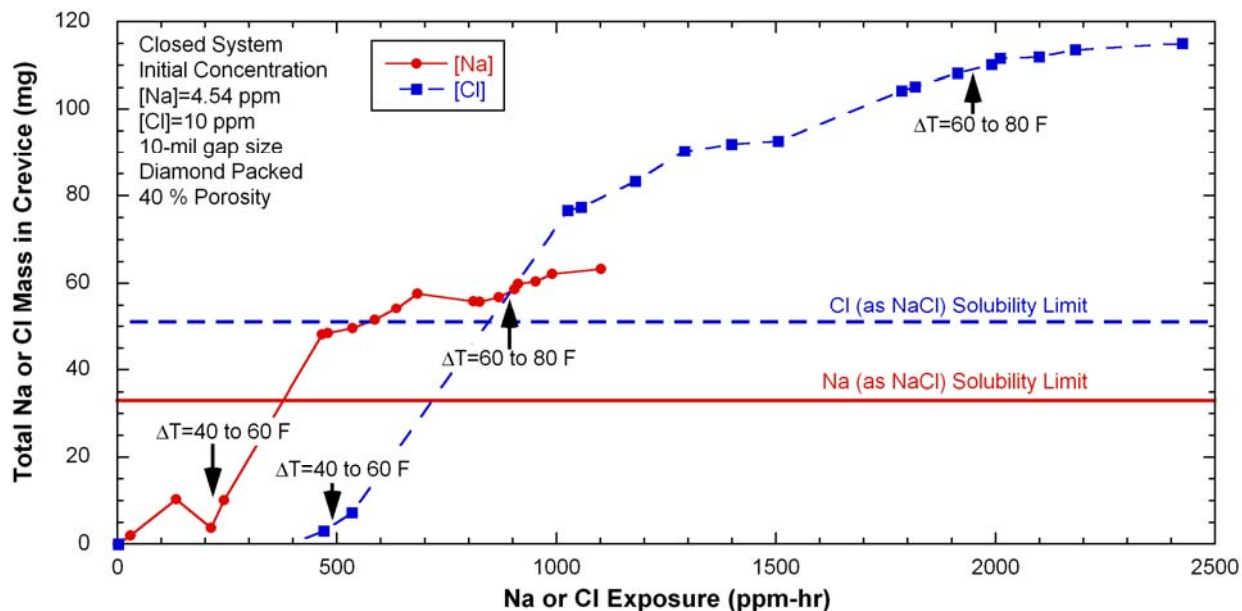


Figure 131. Total mass of Na or Cl in crevice as a function of bulk Na or Cl exposure for the previous MR=0.7 test with single diamond-packed crevice (estimates from the analysis of bulk samples; NaCl-05).

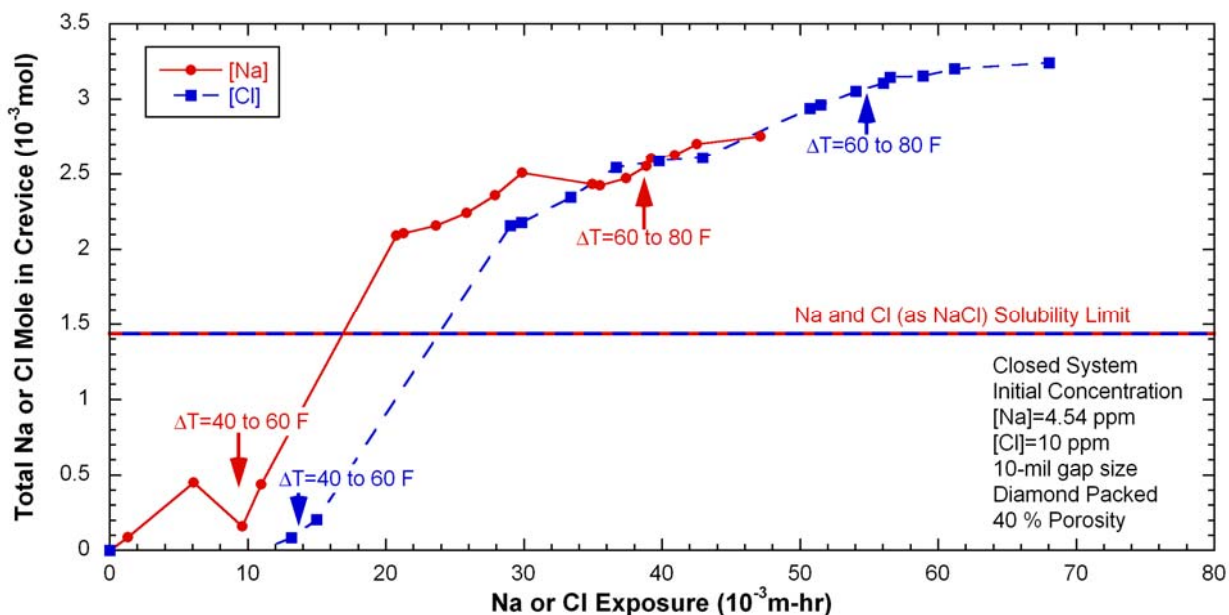


Figure 132. Total moles of Na or Cl in crevice as a function of bulk Na or Cl exposure for the previous MR=0.7 test with single diamond-packed crevice (estimates from the analysis of bulk samples; NaCl-05).

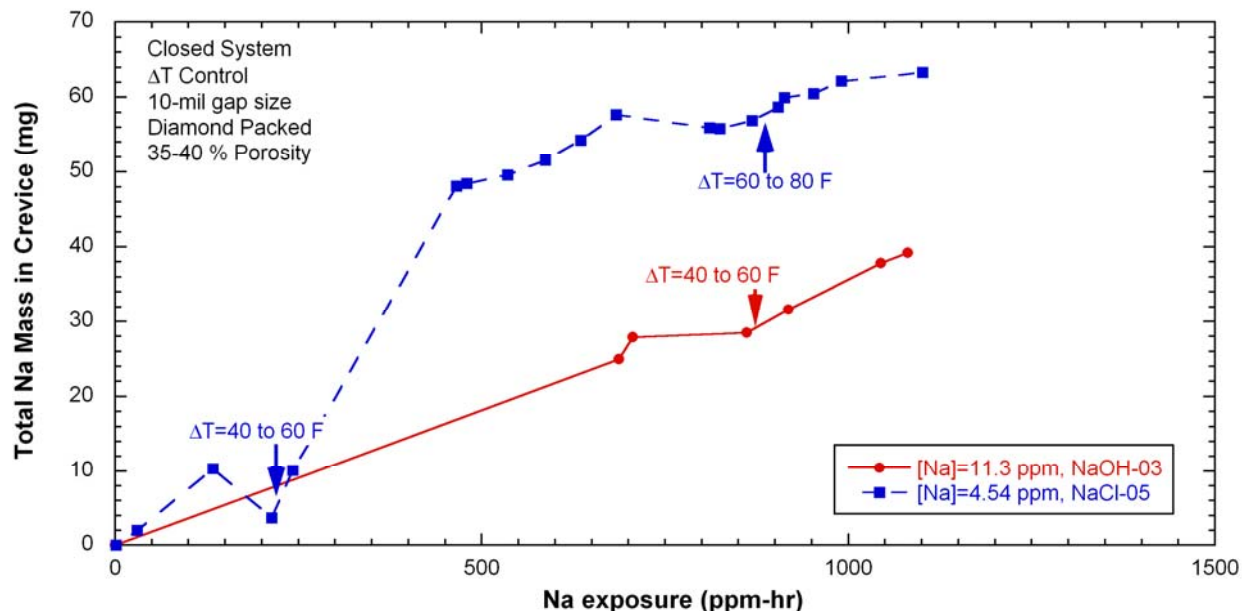


Figure 133. Total Na mass variation in crevice with Na exposure for two tests: NaOH-03 and NaCl-05 with a Na-to-Cl molar ratio of 0.7.

5.3.7 Summary

A NaCl solution test has been conducted with a single crevice packed with diamond and having a bulk MR of 0.7. As seen in the previous NaCl tests, the crevice tungsten potentials indicated that, at the beginning of crevice boiling, the crevice pH became alkaline but then changed to acidic, followed by pH stabilization at the weakly acidic condition. Based on the mass balance analysis, Na was preferentially concentrated in the diamond-packed crevice at lower ΔT , which indicates the volatility effect of Cl. However, at higher ΔT , Na and Cl hideout results were comparable, and sometimes Cl was preferentially concentrated; this concentration appears to have been caused by ion migration due to the excess metal cations formed by severe corrosion in the crevice. Post-test examination showed that severe gouging occurred on the alloy 690 TT tube surfaces. It indicates that strongly acidic crevice chemistry developed on the tube surfaces. The dye penetrant test showed no surface cracks. It appears that it is more difficult to cause stress corrosion cracking in alloy 600 or 690 tubing with a strong acid than with a strong base.

5.4 NaCl-06: NaCl (MR=0.7) Test with Magnetite Packing

5.4.1 Background

Another NaCl test has been conducted with only one crevice simulator packed with magnetite. The crevice was intentionally packed more tightly than in past tests with magnetite to evaluate the influence of packing on flow permeability and hideout. The crevice in NaCl-06 was packed with high-purity magnetite powder, and the porosity of the packed crevice was 54 %, which is much lower than the porosity of the previous magnetite-packed crevice (78 %) and higher than that of the previous diamond-packed crevice (40 %). Test results, data analysis, and post-test examination results are discussed.

5.4.2 Temperature Data

Figure 134 shows the crevice temperature variation with time in NaCl-06. Three thermocouples were installed to monitor crevice temperature. Thermocouples T2 and T4 are located 0.57 in. below the crevice top opening and they were fixed by soft Teflon ferrules, as described in Section 2.3.2. The third thermocouple labeled “Near Electrodes” is located near a crevice electrode assembly so that it monitors the temperature at the electrode tip. To obtain reference data on crevice behavior, the secondary chamber was initially run with pure water at primary/secondary temperatures of 540/500°F. After a period of time, NaCl was injected into the secondary chamber while maintaining the initial temperature. After steady state was reached as indicated by crevice temperatures and chemistry data, the primary temperature T_p was further increased in stages; each time waiting for a “steady state” to be reached. The overall test lasted for 720 hours without any cracking in the alloy 690 tube. Table 6 shows the test temperatures and dwell times for each test period.

Table 6. Test conditions and dwell times for each test period of the NaCl-06 test.

Test Period #	Water Chemistry	Secondary Temperature (°F)	Max Crevice Temperature (°F)	Primary Temperature (°F)	Dwell Time (hr)
1	High purity water	493	500.5	540	15
2	NaCl, MR=0.7	500	516.3	540	362
3	NaCl, MR=0.7	500	524.6	560	194
4	NaCl, MR=0.7	500	533.4	580	146

The crevice temperatures under the high purity water were around 500°F, which is about 6-7°F higher than the secondary saturation temperature at the same time period. For comparison, in the diamond-packed crevice testing, the crevice temperatures with high purity water were about 10°F higher than the saturation temperature due to the high thermal conductivity of diamond. The crevice temperature quickly increased after the NaCl solution injection, as shown in Figure 134. The abrupt temperature change after the solution injection did not occur in the previous tests with the diamond packing or the tests with less-loaded magnetite packing. This difference in behavior might be attributed to the increase in the secondary water temperature of about 7°F after the NaCl solution injection. The thermocouple labeled “Near Electrodes” showed a higher temperature than the two others because its location is deeper in the crevice. Another sudden temperature increase of this thermocouple occurred at 100 hours and is attributed to contact with Na-rich liquid phase, based on the crevice tungsten potential data described in Section 5.4.4. When more stable crevice conditions were achieved after many hours, the “Near Electrode”

thermocouple showed similar temperature to T2 at $\Delta T=40^\circ\text{F}$. The T4 thermocouple data were almost identical to T2 until 120 hours. Under the stable condition at $\Delta T=40^\circ\text{F}$ the deviation between T2 and T4 was about 3°F . This temperature deviation appears to indicate that, in a highly packed magnetite crevice, the local temperature variation increases as the crevice solution concentration proceeds. After ΔT was increased from 40 to 60°F , the three thermocouples quickly responded, but the “Near Electrodes” thermocouple was the most sensitive to the ΔT change. Based on these observations, we inferred that the boundary between the steam-dominant and concentrated liquid-dominant regions was located somewhere between the two crevice depth levels of “Near Electrodes” and T2 or T4 at $\Delta T=60^\circ\text{F}$. The temperature increase and stabilization of the “Near Electrodes” thermocouple suggests that the steam phase was dominant, and the boiling point elevation by the concentrated liquid phase could not occur around the “Near Electrodes” area. The two other thermocouples indicate a gradual temperature elevation due to impurity hideout. The T2 temperature increased and stabilized at 1°F lower temperature than the “Near Electrodes” temperature, but it decreased again and even became lower than T4. Thermocouple T4 showed a sudden temperature increase, as was observed in the “Near Electrodes” thermocouple at $\Delta T=40^\circ\text{F}$. This temperature increase can be attributed to the boiling point elevation due to impurity hideout. However, the temperature decrease suggests that the chemical condition in a highly packed crevice can become locally unstable, or consolidation and redistribution of magnetite particles near the tube wall can affect the thermal conditions. The post-test examination revealed that hard scales had formed on the tube wall. After ΔT was increased from 60°F to 80°F , all three thermocouple readings exhibited a rapid increase, suggesting that at higher ΔT the steam phase is more dominant in highly packed magnetite crevice, especially at the “Near Electrodes” area. Since the T2 temperature was gradually increasing when the MB shut-down was initiated, we concluded that thermal stabilization in the crevice was not achieved after 146 hours of operating at $\Delta T=80^\circ\text{F}$.

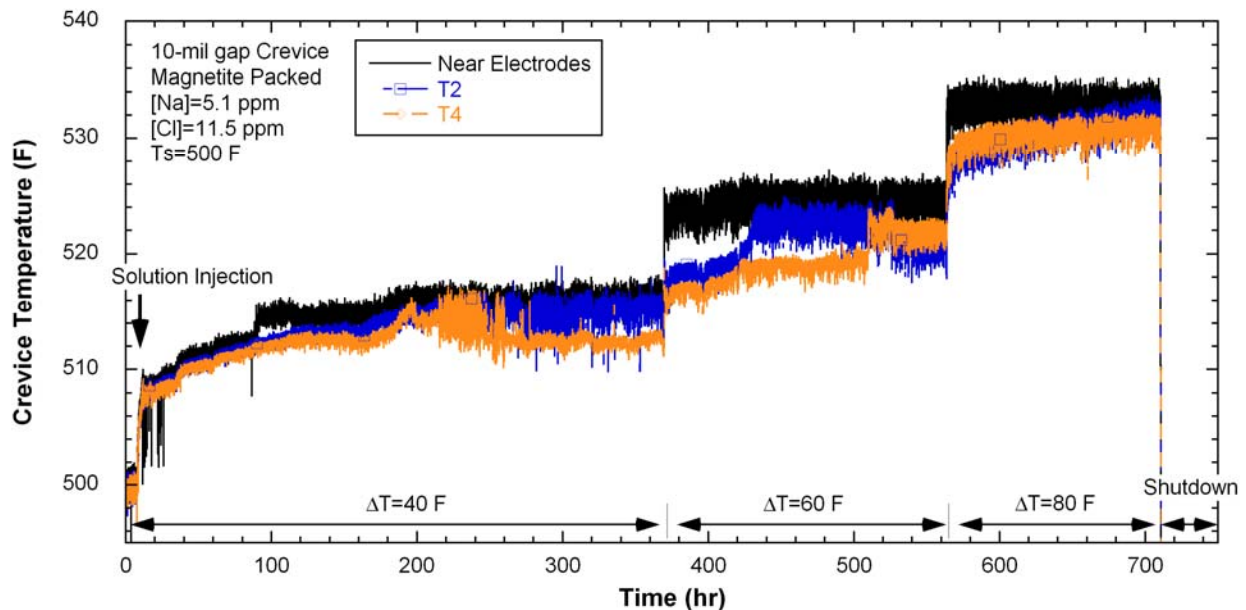


Figure 134. Crevice temperatures as a function of time for the magnetite-packed crevice and secondary water chemistry at Na-to-Cl molar ratio of 0.7 (NaCl-06).

Figure 135 shows the variation in normalized crevice temperature with time for NaCl-06; the crevice temperatures minus the bulk secondary temperature are normalized by the bulk primary-to-secondary temperature difference. The temperature oscillation of T4 observed at $\Delta T=40^\circ\text{F}$ can possibly be explained as follows: The concentrated liquid phase became dominant at the region surrounding T4,

which raised the temperature. The subsequent temperature decrease might be attributed to a local chemistry change. The “Near Electrodes” thermocouple did not show a significant change after ΔT was increased from 40°F to 60°F. However, the normalized temperatures of T2 and T4 slightly decreased, indicating that the boiling heat transfer dominates over single-phase conduction heat transfer. If the single-phase conduction heat transfer is dominant, the normalized temperature remains almost the same value regardless of the ΔT change as observed for the “Near Electrodes” thermocouple. At about 500 hours T4 suddenly increased to the same temperature as T2. Apparently, the tip area of T4 was suddenly surrounded by a concentrated liquid phase, as was observed at $\Delta T=40^\circ\text{F}$. After this abrupt increase of temperature, the normalized T4 temperature did not change significantly, even after the increase of ΔT from 60°F to 80°F. After the increase in ΔT from 40°F to 60°F, T2 started to increase slowly and about 60 hours later T2 became stabilized, followed by a temperature decrease. The observed temperature oscillation for T2 at $\Delta T=60^\circ\text{F}$ looks similar to that observed at $\Delta T=40^\circ\text{F}$ for T4. The temperature increase can be explained by the impurity hideout and boiling point elevation, and the temperature decrease, by the movement or consolidation and redistribution of magnetite particles near the tube wall. After the ΔT increase from 60°F to 80°F, the normalized temperatures were almost the same as before. This finding indicates that the ratio between steam and liquid phase was not much different after the ΔT change. The gradual increase of T2 indicates the gradual replacement of steam phase with concentrated liquid. We concluded from these results that there is much spatial variation within the crevice in that zones of steam or water change location randomly as different paths of boiling-induced expulsion and ingress of secondary bulk water occur.

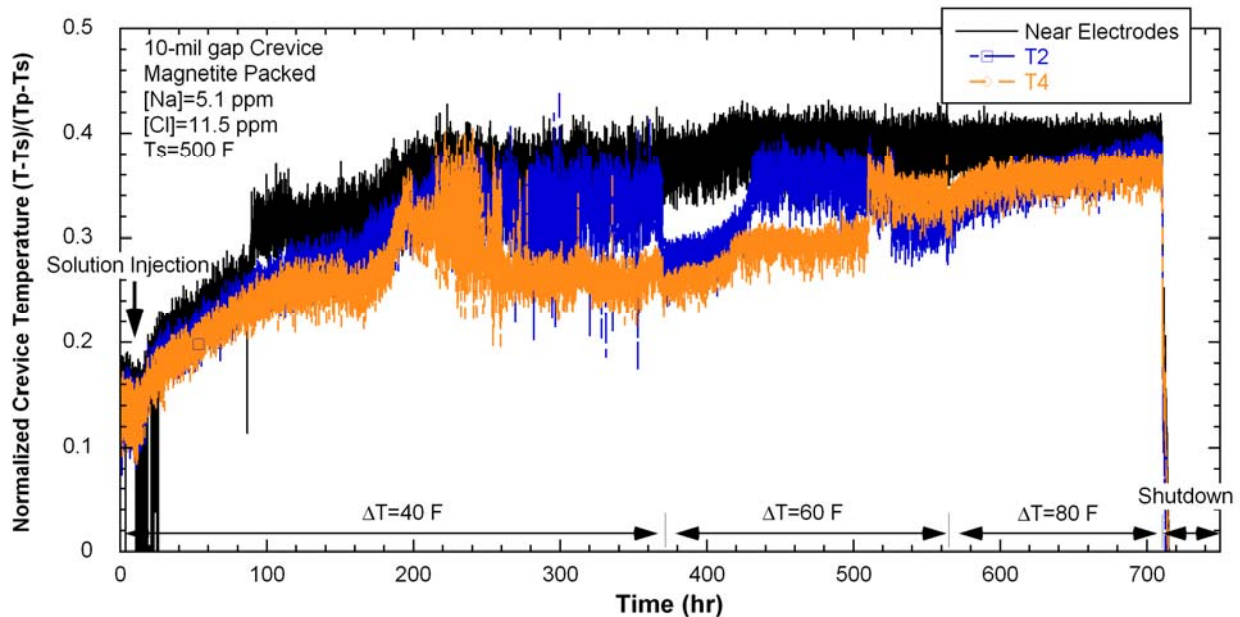


Figure 135. Normalized crevice temperatures as a function of time for the magnetite-packed crevice and secondary water chemistry at Na-to-Cl molar ratio of 0.7 (NaCl-06).

5.4.3 Bulk and Crevice Chemistry

Bulk conductivity and the secondary chemistry variations with time are shown in Figure 136, as measured by an *in situ* conductivity probe and ICP/OES of bulk water samples extracted during the NaCl-06 test. At $\Delta T=40^\circ\text{F}$ the bulk water conductivity stabilized about 200 hours after the NaCl solution injection. The samples analysis indicates that the bulk Na and Cl concentrations behave in a very complex

manner as hideout progresses. Apparently, Na and Cl concentrated in the crevice in a different manner because of the volatility effect of Cl. This issue is discussed again in Section 5.4.6. At $\Delta T=60^\circ\text{F}$ the rate of bulk conductivity reduction is similar to that at $\Delta T=40^\circ\text{F}$. The bulk conductivity quasi-stabilized for a period but it then started to decrease again. The bulk conductivity showed continuous hideout of impurity after the ΔT change from 60°F to 80°F . The chemical analysis for bulk samples at $\Delta T=60^\circ\text{F}$ and 80°F also indicated the continuous hideout of Na and Cl in the crevice. The MB was shut down before a steady state was reached at $\Delta T=80^\circ\text{F}$ because the test time was limited.

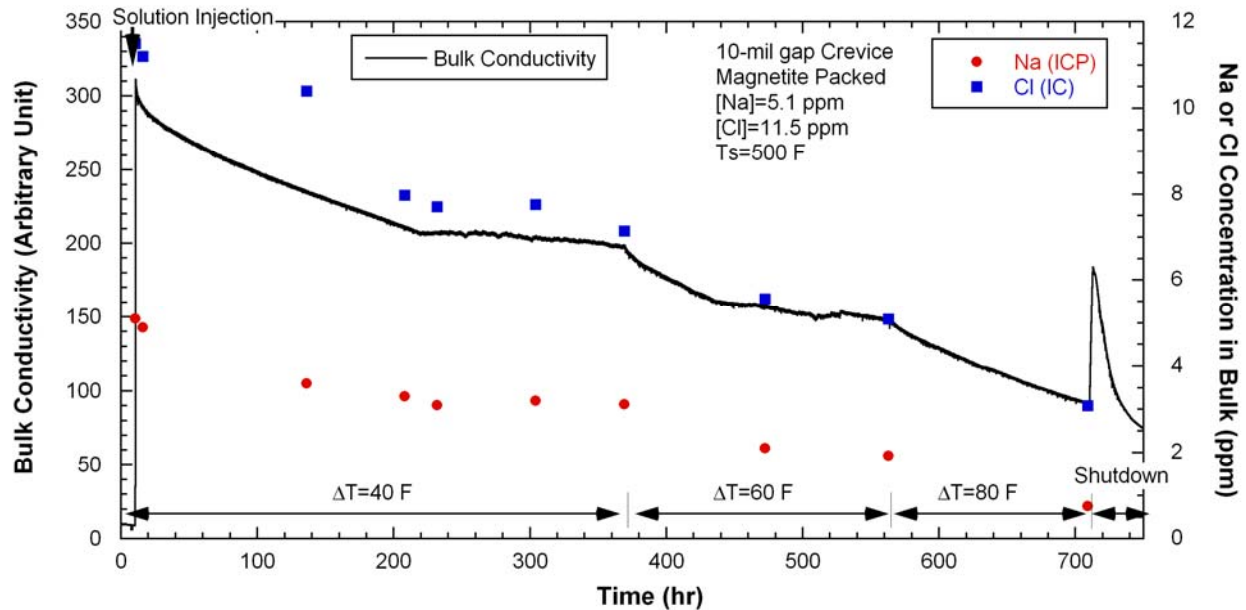


Figure 136. Bulk conductivity as a function of time for the magnetite-packed crevice and secondary water chemistry at Na-to-Cl molar ratio of 0.7 (NaCl-06).

Figure 137 shows the crevice and bulk conductivity versus time. At 100 hours the crevice conductivity suddenly increased and became stable, followed by a gradual decrease. It appears that, initially, the area around the conductivity probes was steam-blanketed or the fraction of concentrated liquid phase was relatively small. As concentrated liquid phase penetrated into the crevice, steam in the crevice pores was replaced by the concentrated liquid, causing the local conductivity to rapidly increase. As compared with the diamond-packed crevice conductivity shown in Figure 118 for NaCl-05, it took much longer for a liquid path to occur between the two conductivity probes. Even though the porosity of magnetite packing is higher than that of diamond packing, the smaller particle size of magnetite likely made the flow between crevice pores more restrictive and caused the time delay. The subsequent gradual decrease of the crevice conductivity is unexpected; NaCl precipitation is impossible at $\Delta T=40^\circ\text{F}$ because it can only occur above $\Delta T=46^\circ\text{F}$, which is the highest obtainable boiling point elevation corresponding to the solubility limit of NaCl at 500°F predicted by MULTEQ. Therefore, we cannot confidently explain the conductivity decrease. It might be caused by the return of steam domination around the probe location.

After ΔT was increased from 40°F to 60°F , the crevice conductivity signal became noisy, but the conductivity value did not increase much. Occasionally, the conductivity signal showed a spike, but it quickly returned to the original value because of a momentary increase of single-phase liquid. The increase of ΔT from 60°F to 80°F made the crevice conductivity signal even more noisy, followed by very low signal, possibly indicating steam blanketing or local dryout. The NaCl precipitation in this zone

may have increased the flow resistance of the packing, resulting in local dryout around the conductivity probe. Even though the liquid path between two probe wires was lost, a thin liquid film may have formed on the tip area of the conductivity probes or the crevice electrodes, which would still have permitted measurement of the crevice electrode potentials even at $\Delta T=80^\circ\text{F}$.

The normalized bulk conductivity as a function of ΔT is plotted in Figure 138. All conductivity data for each ΔT test were normalized with the initial conductivity value immediately after the ΔT change. The reduction rate appears to increase with the increase of ΔT , except for the beginning of testing at $\Delta T=40^\circ\text{F}$. The relatively high rate of bulk conductivity reduction at the beginning of $\Delta T=40^\circ\text{F}$ may indicate the initial adsorption of Cl to the magnetite particles, which is supported by the chemical analysis of bulk samples shown in Figure 136. Figure 139 shows the bulk conductivity variation for the magnetite-packed crevice in comparison with previous data from the diamond-packed crevice test. As shown in Figure 139, the rate of bulk conductivity reduction is much higher for the diamond-packed crevice, which suggests that the impurity hideout rate is much higher in a diamond-packed crevice than in a magnetite-packed crevice. The impurity hideout rate is proportional to various factors like heat flux, liquid penetration depth related to total nucleate boiling area, etc. As compared with the magnetite-packed crevice, the diamond-packed crevice has a deeper liquid penetration depth because it is more permeable, and this condition provides more nucleate boiling area. Greater boiling area will eventually cause faster hideout of bulk impurity if the heat flux is the same. The impurity hideout rate can be increased by not only the higher permeability of the diamond packing, but also the higher thermal conductivity of the diamond powder in the area adjacent to the tube surface, which can serve as an additional site for bubble nucleation and increase the nucleate boiling area. However, due to its lower thermal conductivity, we do not expect that the magnetite powder can provide additional bubble nucleation sites and increase the boiling area near the tube surface.

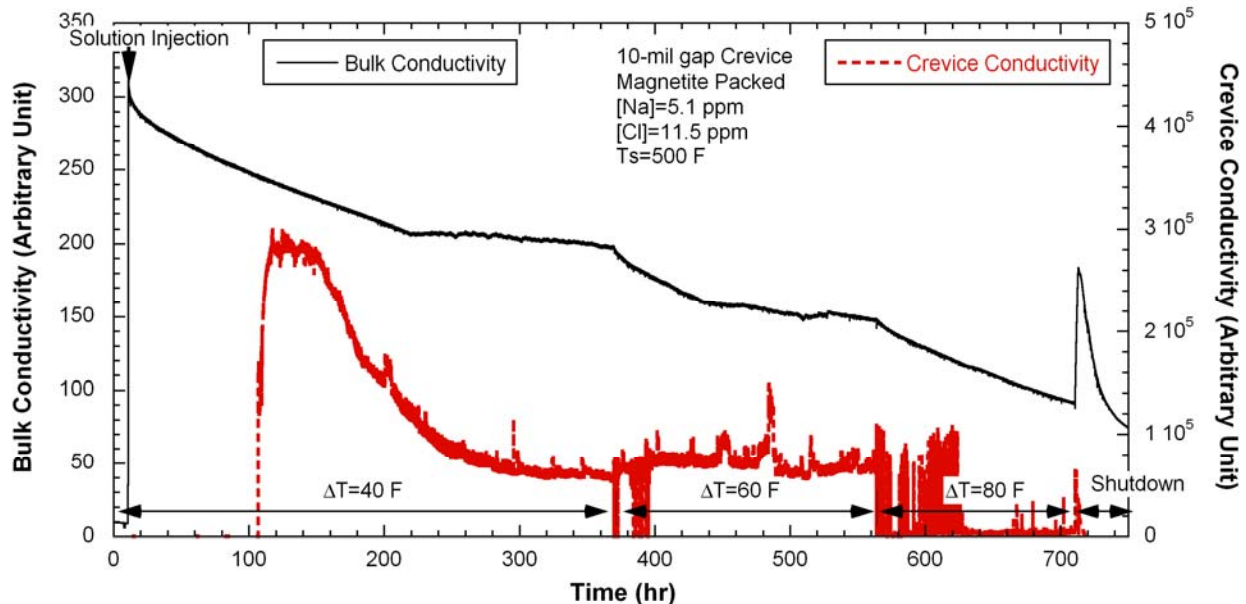


Figure 137. Crevice and bulk conductivities as a function of time for the magnetite-packed crevice and secondary water chemistry at Na-to-Cl molar ratio of 0.7 (NaCl-06).

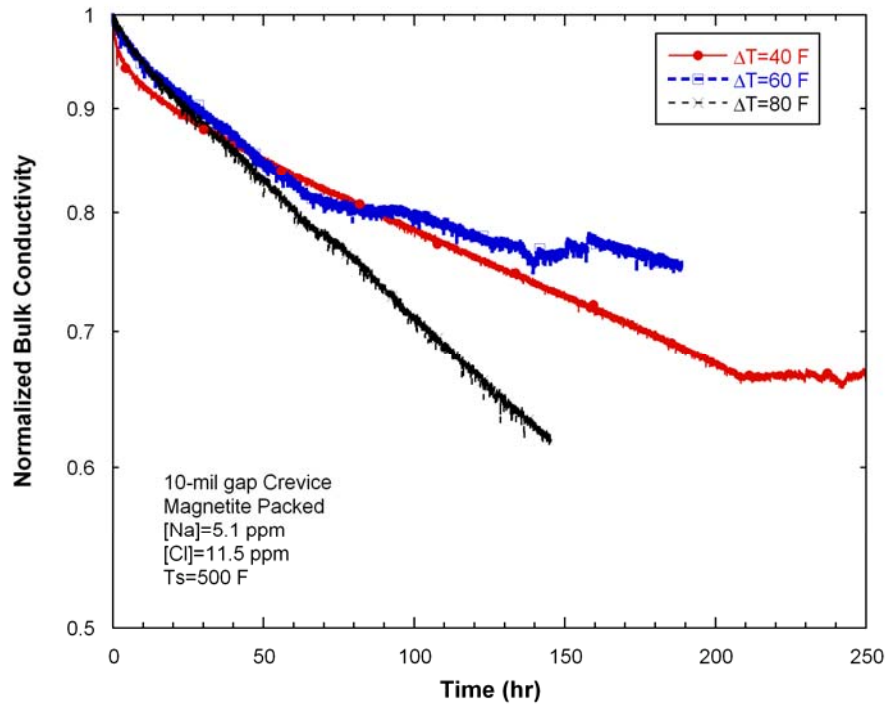


Figure 138. Normalized bulk conductivity variation as a function of ΔT for the magnetite-packed crevice and secondary water chemistry at Na-to-Cl molar ratio of 0.7 (NaCl-06).

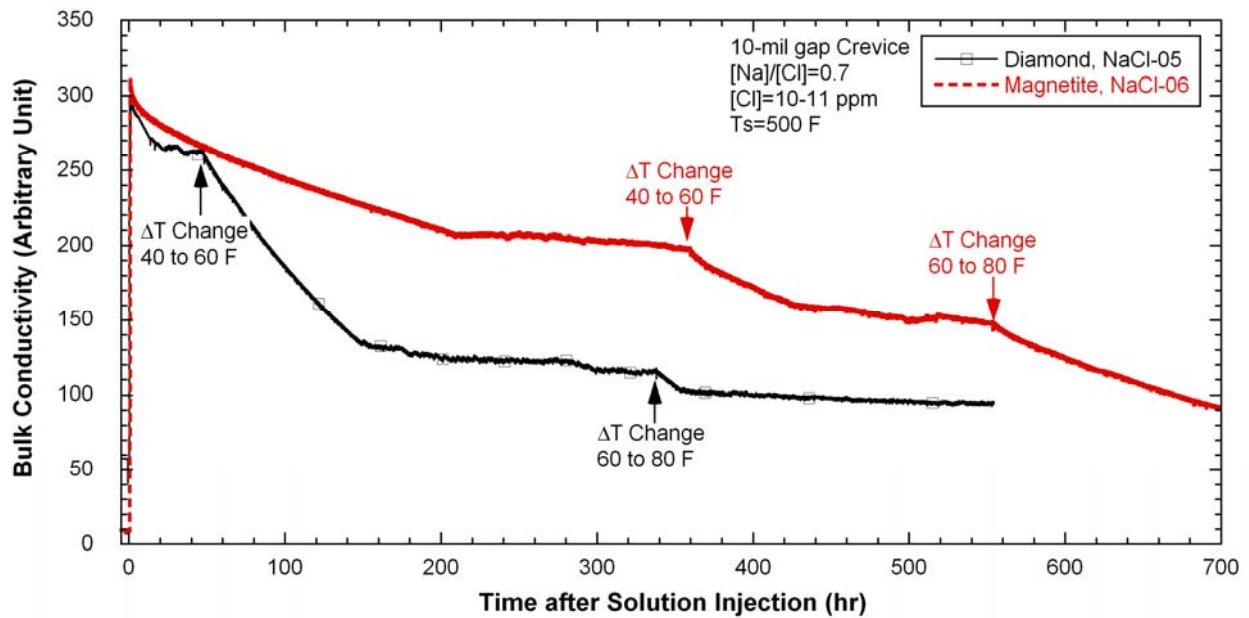


Figure 139. Bulk conductivity variation for the magnetite-packed crevice in comparison of that for the diamond-packed crevice.

5.4.4 ECP Measurement

Figure 140 shows the tungsten electrode potential variations for the bulk water and crevice (electrodes A1 and A2) after the initial NaCl injection into the secondary chamber. The overall decrease of bulk tungsten potential from the start to $\Delta T=60^{\circ}\text{F}$ was caused by the decrease of total bulk concentration rather than the Na-to-Cl molar ratio change, as shown in Figure 44. The bulk tungsten potential changed very slowly after ΔT changed from 60°F to 80°F , even though the bulk conductivity was still decreasing. Two tungsten crevice electrodes were installed 30 degree apart at the same level. As shown in Figure 140, the two crevice tungsten potentials (A1 and A2) show significant differences. Crevice A1 does not vary much except in the initial 50 hours, and A2 does not indicate electric contact until 90 hours after the solution injection. The curve for A1 indicates the development of a weakly acidic crevice throughout the test periods. The region around A2 may have become steam-blanketed before becoming wetted. The time when the potential signal indicated wetting corresponds to the time when the crevice conductivity started to increase drastically, as described earlier. Although it is difficult to determine quantitatively, but the electrode tip of A2 was closer to the tube surface than that of A1. Therefore, the potential discrepancy between the two tungsten electrodes suggests a radial pH gradient in the magnetite-packed crevice. Based on the results in Figure 140 for A2, we inferred that pH variation becomes more dynamic closer to the tube surface. Near the tube surface the pH is likely initially alkaline, which would result in preferential Na hideout around the tube surface because of the volatility effect of Cl. As the test proceeds, the pH near the tube surfaces becomes more acidic, and the radial pH difference becomes smaller because of the preferential Cl hideout. Since the boiling point elevation causes a reduction of boiling rate at the tube surfaces, the volatility effect of Cl may become less significant. Eventually, the steady-state potentials of the two tungsten electrodes become very close to each other near the end of the test time at $\Delta T=40^{\circ}\text{F}$, and this indicates the development of a slightly acidic crevice. Before reaching the steady-state potential at $\Delta T=40^{\circ}\text{F}$, the crevice A2 potential decreased from -400 mV to -450 mV (with respect to an Ag/AgCl reference electrode) during the test period of 220-300 hours, even though bulk chemistry showed no significant change. During this time period, the crevice temperatures and conductivity still varied. Inside the highly packed magnetite crevice, thermal-hydraulic and chemical changes appear to occur without altering the bulk chemistry. This result shows the limitation of estimating the crevice behavior from the bulk solution data and supports the importance of direct crevice chemistry monitoring. Another possibility to explain the crevice A2 potential decrease is the dissolution of magnetite. At a slightly acidic condition, the solubility of magnetite increases, as does the concentration of Fe cation. To retain the charge neutrality, anion concentration like OH^- or Cl^- needs to increase. Among the previous tests with diamond packing, NaCl-03 and NaCl-05 clearly showed evidence of an electromigration effect by the simultaneous decrease of Cl and increase of Na in bulk solution. But during the test period of 220-300 hours, the concentration of these two ions in the bulk solution did not show any significant variation. The magnetite packing is more flow restrictive and less permeable than the diamond packing, which makes it more difficult for ions to move into and out of the crevice. Therefore, the migration of Cl^- is not likely. Another way for the charge neutrality to be retained is an increase of OH^- ion concentration and decrease of H^+ ion; this condition leads to an increase of crevice solution pH and a decrease of the crevice tungsten potential.

Crevice A2 responded quickly to the change of ΔT from 40°F to 60°F , but A1 was not sensitive to the temperature change. The results shown in Figure 140 indicate that the pH near the tube surfaces became more acidic when ΔT was increased. A pH increase near the tube surfaces was anticipated after the increase of ΔT because of the volatility effect of Cl, but the measured pH became slightly more acidic. This inconsistency might occur because the location of A2, which was closer to the tube wall than A1, still was not close enough to the tube surfaces to observe the Cl volatilization and pH increase occurring right on the tube wall. After the increase of ΔT from 60°F to 80°F , A1 did not show any significant

change, but A2 became unstable and showed potential fluctuation. The increase of ΔT appears to have produced a steam-dominant condition near the electrode tip area of A2. The noisy signal became quiet about 40 hours later, and the potential became similar to the value before the ΔT was increased.

These results appear to contradict the observation by Baum that pH increased near the tube surface with an increase of ΔT .³⁹ The tungsten potential difference between the magnetite-packed crevice and bulk solution in Baum's test is plotted as a function of ΔT in Figure 141. The bulk concentration is $[Cl]=2.7$ ppm, lower than our test condition of $[Cl]=10$ ppm. At $\Delta T=22^\circ C$ ($40^\circ F$), the tungsten potential at the tube surface gradually increased, indicating crevice acidification. Overall, the potential variation at $\Delta T=22^\circ C$ ($40^\circ F$) looks very similar to the observed tungsten potentials in our test, designated as A2 in Figure 140. Our test results showed that the minimum crevice tungsten potential was lower than the bulk tungsten potential, but Baum's work indicated that the crevice tungsten potential was always higher than the bulk tungsten potential. This difference can be attributed to the total Na bulk concentration being higher than that in Baum's work. Explaining the discrepancy of the crevice tungsten potential variation at higher ΔT in our work and Baum's is difficult, but it should be noted that in our test the crevice tungsten wire tip was not located on the tube surface as in Baum's work, and our total exposure time before changing ΔT from $40^\circ F$ to $60^\circ F$ was more than two times longer.

Figure 142 shows the tungsten potentials in the bulk and crevice after the MB shut-down. After shut-down of the primary and secondary heater power, the tungsten potential for A1 decreased while that for A2 quickly increased. This behavior means that A1 became slightly alkaline and A2 moved in the acidic direction, even though there were large potential fluctuations followed by stabilization. After the shut-down, Cl ion might have moved toward the tube surface; this condition would cause a decrease of pH near the tube surface and a slight increase of pH away from the tube surface. Crevice A1 returned to the bulk potential value at room temperature, while A2 did not. Furthermore, A2 was about 80 mV higher than the tungsten bulk potential at room temperature. These findings suggest that even though the shut-down produced chemical homogenization in most of the crevice, the near surface area labeled A2 maintains the acidity probably because of Cl ions adsorbed to the magnetite particles on the surface.

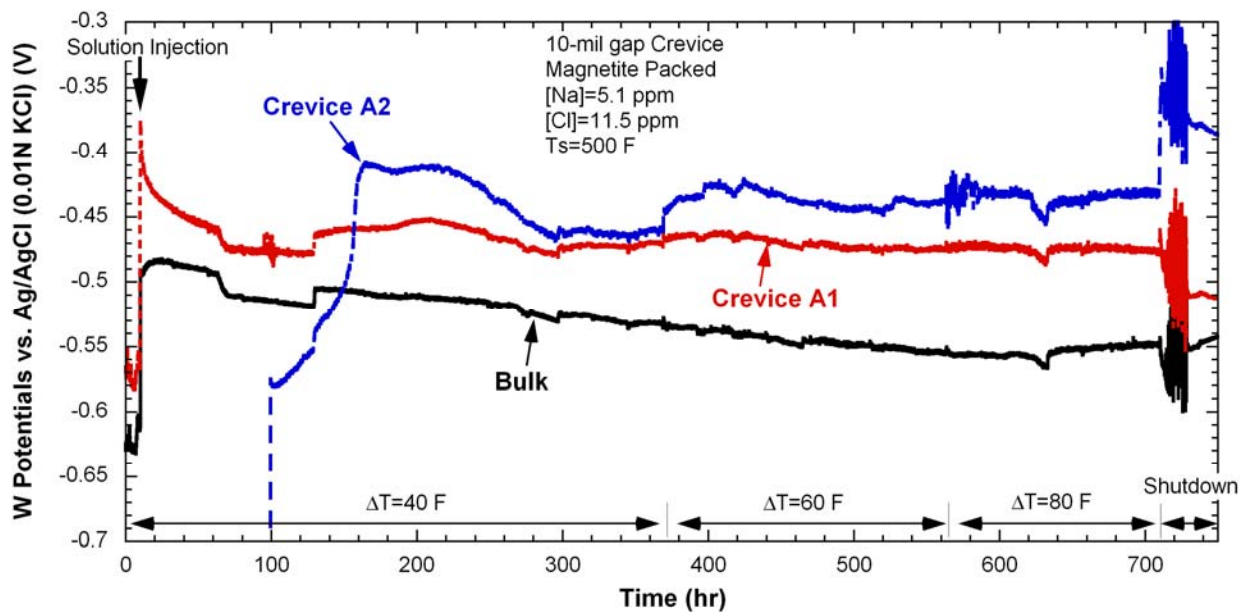


Figure 140. W/ WO_x potentials measured at bulk and crevice as a function of time for the magnetite-packed crevice and secondary water chemistry at Na-to-Cl molar ratio of 0.7 (NaCl-06).

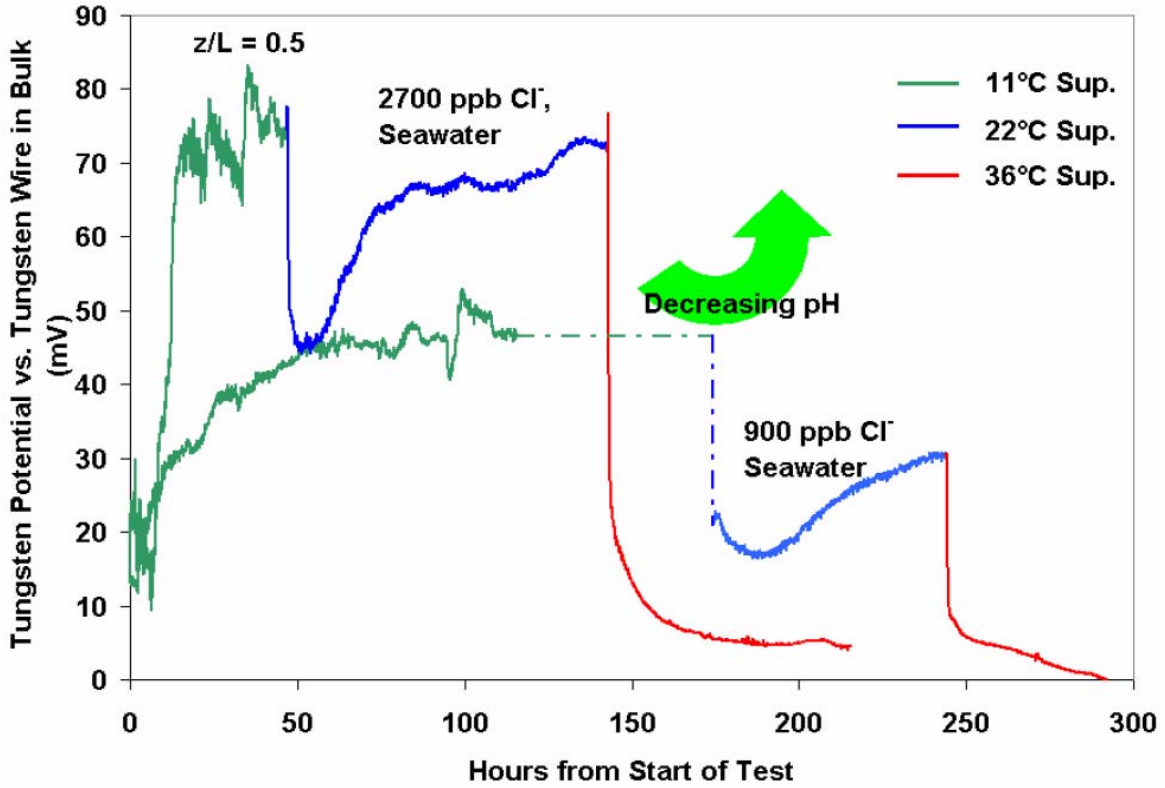


Figure 141. Tungsten potential difference variations as a function of ΔT in seawater addition testing (from Baum).³⁹

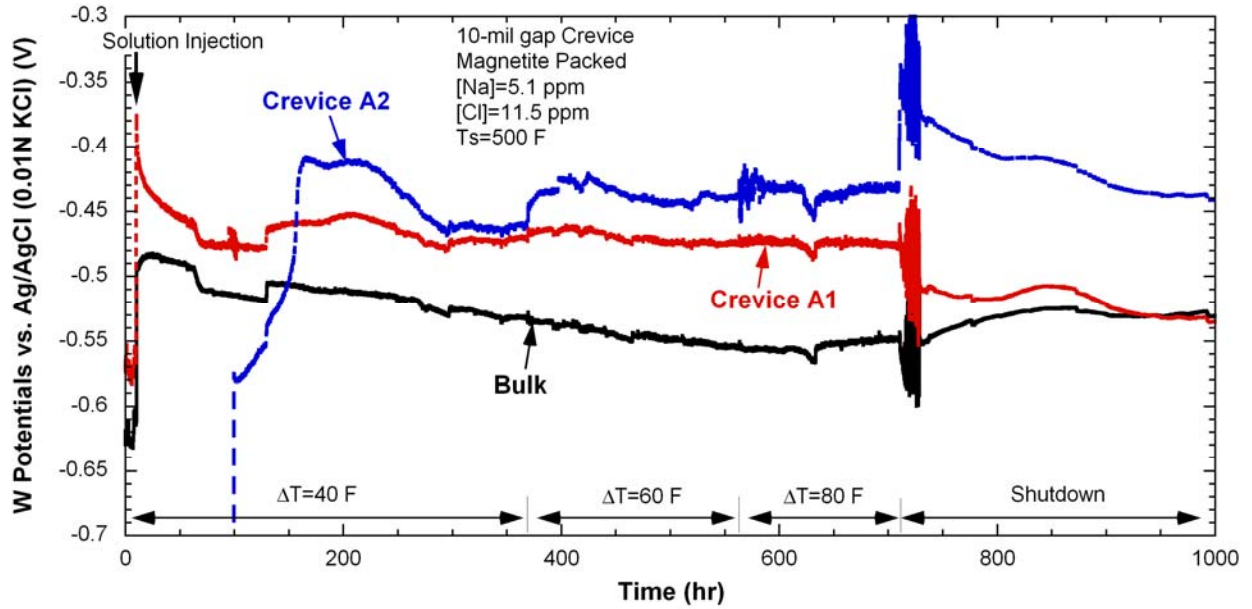


Figure 142. W/WO_x potentials measured at bulk and crevice after the MB shut-down (NaCl-06).

Figure 143 shows the Pt electrode potentials in the bulk water and crevice as a function of time. The crevice Pt potentials showed no significant change with the increased ΔT . A Ta/Ta oxide electrode was also used as a pH electrode as in the previous test, NaCl-05. Figure 144 shows the variations in Ta electrode potential with time. The Ta electrode potentials in the crevice did not show any significant change with the increase of ΔT . The insensitivity of the Pt and Ta electrodes in the crevice, as observed for A1 in Figure 141, is attributed to their not being close enough to the tube wall to represent the chemical change on the tube surface. The Ta electrode potentials for the bulk solution gradually increased, indicating the acidification of the bulk water if the Ta electrode was behaving as a pH electrode. However, the tungsten electrode potentials and the calculated pH from bulk samples suggest the pH of the bulk water increased with time. More experimental study could lead insights on using a Ta/Ta oxide electrode as a pH electrode.

Figure 145 shows the alloy 600 electrode potentials in the crevice as a function of time. About 20 hours after the NaCl solution was injected, the crevice potential indicated the wetting of the alloy 600 wire tip area. The alloy 600 potentials abruptly decreased almost at the same time as the crevice tungsten potentials indicated the wetting. From the alloy 600 and tungsten potential behaviors, we inferred that, initially, alkaline chemistry developed on the tube surfaces due to the volatility effect of Cl, and as impurity hideout proceeded, the Na-rich concentrated liquid film expanded further in the axial and radial direction and touched the tips of the tungsten and alloy 600 electrodes.

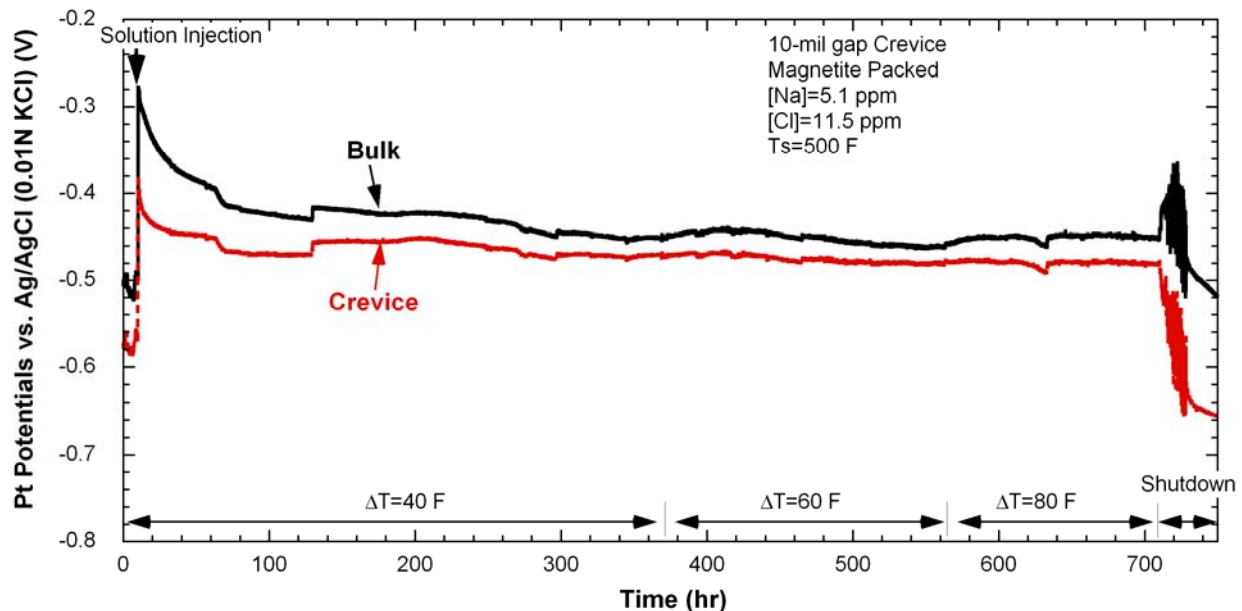


Figure 143. Pt potentials measured at bulk and crevice as a function of time for the magnetite-packed crevice and secondary water chemistry at Na-to-Cl molar ratio of 0.7 (NaCl-06).

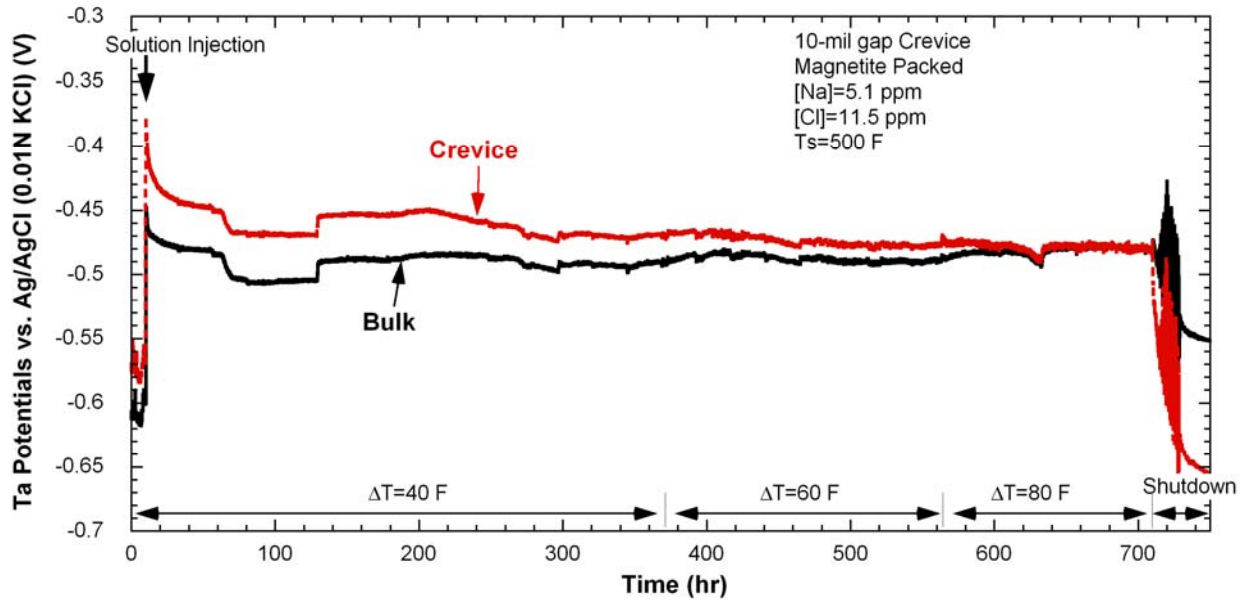


Figure 144. Ta potentials measured at bulk and crevice as a function of time for the magnetite-packed crevice and secondary water chemistry at Na-to-Cl molar ratio of 0.7 (NaCl-06).

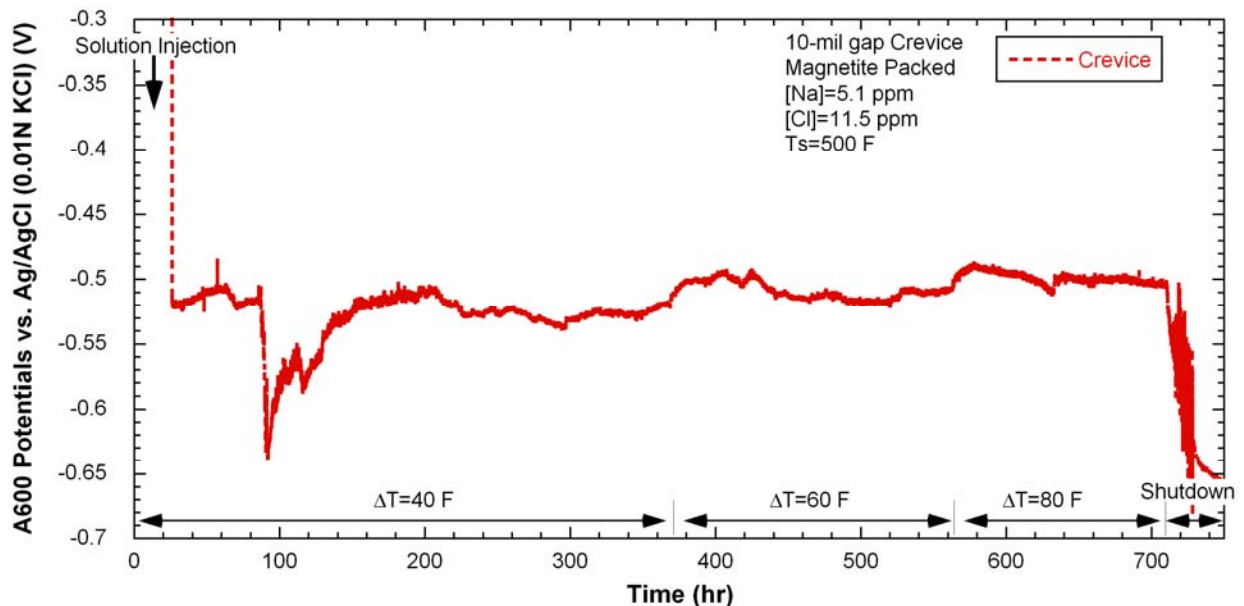


Figure 145. Alloy 600 potentials measured at crevice as a function of time for the magnetite-packed crevice and secondary water chemistry at Na-to-Cl molar ratio of 0.7 (NaCl-06).

In Figure 146, the crevice electrode potentials are compared with the crevice temperature variation. When the tungsten and alloy 600 potentials began to indicate alkaline crevice, the crevice temperature labeled “Near Electrode” increased. The sudden temperature increase can be explained by the contact of the Na-rich liquid phase with the thermocouple tip area. After the sudden potential decreases, the tungsten electrode (WA2), which was installed more closely to the tube surface, and the alloy 600 electrode showed similar behavior.

Figure 147 shows the tungsten potentials for the magnetite- and the diamond-packed crevice with the same Na-to-Cl molar ratio of 0.7. Based on the steady-state potentials, the magnetite-packed crevice appears to be more acidic than the diamond-packed crevice at all ΔT conditions. This result indicates that the magnetite-packed crevice is more flow restrictive, making it more difficult to completely mix the liquid and vapor phases. The initial potential variations after the solution injection are also different. In the diamond-packed crevice, the potential quickly decreased, indicating preferential Na concentration due to the volatility effect of Cl. This decrease was followed by rapid potential increase and stabilization. However, in the magnetite-packed crevice, the pH remained slightly acidic at the location away from the tube surface (WA1). Near the tube surface (WA2), the crevice pH indicated alkaline solution, but it became gradually acidified. With the diamond-packed crevice, the tungsten potential appears to be independent of ΔT , but in the magnetite-packed crevice, the tungsten potential near the tube surface indicated acidification with an increase of ΔT . Based on these tungsten potentials, we concluded that the independence of the tungsten potential in the diamond-packed crevice on ΔT was due to the location of tungsten electrode away from the tube surfaces combined with relatively vigorous mixing inside the crevice as compared with the magnetite-packed crevice.

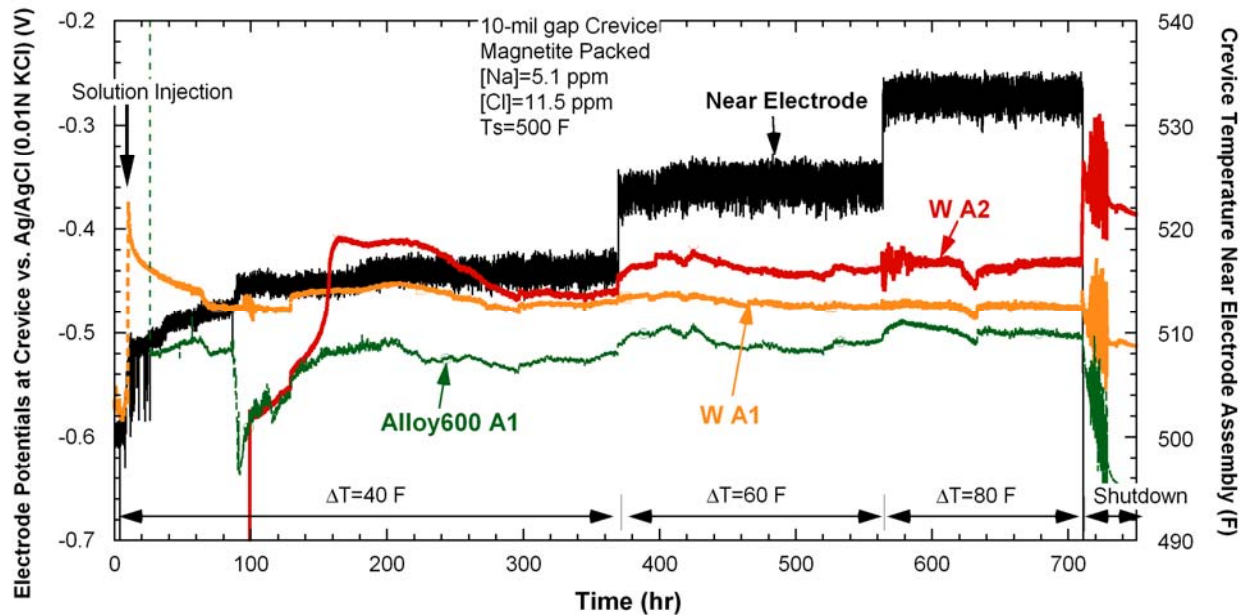


Figure 146. Crevice electrode potentials in comparison of the crevice temperature at the magnetite-packed crevice with the Na-to-Cl molar ratio of 0.7 (NaCl-06).

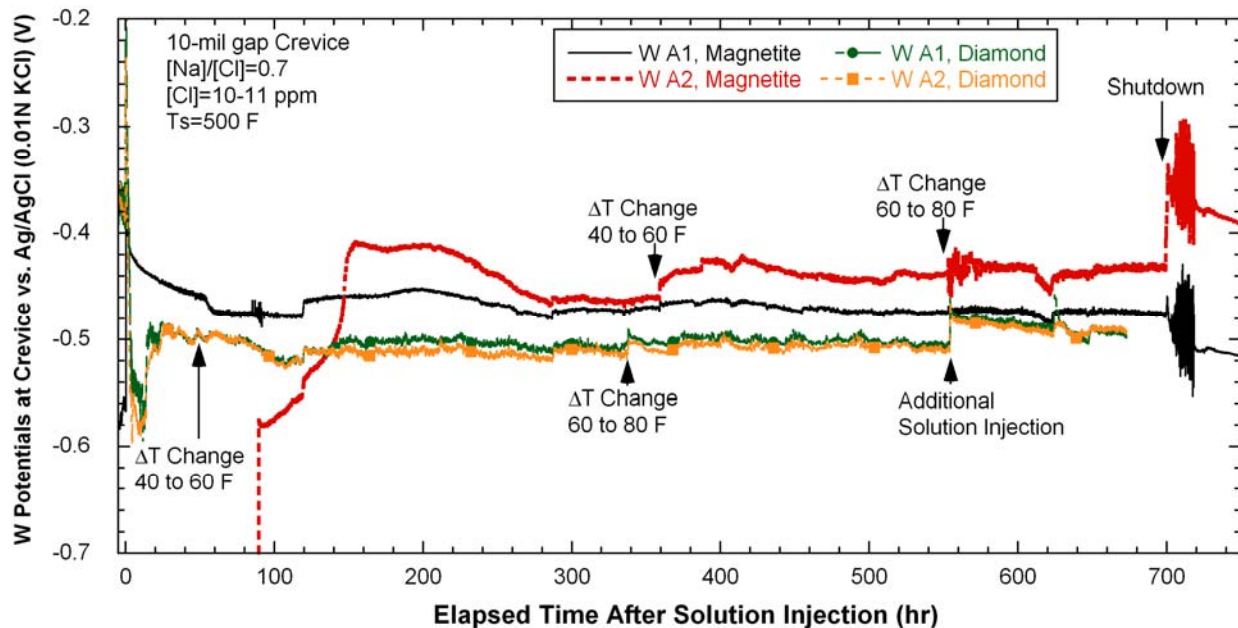


Figure 147. Crevice tungsten potentials measured at the magnetite-packed crevice compared with crevice tungsten potentials at the diamond-packed crevice with the same Na-to-Cl molar ratio of 0.7 (NaCl-06).

5.4.5 Post-Test Examination

The crevice assembly and magnetite powder inside the crevice for NaCl-06 were examined after opening the MB. Figure 148 shows the top area of the crevice assembly, and Figure 149 shows the same area as in Figure 148 but after the top retainer had been removed. These two pictures indicate that the magnetite packing powder remained inside the crevice throughout the test period of 720 hours. Figure 148 also shows two high-pressure fittings welded to the outer wall of the crevice simulator. Visual examination confirmed that the thermocouples installed in the crevice were tight and did not slip throughout the test. Figure 150 shows the crevice mouth area after removal of the foam retaining mesh. Some deposits appear on the crevice ring area, but almost all the magnetite powder was in the crevice. Figure 151 shows the crevice area after we removed the crevice simulator ring. Some magnetite powder was detached from the surface during this removal. With unaided visual observation, we did not find any other deposit except black magnetite powder.

Figure 152 shows that hard scale formed on the alloy 690 tube surfaces underneath the loosely attached magnetite powder. As shown in Figure 152, the area without scale was shiny. Pitting was not evident on the surface except for very small local areas. The tubing under the hard scale regions was not likely damaged. The shiny tube surfaces indicate that tube corrosion was not severe in the magnetite-packed crevice as compared with the diamond-packed crevice. As shown in Figure 153, severe gouging/pitting did occur on the tube surfaces with the diamond-packed crevice in the NaCl-05 test even though the bulk water chemistry and the total exposure time were similar to the NaCl-06. This discrepancy is attributed to the fact that, as shown in Figure 139, the hideout kinetics was much faster in the diamond-packed crevice test, so that the tube corrosion might start earlier than in the magnetite-packed crevice. However, if the NaCl-06 test had been exposed to NaCl water chemistry for a longer time, we expect that similar corrosion phenomena would occur on the tube surfaces. Since the post-test

examination of the tube/crevice as shown in Figure 152 did not show any significant corrosion, an electromigration effect caused by the metal corrosion does not appear to occur in the NaCl-06. Therefore, the preferential Cl hideout in the NaCl-06 test cannot be explained by the electromigration effect. The NaCl-06 test showed that hard scale consisting of magnetite can form on the tube wall in a relatively short time. Similarly, soft magnetite particles can attach and consolidate on the tube surface under the prototypic SG thermal condition.

To detect any crack formed on tube surface for NaCl-06, a dye penetrant test was performed. Figure 154 shows the dye penetrant results for the area shown in Figure 152. The red areas are from the deposit. No cracks were visible on the tube surface except for the regions under the scaly particles shown in Figure 152. We did not inspect underneath the scaly particles but crack is not likely to be present underneath them.

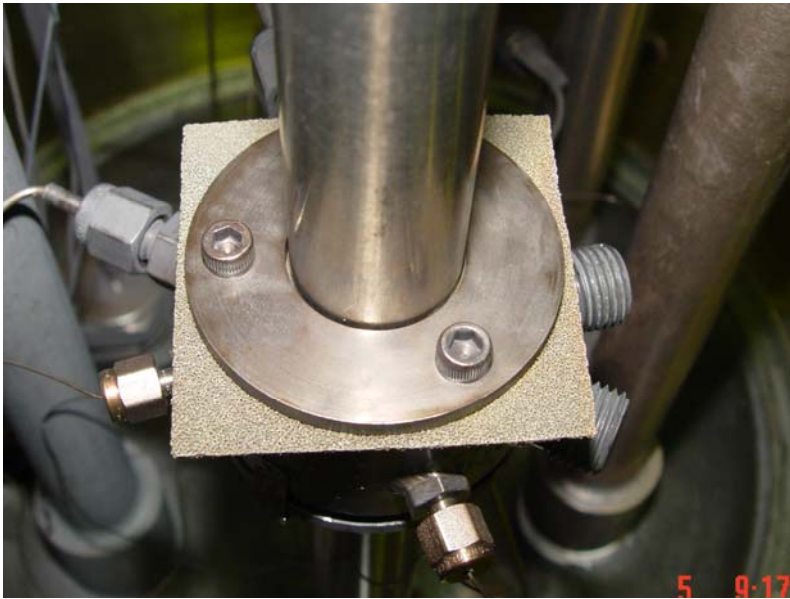


Figure 148.
Top area of crevice
assembly exposed to the
test solution with MR=0.7 for
720 hours at 500°F (260°C).



Figure 149.
Top area of crevice assembly
after removal of a top retainer
exposed to the test solution
with MR=0.7 for 720 hours at
500°F (260°C).



Figure 150.
Crevice mouth after removal
of a foam mesh showing that
magnetite powder remains in
place.



Figure 151.
Magnetite powder clinging to
the alloy 690 tubing surfaces
after removal of the crevice
ring.



Figure 152.
Hard scale formed on alloy 690 tube surface exposed to the NaCl-06 test solution with MR=0.7 and magnetite packing for 720 hours at 500°F (260°C) (crevice top: left; crevice bottom: right).

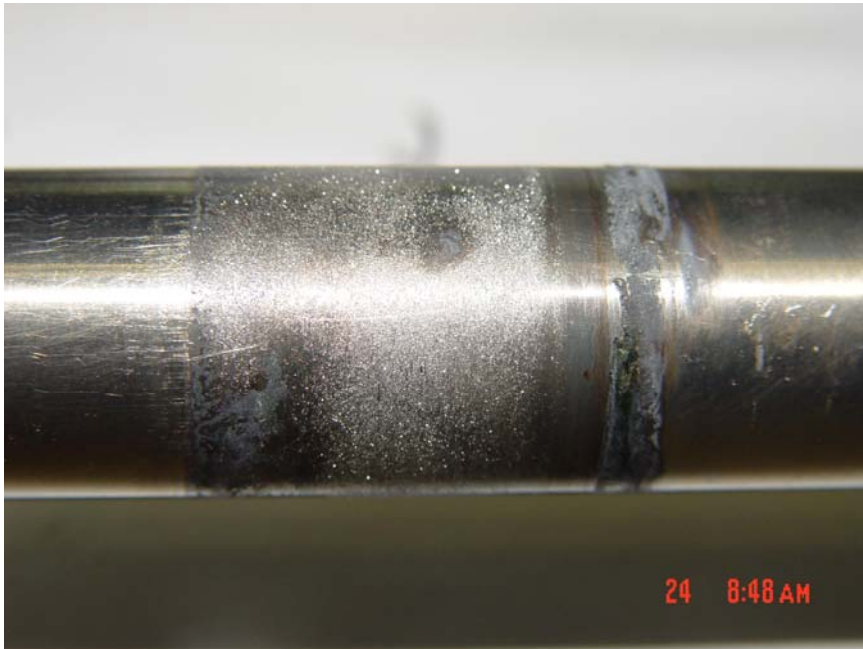


Figure 153.
Alloy 690 tube surface exposed to the test solution of NaCl-05 with MR=0.7 for 700 hours at 500°F (260°C) and diamond-packed crevice (crevice top: left; crevice bottom: right).

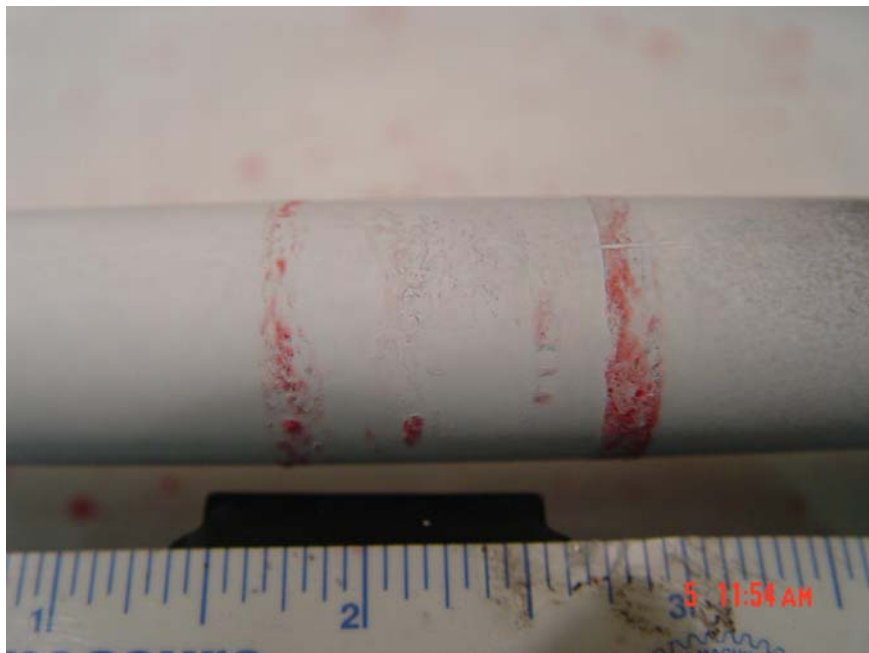


Figure 154.
Dye penetrant test results in the same area as shown in Figure 152 (crevice top: left; crevice bottom: right).

5.4.6 Discussion

Analysis for ECP and pH Data

Samples were taken from the crevice and bulk solution of NaCl-06 and analyzed by ICP/OES and IC for Na and Cl, respectively. As observed in the previous tests, the crevice samples showed a time delay effect because the volume in the sampling line and shutoff valve is comparable with that of the crevice solution sample. The bulk solution sample size is sufficiently large to overcome the sampling volume issue. In this test, to minimize the time delay effect and evaluate crevice concentration more accurately, crevice samples were taken only before changing ΔT . Sampling procedures are composed of three steps: first, 2-drop sampling; second, 2-drop sampling; and third, 5-drop crevice flushing. The volume of the 2-drop sample is roughly equivalent to the dead volume of the sampling line, 90 μL . Therefore, the first 2-drop sample will be the stagnant solution in the sampling line, and the second 2-drop sample will represent the actual crevice solution. After the second step, remaining concentrated crevice solution may still be in the sampling line because the total available crevice volume, excluding the space occupied by magnetite particles, is 250 μL in this test. The third step, a 5-drop sampling, is intended to flush all crevice solution in the sampling line. We anticipated that the first 2-drop sample would show relatively low impurity concentration, and the second 2-drop sample would show high concentration. Since the Na and Cl in the first 2-drop sample, if there is, eventually come from the crevice solution by diffusion, the concentrations are adjusted by the summation of the first and second 2-drop samples to account for the dilution effect. Assuming the first sample's volume is the same as the second sample's one, no other volume correction is necessary. Table 7 shows the Na and Cl concentration for the first and second 2-drop samples. "Adjusted Conc." means the summation of the first and second samples' concentrations. The first samples showed lower concentrations than the second samples for both Na and Cl, except for $\Delta T=40^\circ\text{F}$. At this ΔT , the concentrated liquid phase appears to have been dominant around the sampling port so that the diffusion of Na and Cl ions was easier. At higher ΔT , the steam phase became more dominant so that ionic diffusion through the liquid phase was limited. The decrease in total concentration with the increase in ΔT can also be attributed to the steam phase growing with the increase in ΔT .

The dissolved Fe and Ni concentrations are summarized in Table 7. The bulk concentrations of Fe and Ni were about 0.7 and 0.2 ppm, respectively, which might come from the internal surface of the secondary chamber and partly from alloy 600 and 690 tubing. The high Fe concentration in the crevice is partially attributed to the presence of magnetite. The molar ratio of the crevice sample at $\Delta T=80^\circ\text{F}$ is much lower than before. This difference might be caused by two effects: dilution and steam condensation. The extracted samples from the crevice could have been mixed and diluted with bulk solution during the sampling procedures. This dilution effect by bulk solution is difficult to avoid unless the crevice mouth is shut off so that the bulk liquid cannot penetrate into the crevice during the sampling procedure. At higher ΔT , more steam may be sampled and the concentration of Na and Cl in the steam may result in the lower MR. The crevice samples at higher ΔT should be analyzed carefully because of these two effects (i.e. the dilution effect or steam condensation).

Table 7. Na and Cl concentration results for crevice samples and adjusted Fe and Ni concentrations in the same crevice samples.

#	Sample Description	1 st 2 Drops (ppm)		2 nd 2 Drops (ppm)		Adjusted Conc. (ppm)		[Na]/[Cl]	Adjusted Fe Conc. (ppm)	Adjusted Ni Conc. (ppm)
		Na	Cl	Na	Cl	Na	Cl			
1	$\Delta T= 40^\circ\text{F}$ after 362 hr	1514	2984	516	975	2030	3959	0.79	202.4	16.6
2	$\Delta T= 60^\circ\text{F}$ after 194 hr	14.2	59.5	738	1599	752.2	1658.5	0.70	190.5	26.8
3	$\Delta T= 80^\circ\text{F}$ after 146 hr	0.0	28.0	7.7	165	28.0	172.7	0.25	59.5	6.6

Figure 155 shows the tungsten potentials measured in the bulk water and crevice as a function of pH calculated from the solution sample analysis. In previous tests, only Na and Cl were considered as impurities, but in this analysis dissolved Fe and Ni were included as well. As shown in Figure 155, Fe and Ni tend to increase the solution pH. Additional metal cations need additional anions to maintain charge neutrality. Therefore, when metal cations are introduced in the bulk solution, the concentration of OH^- ions increases and the solution pH increases. The slopes of the bulk tungsten potential data with respect to bulk solution pH were dependent on the presence of Fe and Ni. When dissolved Fe and Ni are considered, the bulk potential/pH slope of -88 mV/pH is closer to the Nernstian slope of -106 mV/pH at 500°F than when Fe and Ni are not considered. The two bulk data sets with and without considering Fe and Ni are sensitive to the solution pH change, suggesting that the W/WO_x electrode can behave as a pH electrode in dilute NaCl solution with $\text{MR}=0.7$ at 500°F . However, a decreasing trend of the potential with the increase of pH is not apparent for crevice tungsten potentials even after the pH correction using Fe and Ni concentration. However, the crevice tungsten potentials are always higher than the bulk tungsten potentials; this finding is consistent with the crevice solution pH always being lower than the bulk solution pH.

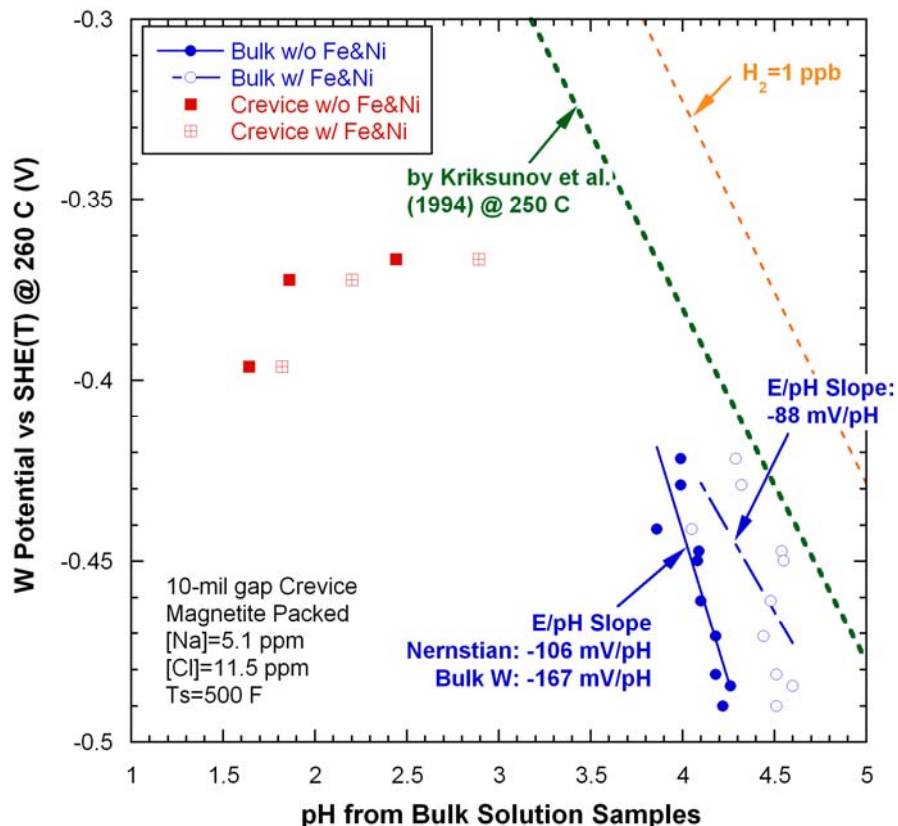


Figure 155. Tungsten potentials in bulk and crevice as a function of pH calculated from solution sample analysis with and without Fe and Ni (NaCl-06).

In Figure 156 the potential data for the crevice and bulk solution are compared with the previous test results in a W-H₂O phase diagram. The bulk solution data are slightly shifted toward the alkaline direction as compared with earlier data, and this shift is attributed to including the dissolved Fe and Ni ions. In earlier ICP/OES analysis, Fe and Ni were not included. If Fe and Ni ions had been considered for the previous bulk solution data, the tungsten potential data would have likely fit a single line. If we consider only the bulk solution data in this test (NaCl-06) and the previous alkaline data (NaOH-03), for which the pH is higher than 6, the potential/pH slope is -103 mV/pH, which is very close to the Nernstian value of -106 mV/pH at 500°F. These results are consistent with the earlier work done by Kriksunov et al.²⁹ They reported that the W/WO_x electrode followed the Nernstian slope in the pH range of 2-11 at high temperature. In Figure 156, the Kriksunov et al. test results are plotted. Considering the test temperature of the earlier work is 250°C (482°F), the results from NaCl-06 appear to be consistent with the earlier work. The crevice tungsten potential data of this test is 30-60 mV higher than the previous NaCl test data. This discrepancy appears to be attributed to two changes: the location of tungsten wire tip and packing materials. As indicated by Figure 140, in the NaCl-06 test, one crevice tungsten wire tip located closer to the tube surface than the other represented the active chemistry change near the tube surface area, which caused different crevice potentials from the previous crevice potential data at the same crevice sample pH. This test (NaCl-06) used magnetite powder as packing materials, which caused lower permeability and less volatility effect of Cl than diamond powder. Therefore, the magnetite-packed crevice might maintain acidity more efficiently than the diamond-packed crevice, which led to higher crevice W/WO_x electrode potentials.

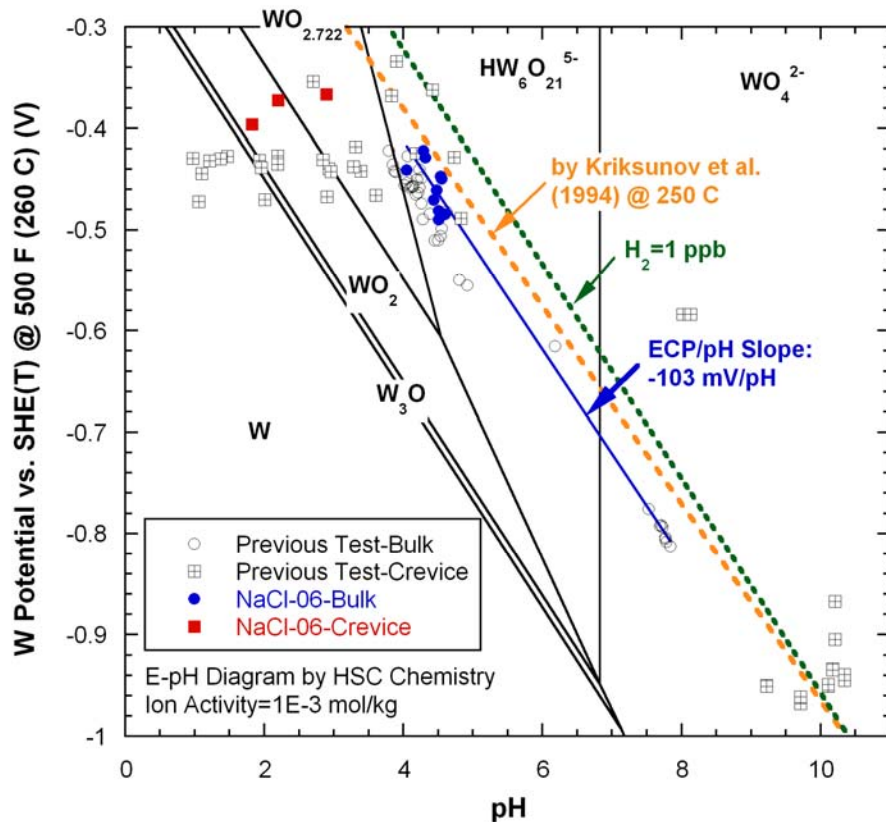


Figure 156. Measured tungsten potentials in the NaCl-06 test in comparison with the previously measured tungsten potentials in a W-H₂O phase diagram predicted by the thermodynamic code HSC Chemistry.

The plateau in the crevice tungsten potential data with respect to solution pH may be caused by a metal-to-metal cation reaction. However, as shown in Figure 156, the tungsten-to-tungsten cation reaction is not thermodynamically stable at 500°F, but tungsten oxides are stable in the low pH region. Therefore, the insensitivity of crevice tungsten potential data to crevice pH cannot be attributed to the metal-to-metal cation reaction. Instead, as discussed before, the tungsten wire tip location relative to the tube wall should be considered.

Mass Balance Analysis

One advantage of a closed MB system is that the impurity amount in a crevice can be estimated from the changes of bulk impurity concentration. Based on the analysis for Na and Cl concentration in the secondary bulk samples, we estimated the total accumulated Na and Cl masses in the crevice at corresponding points of time. Figure 157 shows the total mass of Na and Cl in the crevice as a function of time. Figure 158 shows the same results in terms of total moles. Since Na and Cl have different atomic mass, mole units are better than mass units for evaluating and comparing each ion's hideout. At the very beginning of the concentration process, the accumulated Na and Cl moles were the same. However, Na was initially concentrated preferentially, and then Cl started to be concentrated as the Na concentration became saturated at $\Delta T=40^\circ\text{F}$. In the time period when Cl was preferentially concentrated in the crevice, the crevice tungsten potential near the tube surface also indicated the acidification of the crevice, as shown in Figure 140. Possible explanations for this behavior are as follows. Preferential concentration of Na indicates the volatility effect of Cl in the crevice, and the subsequent preferential concentration of Cl might be caused by the boiling rate reduction due to the boiling point elevation by Na concentration and the resultant reduction of the volatility effect. Also, if metal corrosion occurred in the crevice, the metal cations can drive the Na ion out and the Cl ion into the crevice to maintain charge neutrality, which is

called the “electromigration effect.” However, from the post-test examination discussed in the previous section, the tube corrosion in the crevice was not significant. After steady state was reached at almost 200 hours, the total mole of Cl was higher than that of Na, indicating the development of an acidic crevice. Preferential concentration of Na or Cl was not evident at $\Delta T=60^\circ\text{F}$ and 80°F . The test was stopped prior to the crevice reached a saturation condition at $\Delta T=80^\circ\text{F}$.

Using MULTEQ[®], a thermodynamic concentration limit was calculated for Na or Cl at $\Delta T=40^\circ\text{F}$, assuming that all unoccupied empty space in the crevice was filled with concentrated solution. The calculation indicated that the Na concentration was close to the thermodynamic limit at the given conditions, and the Cl concentration was a little higher than the limit. In a highly packed magnetite crevice, the Na concentration process appears to be thermodynamically limited, but this is only a hypothesis. Actually, the Cl concentration was expected to be lower than the thermodynamic limit due to the volatility effect. The higher Cl concentration than the thermodynamic limit at $\Delta T=40^\circ\text{F}$ might be attributed to the adsorption of Cl to magnetite particles. The adsorption can occur as long as adsorption sites are available regardless of ΔT . At $\Delta T=60$ and 80°F , the Na and Cl concentrations exceeded their solubility limit as NaCl, and NaCl precipitation might have occurred. The NaCl solubility is dependent on temperature but the solubility limits at $\Delta T=60$ and 80°F are identical because the bulk saturation temperature is constant (500°F). Note that the results in Figures 157 and 158 show only the average crevice concentration, not the local variation in crevice chemistry, which would actually be large due to the significant variations in boiling and flow path behavior in the crevice introduced by the packing.

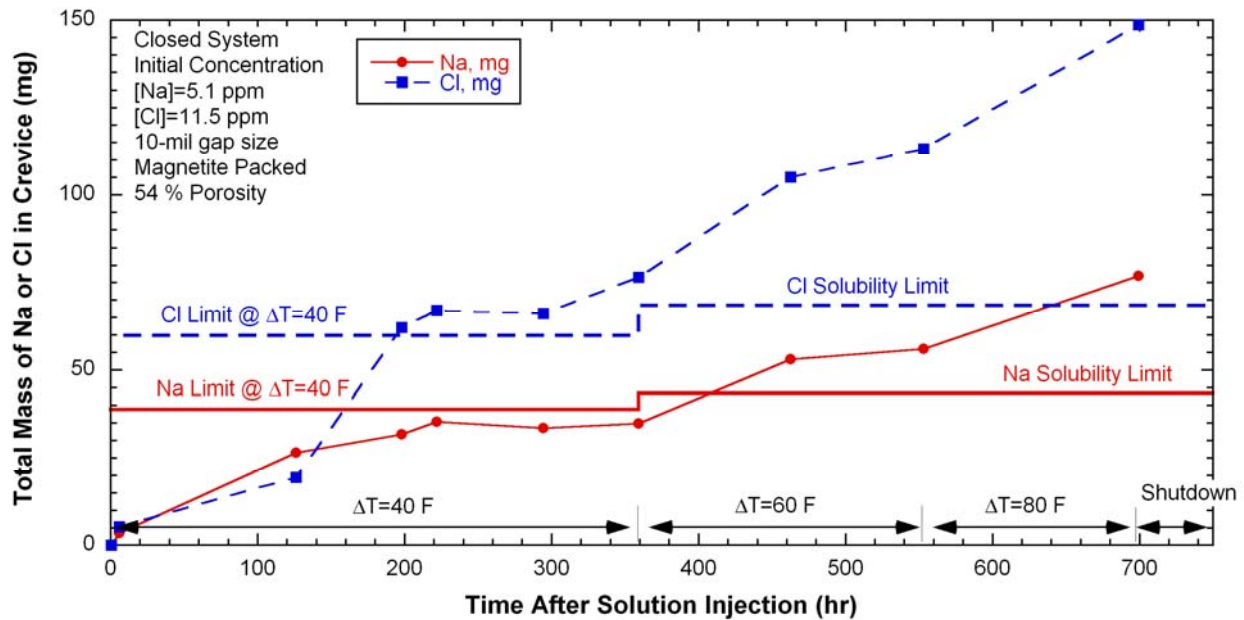


Figure 157. Total mass of Na and Cl accumulated in the crevice as a function of time based on the results of bulk solution analysis (NaCl-06).

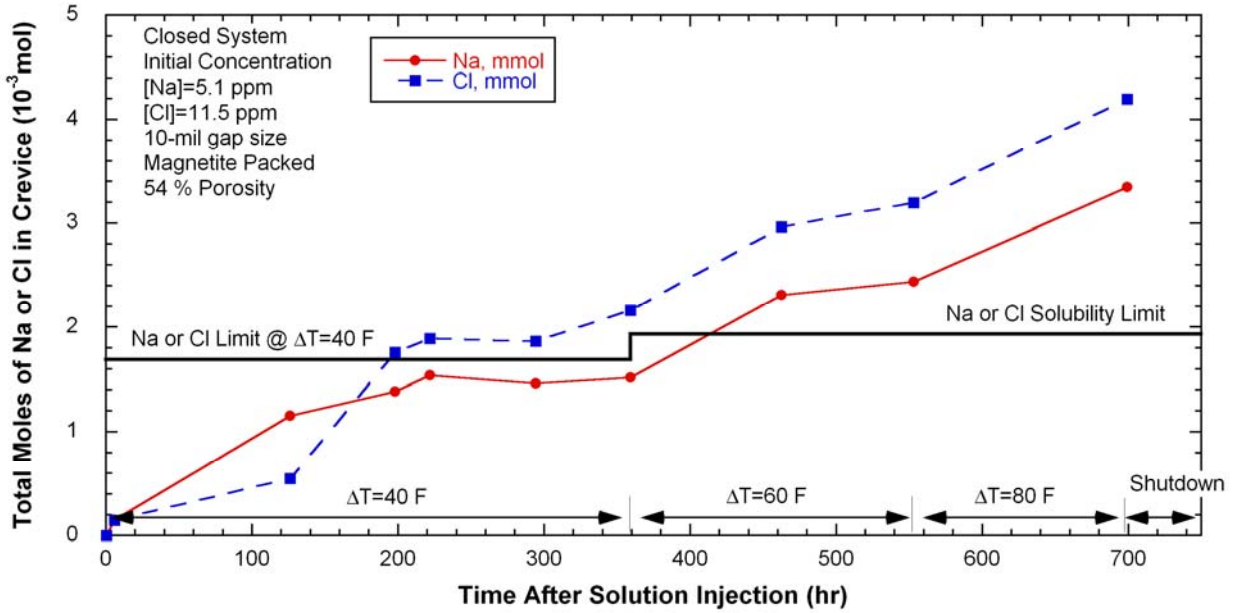


Figure 158. Total moles of Na and Cl accumulated in the crevice as a function of time based on the results of bulk solution analysis (NaCl-06).

The results shown in Figures 157 and 158 do not account for the bulk concentration difference between Na and Cl. To account for this effect, “exposure” was introduced. As mentioned earlier, “exposure” is defined as the time integration for the variation in bulk impurity concentration. Figure 159 shows the total mass of Na and Cl as a function of exposure. If the bulk concentrations are the same for Na and Cl, it is expected that Na will reach steady state before Cl at a given ΔT . Since Na and Cl have different atomic mass, the total moles of Na and Cl with respect to molal exposure were plotted, as shown in Figure 160. The “molal exposure” means the time integration for the bulk impurity concentration in a molal unit instead of ppm unit. The preferential Na concentration in the crevice at the early stage of testing is clear. The hideout kinetics of Na is faster than that of Cl under the same molal exposure at $\Delta T=60^\circ\text{F}$ and 80°F . The Na hideout rates are proportional to ΔT and the Cl hideout rates also appear to depend on ΔT except for the delayed preferential Cl concentration at $\Delta T=40^\circ\text{F}$. The delayed preferential Cl concentration, as discussed before, is attributed to the adsorption of Cl on magnetite particles or the reduced volatility of Cl due to the boiling point elevation and the resultant steam-phase reduction.

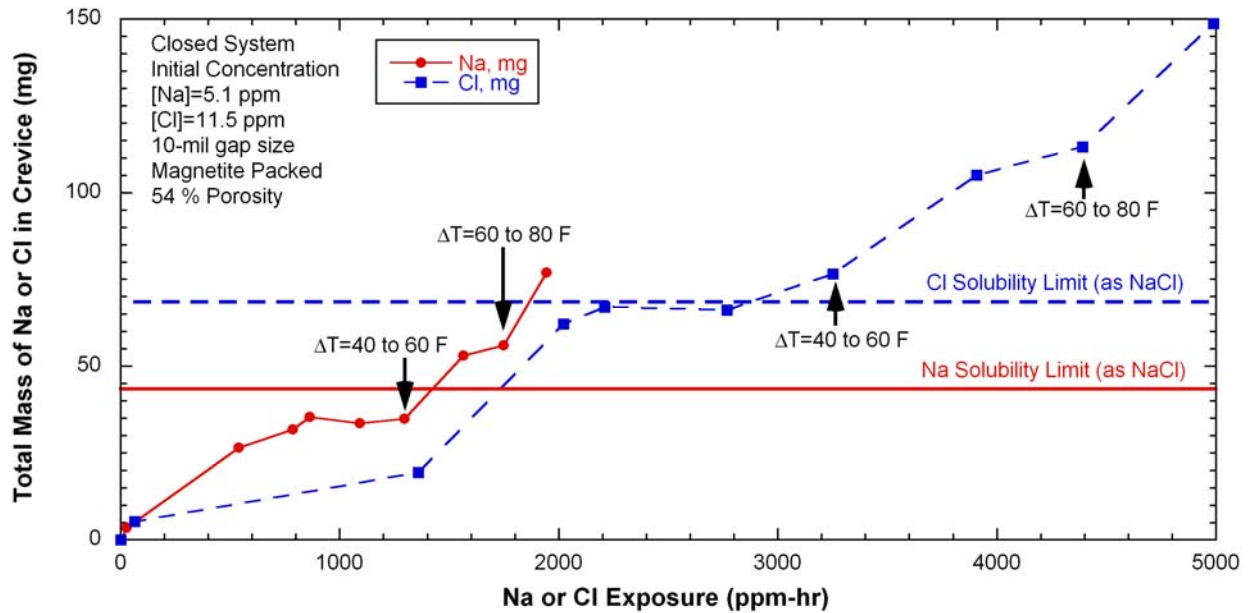


Figure 159. Total mass of Na and Cl accumulated in the crevice as a function of exposure based on the results of bulk solution analysis (NaCl-06).

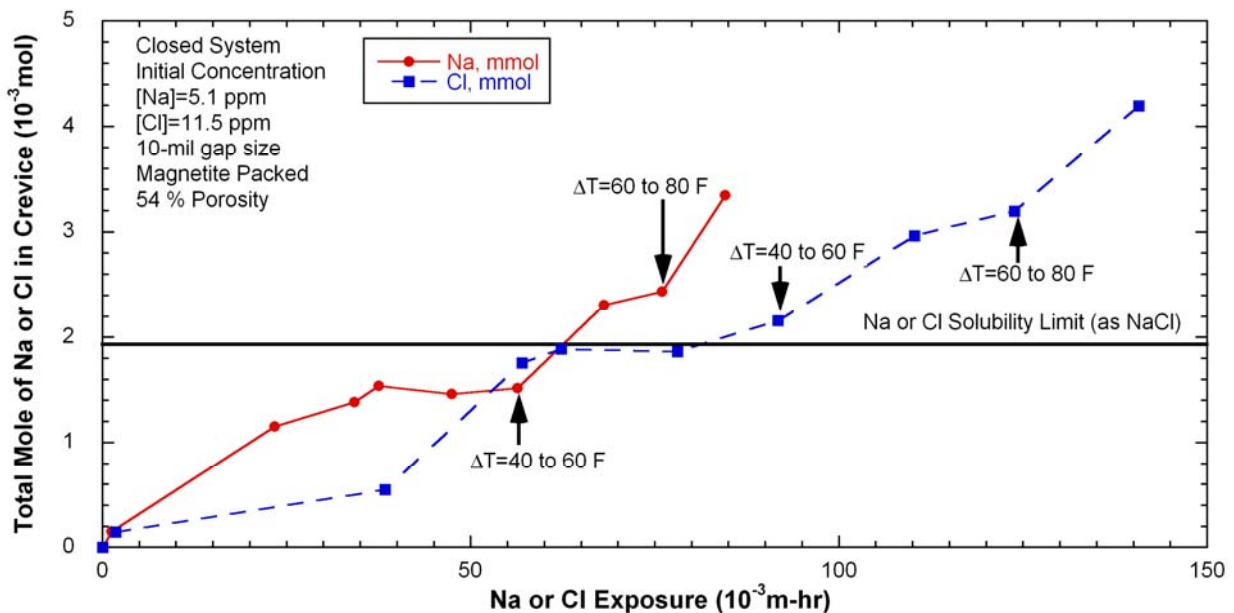


Figure 160. Total moles of Na and Cl accumulated in the crevice as a function of molal exposure based on the results of bulk solution analysis (NaCl-06).

Figure 161 shows the Na-to-Cl MR variation in the bulk and crevice for NaCl-06. The crevice MR was calculated from the total accumulated amount of Na and Cl estimated from bulk-sample chemical analysis. The initial MR was 0.7 in the bulk solution, but this MR decreased as the crevice MR increased up to 2. As the bulk MR increased, the crevice MR decreased and stabilized at MR=0.8, which is higher than the initial MR=0.7 but still lower than 1.0. This finding suggests that the magnetite-packed crevice became initially alkaline due to the volatility effect of Cl but then acidified due to the delayed preferential Cl concentration. The decrease of bulk MR with the increase of ΔT also suggests that the preferential Na

concentration occurred at higher ΔT as well as at 40°F because the volatility effect of Cl became more significant at higher ΔT ; this is consistent with earlier Baum's test results³. However, the crevice MR did not significantly increase, and the crevice tungsten potential also indicated slight acidification rather than alkalization. Prior to the ΔT change from 60°F to 80°F the formerly accumulated impurity levels may have been so high, as compared with the newly accumulated impurity amount, that the impact of changing ΔT was not significant. If the temperature condition had started with $\Delta T=60^\circ\text{F}$ or 80°F , initial large preferential Na hideout is expected and probably would be followed by a delayed preferential Cl hideout.

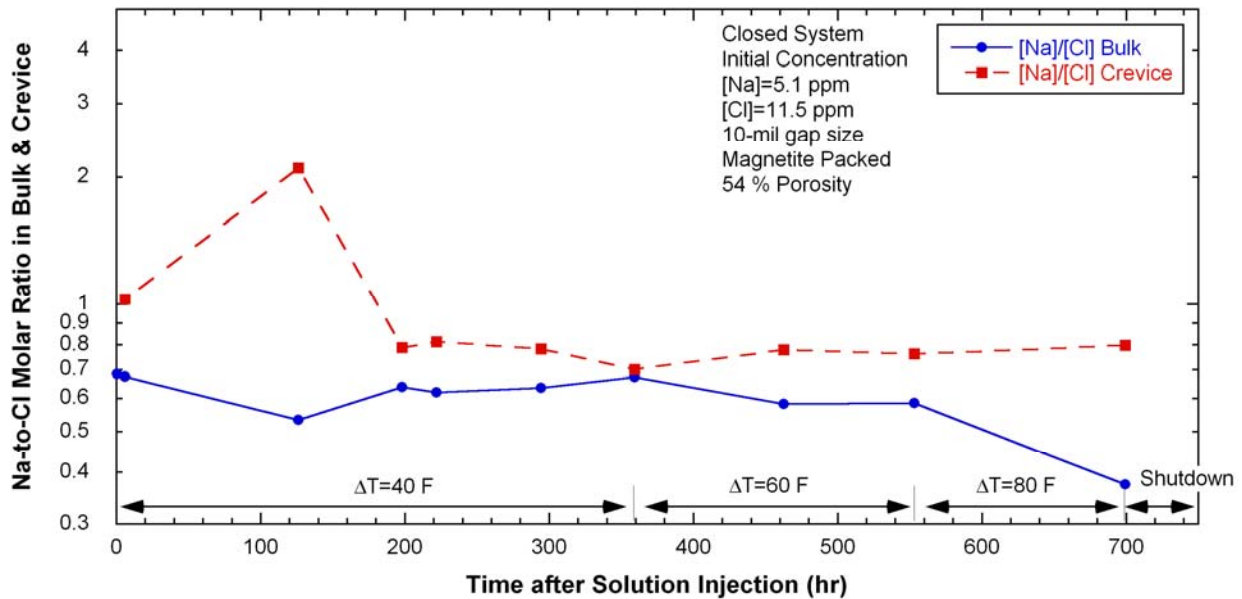


Figure 161. Na-to-Cl molar ratio variation of bulk samples and estimated crevice concentration from bulk chemical analysis (NaCl-06).

To evaluate the dependency of Na concentration on choice of packing material, we compared the Na concentration from two tests (NaCl-05 and NaCl-06) as a function of Na exposure, as shown in Figure 162. To account for the porosity difference in each test, the total accumulated Na mass was divided by the total available unoccupied space in the crevice, which was defined by the integrated-volume average Na concentration. The concentration of the NaCl-05 prior to the ΔT change (40°F→ 60°F) is much lower than that of the NaCl-06. In the NaCl-05 test, the test duration at $\Delta T=40^\circ\text{F}$ was much shorter than the NaCl-06. Although the bulk solution conductivity data showed stabilized behavior, as indicated in Figure 117, we might have increased ΔT from 40°F to 60°F too early. The Na concentration rate in the NaCl-05 test was highest at $\Delta T=60^\circ\text{F}$. At $\Delta T=60^\circ\text{F}$, the maximum concentration rate in NaCl-05 was 3.5 times higher than that in NaCl-06, and the saturation concentration of the NaCl-05 is about two times higher than that of the NaCl-06. This discrepancy suggests that the difference in packing materials can affect the Na concentration at $\Delta T=60^\circ\text{F}$; the magnetite-packed crevice appears to be thermodynamically limited while the diamond-packed crevice is not thermodynamically limited because of NaCl precipitation which could increase the saturated Na concentration above the thermodynamic limit. At $\Delta T=80^\circ\text{F}$, the Na concentration in NaCl-05 was readily saturated, probably because significant NaCl precipitation had occurred at $\Delta T=60^\circ\text{F}$. The Na concentration in NaCl-06 did not saturate as it did for NaCl-05. Further Na hideout would be expected if NaCl-06 was run longer at a $\Delta T=80^\circ\text{F}$.

Figure 163 shows the Cl concentration behavior in the diamond- and magnetite-packed crevice tests (NaCl-05 and NaCl-06 tests). Figure 163 clearly shows the effect of packing materials on Cl concentration. The Cl concentration of NaCl-05 (diamond-packed) prior to the ΔT change ($40^{\circ}\text{F} \rightarrow 60^{\circ}\text{F}$) is much lower than that of NaCl-06 (magnetite-packed). A longer-term test for the diamond-packed crevice $\Delta T=40^{\circ}\text{F}$ could determine whether this is attributed to the shorter exposure time or the discrepancy of packing materials (diamond vs. magnetite). At $\Delta T=60^{\circ}\text{F}$, the maximum Cl concentration rate in NaCl-05 is 4.4 times higher than that in NaCl-06. At $\Delta T=80^{\circ}\text{F}$, the final Cl concentration of NaCl-06 is slightly lower than that of NaCl-05. It is expected that if the NaCl-06 test was run longer, the Cl concentration would have increased further and might be saturated at a similar level to that of NaCl-05.

The hideout rate depends on the heat flux and the total area where the nucleate boiling can occur. The heat flux difference on the tube surface between diamond and magnetite would not be significant. The total area for the boiling is expected to be much different. The magnetite-packed crevice is less permeable so that the liquid phase cannot penetrate as deep into the crevice as it can when the crevice is packed with diamond powder. Based on the temperature data shown in Figures 134 and 135, at $\Delta T=60^{\circ}\text{F}$ the liquid phase appears to penetrate at least 50 % of the depth of the magnetite-packed crevice. Assuming that the whole crevice tube surface was wetted in the diamond-packed crevice at $\Delta T=60^{\circ}\text{F}$, the difference in the hideout rates between the diamond- and magnetite-packed crevices should not exceed a factor of two. The present results suggest another source of the difference. The diamond has very high thermal conductivity so that the diamond surface itself near the tube wall may be able to behave as the boiling site. In this case, the total boiling area is increased more than two times.

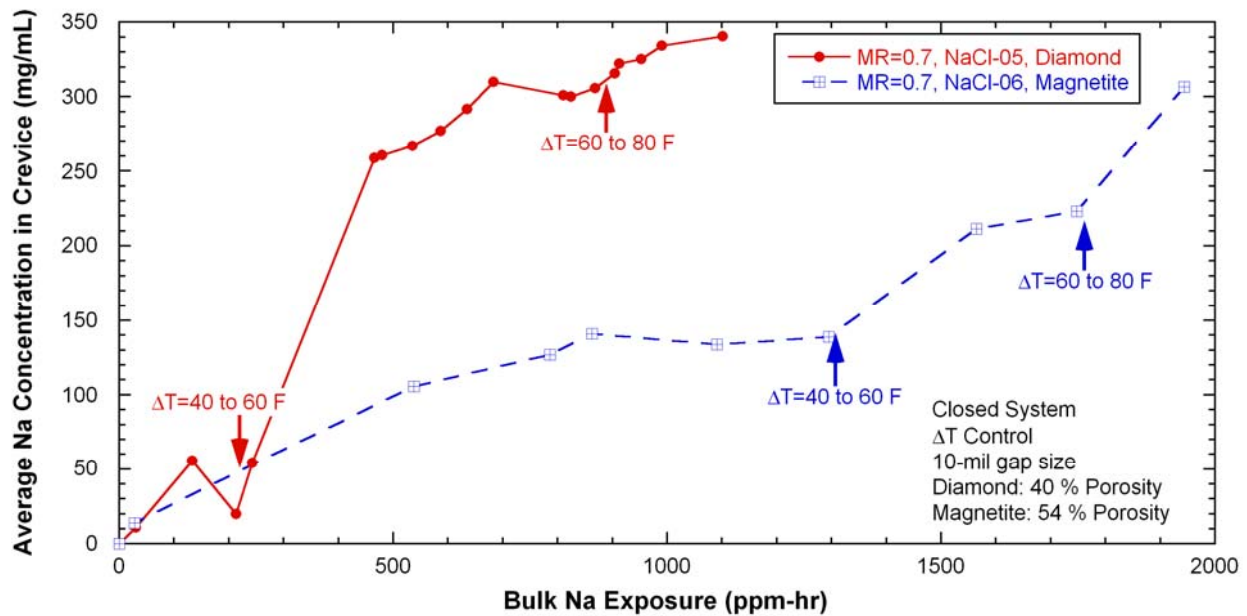


Figure 162. Integrated-volume average Na concentration variations with exposure for NaCl-05 and NaCl-06 tests.

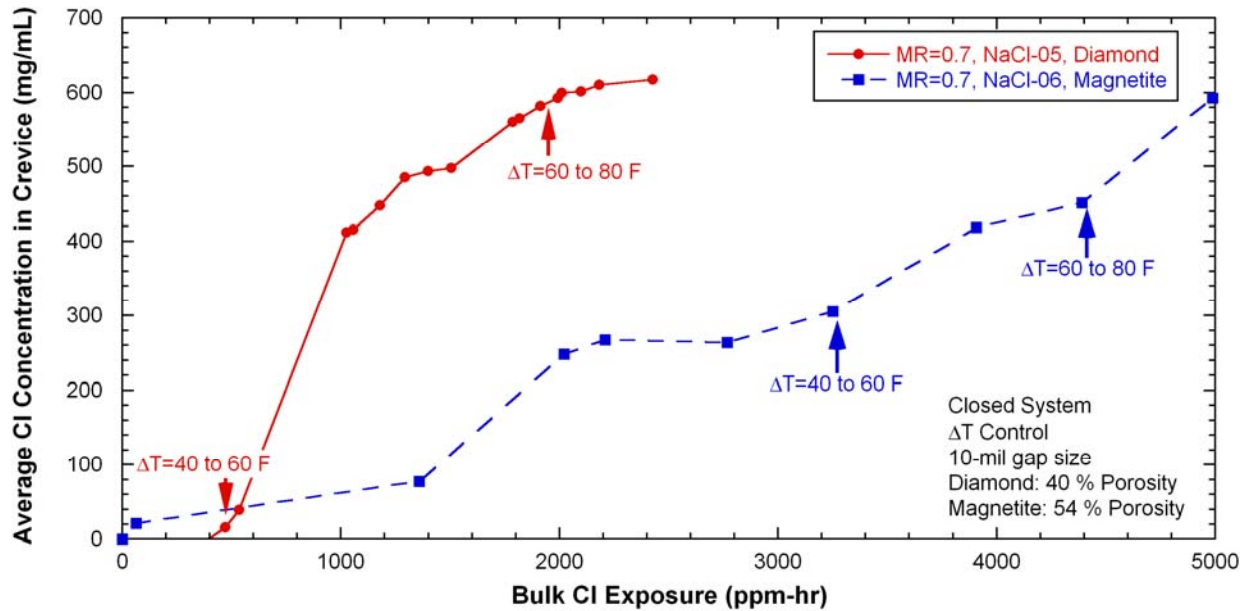


Figure 163. Integrated-volume average Cl concentration variations with exposure for NaCl-05 and NaCl-06 tests.

Permeability

Porosity and permeability are measures of restriction to flow into and out of the crevice packing. Our test results show that these factors are important with regard to crevice hideout behavior and strongly relate to how rapidly stable conditions are achieved in the crevice. Figure 164 shows the permeability of our diamond-packed and magnetite-packed crevices as predicted by the Carman-Kozeny equation⁴⁰:

$$k = \frac{D_p^2 \varepsilon^3}{72\tau(1 - \varepsilon)^2}$$

where k = permeability, m^2

D_p = particle diameter, m

ε = porosity

τ = tortuosity

(6)

Eq. (6) is valid for a uniform porous material packed with spheres having the same diameter. As shown in Figure 164, the mean diameter of our diamond particles is 146 μm , and the porosity is 40 %. The estimated permeability for the diamond-packed crevice is 44 Darcy units. One Darcy unit is equivalent to $9.87 \times 10^{-13} m^2$. The tortuosity of the diamond-packed crevice was derived from the estimated value for a carbon fiber-filled crevice by Millett.¹⁹ The tortuosity is a measure of how much the flow path wanders or turns in a packed crevice as compared with the non-packed condition and strongly influences effective flow resistance. Millett estimated the tortuosity for carbon fiber-filled crevice and synthetic magnetite-filled crevices. He also established the reference permeability value for the magnetite-packed crevice, which is 0.1 Darcy. Therefore, the permeability difference between diamond- and magnetite-packed crevices is almost three orders of magnitude, as shown in Figure 164. For a low-permeable crevice, the liquid and steam flow into and out of the crevice is slow and limited, and mixing inside the

crevice becomes more difficult, producing spatial variations both thermally and chemically. For a low-permeability crevice, it takes longer to reach steady state.

A low-permeability crevice can have a different crevice chemistry compared with a high-permeability crevice at given bulk chemistry and thermal conditions. The mixing between liquid and steam phases and Cl escaping from the heat transfer tube surface become harder in a low-permeability crevice. The two effects (induced mixing and Cl escaping) result in a decrease in pH (acidification) on the tube surface.

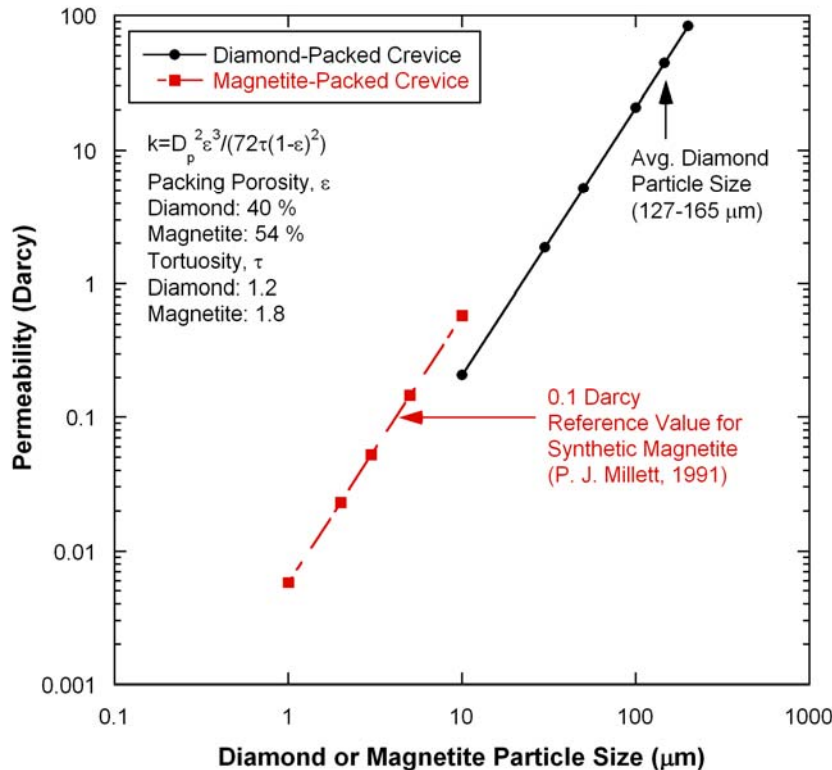


Figure 164. Permeability of single-crevice tests for diamond- and magnetite-packed crevices predicted by Carman-Kozeny equation (1 Darcy = $9.86923 \times 10^{-13} \text{ m}^2$).

Magnetite Dissolution

Diamond powder is inert under highly acidic or caustic chemistry, but magnetite's solubility depends on the pH. If the chemistry in a magnetite-packed crevice becomes strong acid or alkaline, consideration should be given to the dissolution of packed magnetite and its effect on the solution chemistry. Figure 165 shows a potential-pH diagram of Fe in water that contains Na and Cl ions of 0.1 mol/kg at 500 °F, predicted by the thermodynamic code HSC Chemistry. In deaerated acid solution FeCl^+ is a predominant ion. If an acidic crevice is formed in a magnetite-packed crevice, dissolved ferrous ions from the magnetite react with chloride ions and form FeCl^+ . The formation of FeCl^+ will increase the solution pH. This prediction is supported by the pH estimation by MULTEQ shown in Figure 155. We can expect that if a magnetite-packed crevice becomes acidic by the chloride ions, dissolved ferrous ions react with the chloride ions so that the crevice pH becomes less acidic to some extent. However, the quantitative estimation of the pH variation due to magnetite dissolution could benefit from additional study.

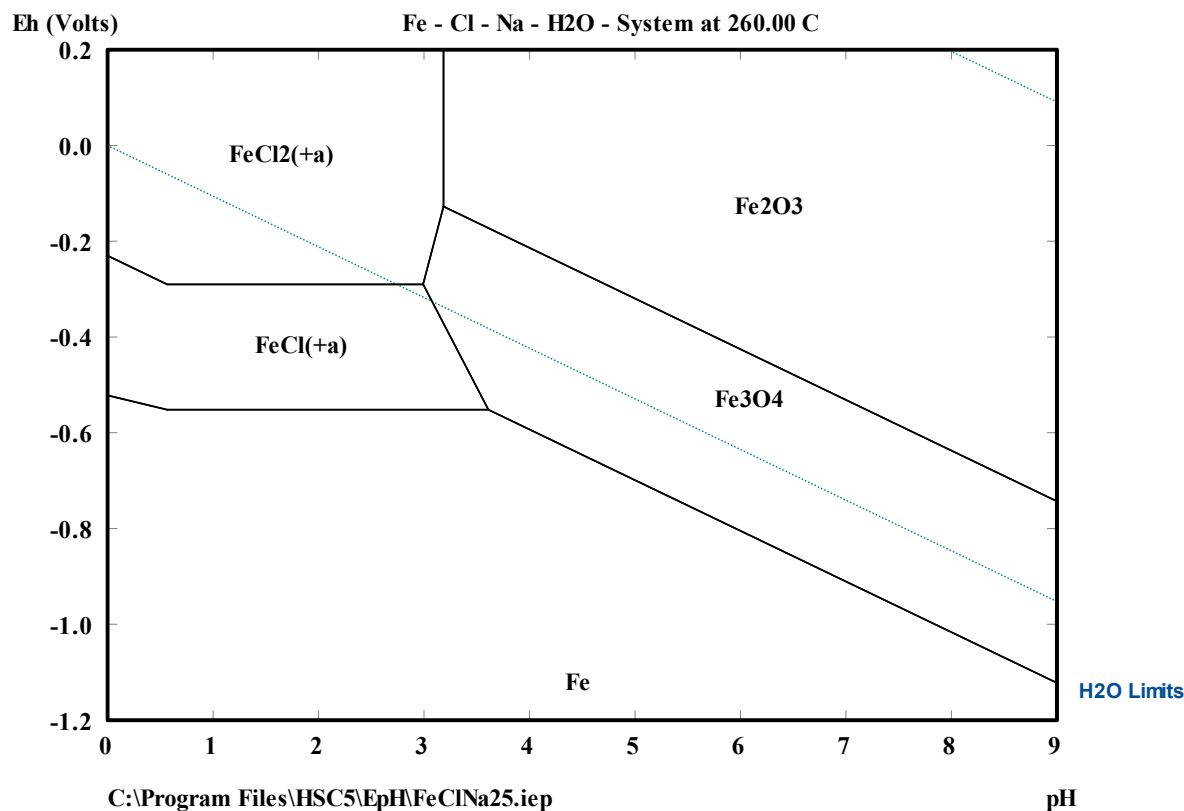


Figure 165. Potential-pH diagram of Fe-Cl-Na-H₂O system at 260°C (500°F) predicted by the thermodynamic code HSC Chemistry.

5.4.7 Summary

The NaCl-06 test at $\Delta T=40$ °F took about 300 hours to reach a steady state in the magnetite-packed crevice. This duration means the kinetics are slower than in the previous diamond-packed crevice test (NaCl-05) because of the lower permeability and higher flow restriction with the magnetite packing. We inferred from the crevice conductivity and tungsten potential that initially, at the deep crevice region, pores were filled mainly with steam and then replaced by the Na-rich liquid phase as the process continued. Crevice tungsten potential measurements indicated the presence of a radial pH gradient near the tube wall. While the tungsten potential located away from the tube surface was not much changed, the potential closer to the tube surface indicated larger fluctuation of crevice pH. At $\Delta T=40$ °F, an initially alkaline pH solution developed near the tube surface but gradually became acidified, which was supported by the bulk solution analysis. The preferential concentration of Na in the crevice will cause a boiling point elevation, which will decrease the steam phase at the tube surface and will make the volatility effect of Cl less significant. The crevice tungsten potential near the tube surface maintained the acidity with the further increase of ΔT from 40 °F to 60 °F and 80 °F, which contradicts the results of earlier literature. However, the molar ratio of bulk samples indicated that the volatility of Cl became more

significant with increasing in ΔT , which is consistent with earlier literature. During the same time period the diamond-packed crevice will result in more severe corrosion of the tube than the magnetite-packed crevice at $\Delta T=60$ °F or higher because of the faster impurity hideout kinetics.

This page is intentionally left blank.

6. Overall Discussion

6.1 Comparison with Literature Data

6.1.1 NaOH Test

Lumsden⁴¹ performed crevice hideout tests with a diamond-packed crevice and NaOH bulk chemistry. Figure 166 shows the total mass of Na in the crevice as a function of time. The bulk Na concentration for each test is specified in the figure. A constant heat flux was applied during the test instead of the ΔT control used in our test. A ΔT control test is considered to be closer to the thermal conditions in SGs than a constant heat flux test. The porosity in the crevice after packing with diamond powder was 52 %. The radial gap size and depth of the crevice were 0.25 mm (10 mil) and 25 mm (1 in.), respectively.¹² The crevice geometry of Lumsden's test is almost identical to ours. A feed/bleed system was used to try to maintain the secondary water chemistry at constant condition.

Lumsden's data were recalculated to the "exposure" base and compared with our single-packed crevice data from NaOH-03, as shown in Figure 167. Considering the differences of the primary heating method and crevice porosities, the hideout rate for the NaOH-03 test appears to be consistent with Lumsden's data for the 20 ppm and 2 ppm bulk Na tests. Lumsden's data show similar behavior in an "exposure" scale, suggesting that the Na hideout rate is directly proportional to the bulk Na concentration. In Figure 167 the Na concentration limits calculated by MULTEQ were specified as parallel lines for each ΔT . Since NaOH has a very high solubility limit, the Na concentration in the crevice is expected to be thermodynamically limited by available superheat if the crevice packing has enough flow restriction. At $\Delta T=40^\circ\text{F}$, the saturation Na mass is slightly higher than the thermodynamic limit. When the crevice gap is being filled with diamond powder, some excess diamond powder usually remains at the crevice mouth, and this condition may result in an overestimate of the crevice porosity. If the crevice becomes more porous, the thermodynamic limit of the total Na mass becomes higher due to the larger crevice volume. From the data in Figure 167, we inferred that the crevice was fully wetted, and the steady-state crevice concentration was thermodynamically limited for the diamond-packed crevice and NaOH bulk chemistry; this behavior is expected in the case of highly soluble solutes like NaOH.

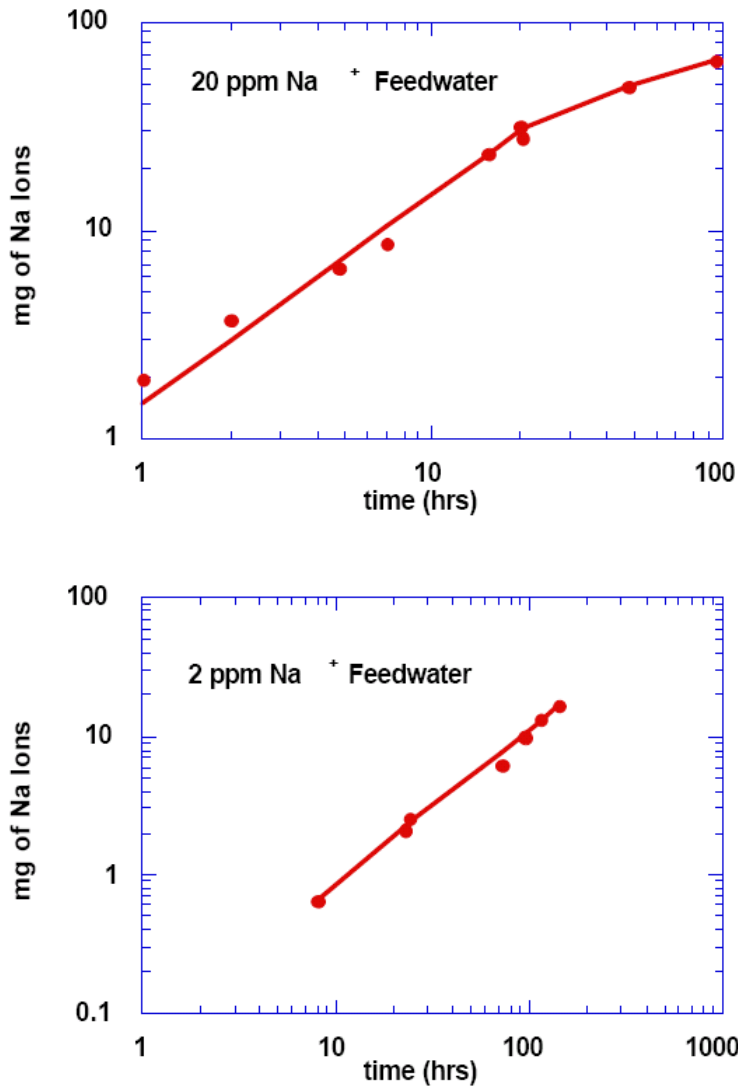


Figure 166. Total Na mass in crevice as a function time with two bulk Na concentrations: 20 ppm Na for upper figure and 2 ppm Na for lower figure. Test conditions are as follows: constant heat flux, diamond packed (52 % porosity), $T_{\text{sat}}=280^{\circ}\text{C}$.⁴¹

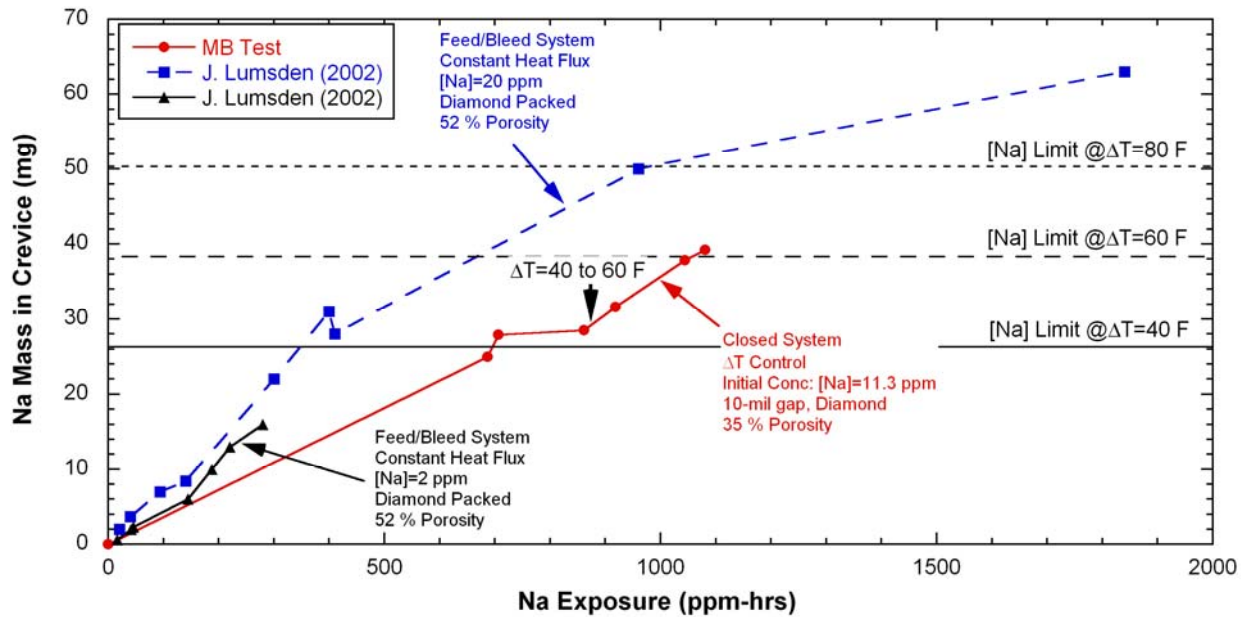


Figure 167. Comparison of 20 ppm NaOH ([Na]=11.3 ppm) test results with available NaOH test data from Lumsden's earlier work⁴¹ (Note: Lumsden's data are the same as shown in Figure 166).

6.1.2 NaCl Test

Mann and Castle performed NaCl hideout tests with carbon-fiber packed crevices.² The porosity of the carbon-fiber packed crevice was 51 %, and its permeability was 43 Darcy. Mann and Castle's data were compared with our crevice test results. The measured permeability is very close to the estimated permeability of our diamond-packed crevice shown in Figure 164. In Figure 168 the total NaCl hideout mass as a function of Cl exposure is compared with our test results for NaCl water chemistry: NaCl-02, -05 and -06. The NaCl-02 test had a molar ratio of 1.0, and NaCl-05 and -06 had a molar ratio of 0.7. Even though there are experimental differences like ΔT and porosity, the initial hideout rate of NaCl-02 is very similar to that of literature data. The NaCl-05 and -06 results differ from the literature data, probably because of the different molar ratio and ΔT conditions. The NaCl-06 test also has a lower permeability than that of Mann and Castle's test. To evaluate the hideout rate of diamond- and magnetite-packed crevices at a certain ΔT , a test such as NaCl-05 or -06 that increases ΔT stepwise is not appropriate. A NaCl hideout test in which ΔT remains constant is more appropriate and would permit this evaluation.

Figure 169 shows the steady-state NaCl mass in the crevice as a function of ΔT . Mann and Castle's test results were obtained with the same crevice geometries and experimental conditions as given in Figure 168. The absolute NaCl masses from our tests cannot be compared with the literature data due to the difference in experimental parameters. Figure 169 plots the overall dependency of the steady-state mass on ΔT . Mann and Castle's test shows the results at MR=1.0, and our tests show the steady-state NaCl mass at MR=0.7. The NaCl-05 test results show an irregular variation with the increase of ΔT . The NaCl-05 test underwent electromigration, which might have affected the steady-state concentration in the crevice. Even though a steady state was not reached at $\Delta T=60^\circ\text{F}$ and 80°F in the NaCl-06 test, the NaCl mass shows a similar variation to Mann and Castle's test.

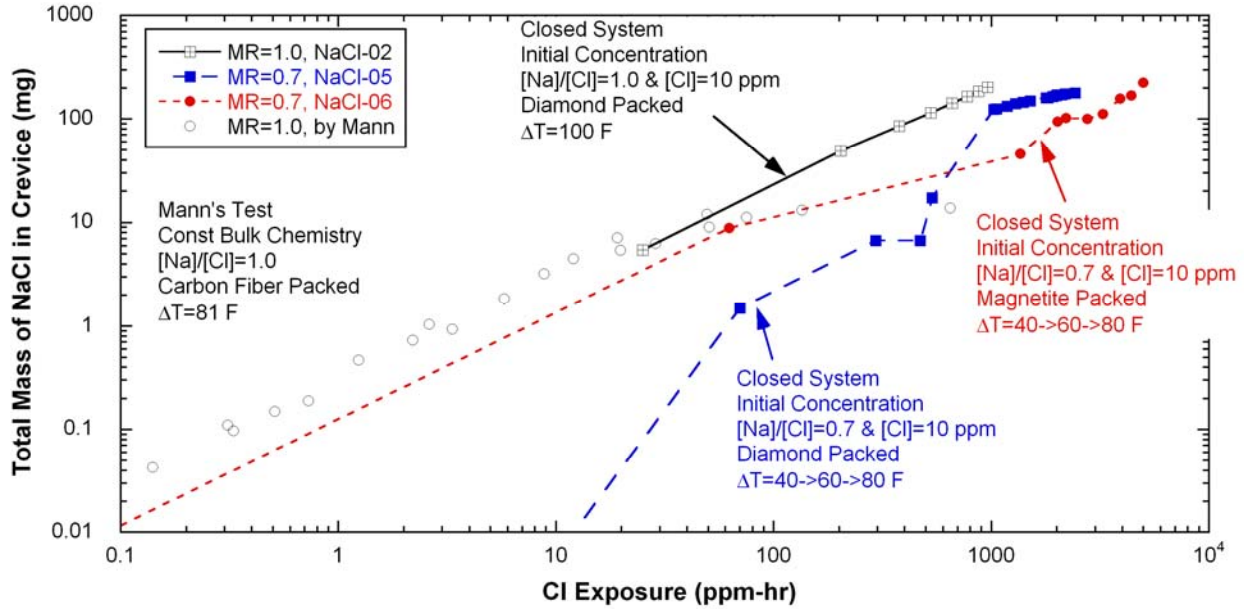


Figure 168. Comparison of NaCl hideout mass as a function of Cl exposure determined by Mann and Castle² and our test results for molar ratios of 1.0 (NaCl-02) and 0.7 (NaCl-05 and -06).

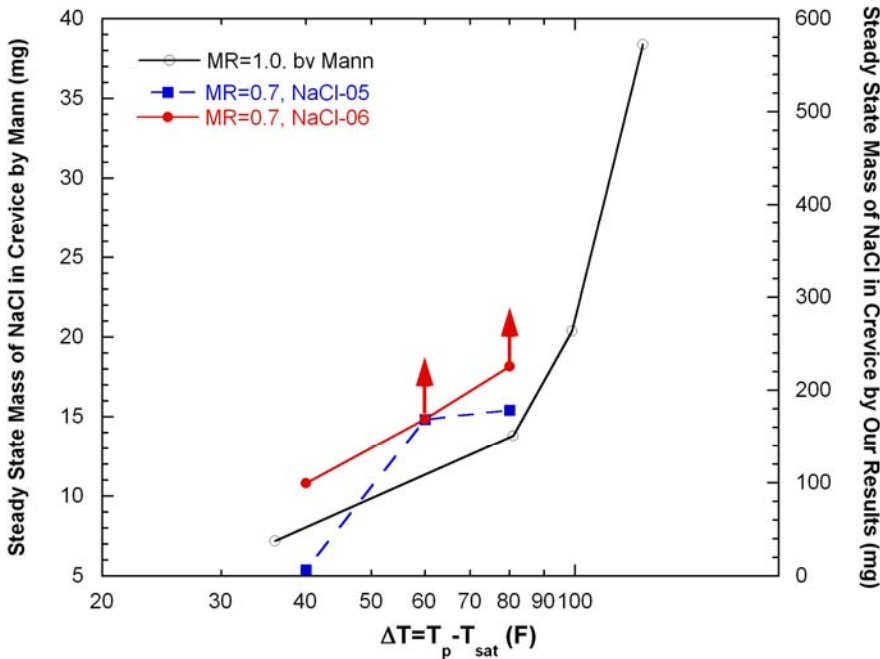


Figure 169. Comparison of the steady-state NaCl mass in the crevice as a function of ΔT from NaCl-05 and -06 tests and tests by Mann and Castle.²

Figure 170 shows the results of NaCl hideout as a function of Cl exposure in the corroded carbon-fiber packed crevice of Mann and Castle² and the magnetite-packed crevice of NaCl-06. In Mann and Castle's test the carbon-fiber filled crevice was exposed to acidic bulk chemistry, which caused corrosion of a tube support plate and formation of magnetite inside the crevice region. Therefore, the corroded crevice of Mann and Castle's test may be considered to be packed with a mixture of carbon fiber and magnetite. The crevice packing permeability in Mann and Castle's test was about 100 times lower than that in NaCl-06, which is expected to result in a lower hideout rate. As compared with the hideout rate at $\Delta T=80^\circ\text{F}$ in NaCl-06, the hideout rate of Mann and Castle's test with $\Delta T=81^\circ\text{F}$ is about three times lower,

which supports the effect of lower permeability qualitatively. Quantitative effect of permeability on the impurity concentration in the crevice could be evaluated through a modeling work.

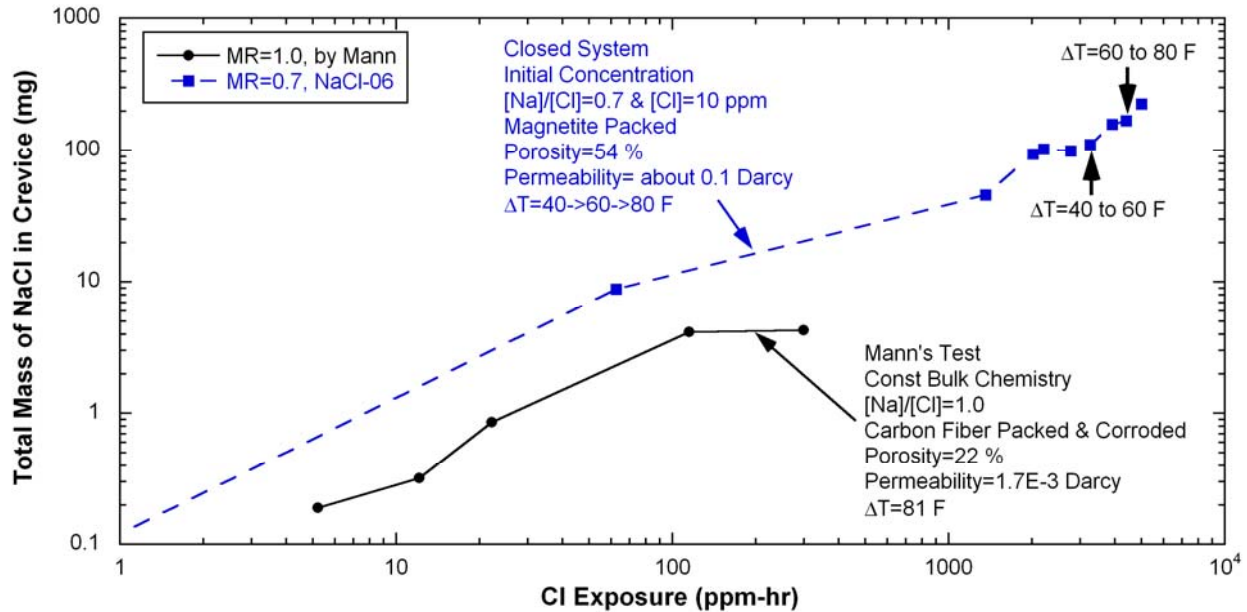
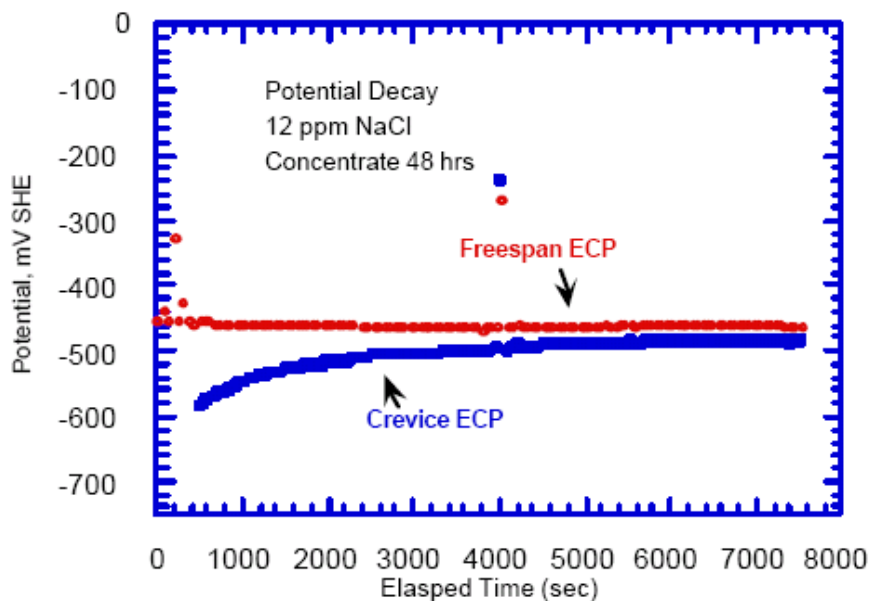


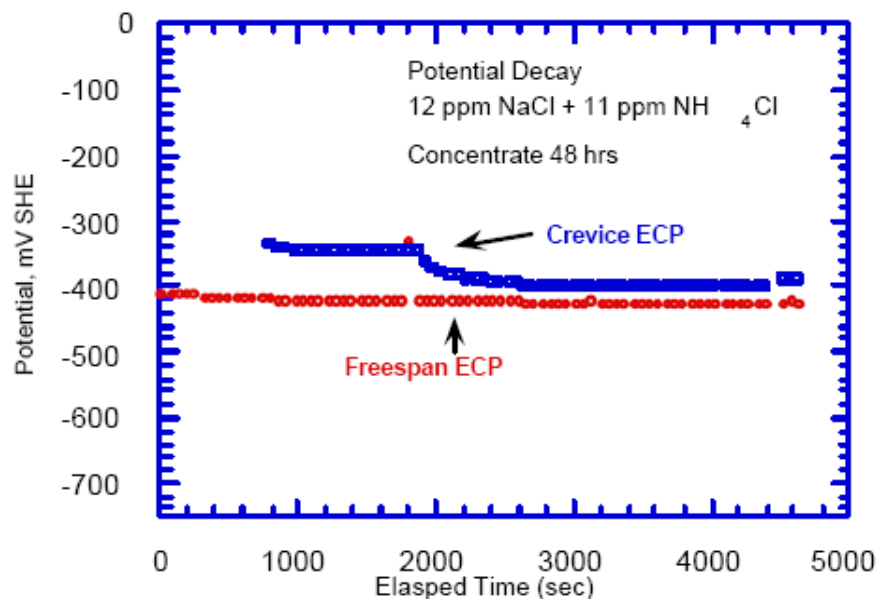
Figure 170. Comparison of NaCl hideout mass as a function of Cl exposure in the corroded carbon-fiber packed crevice of Mann and Castle² and in the magnetite-packed crevice of NaCl-06.

6.1.3 ECP Data Comparison

Figure 171 shows the ECP measurements in the crevice and bulk solution after exposure to the NaCl solution for 48 hours, from a test conducted by Lumsden.⁴¹ Lumsden's test explored the effect of Na-to-Cl molar ratio on crevice ECP. An electric heater inside the primary tubing was turned off after 48 hours, and the crevice ECP variation was monitored. As shown in Figure 171(a), the crevice ECP of alloy 600 was lower than that of the bulk solution at MR=1.0, indicating that crevice pH is more alkaline. At MR=0.2 the crevice ECP was higher than that of the bulk solution, indicating that crevice pH is slightly more acidic, as shown in Figure 171(b). Figure 172 shows the measured crevice and bulk Pt potentials in our MR=1.0 test, NaCl-02. When ΔT was changed from 80°F to 40°F, the crevice Pt potentials quickly dropped and gradually recovered, which is a similar behavior to the results in Figure 171(a). As shown in Figure 59 (NaCl-03, MR=0.3), the crevice pH where the molar ratio was 0.3 was more alkaline at $\Delta T=40^\circ\text{F}$ and the beginning of the $\Delta T=60^\circ\text{F}$ test than the bulk solution, but then the crevice pH became gradually acidic. In our MR=0.7 tests, NaCl-04 and -05, the crevice pH was slightly more acidic than the bulk solution, as shown in Figures 76 and 120. Our crevice ECP results where the molar ratio was less than unity appear to be in reasonable agreement with Lumsden's data shown in Figure 171(b).



(a) $[\text{Na}]/[\text{Cl}]=1.0$



(b) $[\text{Na}]/[\text{Cl}]=0.2$

Figure 171. Crevice ECP after exposure to NaCl solution for 48 hours when the molar ratios of bulk solution was (a) $[\text{Na}]/[\text{Cl}]=1.0$ and (b) $[\text{Na}]/[\text{Cl}]=0.2$.⁴¹

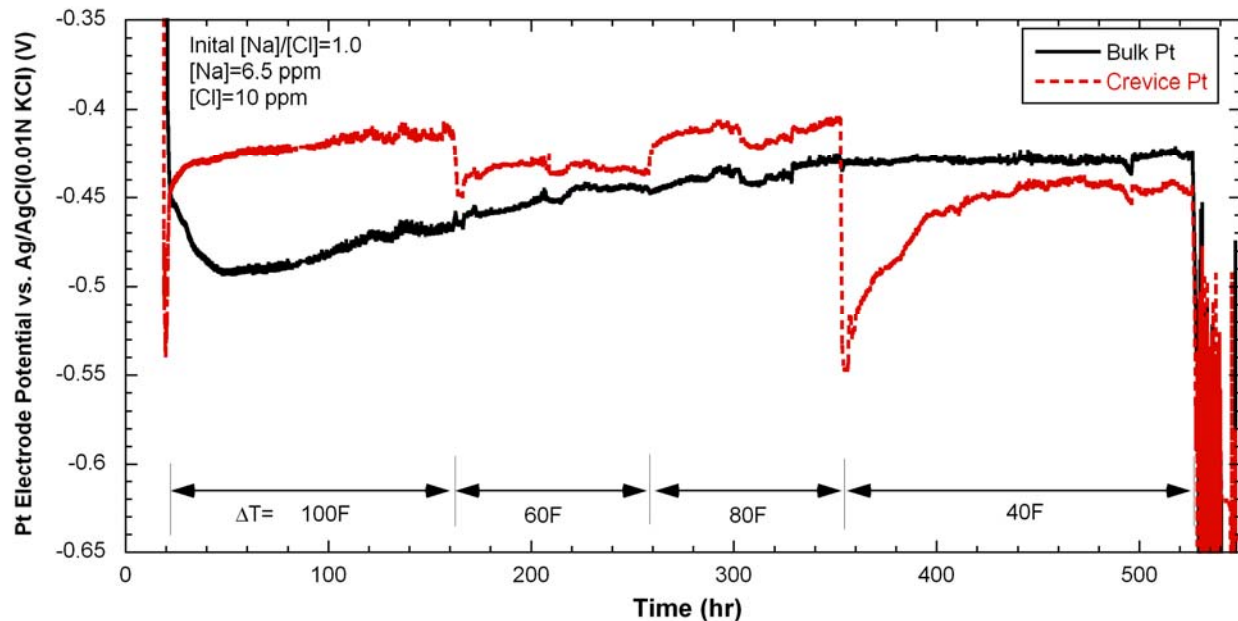


Figure 172. Pt electrode potential variations in bulk and crevice with the molar ratio of 1.0 (NaCl-02 test).

6.2 Comparison with MULTEQ Prediction

The test results for crevice pH and crevice temperature elevation were compared to calculations by the thermodynamic equilibrium code, MULTEQ. Figure 173 shows the crevice pH calculated by the MULTEQ code as a function of boiling point elevation. For the MULTEQ prediction, we assumed that the bulk water chemistry is the same as that in the NaOH-03 test. We selected the “static system” option, which has suboptions: “steam retained” and “steam removed.” It was assumed that precipitates are retained in the system. A static system with “steam retained” means that the liquid phase, the solid precipitates, and the vapor phase stay within the system and no mass exchange occurs through the system boundary.²⁴ It was also assumed that all phases are in thermodynamic equilibrium. In this option, as the calculation step increases, the steam mass fraction increases and the liquid mass fraction decreases. This condition leads to an increase of the impurity concentration in the liquid phase. A static system with “steam removed” is the same system as that with “steam retained” except that the vapor phase formed in each step is removed from the system.²⁴ This system is not closed since vapor can cross the system boundaries. The concentration process is assumed to take place in a series of finite steps, which are specified by the operator. Since this system constitutes a continuous process modeled as finite steps, the final composition is a function of the step size selected by the operator.²⁴ The static system with the “steam removed” models a system with incomplete mixing; the static system with the “steam retained” models a perfectly mixed system. Therefore, if the step size in the “steam removed” option is increased, it is assumed that mixing in the system will become more difficult. Two options can be considered as extreme cases that may occur in actual SG crevices. An actual crevice condition is expected to be somewhere between the two extreme cases. Baum has discussed the crevice pH variation in magnetite-packed crevice as a function of ΔT .³ Figures 173-175 and 178-179 present the calculated results for different options and system conditions.

Figure 173 shows that the calculated crevice pHs with the options of “steam retained” and “steam removed” are the same under the NaOH-03 test condition. The crevice pH increases with increasing

elevation of the boiling point. The largest rate of increase in pH occurs when the boiling point elevation is less than 5°F. The slope of the curve for crevice pH as a function of boiling point elevation is low at relatively high concentrations of Na mainly because the activity coefficient of the Na⁺ ion is lower at higher concentration and soluble NaOH becomes more stable than Na⁺ ion at high Na concentration. The measured crevice pH by the crevice tungsten electrode in the NaOH-03 test as a function of measured crevice boiling point elevation is also plotted in the same figure. The measured boiling point elevation was determined by the difference between the measured crevice temperature and bulk temperature (500°F). The crevice pH becomes close to the prediction results as the boiling point elevation increases and tends to fit with the prediction line. The initial discrepancy at lower elevations in the boiling point appears to be due to the crevice concentration being transient rather than in equilibrium because the lower elevation data in the boiling point were acquired during the transient condition before reaching the saturated state at ΔT=40°F and MULTEQ prediction is valid in equilibrium state. Based on the comparison, we inferred that the MULTEQ code prediction and the experimental data at equilibrium state with NaOH bulk chemistry showed a reasonable agreement.

Figure 174 shows the calculated crevice pH as a function of boiling point elevation for a molar ratio of 1.0 and Cl concentration of 10 ppm. As observed in Figure 173, the crevice pH increases with the increase in boiling point elevation, but the crevice pH is about 3 units lower than that of the NaOH-03 test. In Figure 174, the discrepancy between “steam retained” and “steam removed” is not significant but becomes larger as the boiling point elevation increases. This change can be interpreted as the volatility effect of Cl. The NaCl-02 test had a molar ratio of 1.0 but employed no crevice pH electrode. The crevice Pt electrode potential was about 100 mV lower than the bulk Pt potential at ΔT=40°F, and the bulk pH was 4.4. Assuming the crevice Pt electrode behaves as a hydrogen electrode, the estimated crevice pH is roughly 5.4, and the corresponding crevice temperature elevation is 12°F. The estimated pH from the Pt potentials (pH=5.4) is much lower than the predicted crevice pH (pH=7.5) by MULTEQ at the same temperature elevation. This discrepancy was discussed in Section 4.2.3.

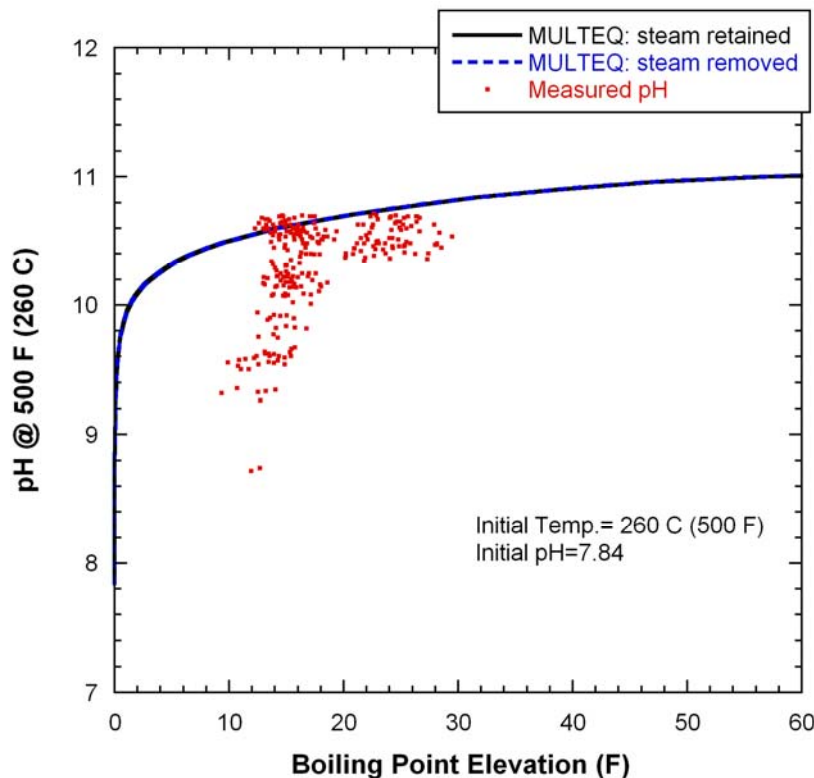


Figure 173. Calculated crevice pH by MULTEQ as a function of boiling point elevation in comparison to the measured crevice pH based on the crevice tungsten potential data in the NaOH-03 test (nominal [Na]=11.3 ppm and [Cl]=0.6 ppm).

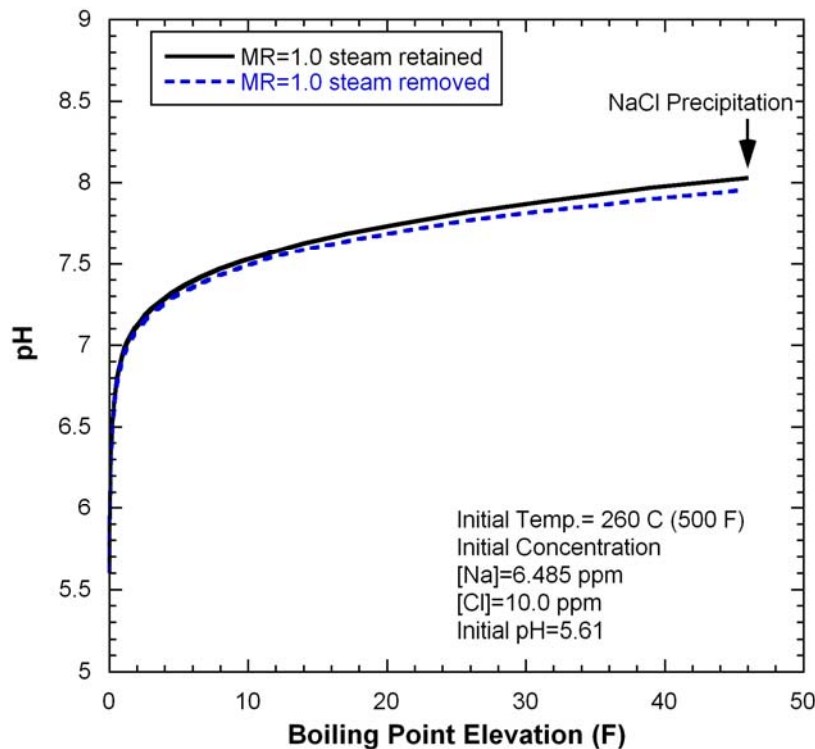


Figure 174.
Calculated crevice pH by
MULTEQ as a function of boiling
point elevation at MR=1.0.

Figure 175 shows the calculated crevice pH by MULTEQ as a function of boiling point elevation for the molar ratio of 0.7 and Cl concentration of 10 ppm. Figure 175 shows a large difference between the two options: “steam retained” and “steam removed.” To interpret the calculation results, each ion’s concentration variation was plotted as a function of concentration factor. The “concentration factor” in MULTEQ is defined as the ratio between the total mass of the system and liquid mass at each calculation step. Figure 176 shows the ion concentration calculation results as a function of concentration factor for the steam retained option. The initial pH decrease can be attributed to the concentration of impurities, as discussed in Figure 44. As the concentration progresses, the molar ratio becomes higher and closer to one due to the volatility of Cl, which makes the crevice pH increase. The further increase of the crevice pH, even though the molar ratio had already reached one, was attributed to the decrease of aqueous HCl concentration. To maintain the equilibrium constant among HCl(aq) , H^+ , and Cl^- , H^+ should decrease when HCl(aq) decreases because Cl^- increases. Figure 177 shows the predicted ion concentrations for the “steam removed” option. The molar ratio becomes close to one at higher concentration factors as compared with the “steam retained” option. This condition makes the crevice pH decrease continuously even at a relatively high concentration factor. The increase in crevice pH can be interpreted as the result of the increase in the molar ratio and the decrease of aqueous HCl concentration. The HCl(aq) concentration in liquid phase with the “steam removed” option is higher than that with the “steam retained” option. In the case of “steam retained”, HCl(aq) should be in equilibrium with the HCl in the vapor phase so that the HCl(aq) concentration cannot be increased continuously. However, in the “steam removed” option, the total mass of the steam phase at each calculation step is much smaller than that of the “steam retained” option. Therefore, the volatilized and lost HCl amount from the liquid phase is smaller, which enables the continuous increase of HCl(aq) concentration as the concentration progresses.

The measured crevice pH as a function of measured crevice boiling point elevation from the NaCl-05 test is also plotted in Figure 175. As was observed for Figure 173, transient phenomena are initially observed at lower boiling point elevations. As the boiling point elevation increases, the crevice pH deviates from the “steam retained” condition. This trend could be attributed to the location of the crevice pH electrode in relation to the tube wall. In the NaCl-05 test the crevice pH electrode was apparently far from the tube wall so that the measured crevice pH does not accurately represent the crevice chemistry on the tube wall.

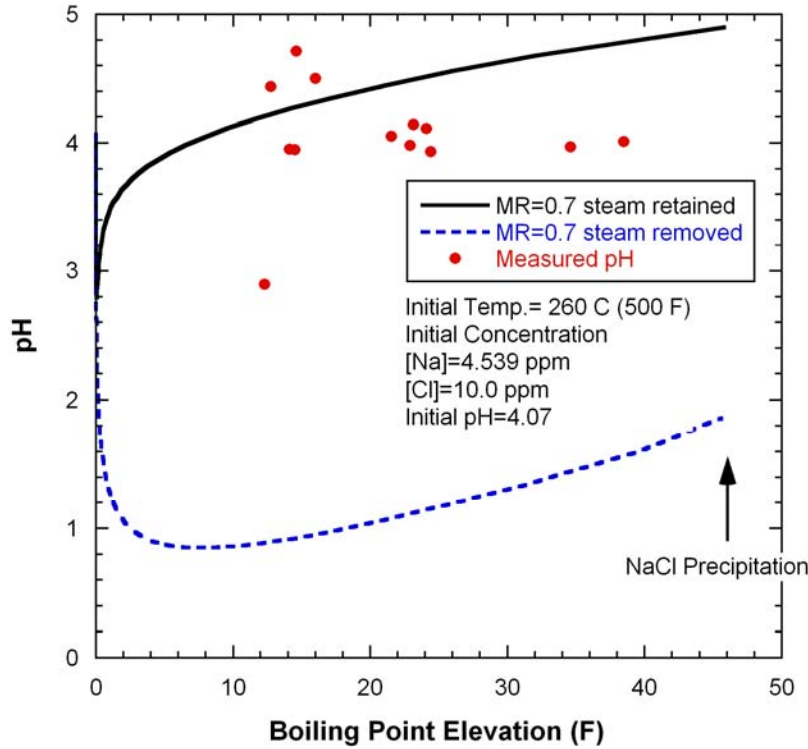


Figure 175. Crevice pH calculated by MULTEQ as a function of boiling point elevation compared to the measured crevice pH based on the crevice tungsten potential data in the NaCl-05 test (MR=0.7).

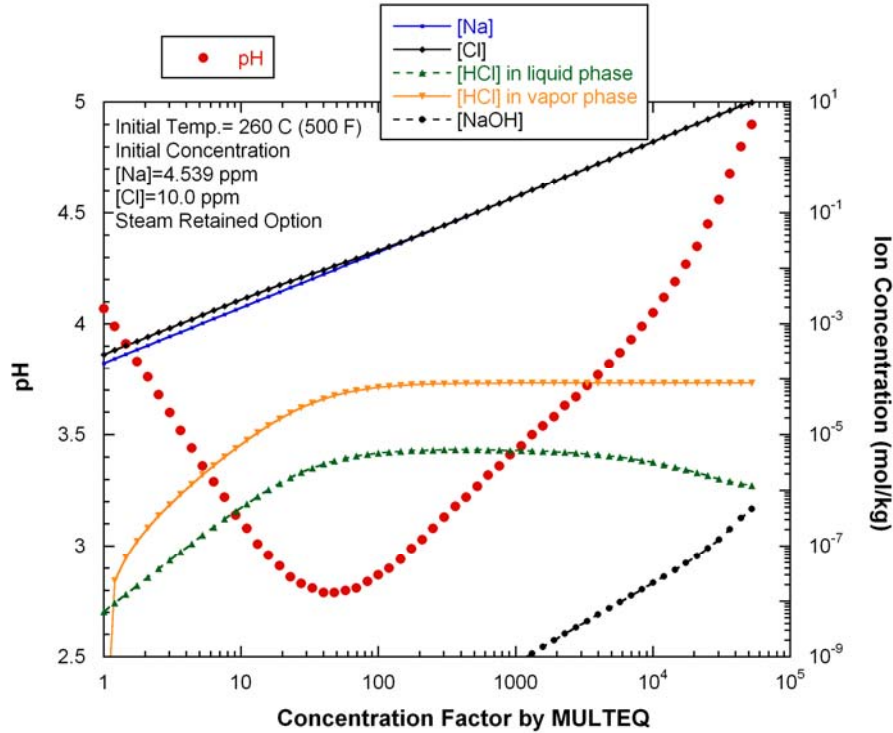


Figure 176. Crevice pH and ion concentration as a function of concentration factor calculated by MULTEQ assuming the "steam retained" condition and MR=0.7.

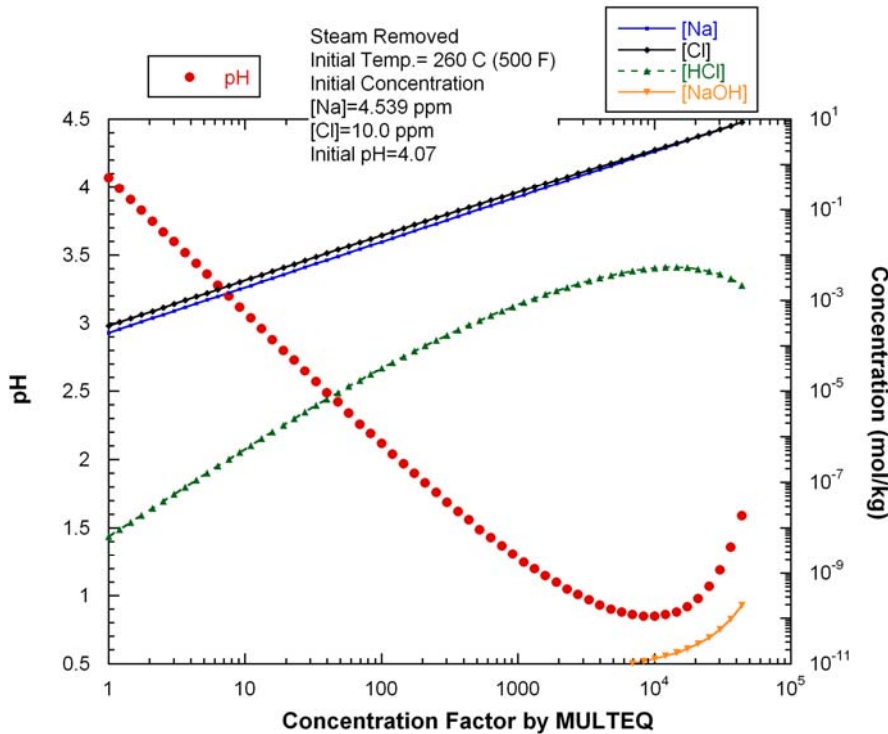


Figure 177. Crevice pH and ion concentration as a function of concentration factor calculated by MULTEQ assuming the "steam removed" condition and MR=0.7.

The crevice pH with respect to the boiling point elevation from the NaCl-06 test is shown in Figure 178. As discussed in Section 5.4.4 and 5.4.6, the crevice pH took a long time to reach steady state because of the complex Na and Cl concentration behavior. The data scatters at lower boiling point elevations

represent the transient crevice condition. The NaCl-06 data show lower crevice pH values than the NaCl-05 data at the same boiling point elevation. This difference appears to be reasonable because the magnetite-packed crevice in NaCl-06 has higher flow restriction and lower permeability than the diamond-packed crevice in NaCl-05, and this condition results in less mixing between liquid and vapor phases, moving the crevice pH closer to the “steam removed” option.

Figure 179 shows the calculated pH as a function of boiling point elevation for a molar ratio of 0.3. The overall pH trend with respect to the boiling point elevation is similar to that with the molar ratio of 0.7 shown in Figure 175, but the absolute pH value is lower at the same boiling point elevation because of the lower Na concentration and molar ratio. The measured crevice pH as a function of the measured boiling point elevation is plotted in the same figure. Even though there is some data scatter, the crevice pH data follow the “steam retained” option curve. Since the diamond-packed crevice in the NaCl-03 test has higher permeability than the magnetite-packed crevice, the measured data were expected to be close to the “steam retained” results. As can be deduced from Figures 176 and 177, the molar ratio does not exceed unity in the MULTEQ calculations. However, the measured or estimated molar ratios in our experiments exceeded unity because of the preferential hideout of Na. Some data located above the line for the steam retained option shown in Figures 178 and 179 may represent more prototypic crevice concentration phenomena. Since these phenomena occur during transient conditions, they are difficult to predict with a chemical equilibrium model like MULTEQ code.

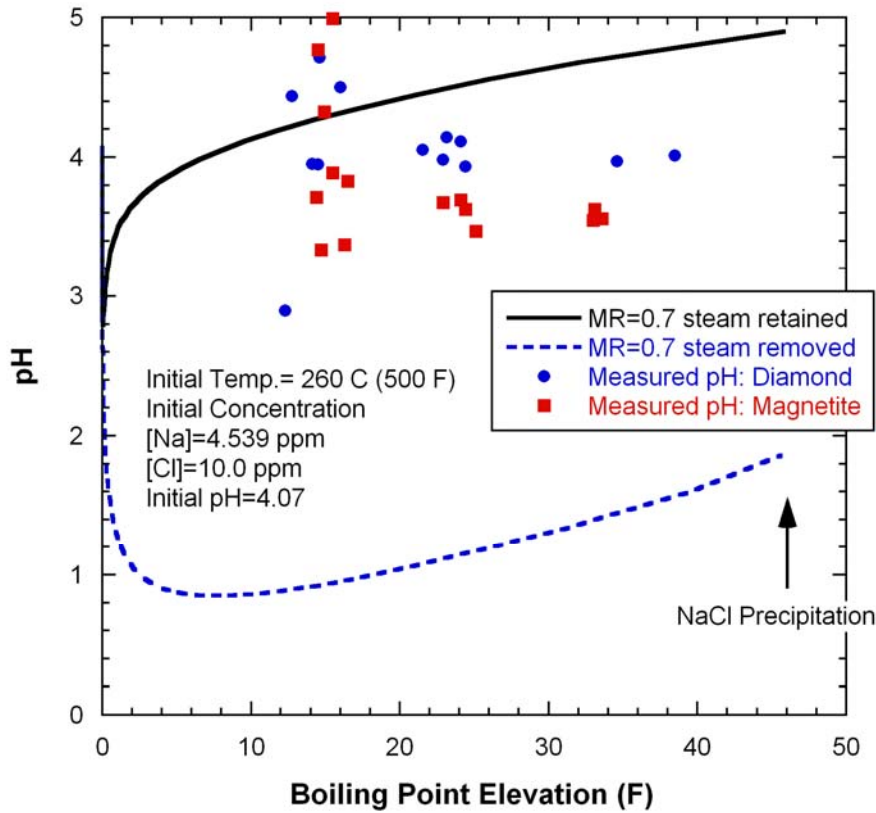


Figure 178. Measured crevice pH based on the crevice tungsten potential data in the NaCl-06 test in comparison with the NaCl-05 test and calculated pH by MULTEQ.

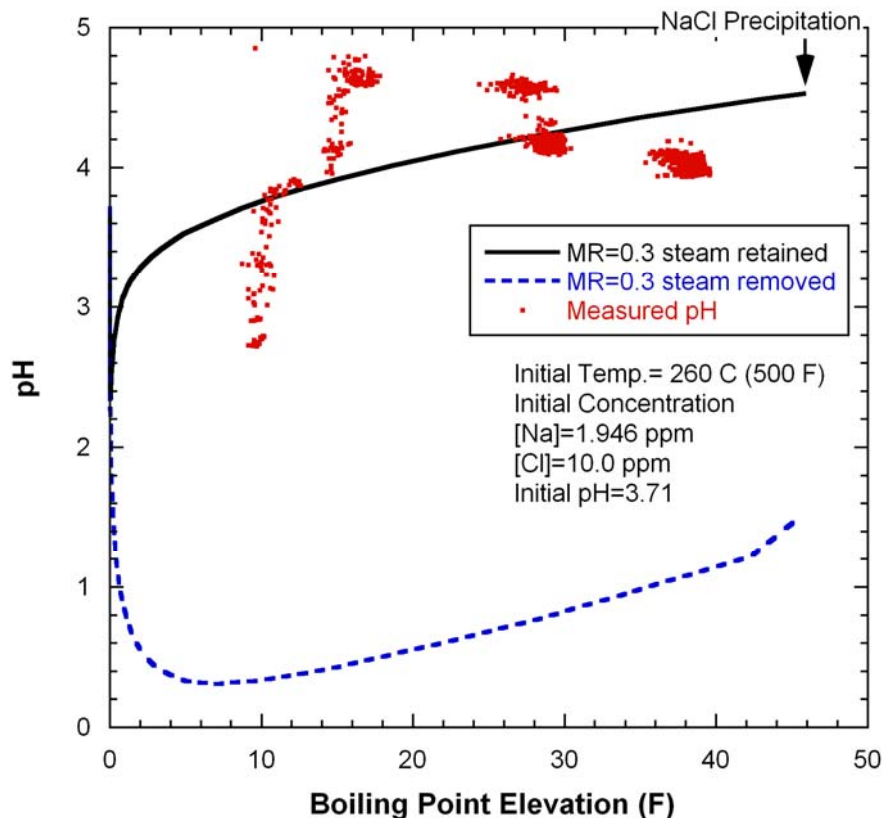


Figure 179. Calculated crevice pH by MULTEQ as a function of boiling point elevation in comparison with measured crevice pH based on the crevice tungsten potential data in the NaCl-03 test.

6.3 Implication of MB Test Results for Operating Steam Generator

6.3.1 Crack Propagation in an Unpacked Crevice

As discussed in Section 5.2.4, we have some preliminary experimental evidence that once a tube crack is formed, the crack itself can act as a crevice that causes, in the presence of NaOH bulk chemistry, the crack to grow even if the sludge or debris is cleaned out of the SG. The alloy 600 tube has been used in the NaOH-01 through NaCl-05 tests. Through-wall cracks in the unpacked crevice were initiated during the NaOH-01 and -02 tests and grew to completely through-wall during the NaOH-03 test which followed the NaCl-01 through NaCl-04 tests. Crack growth under the NaCl-01 and -02 tests where the MR=1.0 was not expected because the 20-mil gap crevice packed with diamond would be in a well-mixed condition, and the molar ratio would be close to a neutral condition. The NaCl-03 and -04 tests where the MR<1.0 may have a chance for crack growth to occur because they had the magnetite-packed crevices which seem to show an initial preference for Na concentration. However, since the initial Na preference was followed by pH neutralization, as observed in the NaCl-06 test, and the magnetite packing porosity of NaCl-03 and -04 was much higher than that of NaCl-06, crack growth in the 20-mil gap crevice did not likely occur during the NaCl-03 and -04 tests. The SCC growth data³⁷ indicated that the crack growth rate at pH=11 is about one order of magnitude higher than that at pH=1 and also suggested that the cracks were more likely to grow in the NaOH test than the NaCl test. However, we did not experimentally confirm that a crack will grow without flow restriction under NaCl rather than NaOH bulk water chemistry. If a crack does not grow in a NaCl solution where there is no restriction to flow, crack growth

would not be expected in an actual SG since the Na-to-Cl MR in most SGs is close to the neutral condition. If a crack does grow under a NaCl solution where there is no restriction to flow, crack growth may occur. It may be worthwhile to grow 50 % through-wall cracks, and then test them in the MB to determine if they will become 100% through-wall without any crevice or packing present under the NaCl and the NaOH bulk water chemistry.

6.3.2 Diamond vs. Magnetite

Diamond has a much higher thermal conductivity than magnetite, which enhances the boiling rate in the crevice and increases the impurity hideout rate. Two parameters characterize packing materials: porosity and permeability. Porosity provides an indication of the available space for liquid to concentrate in the crevice. If the impurity hideout rates are the same, a crevice having lower porosity will reach steady state earlier. Permeability determines how quickly the liquid or vapor phase can penetrate into or escape out of the packed crevice, and how much the liquid and vapor phases can mix in the crevice. The diamond-packed crevices in the MB tests had lower porosity but higher permeability than the magnetite-packed crevice. The diamond-packed crevices can result in an overestimate of the impurity hideout rate. To evaluate the hideout rate realistically, the magnetite-packed crevice test appears to be more appropriate. In one MB test, the packing porosity of the magnetite-packed crevice was 54%, and its permeability was about 0.1 Darcy. The examination of the tubes removed from SGs showed that there was a considerable radial variation in the physical and chemical characteristics of the crevice deposits.⁴ The deposits on the tube side of the crevice were enriched in calcium, magnesium, phosphate, and silicate, while the deposits on the tube support plate side of the crevice were composed of almost 100 % dense (0 % porosity) magnetite. Highly porous magnetite separated the two regions. The tube-side crevice deposits in actual SGs are much denser and have a lower porosity than the magnetite packing in the MB test. The hideout rate in the crevice in actual SGs is expected to be lower than that of our magnetite-packed crevice and the crevice pH is expected to be closer to the prediction result by MULTEQ with the “steam removed” option because of the difficulty in mixing between the liquid and steam phases. These differences suggest that an actual SG crevice compared with our MB test is more acidic at the same ΔT . Further experimental and analytical studies would aid in our understanding of what would occur in actual SG crevices.

6.3.3 Hideout Kinetics Estimation in Actual SG Crevices

In an actual SG crevice packed with magnetite, the kinetics of the impurity concentration will be much slower than experienced in the MB tests because the impurity concentrations in the SG will be much less (i.e. in the ppb range), even if the packing porosity and permeability are assumed to be the same as in the current MB test. Also, the total exposed time in an actual SG crevice will be much longer than that in the MB test. If the exposed time is long enough, however, the crevice impurity concentration in an actual SG crevice can become as high as in the MB test. If the exposed time is not long enough, the actual SG crevice may not reach a steady-state condition after one fuel cycle. Longer-term MB experiments with more dilute impurity concentration in the bulk solution and a theoretical model for predicting the long-term crevice concentration behavior with ppb-range impurity may be useful.

Based on the Na and Cl hideout behavior in the magnetite-packed crevice test, NaCl-06 (Figure 159), the hideout rates of Na and Cl as a function of ΔT were estimated, as shown in Figure 180. The hideout rates of Na are always higher than those of Cl. One data point, labeled “Cl hideout rate after Na saturation,” indicates the measured hideout rate when the delayed preferential Cl concentration occurred at $\Delta T=40^\circ\text{F}$, as shown in Figure 159. This hideout rate data can be used to independently estimate the hideout rate for Na and Cl in an actual SG crevice.

To determine the hideout rate in an actual SG, the physical characteristics in an actual SG crevice must be known. Baum's assumption⁵ for the tube-side deposits was introduced in this estimation; the deposit layer was assumed to extend 38 μm and have 10 % porosity. The total crevice depth was assumed to be 25.4 mm (1 in.). Actual crevice gap size would be larger than 38 μm , but in this estimation we focus on the hideout characteristics of the tube-side deposits. The total pore volume is about 7×10^{-3} mL. The assumed crevice would have a lower permeability than that in the NaCl-06 test, but for a simple estimation, we assumed that the deposits have a similar permeability to that in the NaCl-06 test. Because the bulk impurity concentration in an actual SG is much lower than that of MB tests, it will take more time to reach a certain concentration level for Na or Cl. The ΔT was assumed to be 60°F because this temperature is closer to the ΔT in an actual SG. The bulk solution concentration for Na and Cl was assumed to be 1 and 2 ppb, respectively, to maintain the molar ratio of 0.7 used in NaCl-06 and to represent actual impurity concentrations in SGs. For the Na hideout rate, the measured hideout rate at $\Delta T=60^\circ\text{F}$ was chosen, and the Na concentration was assumed to continuously increase until it reached the thermodynamic limit of NaOH at $\Delta T=60^\circ\text{F}$. For the initial Cl hideout rate, the measured Cl hideout rate at $\Delta T=40^\circ\text{F}$ was used instead of that at $\Delta T=60^\circ\text{F}$. Baum noted that the loss of acidity on the tube wall becomes more significant with the increase in ΔT ,³ and NaCl-06 started with a ΔT of 40°F, which was increased 362 hours later to 60°F. Therefore, the measured Cl hideout rate at $\Delta T=60^\circ\text{F}$ is expected to be affected by the test results at $\Delta T=40^\circ\text{F}$. If the ΔT starts at 60°F, the Cl hideout rate is expected to be similar or even lower than the one measured at 40°F in the NaCl-06 test. The Cl hideout rate is assumed to change when the Na concentration reaches the thermodynamic limit at $\Delta T=60^\circ\text{F}$. Based on the results at $\Delta T=40^\circ\text{F}$ in the NaCl-06 test, the Cl concentration started to increase rapidly when the Na concentration reached about 80 % of the saturation level, and the Na hideout rate became lower. In this estimation, the hideout behavior of an actual SG crevice is determined qualitatively rather than quantitatively, so that a simple assumption for the Cl hideout rate change was introduced.

Figure 181 shows a schematic of Na and Cl hideout mass variations in the assumed crevice deposits as a function of time. Even after a typical fuel cycle (approximately 15 months or 10,800 hours), the Na concentration did not reach the solubility limit at $\Delta T=60^\circ\text{F}$. The average Na-to-Cl molar ratio in the crevice always remains higher than one, indicating the development of an alkaline crevice during one fuel cycle. If the actual hideout rate in a SG crevice is lower than the estimated value, which is a credible assumption because the crevice deposits in a SG would have lower permeability than that in the MB test, the actual crevice condition could be more likely in an alkaline condition during one fuel cycle. Even though the assumptions for this estimation introduce uncertainties, the estimated concentrations in the actual SG crevice deposits near the tube wall indicate that the crevice concentration is likely to be in a transient condition during a typical fuel cycle. It is also expected that the crevice pH near the tube wall remains alkaline for this time period. Therefore, to lead additional insights into the behavior of an actual SG crevice, it may be more important to focus on the kinetics of impurity hideout rather than the steady-state conditions. However, this estimation assumes that impurity in the actual SG crevice is not present at the beginning of a fuel cycle, which may not be true. Some of impurities accumulated during a typical fuel cycle may remain in the crevice after shutdown rather than return to the bulk water. These remaining impurities can affect the crevice chemistry for the next fuel cycle.

A magnetite-packed crevice test having low bulk impurity concentration could be conducted for a relatively long time. The total exposure of Na or Cl under actual SG conditions during one fuel cycle is less than 100 ppm-hr. If the bulk concentration in a laboratory test is 1 ppm, the total test time should be more than 100 hours to simulate one fuel cycle. Whether or not the ppm-range bulk concentration test results can be extrapolated to the ppb range is a different issue. Baum suggested that the acidity loss is likely to become more significant with a decrease in bulk concentration, which will make the crevice pH more alkaline.³ To evaluate how the remaining impurities in the crevice after shutdown affect the crevice

chemistry for the next fuel cycle, the test can be stopped after 100 ppm-hr operation and resumed without opening the MB secondary chamber.

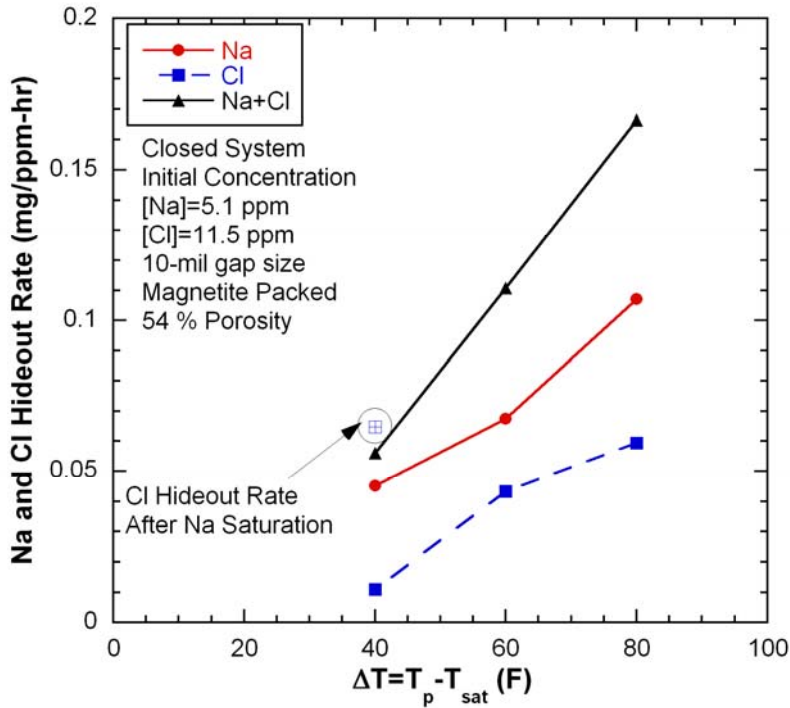


Figure 180. Initial Na and Cl hideout rates as a function of the temperature difference between primary and secondary saturation temperatures (NaCl-06).

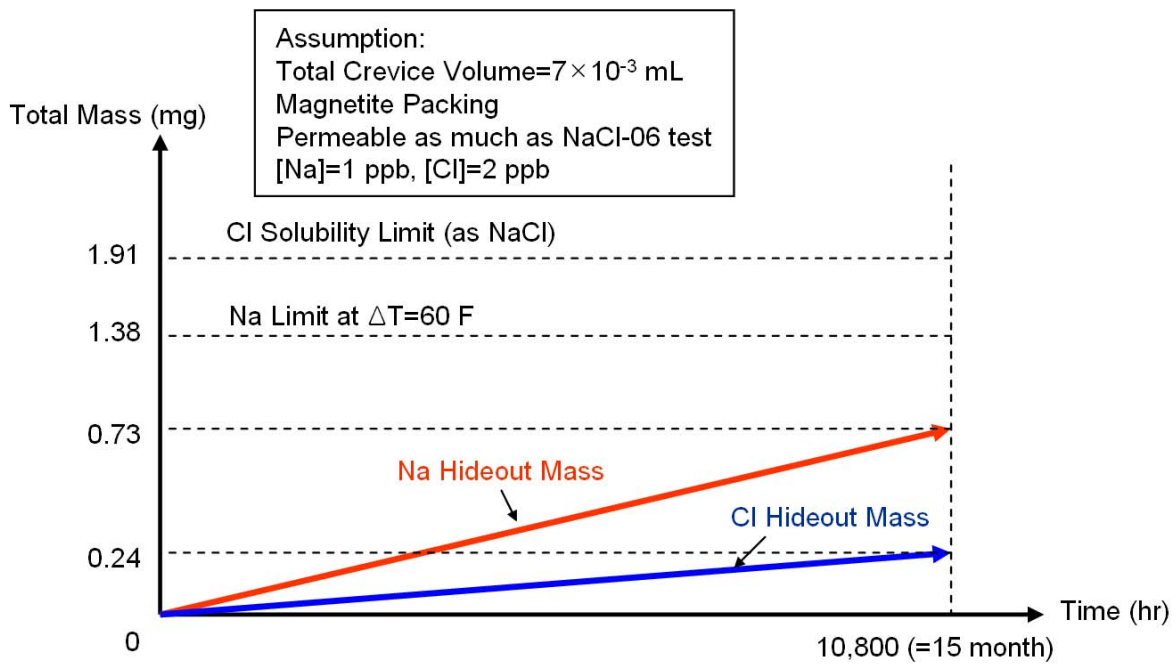


Figure 181. Schematic of Na and Cl hideout mass variations as a function of time in a crevice where the porosity and secondary impurity level are assumed to be similar to those in actual SGs.

6.3.4 Dependency of Cl Volatility Effect on Molar Ratio

The dependency of the Cl volatility effect on bulk concentration and ΔT was discussed by Baum.³ Lower bulk concentration and higher ΔT tends to make the volatility effect of Cl more significant. The dependency of the Cl volatility effect on the Na-to-Cl molar ratio has not been discussed before. This issue is discussed from two points of view here: molar ratio and crevice and bulk tungsten potentials.

Figure 182 shows the molar ratios in crevice samples with respect to those in bulk samples for the diamond-packed crevices. The crevice MRs decrease with the decrease of bulk MRs. The crevice MR data for MR=1.0 is scattered, depending on ΔT . If the Cl volatility effect does not depend on molar ratio, all data points should fit on a single line parallel to the solid line in the figure representing a 1:1 correlation line. In Figure 182, as the bulk MR decreases, the crevice MR tends to deviate from the 1:1 line; this deviance suggests that the Cl volatility effect becomes more significant with the decrease in the bulk MR. If experimental data are acquired for a bulk solution MR of 0.1 or 0.2, the data trend should become clearer.

Figure 183 shows the molar ratio of crevice samples as a function of the MR in the bulk sample for a magnetite-packed crevice. As compared with the diamond-packed crevice data, the number of data points is relatively small with regard to deriving a firm conclusion. One clear difference from the results shown in Figure 182 is that the crevice MRs are close to the bulk MRs, and some data show even lower values than the bulk MRs. This finding needs to be carefully interpreted because all these data were obtained at $\Delta T=80^\circ\text{F}$. At high ΔT a less permeable crevice like a magnetite-packed crevice tends to be filled with steam, and the extracted samples from this crevice show higher Cl concentrations because the steam contains HCl which is condensed and extracted from the crevice. In the magnetite-packed crevice, as discussed in Section 6.3.3, the crevice chemistry is dependent on the exposure time. The crevice data used in Figure 183 represent only the data under a saturated state at each ΔT . Although the data sets are limited, we concluded that, as compared with a relatively permeable crevice like the diamond-packed crevice, the Cl volatility effect in the magnetite-packed crevice is less significant at a saturated state because it becomes more difficult for Cl to escape from the heated tube-wall surface in less permeable packing. Baum also mentioned that the acidity loss on the tube wall becomes less significant with a decrease in packing porosity.³ To further evaluate the dependency of Cl volatility on the molar ratio in the magnetite-packed crevice quantitatively, additional tests should be considered.

We evaluated the dependency of Cl volatility on the molar ratio from the crevice and bulk ECPs. At a molar ratio of 0.3, as shown in Figure 59, the crevice tungsten potentials were lower than the bulk tungsten potentials at $\Delta T=40^\circ\text{F}$ and were mixed (some higher, some lower) at $\Delta T=60^\circ\text{F}$. When the bulk MR was 0.7, the NaCl-04 and -05 test results showed that, during most of the test time, the crevice tungsten potentials did not deviate much from the bulk tungsten potentials, as shown in Figures 76 and 120, respectively. At a bulk MR of 1.0, as shown in Figure 43, the Pt potentials indicated alkaline crevice chemistry at low ΔT . The crevice tungsten potentials in the diamond-packed crevices are reasonably consistent with the results from the molar ratio analysis shown in Figure 182. Since we conducted only one highly packed crevice test with magnetite, we cannot reach a firm conclusion about the Cl volatility dependency on molar ratios. For the magnetite-packed crevice, it is more important to focus on the effect of molar ratio on the hideout kinetics rather than the saturation condition in the crevice as a function of molar ratio.

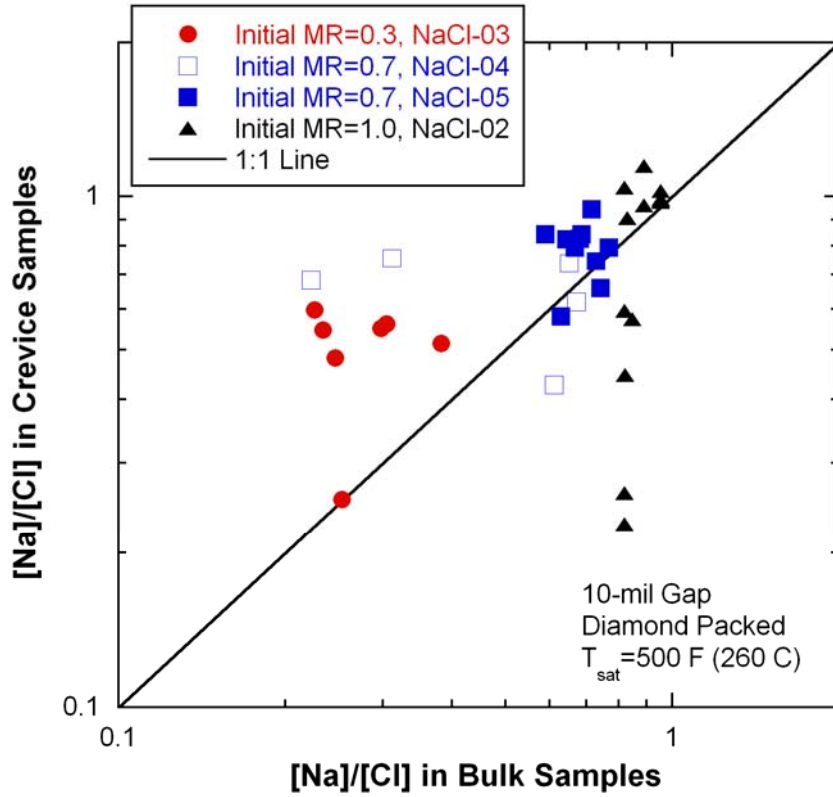


Figure 182.
Molar ratio in crevice sample as a function of the molar ratio in the bulk sample for a diamond-packed crevice.

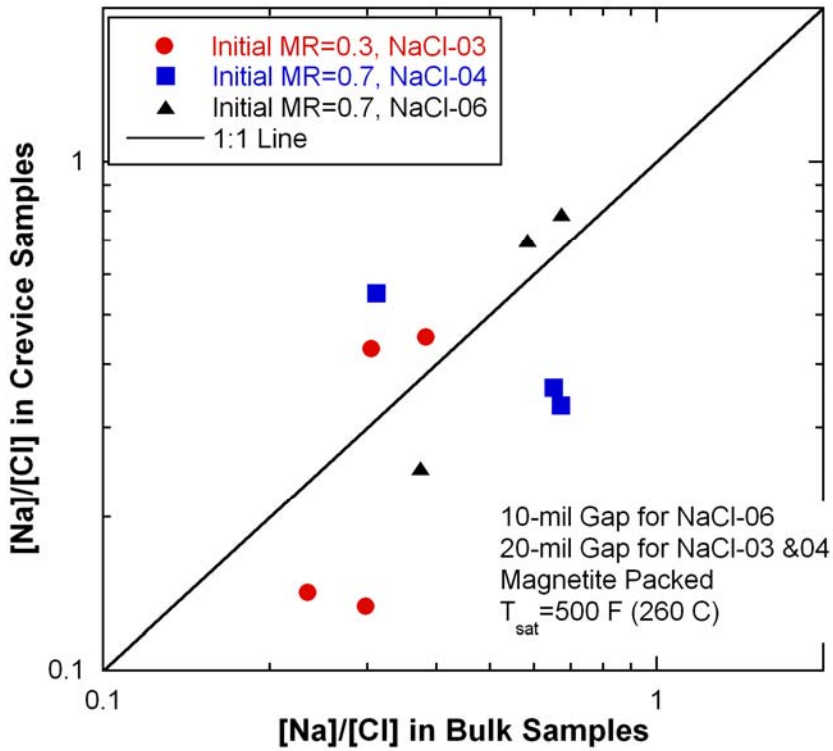


Figure 183.
Molar ratio in crevice sample as a function of the molar ratio in the bulk sample for a magnetite-packed crevice.

6.3.5 Cl Adsorption to Magnetite

The Cl adsorption to magnetite was not likely to be verified experimentally through the MB crevice tests. However, the initial bulk conductivity reduction in the magnetite-packed crevice tests indicates the possibility of Cl adsorption to magnetite. Figure 184 shows the normalized bulk conductivity variation with time from the beginning of each test for $\Delta T=40^\circ\text{F}$. All test results for a magnetite-packed crevice showed rapid reductions of bulk conductivity for 1-2 hours from the beginning of the test. Then, the rate of reduction in bulk conductivity became smaller until they were nearly constant. The bulk conductivity data for the diamond-packed crevice tests did not exhibit this behavior. The hideout rate mainly depends on the heat flux and the total area where nucleate boiling can occur. At the given crevice physical and thermal conditions, the hideout rate will not change until it becomes close to the saturation limit. Therefore, the initial rapid reduction in bulk conductivity suggests a different hideout mechanism for the magnetite-packed crevices. The Cl adsorption to magnetite can be considered as a driving force for impurity hideout at the beginning of a test. This factor becomes less significant with time because the available adsorption sites are limited under a given magnetite-packing condition.

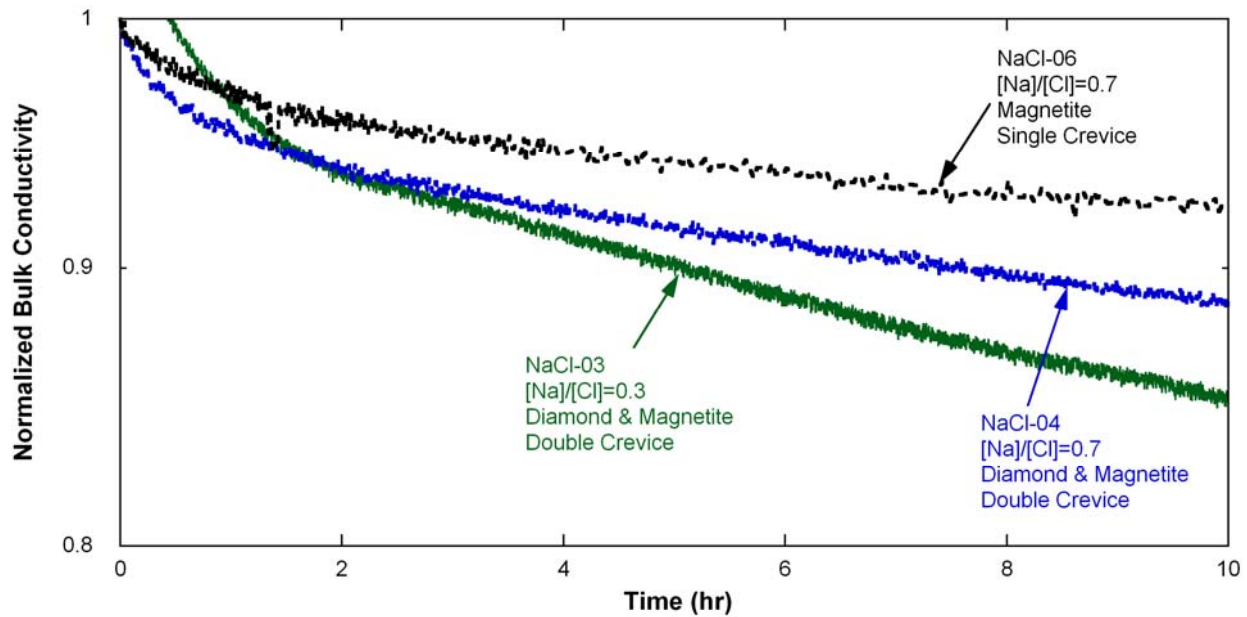


Figure 184. Normalized bulk conductivity variations with time (hr) from the beginning of each test at $\Delta T=40^\circ\text{F}$.

6.3.6 Electromigration Effect in the Crevice

Electromigration refers to ion movement due to a difference in electrical potential. The mass transport in solution usually depends on convection and diffusion. If the solution has a charge, electromigration is possible. In a heated crevice where boiling occurs, there are liquid and steam phases. The dissolved oxygen level is very low. Therefore, electromigration is not likely to be a dominant factor for impurity transport. However, electromigration was experimentally observed for some crevice tests. Electromigration requires an electric potential gradient between the crevice and bulk solution. Under a deaerated condition, if metal cations are dissolved in the crevice as a result of tube corrosion or magnetite dissolution, the electric potential in the crevice becomes higher than that in the bulk solution, and this condition drives Cl ions into and Na ions out of the crevice. In the NaCl-03 test, at $\Delta T=60^\circ\text{F}$ the bulk

conductivity increased slightly when the bulk Na concentration increased and Cl concentration remained almost constant, as shown in Figure 53. In the NaCl-05 test at the same ΔT , the bulk conductivity did not vary significantly but the Na concentration increased and the Cl concentration decreased in the bulk solution, as shown in Figure 117. The post-test examinations for the two tests indicated heavy gouging of the tubing. The two test results appear to prove that electromigration occurred in the diamond-packed crevice. Whether electromigration occurred in the magnetite-packed crevice is not clear from our test results. The tube surfaces after NaCl-06 did not show any gouging, and it is uncertain whether metal cations might have come from the dissolution of the magnetite packing materials. Electromigration in a magnetite-packed crevice, if it will happen, appears to take a long time because the impurity hideout rate is very low. Furthermore, it takes time to reach an impurity level that can generate tube corrosion. In an actual SG crevice packed with deposits, as discussed in Section 6.3.3, the crevice pH would be alkaline or neutral during a typical fuel cycle. In an actual SG crevice, one fuel cycle is not long enough for tube corrosion and electromigration to occur. Also, the high packing density of the actual crevice will hinder the movement of ions. However, if some of impurities remain in the crevice after each fuel cycle, tube corrosion and electromigration may occur after several fuel cycles.

6.3.7 Hard Scales Formed on the Tube Surfaces

Black and hard magnetite deposits were observed on the tube surfaces in the crevice region during several crevice tests: NaOH-03 and NaCl-05 packed with diamond and NaCl-06 packed with magnetite. In the NaOH-03 test, black deposits were found mainly near the crevice mouth region, as shown in Figure 102. Similar black deposits were also found in the NaCl-05 test at similar locations, as shown in Figure 123. At the crevice mouth region, mixing between the crevice and bulk solution is active so that concentration of the impurities will be relatively low, and the resultant chemical condition such as pH will not be severe, near to a neutral condition. Therefore, magnetite solubility is expected to be low, and this low solubility makes it easy for magnetite deposits to be formed in that area. Deeper into the crevice, the impurities are further concentrated, and the resultant crevice pH becomes corrosive. Consequently, tube corrosion occurs so that the black deposits are not likely to be formed.

In the NaCl-06 test, black deposits were also formed in the crevice mouth area, as shown in Figure 152. Since the magnetite particles filled the crevice, the hard magnetite deposits appear to form and consolidate easier than for the two tests packed with diamond powders. In an actual SG, the bulk Fe concentration is roughly estimated as 1 ppb, and the total operation time for one cycle is roughly 10^4 hours. Therefore, the total Fe exposure is 10 ppm-hr. The bulk Fe concentration in the NaCl-06 test was within the range of 0.5-1.0 ppm, and the total test time was 700 hours. The total test times of NaOH-03 and NaCl-05 tests were 400 and 700 hours, respectively. If the bulk Fe concentration of the three tests were within the same range, the estimated total Fe exposure of our tests would be 200-700 ppm-hr, which is equivalent to at least 20 fuel cycles for an actual SG. Since we do not know when the deposits actually started to form during the MB tests, the deposits in actual SGs are expected to form earlier than 20 cycles.

7. Summary

7.1 Conclusions

At Argonne National Laboratory, a MB system that can simulate prototypical thermal hydraulic and chemistry conditions of the secondary side of SGs in PWRs was developed. The facility has prototypic crevice heat fluxes and temperatures thus permitting the development of more prototypic crevice chemistry conditions. A crevice simulator equipped with various instrumentations, including thermocouples, ECP electrodes, pH electrodes, conductivity probes, and solution sampling lines, was developed and successfully operated. To measure the pH in the bulk solution and crevice, we used a tungsten/tungsten oxide (W/WO_x) electrode. The W/WO_x electrode served as a pH electrode in the pH range of 4-8 under NaCl or NaOH water chemistry. The potential slope with respect to pH variation was -103 mV/pH, which is close to the Nernstian slope of -106 mV/pH at 260°C (500°F). The behavior of the W/WO_x electrode was consistent with that reported in earlier work²⁹.

We reached the following conclusions from the MB test results:

- ◆ Diamond powder has a very high thermal conductivity as compared with magnetite powder, which can enhance the boiling rate and lead to higher impurity hideout rates. High permeability of diamond packing allows active mixing inside the crevice and the liquid and steam phases can transport easily in and out of the crevice. In some tests, the diamond-packed crevice concentration did not reach the thermodynamic limit, while in the magnetite-packed crevice the concentration was thermodynamically limited under the same thermal conditions. To simulate actual SG crevices, a magnetite-packed crevice having a lower permeability is more appropriate than a diamond-packed crevice, since a diamond-packed crevice can lead to an overestimate of the crevice hideout rate.
- ◆ In a magnetite-packed crevice test (NaCl-06), bulk sample analyses indicated that Na was preferentially concentrated until it reached the thermodynamic limit at a given ΔT , followed by delayed Cl preferential concentration. The W/WO_x electrode installed near the tube wall supported the observations of these Na and Cl concentrations and also the W/WO_x electrodes indicated the radial chemistry gradients in the magnetite-packed crevice, which is consistent with literature information³.
- ◆ Based on the hideout rates for Na and Cl in the magnetite-packed crevice (NaCl-06), the chemistry variation in the deposits in an actual SG crevice near the tube wall was estimated. During a typical fuel cycle, the crevice chemistry was in a transient rather than a steady-state condition, mainly because of the low impurity concentration in the bulk solution. The estimated average crevice pH was always alkaline because of the initial preferential Na concentration unless some impurities remain and accumulate in the crevice after each fuel cycle. The kinetic data for the crevice hideout with low bulk impurity concentration are helpful for estimating the actual variations in SG crevice chemistry.
- ◆ Based on the analyses of the crevice and bulk solution samples at a saturated state, the volatility effect of Cl for the diamond-packed crevices becomes significant as the MR decreases. For the magnetite-packed crevice, available data are limited, but it is likely that the volatility effect of Cl at a saturated state is not as significant as it is for the diamond-packed crevice and it is not dependent on the bulk MR variation.
- ◆ The Cl adsorption onto magnetite was not verified through our current series of tests. However, the reduction in bulk conductivity from the initial value in the magnetite-packed crevice tests indicates possible Cl adsorption to magnetite.
- ◆ Electromigration in the crevice was observed especially when the tube corrosion was severe

under strongly acidic crevice chemistry. But in an actual SG crevice, electromigration in the packed crevice is not likely because bulk impurity concentration is very low and one fuel cycle (about 10^4 hr) is not long enough for tubes to corrode to the point that it results in electromigration unless some impurities remain in the crevice after each fuel cycle and accumulate over several fuel cycles.

- ◆ The crevice pH predicted by the MULTEQ[®] code was compared with the measured crevice pH as a function of boiling point elevation. The test results in diamond-packed crevices followed the “steam retained” option. In a magnetite-packed crevice, the measured pH at steady state was lower than that in the diamond-packed crevice and deviated from the “steam retained” option. In a less permeable crevice, the volatility of Cl becomes less significant because Cl does not easily escape. This condition led to a lowering of the crevice pH near the tube wall. However, since the transient behavior is more important in actual SG crevice deposits, the calculations with a thermodynamic equilibrium code have limited applicability.
- ◆ The MB tests showed some initial evidence that once a crack is formed, the crack itself can act as a crevice. In the NaOH bulk chemistry, this crack can grow even if the sludge or debris is cleaned out of the SG. It would be valuable to confirm whether the crack itself can act as a crevice in other bulk water chemistry regimes such as a NaCl chemistry regime.

7.2 Future Work

From the current test results and analyses, the following additional investigations may provide a better understanding of SG heated crevices:

- ◆ Conduct MB experiments to determine whether a 50 % through-wall crack would grow in the absence of any crevice or packing under NaOH or NaCl bulk water chemistry.
- ◆ Further evaluate the permeability effect on the crevice hideout kinetics in magnetite-packed crevice tests with a lower packing porosity. Considering the porosity of actual SG crevice deposits, a porosity of less than 50 % is required.
- ◆ Conduct MB hideout tests with magnetite-packed crevice and MR=0.3 and 1.0 for comparison with the MR=0.7 test results. From these tests, the molar ratio effect on the crevice hideout behavior in the magnetite-packed crevice can be further explored.
- ◆ Perform MB tests with low impurity concentration in the bulk solution. The impurity level in the secondary water of an actual SG is in the ppb range. Since the total impurity exposures of Na and Cl during one fuel cycle are around 100 ppm-hr, tests having 1-ppm bulk impurity may be appropriate. However, the volatility effect of Cl tends to become significant as the Cl concentration becomes low. Therefore, theoretical modeling should be considered for extrapolating the MB test results to actual SG crevices.
- ◆ Explore the complex solution chemistry involved with sodium, chloride, and sulfate. Sulfate is another major impurity in the secondary water of SGs. Since the concentration of sulfate is likely to be affected by adsorption onto magnetite powder, the magnetite-packed crevice tests with sulfate water chemistry should be considered.

8 References

1. D. R. Diercks, W. J. Shack, and J. Muscara, "Overview of Steam Generator Tube Degradation and Integrity Issues," Nucl. Eng. Design, 194: 19-30, 1999.
2. G. M. W. Mann and R. Castle, "Hideout and Return of Chloride Salts in Heated Crevices Prototypic of Support Plates in Steam Generators," EPRI NP-5015, Electric Power Research Institute, January 1987. Copyright permission is granted by EPRI.
3. Allen Baum, "Experimental Evaluation of Tube Support Plate Crevice Chemistry," Proc. 10th Int. Conf. Environmental Degradation of Materials in Nuclear Power Systems-Water Reactors, National Association of Corrosion Engineers, 2002.
4. L. Albertin et al., "Characterization of Deposits in Dampierre-1 Steam Generator Support Plate Crevices," Proc. 7th Int. Symp. Environmental Degradation of Materials in Nuclear Power Systems-Water Reactors, Breckenridge, Colorado, National Association of Corrosion Engineers, pp. 399-409, 1995.
5. A. Baum and K. Evans, "Modeling Concentrated Solution Transport and Accumulation in Steam Generator Tube Support Plate Crevices," 12th Int. Conf. Environmental Degradation of Materials in Nuclear Power System-Water Reactors, Minerals, Metals & Materials Society, 2005. Copyright permission is granted by TMS.
6. A. J. Baum, "Restricted Geometries and Deposits," in *The ASME Handbook on Water Technology for Thermal Power Systems*, ed., P. Cohen, American Society of Mechanical Engineers, Chapter 6-3, 1989.
7. R. W. Staehle and J. A. Gorman, "Progress in Understanding and Mitigating Corrosion on the Secondary Side in PWR Steam Generators," Special Bonus Paper, Proc. 10th Int. Conf. Environmental Degradation of Materials in Nuclear Power Systems-Water Reactors, Lake Tahoe, Nevada, National Association of Corrosion Engineers, Aug. 5-9, 2001.
8. "Heated Crevice Seminar," NUREG/CP-0189, U.S. Nuclear Regulatory Commission, Washington D.C., February 2005.
9. R. E. Hermer, R. J. Jacko, A. Kishida, and H. Takamatsu, "The Measurement of Simulated Steam Generator Crevices," Proc. 3rd Int. Symp. Environmental Degradation of Materials in Nuclear Power Systems-Water Reactors, Traverse City, Michigan, Metallurgical Society, pp. 199-207, 1987.
10. Damien Feron, "Electrochemical Measurements in PWR Steam Generators to Follow Crevice Chemistry," Paper No. A-44, Proc. JAIF Int. Conf. Water Chemistry in Nuclear Power Plants, Fukui City, Japan, 1991.
11. A. M. Brennenstuhl, A. McBride, and D. Graham, "An Assessment of High Temperature Electrochemical Noise to Monitor the Effects of Chemical Excursions on the Corrosion Response of UNS N08800 Nuclear Steam Generator Tubes," Proc. 8th Int. Symp. Environmental Degradation of Materials in Nuclear Power Systems-Water Reactors, Amelia Island, FL, American Nuclear Society, pp. 3-10, 1997.

12. J. B. Lumsden, G. A. Pollock, P. J. Stocker, P. J. Millett, and C. Fauchon, "Hideout in Prototypic Tube/Tube Support Plate Heated Crevices," Proc. 8th Int. Symp. Environmental Degradation of Materials in Nuclear Power Systems-Water Reactors, Amelia Island, FL, American Nuclear Society, pp. 108-112, 1997.
13. J. B. Lumsden, G. A. Pollock, P. J. Millett, N. Torigoe, and H. Takamatsu, "Effects of the Feedwater Sodium/Chloride Ratio and Hydrazine on Crevice Chemistry," Proc. 9th Int. Symp. Environmental Degradation of Materials in Nuclear Power Systems-Water Reactors, Newport Beach, CA, Minerals, Metals, and Materials Society, August 1-5, 545-554, pp. 1999.
14. H. Kawamura and H. Hirano, "Estimation of Impurity Concentration Factor on Boiling Heat Transfer Surface within Tube-Tube Support Plate Crevice using Corrosion Potential Measurement Technique," Proc. Int. Conf. Water Chemistry in Nuclear Power Plants: Water Chemistry '98, JAIF, Kashiwazaki, Japan, pp. 546-553, October 1998.
15. H. Kawamura and H. Hirano, "Estimating the Impurity Concentration Factor on the Boiling Heat Transfer Surface of a Simulated Steam Generator Tube-Support-Plate Crevice Using an In Situ High-Temperature Conductivity Measurement Technique," Nucl. Tech. 129: 398-406, 2000.
16. A. Baum, "Relationships between Boiling Regimes and Chemical Concentration Processes in Tube Support Plate Crevices," Int. Conf. Water Chemistry in Nuclear Power Systems, SFEN, Avignon, France, April 2002.
17. P. V. Balakrishnan and G. L. Strati, "Laboratory Experiments on Steam Generator Crevice Chemistry," Heated Crevice Seminar, NUREG/CP-0189, U.S. Nuclear Regulatory Commission, Washington D.C., p. 319, February 2005.
18. C. B. Bahn, S. H. Oh, B. G. Park, I. S. Hwang, I. H. Rhee, U. C. Kim, and J. W. Na, "Impurity Concentration Behaviors in a Boiling Tubesheet Crevice: Part II. Packed Crevice," Nucl. Eng. Design, 225: 145-157, 2003.
19. P. J. Millett, "Theoretical and Experimental Investigation of Local Concentration Processes in PWR Steam Generators," Ph.D. Thesis, University of Connecticut, 1991.
20. P. J. Millett and J. M. Fenton, "A Modeling Study of Parameters Controlling Local Concentration Processes in Pressurized Water Reactor Steam Generators," Nucl. Tech. 108: 256-265, 1994.
21. G. R. Engelhardt and D. D. Macdonald, "Transport Processes in Steam Generator Crevices. I. General Corrosion Model," Corr. Sci. 41: 2165-2190, 1999.
22. G. R. Engelhardt, D. D. Macdonald, and P. J. Millett, "Transport Processes in Steam Generator Crevices. II. A Simplified Method for Estimating Impurity Accumulation Rates," Corr. Sci. 41: 2191-2211, 1999.
23. Céline L. Fauchon, "Development and Testing of an Electrochemical Model for PWR Steam Generators Crevice Environment," Master Thesis, Massachusetts Institute of Technology, February 2000.

24. "MULTEQ: Equilibrium of an Electrolytic Solution With Vapor-Liquid Partitioning," Volume 3, *Theory Manual*, EPRI NP-5561-CCML, Electric Power Research Institute, Palo Alto, CA, August 1992.
25. K. E. Kasza, J. J. Oras, B. L. Fisher, J. Y. Park, J. E. Franklin, and W. J. Shack, "Argonne Model Boiler Facility: Topical Report," NUREG/CR-6880, U.S. Nuclear Regulatory Commission, Washington D.C., 2005.
26. Gilbert W. Castellan, *Physical Chemistry*, 3rd Ed., Addison Wesley Publishing Company, Reading, MA, p. 378, 1983.
27. S. E. S. El Wakkad, H. A. Rizk, and I. G. Ebaid, "The Electrochemical behavior of the Tungsten Electrode and the Nature of the Different Oxides of the Metal," *J. Phys. Chem.* 59: 1004-1008, 1955.
28. L-A. Yao, F-X. Gan, Y-X. Zhao, C-L. Yao, and J. L. Bear, "Microelectrode Monitoring the Crevice Corrosion of Titanium," *Corrosion* 47(6): 420-423, 1991.
29. L. B. Kriksunov, D. D. Macdonald, and P. J. Millett, "Tungsten/Tungsten Oxide pH Sensing Electrode for High Temperature Aqueous Environments," *J. Electrochem. Soc.* 141(11): 3002-3005, 1994.
30. D. D. Macdonald, A. C. Scott, and P. Wentreck, "External Reference Electrodes for Use in High Temperature Aqueous Systems," *J. Electrochem. Soc.* 126(6): 908-911, 1979.
31. M. J. Danielson, "A Long-Lived External Ag/AgCl Reference Electrode for Use in High Temperature/Pressure Environments," *Corrosion* 39(5): 202-203, 1983.
32. Gilbert W. Castellan, *Physical Chemistry*, 3rd Ed., Addison Wesley Publishing Company, Reading, MA, pp. 770-773, 1983.
33. S. Bakhtiari, K. E. Kasza, D. S. Kupperman, S. Majumdar, J. Y. Park, W. J. Shack, and D. R. Diercks, "Second U.S. Nuclear Regulatory Commission International Steam Generator Tube Integrity Research Program Final Project Summary Report," NUREG/CR-6804, U.S. Nuclear Regulatory Commission, Washington, D.C., 2003.
34. *CRC Handbook of Chemistry and Physics*, ed., David R. Lide, 83rd Ed., CRC Press, Boca Raton, LA, 2002.
35. J. Molgaard and W. W. Smeltzer, "Thermal Conductivity of Magnetite and Hematite," *J. Appl. Phys.* 42(9): 3644-3647, 1971.
36. James F. Shackelford, *Introduction to Materials Science for Engineering*, 5th Ed., Prentice Hall, New Jersey, p.65, 2000.
37. "PWR Secondary Water Chemistry Guidelines," Revision 5, TR-102134-R5, Electric Power Research Institute, Palo Alto, CA, p. 2-21, May 2000.
38. A. S. Quist and W. L. Marshall, "Assignment of Limiting Equivalent Conductances for Single Ions to 400°C," *J. Phys. Chem.* 69(9): 2984-2987, 1965.

39. A. Baum, "Limits to Crevice Concentration Processes," Heated Crevice Seminar, NUREG/CP-0189, U.S. Nuclear Regulatory Commission, Washington D.C., pp. 203-240, February 2005.
40. M. N. Panda and L. W. Lake, "Estimation of Single-Phase Permeability from the Parameters of a Particle-Size Distribution," AAPG Bulletin 78(7): 1028-1039, 1994.
41. J. Lumsden, "Heated Crevice-Design, Experimental Methods, and Data Interpretation," in Heated Crevice Seminar, NUREG/CP-0189, U.S. Nuclear Regulatory Commission, Washington D.C., pp. 98-136, February 2005.

Appendix A: Preliminary Crevice Test with NaOH Bulk Chemistries

A.1 Packed Crevice Test: NaOH-01

Packed crevice tests were conducted for two crevice simulators with radial gap sizes of 10 and 20 mils, respectively. Each crevice was filled with synthetic diamond powders. The secondary bulk solution contained 11.5-ppm Na as NaOH, as was the case for the unpacked crevice test. The test solution was poured into the secondary chamber before heat-up. A high-pressure injection pump was not available at that time. More information for the crevice simulator and crevice/bulk instrumentations is given in Sections 2.2 and 2.3.

A.1.1 Test Results

Four initial series of tests were conducted. The primary/secondary temperature was maintained at 600/500 °F. The first test involved about 2 days of testing, after which the model boiler (MB) was shut down and allowed to cool over a weekend. The second test involved about 4.5 days of testing and was performed as a check on the reproducibility of the first test and the possibility of achieving increased concentration of the impurity with longer time. The third test extended for 14 days to explore the ultimate crevice concentration achievable and the influence of the micro-bore tube sampling procedures on the impurity concentration data. Also evaluated was the influence of upsetting a crevice by extracting large volumes of crevice contents and determining the time constant associated with re-establishment of crevice hideout. The fourth test involved, without interrupting the third test, raising the primary temperature from 316°C to 329°C (600°F to 625°F), as was done for the unpacked crevices, to determine if crevice hideout changes.

Test Series 1

Figure A1 shows the temperature variations with time in the 10-mil radial gap crevice as well as the primary water temperature (T_p). Thermocouple (TC) T3 shows more gradual temperature elevation than the others. The temperature elevations are dependent on the location of the thermocouples. Figure A2 shows the temperature variations in the 20-mil gap crevice. All thermocouples are close to the secondary saturation temperature of 500°F, except the TC labeled T6. Based on the post-test examination, the diamond packing in the 20-mil gap crevice had blown out during the test, which might explain the lower temperature in this crevice. For test series 1, a maximum Na concentration of 5930 ppm, corresponding to a hideout factor of 560, was observed in the 10-mil gap crevice. For the 20-mil gap crevice, the maximum Na concentration was 54 ppm, corresponding to a hideout factor of 5. The MB was shut down and cooled during the weekend. This 2-day test appeared to be too short to evaluate the steady-state concentration in the crevice. Without opening the MB, test series 2 was conducted under the same test conditions.

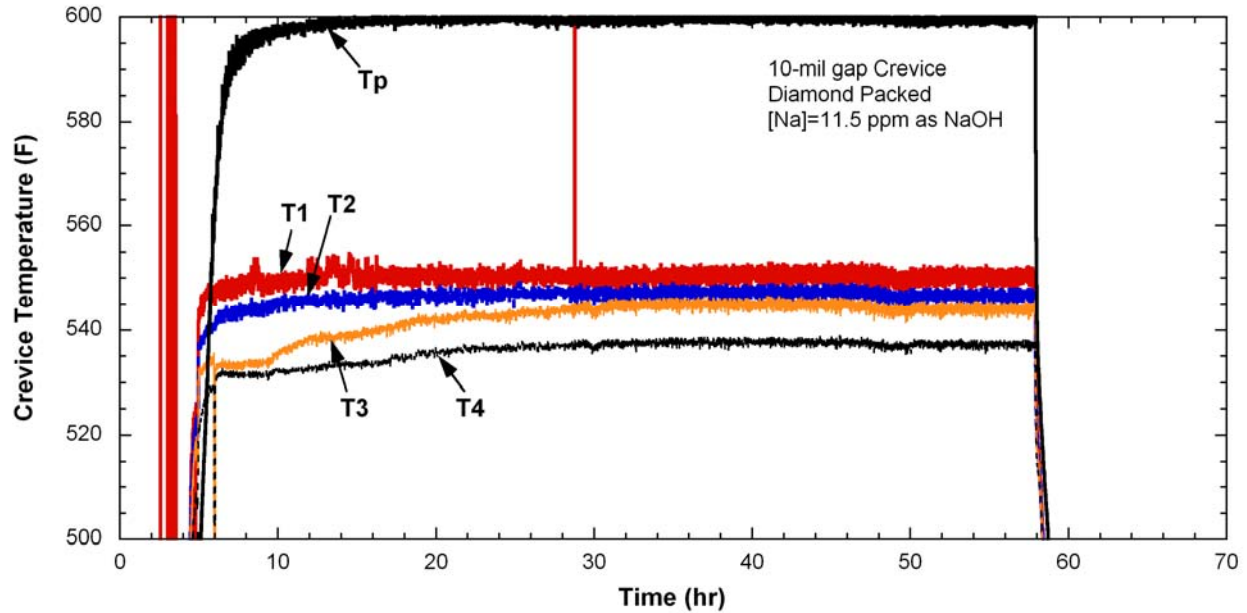


Figure A1. Primary water ($T_p=600^{\circ}\text{F}$) and crevice temperature variations with time in 10-mil gap crevice packed with diamond powder during series 1 of NaOH-01 test.

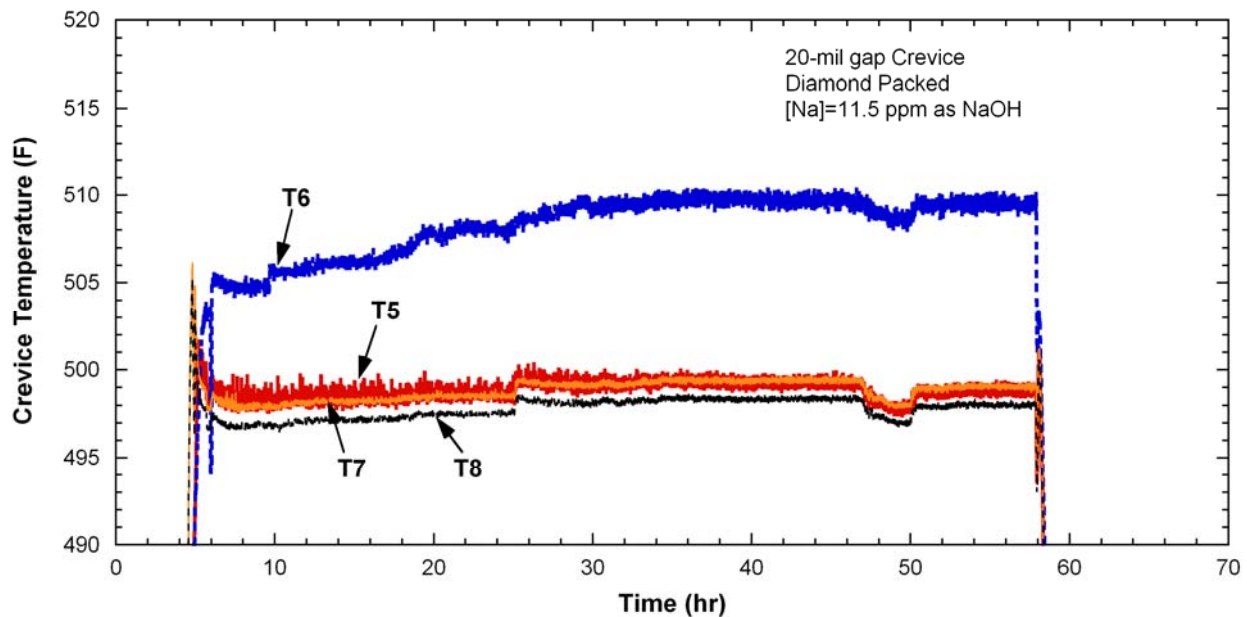


Figure A2. Crevice temperature variations with time in 20-mil gap crevice packed with diamond powder during series 1 of NaOH-01 test.

Test Series 2

Figure A3 shows the crevice temperature variation with time in the 10-mil radial gap crevice. Substantial crevice superheating was observed, in marked contrast to the unpacked crevice of the same gap. As compared with the series 1 results shown in Figure A1, the temperatures did not undergo gradual elevation after the stabilization of the primary water temperature, which might be an effect of the series 1

test. The maximum stabilized temperatures varied from 279°C to 287°C (534°F to 549°F), depending on the TC location. These temperatures are 19°C to 27°C (34°F to 49°F) higher than the secondary bulk temperature of 260°C (500°F). Figure A4 shows the temperature variations with time in the 20-mil gap crevice. As observed in the series 1 test shown in Figure A2, temperatures did not undergo significant elevation.

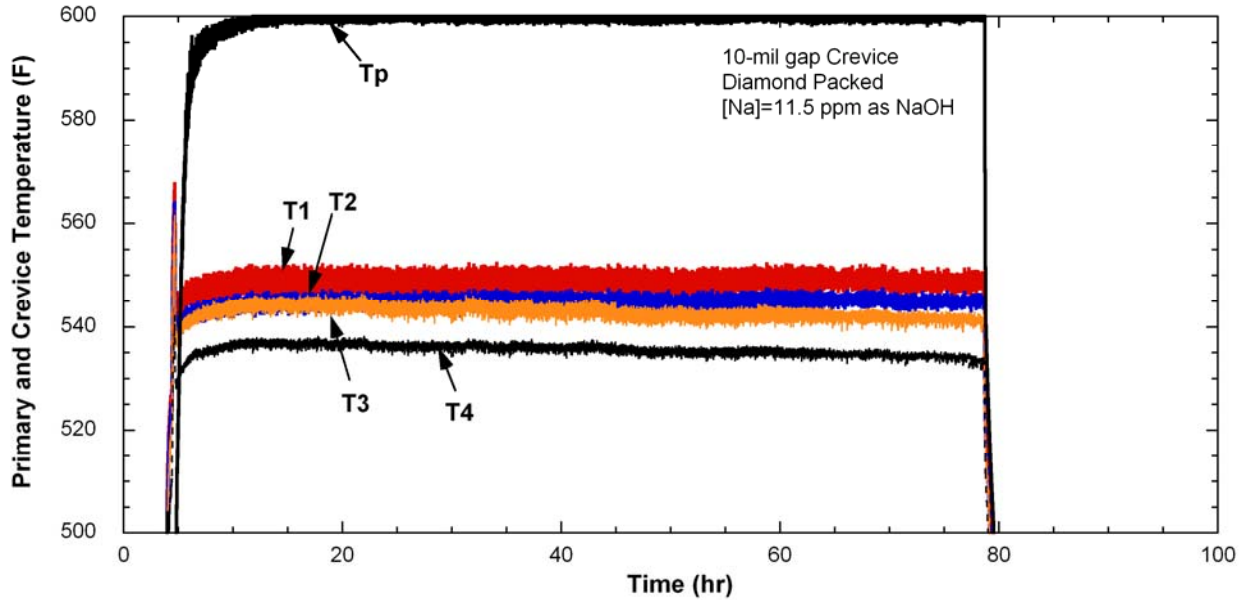


Figure A3. Primary water and crevice temperature variations with time in the 10-mil gap crevice packed with diamond powder during series 2 of NaOH-01 test.

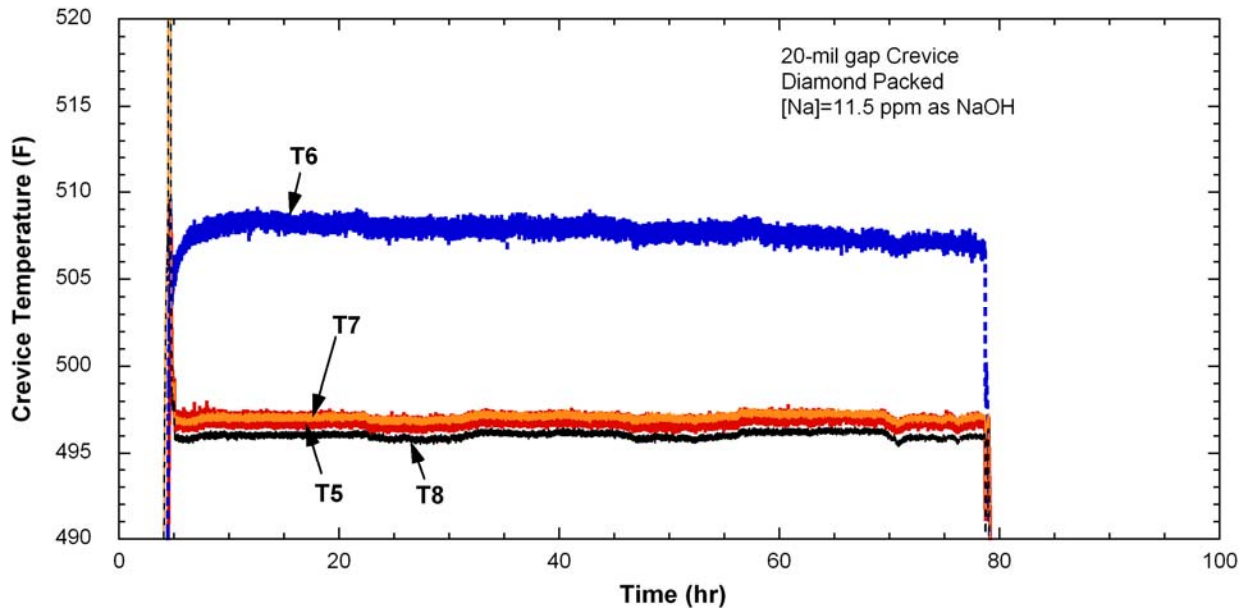


Figure A4. Crevice temperature variations with time in the 20-mil gap crevice packed with diamond powder during series 2 of NaOH-01 test.

For this longer duration test under the same conditions as test series 1, the maximum Na concentrations were 67,700 ppm (concentration factor of 8,600) and 31 ppm (concentration factor of 4) in

the crevices in the 10-mil and 20-mil radial gap, respectively. The increased concentration for the test series 2 appears to be due to the micro-bore extraction tube/valve volumes resulting in a time-delay effect. The calculated internal volume of the micro-bore extraction tubing is about 70 μL . The dead volume of the valve could not be evaluated but should be less than that of the extraction tubing. Assuming that the sampling volume is roughly 50 μL , at least three samples are needed to obtain the actual crevice solution. Since only three samples were taken in the test series 1, the third sample could represent only the beginning stage of the crevice concentration, which led to such a lower Na concentration. With the longer running time and the more frequent sampling of test series 2, we achieved truer indications of maximum hideout. By taking into account the extraction line volume, we are able to better understand the time delay observed in the sampling results compared with the temperature data. As described in the next section, the post-test examination revealed that the diamond powder in the 20-mil gap crevice had been blown out during the test. This result explains the low Na concentration observed in this crevice.

The crevice hideout estimated by the MULTEQ code predicts a maximum Na concentration factor of 45,000 and pH of 11.07, with a neutral pH of 4.88 at the maximum available superheat of 100°F. The estimated concentration factor at the observed maximum superheat of 49°F is 43,000. The maximum concentration factor of 8,600 is less than the MULTEQ predicted value by a factor of five. This discrepancy might be due to significant dilution during the sampling by mixing with secondary water. The samples for the 10-mil crevice were tinted brown. This tinting may indicate dissolved metallic ions, e.g., ferric or ferrous ions or some other species. The ICP/OES analysis confirmed 15-40 ppm Fe in the samples.

Test Series 3 and 4

Figure A5 shows the temperature variations with time in the 10-mil gap crevice. The two thermocouples (T1 and T2) did not work properly presumably because of the thermocouple tip's corrosion in NaOH solution. The crevice temperatures (T3 and T4) did not vary significantly with time except for the period of 20-60 hours. During this period, crevice upset testing caused the temperature fluctuation. Micro-bore tubing crevice extraction was performed to intentionally upset the hideout of the 10-mil gap crevice. An extraction rate of one drop every three seconds had less significant influence on crevice superheat, but a rate of one drop per second caused a significant fluctuation of the crevice temperature at the thermocouple nearest the micro-bore tube (thermocouple T4). With the cessation of crevice extraction, the superheat returned to the initial undisturbed value. Figure A6 shows the temperature variations in the 20-mil gap crevice. The temperature behaviors are almost the same as in the series 2 test shown in Figure A4.

Series 4 involved raising the primary temperature from 315°C to 329°C (600°F to 625°F), as was done for the unpacked crevices, without interrupting the long-term test of series 3. The increased temperature difference between the primary and secondary chambers caused the superheat in the 10-mil gap crevice to increase up to 7-10 °F, as shown in Figure A5. The temperature changes in the 20-mil gap crevice were minor, as shown in Figure A6.

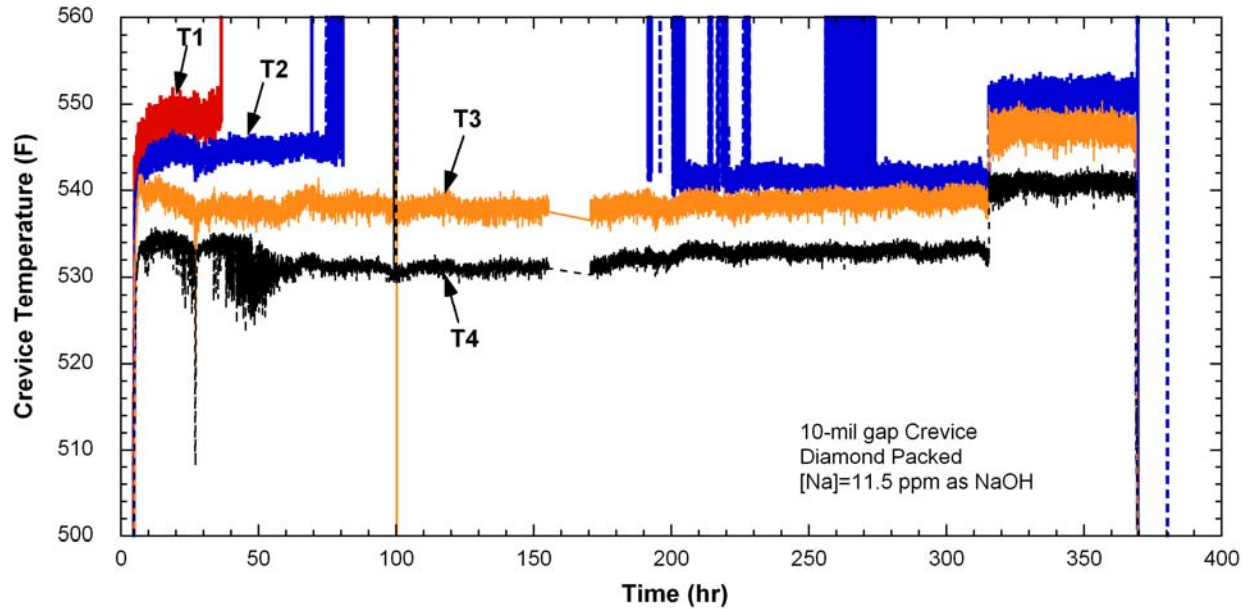


Figure A5. Crevice temperature variation with time in the 10-mil gap crevice packed with diamond powder during series 3 and 4 of NaOH-01 test.

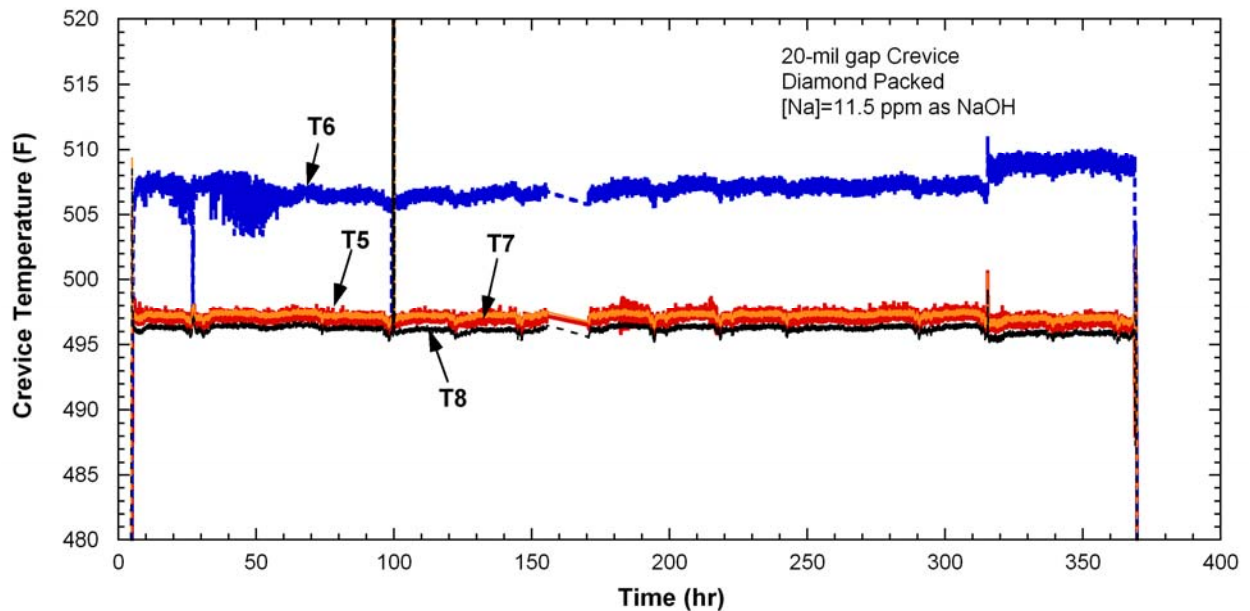


Figure A6. Crevice temperature variation with time in the 20-mil gap crevice packed with diamond powder during series 3 and 4 of NaOH-01 test.

A.1.2 Post-Test Examination

Post-test examination revealed that most of the diamond packing in the 20-mil radial gap crevice had been blown out because of a tear in the nickel foam placed over the crevice entrance. Figures A7 and A8 show the torn nickel foam membrane on the 20-mil gap crevice and the absence of diamond packing

in the crevice, respectively. As evident in Figures A9 and A10 for the 10-mil gap crevice, the nickel foam membrane is intact, and the crevice retains its packing. This finding explains why substantial crevice superheating, approaching 27°C (49°F), was observed in the 10-mil crevice, while only minor superheat occurred in the 20-mil crevice, similar to our previous result for an unpacked crevice of the same radial gap size.



Figure A7.
Photograph of torn nickel membrane on the 20-mil gap crevice and the absence of diamond packing in the crevice.



Figure A8.
Photograph of 20-mil gap crevice and the absence of diamond packing in the crevice.



Figure A9.
Photograph of 10-mil gap
crevice with intact nickel
membrane.

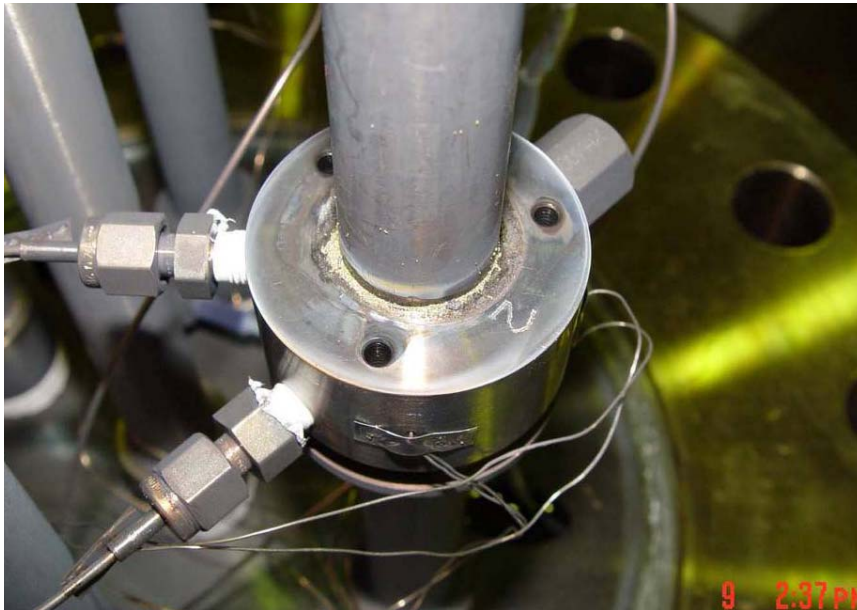


Figure A10.
Photograph of 10-mil gap
crevice with diamond packing.

The inspection of the two steam generator (SG) tubes showed that the outer tube wall in the vicinity of the 10-mil gap crevice had undergone considerable gouging at the end of the NaOH-01 test, as shown in Figure A11. This crevice exhibited a NaOH hideout factor approaching 8,600, and the total time under these conditions was 490 hours. Considering the intergranular attack (IGA) growth rate of alloy 600 MA at a crevice pH of 11 and temperature of 315°C (599°F),¹ the estimated IGA attack depth during the 490-hour exposure is around 25 μm (1 mil), which is comparable to the observation results in Figure A11. No gouging/pitting occurred on the larger 20-mil gap crevice, where the hideout factor was only 5. These same SG tubes and crevices were used in the NaOH-02 test.



Figure A11.
Photograph of gouging in
tube wall in the vicinity of the
10-mil gap crevice.

A.1.3 Summary

In summary, the first packed crevice test, NaOH-01, involved four phases. For the 10-mil radial gap crevice, the nickel membrane was intact and the crevice retained its packing. This crevice exhibited a NaOH hideout factor approaching 8,600. Inspection of the crevices revealed that most of the diamond packing in the 20-mil gap crevice was blown out because of a tear in the nickel foam membrane placed over the crevice exit. This occurrence explains why crevice superheating approaching 27°C (49°F) was observed in the 10-mil crevice, while only minor superheat occurred in the 20-mil gap crevice, similar to our previous result for an unpacked crevice of the same radial gap size. The inspection also showed that the outer tube wall in the 10-mil gap crevice region at the end of NaOH-01 had undergone considerable gouging. No gouging/pitting occurred on the 20-mil gap crevice, where the hideout factor was only 5, mainly because the packed diamond powder had been blown out of the crevice.

A.2 Packed Crevice Test: NaOH-02

A.2.1 Experimental Setup

With completion of the NaOH-01 test, the MB secondary chamber was opened, and the crevices were inspected and cleaned. The 10- and 20-mil gap crevices were repacked, and new nickel-foam grit retention membranes were installed. The 10-mil gap crevice was packed with 50:50 mixture of two mesh sizes of diamond grit (127-165 μm and 75-97 μm), the latter being smaller than that used in the NaOH-01 test in an attempt to achieve a higher packing fraction and further restrict the flow into and out of the crevice. The 20-mil gap crevice was packed with the same grit size (127-165 μm) as used in the NaOH-01 test to obtain data for this grit and crevice size that were not obtained previously because grit was blown out of the crevice through a faulty retention membrane. The estimated crevice porosity is 40 % and 29 %

for the 10- and 20-mil gap crevices, respectively. The larger gap crevice has the same porosity as the NaOH-01 test, but the porosity of the smaller gap crevice was larger even though mixed diamond powders were used.

A.2.2 Test Results

The NaOH-02 test was conducted under the same primary and secondary bulk temperatures and bulk chemistry as the NaOH-01 test. After two days of testing, with the MB achieving a stable thermal-hydraulic state and the two crevices both showing superheat above the bulk saturation temperature of 260°C (500°F), a test was conducted involving 30 min of steam purging from the secondary chamber. The purpose of the steam purging was to remove the possible buildup of hydrogen gas in the secondary chamber, which might have originated from the corrosion of internal metal surfaces, including the secondary chamber and alloy 600 tubing, and to eliminate its influence on the electrochemical potential (ECP) instrumentation. The steam was purged at a rate that ensured maximum nucleate-boiling heat transfer of the SG tube and steam condensation in the vertical finned heat rejection pipe. This purging had no measurable influence on the ECP instrumentation. Hence, the build-up of hydrogen gas in the secondary chamber and its effect appear to be negligible.

Figure A12 shows the temperature versus time in the 10-mil gap crevice. The temperature varied depending on the circumferential location. The temperature variations might have occurred because the thermocouples were located at different locations from the tube surface. Closer locations to the tube surface will show higher temperature. The smaller gap crevice showed nominally the same crevice superheat as the NaOH-01 test packed with the diamond powder of only one grit size (127-165 μm). Figure A13 shows the temperature variations in the 20-mil gap crevice. In the NaOH-01 test, recall that the diamond grit was blown from the 20-mil crevice through a torn nickel membrane and the crevice behaved like an unpacked crevice. In contrast, the 20-mil gap crevice in the NaOH-02 test retained the diamond packing and achieved superheats in the range of 0-20°F, depending on crevice location. The temperature oscillations shown in Figure A13 appear to indicate the active mixing of liquid and steam phases. As described in the next section, axial through-wall cracks were detected in the 10-mil gap crevice region. The temperature oscillations shown in Figure A12 are attributed to a primary-to-secondary leak through the cracks.

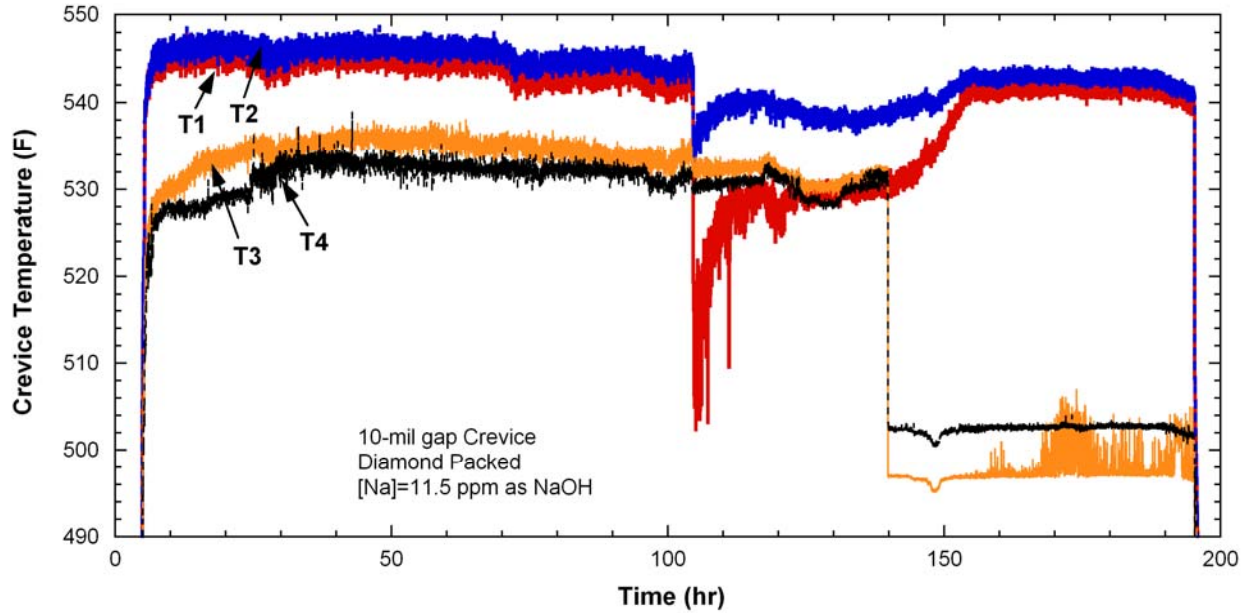


Figure A12. Crevice temperature variation with time in the 10-mil gap crevice packed with diamond powder for NaOH-02 test.

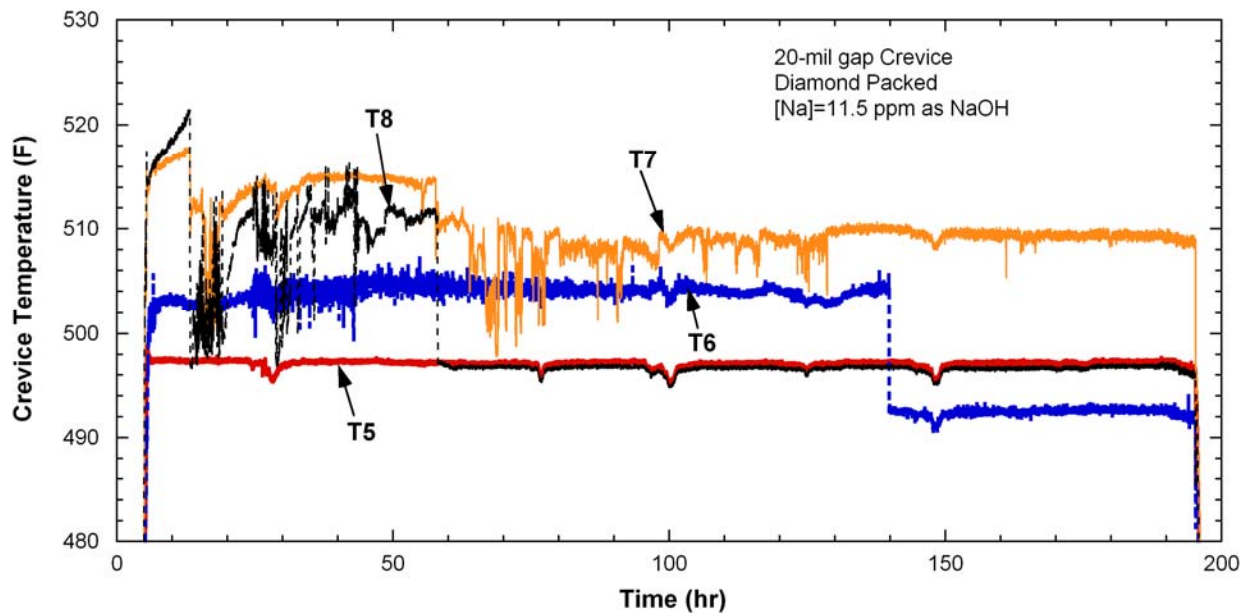


Figure A13. Crevice temperature variation with time in the 20-mil gap crevice packed with diamond powder for NaOH-02 test.

A large temperature drop occurred in the 10-mil gap crevice at about 100 hours, as shown in Figure A12. Another temperature drop occurred at 140 hours. The drastic temperature drops are attributed to the beginning of a leak from the through-wall cracks. Post-test examinations, as discussed in the next section, verified through-wall cracks in the crevice region. To accurately determine the time when the leakage started, the cooling fan speed and the resistances of the level sensors in the bulk water are plotted as a

function of time in Figure A14. The first small change of cooling fan speed was caused by the secondary-chamber purging test. The second change of fan speed occurred at the same time as the drastic temperature drop, at about 100 hours. Also, the resistance of the lower level sensor started to decrease at the same time. This decrease suggests the increase of bulk Na concentration caused by the leakage. The change in the upper level sensor readings indicated a leak from the primary side to the secondary chamber. The time of this event coincided with the time at which two of the 10-mil gap crevice thermocouples indicated the loss of superheat. After running the NaOH-02 test for 190 hours at 316°C (600°F) primary- and 260°C (500°F) secondary-side temperatures, the MB was shut down. After cooling, the secondary chamber was opened to find the source of the primary-to-secondary leak. The total accumulated exposure time of the cracked tubing over the two consecutive series of diamond-packed crevice testing, during which the crevice hideout factor reached 8,600, is 590 hours. The bulk secondary water for all these hours initially consisted of 11.5 ppm Na (20 ppm as NaOH) in deionized water, which decreased to 4.2 ppm due to the Na hideout in the crevices. Considering the stress corrosion crack (SCC) growth rate of alloy 600 MA under a crevice pH of 11 and temperature of 315°C (599°F),¹ we estimated the crack length during the 590-hour exposure to be about 67 mil, which is comparable to the tube wall thickness of 50 mil.

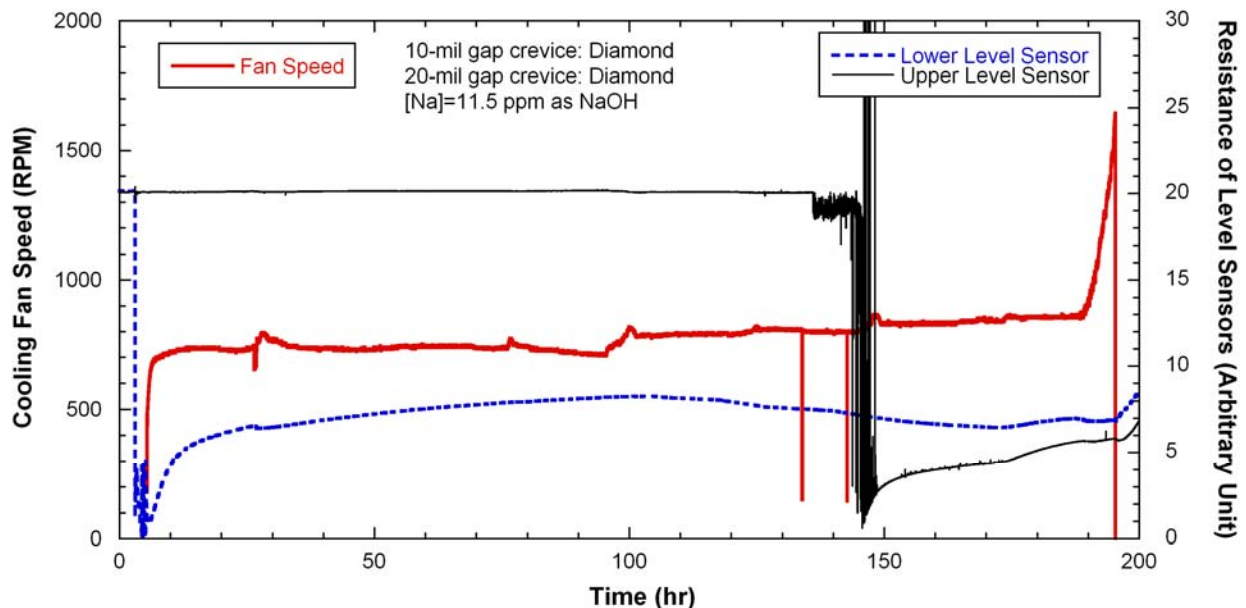


Figure A14. Cooling fan speed and resistance of lower and upper level sensors with time for NaOH-02 test.

A.2.3 Post-Test Examination

After opening the secondary chamber, we examined the two packed crevices prior to disassembly by filling the crevices with water and pressurizing the primary chamber to 4.8 MPa (700 psi) with nitrogen. The outlet of the 10-mil gap crevice exhibited repeated bubble release, as shown in Figure A15, indicating through-wall penetration. Under our primary and secondary chamber test temperatures of 316°C and 260°C (600°F and 500°F), respectively, the pressure differential across the tube was 5.7 MPa (827 psi).

The leaking tube was then removed from the MB, and a low-pressure nitrogen-gas bubble test was performed in a water bath. At 0.34 MPa (50 psi), bubbles were generated at several sites along a ≈ 10 -mm (0.4-in.) long axial SCC located in the bottom half of the crevice, as shown in Figure A16. No other leakage was seen. Because the flaw was very tight, we applied dye penetrant to allow it to be studied and photographed. As shown in Figure A17, the axial SCC flaw on the outside diameter (OD) is longer than 18 mm (0.71 in.).



Figure A15. Photo indicating repeated bubble generation and release at the crevice exit due to an SG SCC flaw in the packed-crevice region for 10-mil gap.



Figure A16. Low-pressure bubble test of MB crevice flaw at 0.34 MPa (50 psi) showing bubbles at several sites along an ≈ 10 -mm (0.4-in.)-long axial SCC located in the bottom half of the crevice.



Figure A17.
Crevice SCC flaw
photographed using dye
penetrant to enhance
visualization. The flaw is
longer than 18 mm (0.71
in.).

A.2.4 Eddy-Current Examination of Cracked Tube

After photographing the flaw, we initiated eddy-current non-destructive examinations to permit further characterization of the tube crevice region. A +Point coil operating at 300 kHz was used to profile the cracks. Standard industry practice was used for all depth measurements. An electro-discharged machine notched reference tube (18 notches) was used for calibration. Figure A18 shows the +Point c-scan for the tube. Four prominent cracks (numbered 1-4) are visible, all axial ODS-SCC. The maximum +Point voltage for these four cracks was about 6 V.

The profile for each crack was established by determining the eddy current depth at intervals along the crack. The depth profiles for the four SCC flaws are shown in Figure A19 through A22. Flaws MB1-1 and MB1-3 are located in the crevice ring-simulator region, and flaws MB1-2 and MB1-4 are located immediately below this region under the Swagelok cone and ring fittings used to seal the bottom of the crevice, as shown in Figure A16. The crevice hideout region produced by the Swagelok fittings is formed by the line contact associated with the fittings and the tube, resulting in a reduced flow region that hinders nucleate-boiling heat transfer. This hideout region has a different flow communication path with the bulk secondary path than the crevice formed by the crevice simulator ring. For MB1-2 and MB1-3, we could not clearly locate one end of the crack from the eddy-current signal. Any signal indicating an EC depth of 90% through-wall or greater is presumed to be a through-wall flaw location. The only crack that leaked during the low-pressure bubble tests and the only one that clearly showed at the tube OD under the initial dye penetrant exam is MB1-1, as shown in Figures A16 and A17. Table A1 shows the crack identifier, maximum +Point voltage, total length, and length where the crack is estimated to be through-wall for all four flaws. As will be discussed shortly, after pressurizing the tube to 8.3 MPa (1200 psi) for the purpose of leak testing, we could see all four cracks, but only MB1-1 exhibited an active leak.

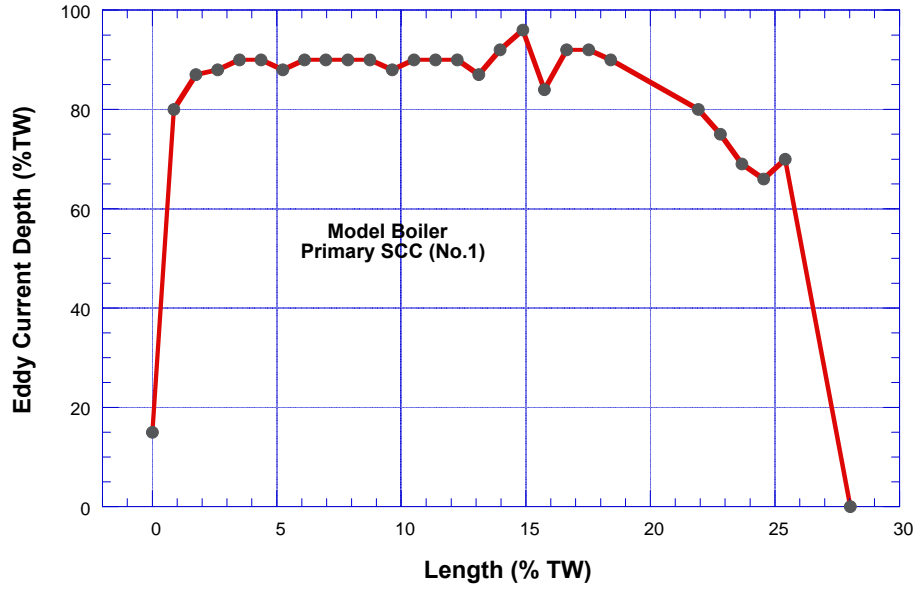


Figure A19.
Eddy current profile for the primary axial ODSCC MB1-1.

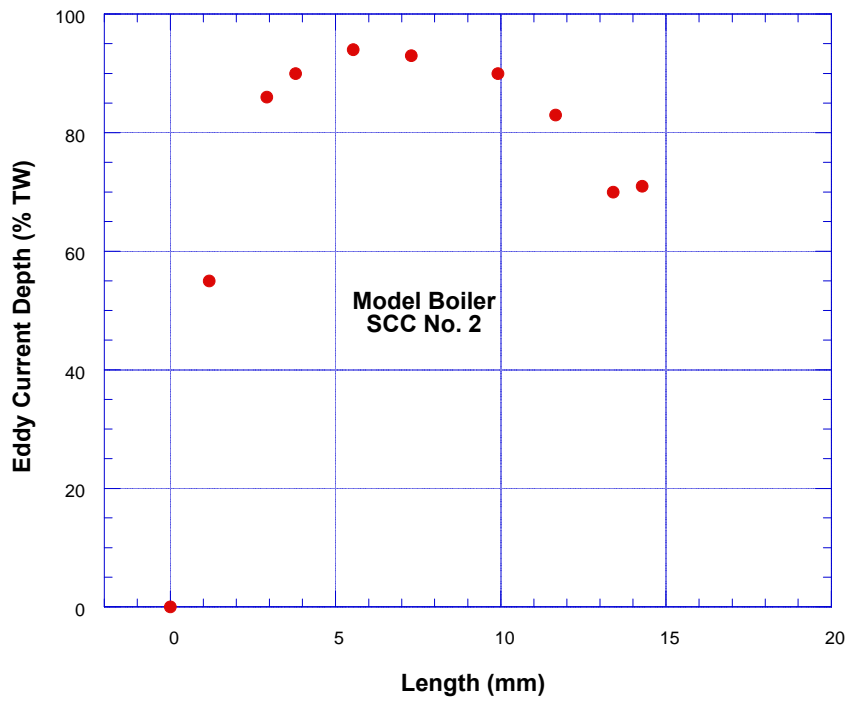


Figure A20.
Eddy current profile for the axial ODSCC MB1-2.

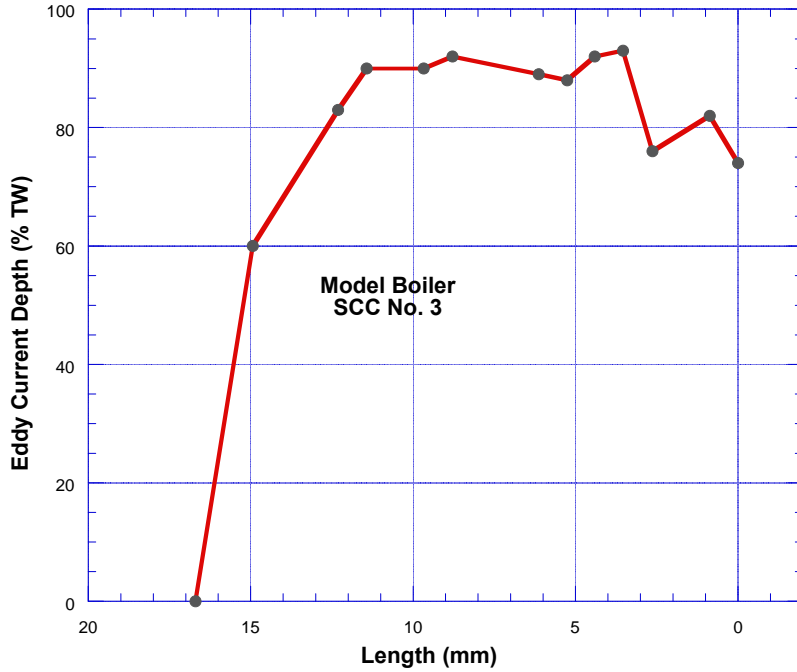


Figure A21.
Eddy current profile for the axial ODSCC MB1-3.

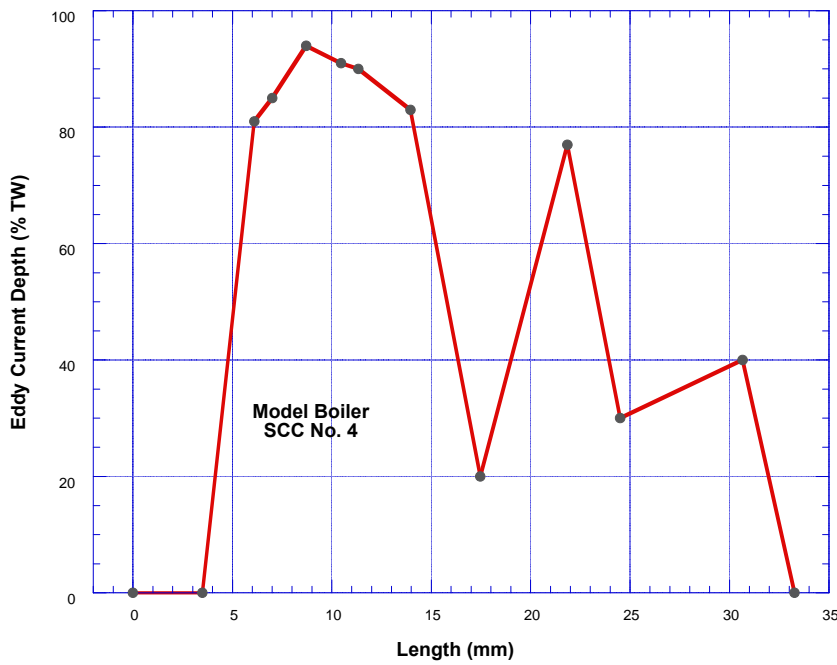


Figure A22.
Eddy current profile for the axial ODSCC MB1-4.

A.2.5 High-Pressure Leak Test for Cracked Tube

After the eddy-current examination, the flaws were heat tinted and subjected to a constant-pressure leak test at 8.3 MPa (1200 psi) in our Room-Temperature High-Pressure Leak Testing Facility.² The objective was to study the leak characteristics and determine if the flaw would exhibit time-dependent constant-pressure tearing. The leak testing was performed by increasing the flow in 1.0 MPa (150 psi)

increments from 0 to 8.3 MPa (0 to 1200 psi) with 2-3 minutes of hold at each intermediate plateau. At each plateau, we monitored the leak. The flaw zone MB1-1 showed no signs of leakage until a pressure of 3.1 MPa (450 psi). The leak was in the form of a single drop with no cyclic behavior. As stated above, our bubble immersion test with nitrogen gas at 0.34 MPa (50 psi) showed active bubble generations at several locations over about 10 mm (0.4 in.) of the OD crack length. At 5.2 MPa (750 psi), we saw drop formation from two distinct locations, one being MB1-1 and the other outside of the crack region highlighted by the bubble test. At 6.2 MPa (900 psi), active multiple jets were issuing from the 10-mm (0.4-in.) axial zone of flaw MB1-1. At 7.2 MPa (1050 psi), the jets became very strong. No other locations showed active jetting. An additional point of water droplet formation may have occurred in another region, but firm confirmation was not possible due to water spray inside the jet confinement tank.

The test pressure was then raised to 8.3 MPa (1200 psi), and the flow rate was measured as a function of time. After 15 min at this pressure, the leak rate was 1.69 kg/min (3.72 lb/min), and 10 min later the leak rate had increased to 2.08 kg/min (4.60 lb/min), which is quite a rapid increase. We stopped the leak test and photographed the leaking flaw as well as other regions of cracking suggested by the pretest eddy-current nondestructive evaluation. As shown in Figure A23, the main axial flaw labeled MB1-1 had widened and grown significantly compared with its pretest length shown in Figures A16 and A17. Figure A24 to Figure A26 show the three additional ODSCC flaw areas on the tube, namely, MB1-2, MB1-3, and MB1-4. The photographic images of the flaws at the OD after leak testing agree well with the flaw locations determined by eddy current techniques, though these flaws did not produce active jets. Flaws 1 and 3 were in the crevice simulator ring region, and flaws 2 and 4 were in the zone of the Swagelok fittings that seal the crevice at the bottom of the crevice simulator ring.

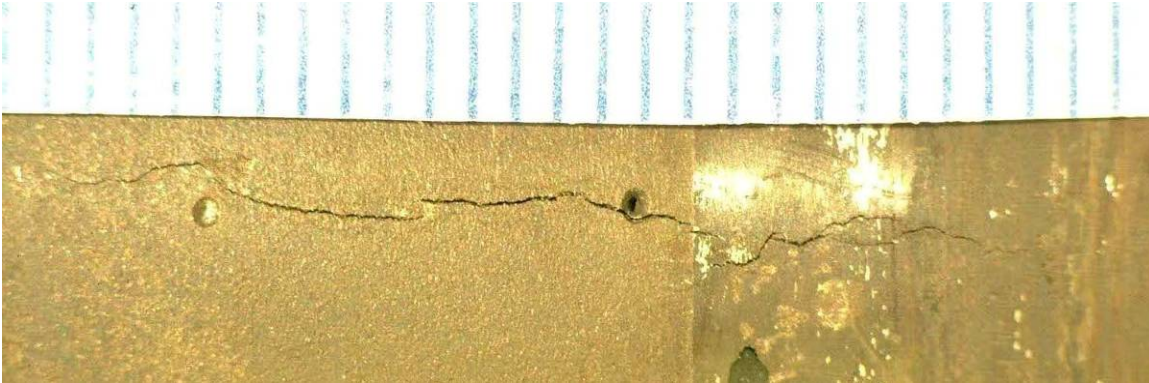


Figure A23. Photograph of crevice SCC OD flaw MB1-1 after leak testing at 8.3 MPa (1200 psi).

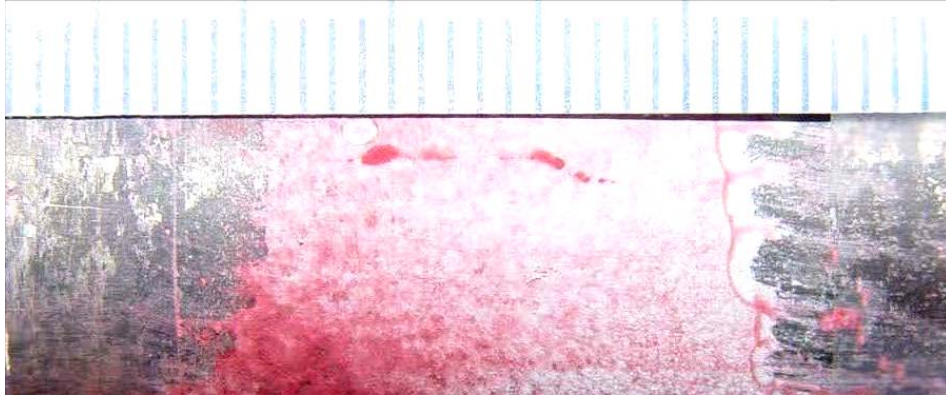


Figure A24. Photograph of crevice SCC OD flaw MB1-2 after leak testing at 8.3 MPa (1200 psi).



Figure A25. Photograph of crevice SCC OD flaw MB1-3 after leak testing at 8.3 MPa (1200 psi).

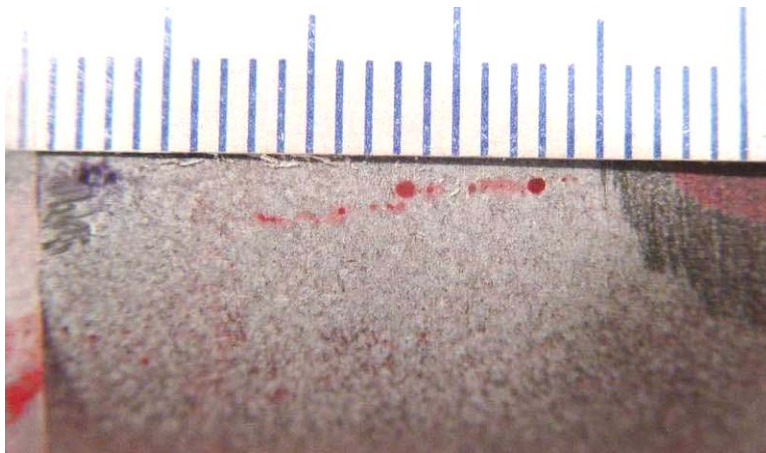


Figure A26. Photograph of MB crevice SCC OD flaw MB1-4 after leak testing at 8.3 MPa (1200 psi).

The MB appears to be a good facility for studying not only chemical hideout induced by prototypic SG-tube crevice heat transfer, but also, in a reasonable length of time, can be used to study the potential for cracking of tubes exposed to various chemicals under a variety of crevice geometry, thermal hydraulic, and tube material conditions. There is the possibility that, in the presence of corrosive chemicals concentrated by crevice hideout, the vigorous nucleate boiling at an SG tube outer surface accelerates the growth of SCC above that which takes place in the absence of heat transfer and nucleate boiling. The MB also allows us to grow SCC flaws in a prototypic heat transfer environment and further evaluate the potential for using eddy-current non-destructive examination to characterize the SCC.

References

1. "PWR Secondary Water Chemistry Guidelines-Revision 5," TR-102134-R5, Electric Power Research Institute, Palo Alto, CA, May 2000, p. 2-21.
2. K. Kasza, S. Majumdar, J. Park, and J. Franklin, "Results for Pressure and Leak-Rate Testing of Laboratory-Degraded Steam Generator Tubing," NUREG/CR-6789, U.S. Nuclear Regulatory Commission, Washington, D.C., 2002.

This page is intentionally left blank.

Appendix B: Mass Balance Analysis with Simple Analytical Model

A simple analytical model for crevice concentration was adopted from earlier work by Cleary and Lindsay.¹ The crevice hideout rate can be established by using a mass balance equation like Eq. (B1).

$$\rho_f \varepsilon V \frac{dc}{dt} = \dot{m}_i c_o - \dot{m}_o c - (\dot{m}_i - \dot{m}_o) \gamma c - \Gamma (c - c_o) \quad (\text{B1})$$

where ρ_f : liquid density in crevice

ε : porosity in crevice

V : total volume in crevice

\dot{m}_i : mass flow rate of liquid into the crevice

\dot{m}_o : mass flow rate of liquid out of the crevice

c : crevice concentration

c_o : bulk concentration

γ : liquid - vapor distribution coefficient

Γ : mass transfer coefficient for diffusion

On the right-hand side of Eq. (B1), the first term reflects the incoming rate of impurity from bulk water and the second term, the mechanical carry-over by the outgoing liquid flow.

For algebraic simplicity, the parameter K_f is defined as follows:

$$K_f = \dot{m}_i / \dot{m}_o \quad (\text{B2})$$

In most cases K_f is much larger than 1. The difference between the incoming and outgoing mass flow rates is equal to the evaporation rate inside the crevice, which can be formulated as follows:

$$\dot{m}_i - \dot{m}_o = \alpha \pi D L q'' / h_{fg}$$

where α : the fraction of wetted length in the crevice

D : steam generator tube diameter

L : crevice depth

q'' : heat flux in the crevice

h_{fg} : heat of vaporization

(B3)

$$\dot{m}_i - \dot{m}_o = \dot{m}_i \left(1 - \frac{1}{K_f} \right) \approx \dot{m}_i = \alpha \beta' q''$$

where $\beta' = \pi D L / h_{fg}$

(B4)

Equation (B1) can be reformulated by using Eq. (B2)-(B4) and assuming $K_f \gg 1$:

$$\begin{aligned}
\rho_f \varepsilon V \frac{dc}{dt} &= \dot{m}_i \left[c_o - \left(\frac{1}{K_f} + \left(1 - \frac{1}{K_f} \right) \gamma \right) c \right] - \Gamma (c - c_o) \\
&= \alpha \beta' q'' \left[c_o - \left(\frac{1}{K_f} + \gamma \right) c \right] - \Gamma (c - c_o) \\
&= (\alpha \beta' q'' + \Gamma) c_o - \left[\alpha \beta' q'' \left(\frac{1}{K_f} + \gamma \right) + \Gamma \right] c
\end{aligned} \tag{B5}$$

Since the MB system is closed, the accumulation rate in the crevice should be balanced by the reduction rate in bulk water, as follows:

$$\begin{aligned}
\rho_o V_o \frac{dc_o}{dt} &= -\rho_f \varepsilon V \frac{dc}{dt} \\
\text{where } \rho_o &: \text{density of bulk water} \\
V_o &: \text{volume of bulk water}
\end{aligned} \tag{B6}$$

The reduction rate of the impurity concentration in the bulk water can be determined by using

$$\begin{aligned}
\rho_o V_o \frac{dc_o}{dt} &= -(\alpha \beta' q'' + \Gamma) c_o + \left[\alpha \beta' q'' \left(\frac{1}{K_f} + \gamma \right) + \Gamma \right] c \\
\frac{dc_o}{dt} &= -\frac{\alpha \beta' q'' + \Gamma}{\rho_o V_o} c_o + \frac{\alpha \beta' q'' \left(\frac{1}{K_f} + \gamma \right) + \Gamma}{\rho_o V_o} c
\end{aligned} \tag{B7}$$

If the second term on the right-hand side does not vary much with time, Eq. (B7) can be integrated and formulated as follows:

$$\begin{aligned}
\ln \frac{c_o - A_i}{c_o^o - A_i} &= -G_i t \\
\text{where } c_o^o &: \text{initial bulk concentration} \\
A_i &= \frac{\left[\alpha \beta' q'' \left(\frac{1}{K_f} + \gamma \right) + \Gamma \right] c}{\alpha \beta' q'' + \Gamma} \text{ and } G_i = \frac{\alpha \beta' q'' + \Gamma}{\rho_o V_o}
\end{aligned} \tag{B8}$$

To estimate A_i and G_i in Eq. (B8), impurity concentration behavior data are needed for the bulk water. Figure B1 shows the theoretically estimated conductivity as a function of Na concentration for the Na-to-Cl molar ratio of 0.7. Since the theoretical calculation assumes an infinitely dilute condition, this calculation method is not applicable to the higher impurity concentration observed inside the crevice. Figure B2 shows the calculated Na and Cl concentrations from the bulk conductivity data. The calculated concentrations are in good agreement with the chemical analysis.

The parameter A_i can be determined by a graphical method as shown in Figure B3 through B5. The A_i value is changed by trial and error until the best-fit linear regression is achieved. The bulk concentration variation data shown in Figure B2 were used to determine A_i and G_i values as a function of ΔT . Only bulk conductivity data logged before reaching the steady-state conditions at each ΔT were used for this analysis. As shown in Figure B3 through B5, the best value of A_i is zero. In the case of $\Delta T=40^\circ\text{F}$ it was difficult to find a best value of A_i . To determine a general trend, the best value of A_i at $\Delta T=40^\circ\text{F}$ was assumed to be zero as used in other cases. If we assume the mass transfer coefficient is small enough to neglect, A_i is dependent on K_f , the liquid-vapor distribution coefficient, and the crevice concentration. Since $1/K_f$ is usually much less than one and the liquid-vapor distribution coefficient for NaCl or NaOH is negligible, A_i is dependent on the crevice concentration, c . The estimated crevice concentration in this series of tests is around 10^5 ppm range. If $1/K_f$ is in the same range as the crevice concentration, A_i will be close to zero.

The obtained G_i values are plotted as a function of ΔT in Figure B6. The plot for G_i is linear with respect to ΔT . In Eq. (B8), if the mass transfer by diffusion is negligible, G_i is proportional to the fraction of wetted length α and heat flux q . If the wetted length is constant and equivalent to the actual depth of the crevice, the heat flux will be proportional to ΔT . Therefore, G_i is proportional to ΔT , as shown in Figure B6. Based on the results in Figure B6, the impurity hideout rate is proportional to ΔT . Strictly speaking, the impurity hideout rate depends on the heat flux and the total tube surface area where nucleate boiling occurs in the crevice, excluding steam-dominant areas.

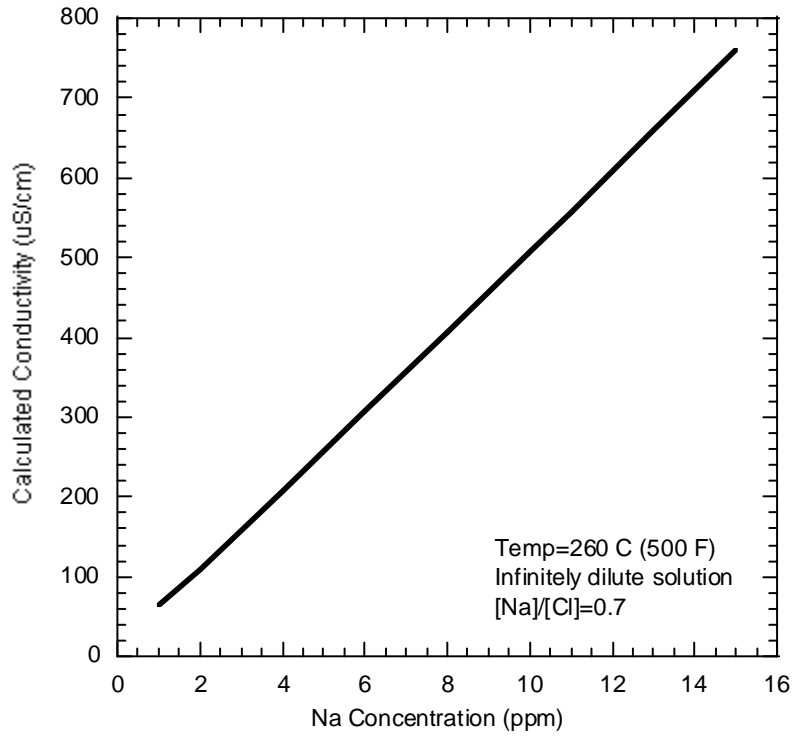


Figure B1.
Theoretically predicted conductivity as a function of Na concentration assuming that Na-to-Cl molar ratio is 0.7.

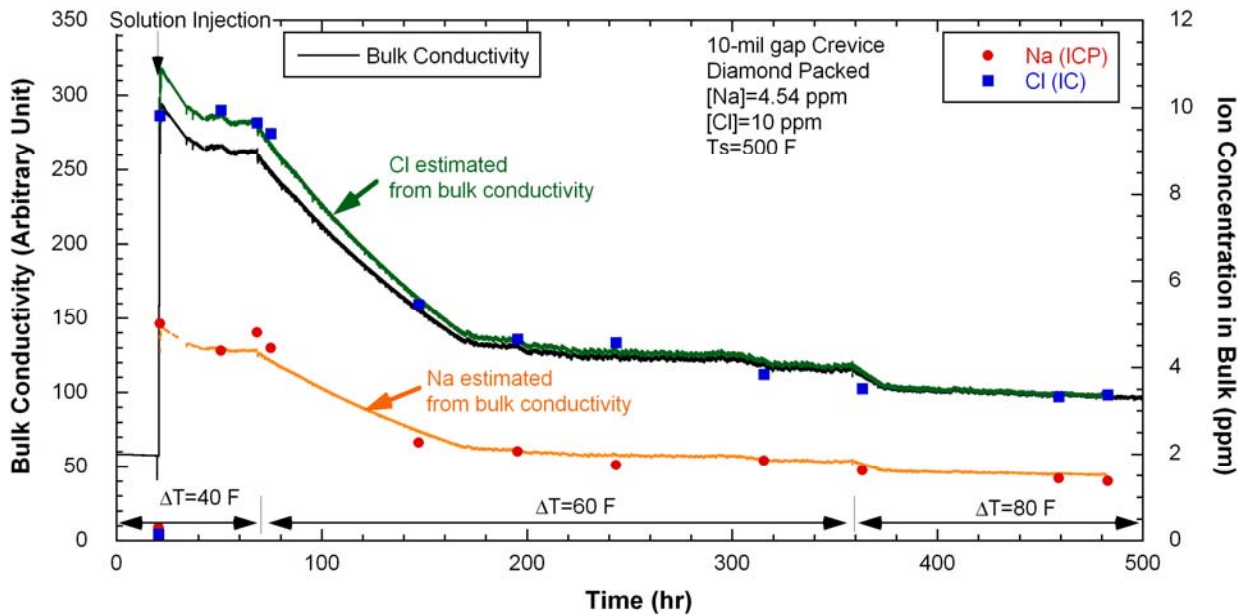


Figure B2. Na and Cl concentration variation estimated from bulk conductivity.

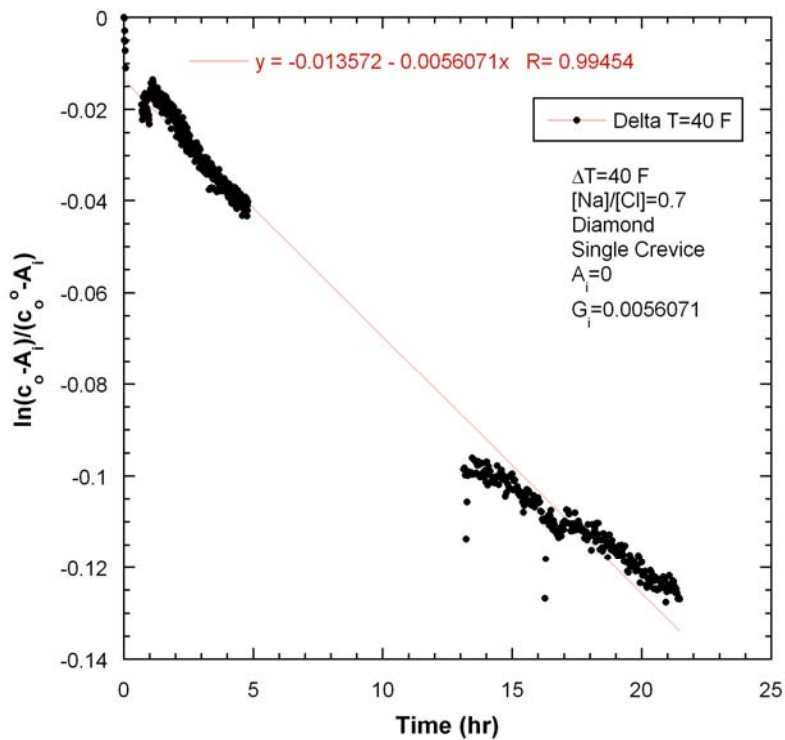


Figure B3.
Normalized bulk concentration
variation as a function of time at
 $\Delta T = 40^\circ\text{F}$.

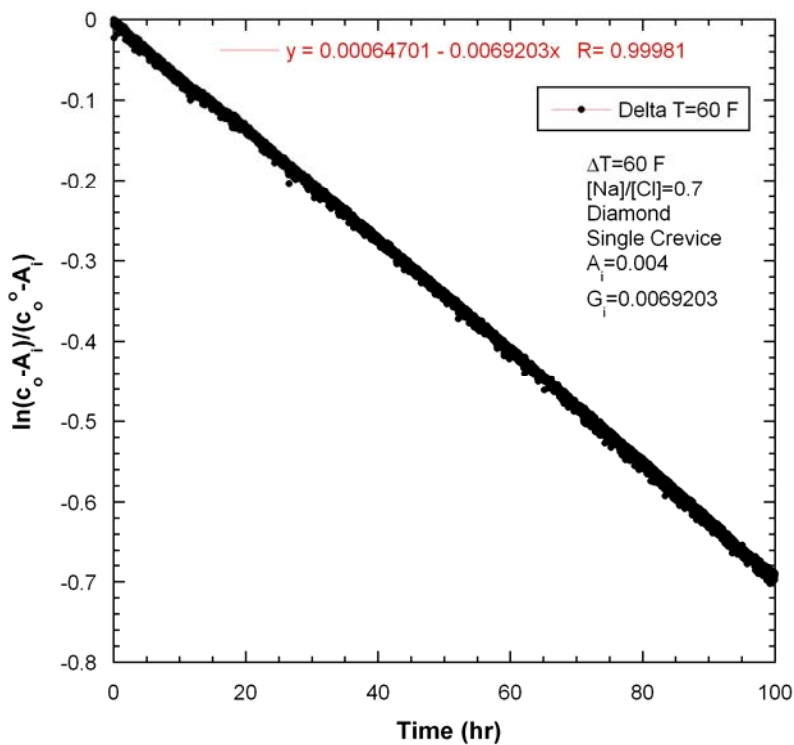


Figure B4.
Normalized bulk concentration
variation as a function of time at
 $\Delta T = 60^\circ\text{F}$.

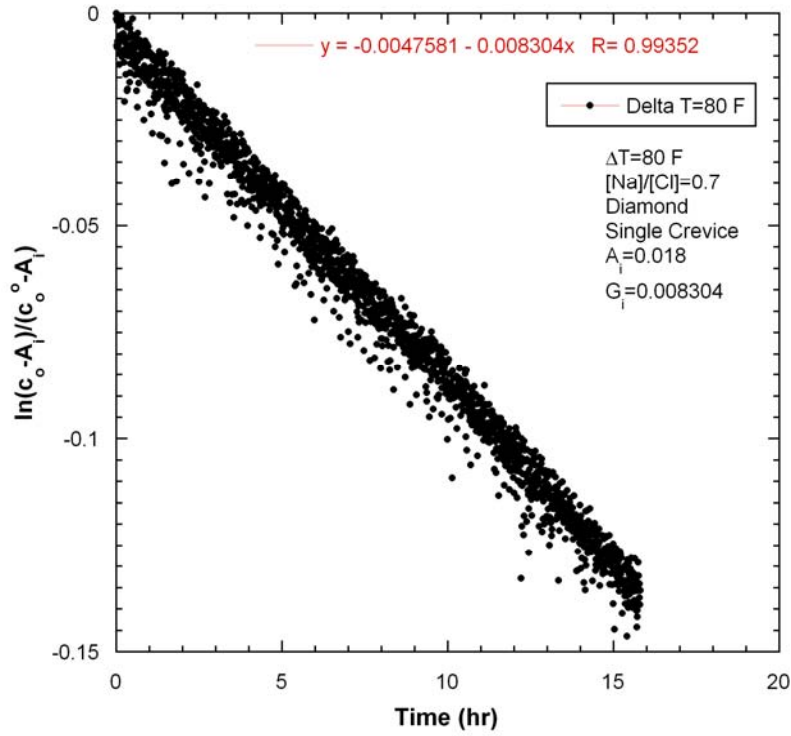


Figure B5.
Normalized bulk concentration
variation as a function of time at
 $\Delta T = 80^\circ\text{F}$.

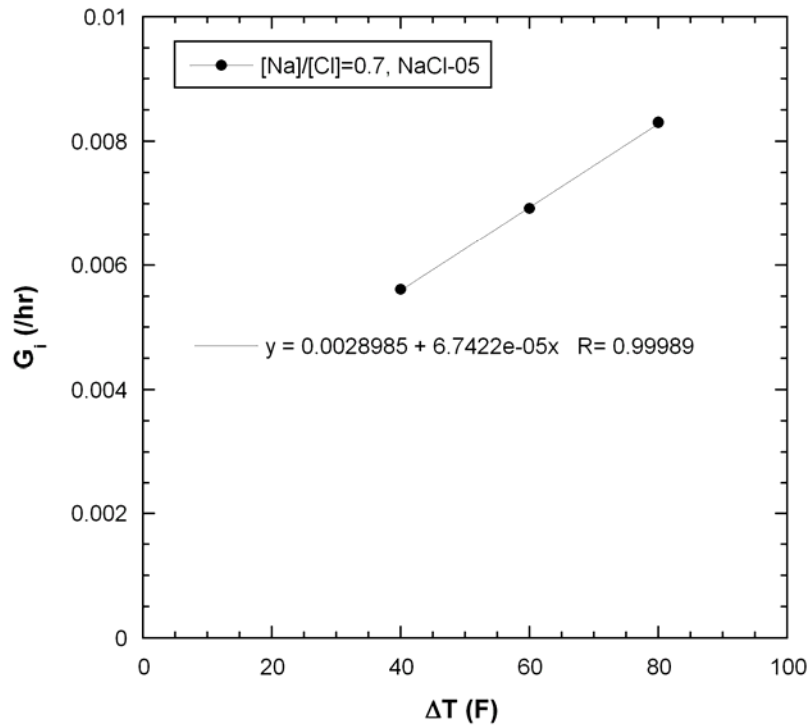


Figure B6.
Time constant G_i variation as a
function of ΔT .

Reference

1. J. G. Cleary and W. T. Lindsay Jr., "Diffusion and Hideout in Crevices, Final Report," EPRI-NP-2979, Electric Power Research Institute, Palo Alto, March 1983.